# SELF PROPAGATED HIGH TEMPERATURE SYNTHESIS OF ELECTROCERAMIC RARE EARTH TITANATES AND THEIR CHARACTERISATION

*Thesis submitted to the Faculty of Science, University of Calicut in partial fulfillment of the requirements for the degree of*

DOCTOR OF PHILOSOPHY

*In Chemistry*

*By*

**K.R. DAYAS**

Forwarded

**NOVEMBER 2006**

**DEPARTMENT OF CHEMISTRY**
**UNIVERSITY OF CALICUT**
**KERALA 673 635**
**INDIA**

# DECLARATION

I hereby declare that the thesis bound herewith is an authentic record of the research work carried out by me under the supervision of **Dr. K. Krishnankutty**, Professor, Department of Chemistry, University of Calicut, in the partial fulfilment of the requirements for the Degree of Doctor of Philosophy in Chemistry of the University of Calicut and further that, no part there of has been presented before for any other Degree.

**K.R. DAYAS**

# CERTIFICATE

This is to certify that the thesis bound herewith is an authentic record of the research work carried out by **Mr. K.R. DAYAS** under my supervision in partial fulfilment of the requirements for the degree of Doctor of Philosophy in Chemistry of the University of Calicut, and further that no part thereof has been presented before for any other degree.

**Dr. K. KRISHNANKUTTY**
*(Supervising Teacher)*

# Acknowledgement

I express my utmost obligation and deep indebtness to my supervising teacher, Dr. K. Krishnankutty, Professor and Head of Department of Chemistry, Calicut University, Kerala for his efficient guidance and excellent directives in successfully completing this investigation. Throughout my research work I was getting very personal attention and healthy criticisms at each and every stage of the work. He was very cordial and friendly, loving, and motivating. It is indeed a matter of pride to me to remember the rewarding moments and accomplishments in this scientific and technological endeavour.

Shri P. Sasidharan, my close friend, was very helpful to me, but I badly missed him. I respectfully dedicate my work to his fond memories.

The former HODs, Dr. M. P. Kannan and Dr. K. Aravindakshan extended their full support and freedom to work in the department. All the faculty members were very cordial with me and extended all the help I needed for my work.

I am very much grateful to my co researchers, Dr. V. D. John, Shri Babu Joseph and Shri. Joseph John provided me valuable help and cooperation in many ways.

I wish to thank Center for Materials for Electronics Technology [C-MET], an R&D institute of Ministry of Communications and Information Technology, Govt. of India for permitting me to do my research work at Calicut University. I am thankful to Dr. T. L. Prakash, Executive Director and Shri. P. I. Sadanandan, Registrar for all their encouragements during the course of my work.

I record my gratitude to my colleagues at C-MET, Dr. A. Seema, Dr. Bindu Krishnan, Shri K. Prasad, Shri Justin. M. Varghese and Shri. N. K. Prasanth for their unstinted help throughout my work. I am thankful to Dr. R. Ratheesh, Dr. SSN Potty, Shri P. A. Abraham and Stanly Jacob for their kind support.

A special thanks are due to Dr. Bindu Krishnan, Dr.V. P. N. Namboodiri and Lyjo Joseph who helped me in accomplishing the photoacoustic studies at CUSAT, Kochi.

My friends, K.R. Girijan and Ajith were encouraging me in my endeavours, I owe much to them also.

My wife and children were all supportive in my activities.

I gratefully acknowledge the characterization services provided by SAIF, Kochi; SAIF, Chennai; II Sc, Bngalore; Sree Vyasa NSS College, Thrissur.

Above all I am immensely grateful to GOD ALMIGHTY for giving me health and strength to carry out this work and complete it to my satisfaction.

**K.R. DAYAS**

# Preface

Advanced ceramic materials have gained considerable importance in recent years mainly because of their actual and potential technological applications. Metal oxide based ceramics constitute an interesting class of industrial material used for several functional applications. Among the metal oxide ceramics so used rare earth titanates have a pride of place. In many modern industrial products they are used as antiferromagnetic and ferromagnetic materials, microwave dielectrics, ceramic capacitors, optical shutters, memory display devices, very high frequency resonators, piezoelectric actuators, sensors, etc. These applications are highly dependent on several structural and physico-chemical properties such as crystal structure, phase purity, particle size, optical characteristics, dielectric properties, etc. These properties of rare earth titanates are virtually controlled by their method of synthesis. Though several methods have been reported, the desired characteristics were seldom obtained. The present investigation has been so designed as to provide ample opportunity for developing new synthetic methods for preparing various rare earth titanates of desired properties.

Rare earths (Lanthanides) constitute the closely related fourteen elements from $^{57}$La to $^{71}$Lu. The element yttrium also exhibit several characteristic properties of lanthanides. The yttrium titanates synthesised in the present study also exhibited properties almost similar to the various rare earth titanates. Therefore, the term "**rare earth** (RE)", in the title of the thesis has been used in a broad sense to embrace yttrium also.

**Chapter 1** is a **General Introduction** on traditional and advanced ceramic materials. Various techniques reported for the

synthesis of advanced ceramic compounds have been briefly discussed. Since in the present investigation, Self propagated High temperature Synthesis method (SHS method) was employed for the preparation of rare earth titanates, salient features of the method have been included. **Chapter 2** is a critical review of reported work on synthesis, structure and applications of rare earth titanates. In **Chapter 3** various materials used, methods adopted and equipments used in the investigation are given.

In **Chapter 4**, details on the synthesis and characterisation of the rare earth titanates of composition $RE_2Ti_2O_7$ by different methods have been discussed. Results are presented as four sections for brevity and better readability. The results showed that SHS method using rare earth nitrates and $TiO_2$ in presence of ammonium acetate on the SHS 'fuel' is a cost effective and efficient method for the synthesis of phase pure monoclinic $RE_2Ti_2O_7$ (RE = La, Pr, Nd) and cubic $RE_2Ti_2O_7$ (RE = Sm, Gd, Dy and Y). The dielectric properties of these compounds revealed that they are good dielectric ceramic materials suitable for high frequency applications.

In **Chapter 5** details on the synthesis and characterisation of rare earth titanates of the type $RE_2TiO_5$ have been presented. **Chapter 6** is mainly on synthesis and characterisation of mixed rare earth titanates, $(RE,RE')Ti_2O_7$ by SHS method. The thermal diffusivity of these compounds obtained from photoacoustic studies showed very low values compared to many standard materials. Therefore these compounds can function as superior thermal barrier coating.

The work described in the Thesis has partly been published, papers accepted, communicated and to be communicated are also listed below.

1. "Photothermal Deflection and Photoacoustic Studies of Rare earth Titanates'. Proceedings of International Conference on Optics & Optoelectronics, ICOL-2005. PP-OMSD-23 (2005).

2. "Photoacoustic Studies of Dysposium Titanate prepared by SHS Method". Proceedings of DAE-BRNS NLS-5. 358-9 (2005).

3. "Self-propagated High-temperature synthesis, characterisation and dielectric properties of some mixed rare earth titanates". National Conference in Chemistry, 2006, Central College, Bangalore (2006).

4. "Photoacoustic studies of rare earth double titanates". Proceedings of Progress on tunable lasers for ultrafast processes and applications", IIT Chennai, 21-22 December 2006 (Accepted).

5. "Preparation and characterisation of monoclinic $RE_2Ti_2O_7$ (RE = La, Pr, Nd) synthesized by modified SHS-AA method" using inorganic activated. Bull. Mat. Sci. (in press).

6. "Synthesis of phase pure nanopowders of cubic $RE_2Ti_2O_7$ (RE = Sm, Gd, Dy) by modified SHS method using inorganic activator", J. Mater. Chem. (Communicated).

7. "A Novel SHS method using Inorganic activator for the synthesis of phase pure nanosized powders of rare earth titanates", $RE_2Ti_2O_7$" (patent to be applied).

8. "Synthesis of mixed rare earth titanates (RE,RE')$Ti_2O_7$ through modified SHS method using inorganic activator" (patent to be applied).

9. Mixed rare earth titanates (RE, RE') $Ti_2O_7$ for thermal protection coating applications, characterised by photoacoustic studies, Mater. Res. Bull. (Communicated).

10. Highly stable dielectric properties of mixed rare earth titanates, synthesized by SHS-AA method using inorganic activator, J. Mater. Sci. Mater. in electronics (to be communicated).

11. IR and Raman spectral studies of rare earth titanates, $RE_2Ti_2O_7$ synthesized by a modified SHS method using inorganic activator, J. of Raman spectrosc. (to be communicated).

# ABBREVIATIONS

| | | |
|---|---|---|
| APS | : | Average Particle Size |
| BET | : | Brunauer Emmett Teller |
| DOT | : | Device Under Test |
| DTA | : | Differential Thermal Analysis |
| DTG | : | Differential Thermo Gravimetry |
| e-$\phi$ | : | electron-phonon |
| EDAX | : | Energy Dispersive Analysis X-rays |
| FSZ | : | Fully Stabilized Zircon |
| FTIR | : | Fourier Transform Infra Red |
| GBBL | : | Grain Boundary Barrier Layer |
| Hz | : | Hertz (frequency) |
| ICDD | : | International Centre for Diffraction Data |
| K | : | Kelvin |
| MHD | : | Magneto Hydro Dynamics |
| MHz | : | Mega Hertz (frequency) |
| MIEC | : | Mixed Ionic Electronic Conduction |
| MLCC | : | Multilayer Ceramic Capacitors |
| MPI | : | Mesh per Inch |
| MRI | : | Magnetic Resonance Imaging |
| nm | : | nanometer ($10^{-9}$ m) |
| $\Omega$ | : | resistance, ohms |
| PA | : | Photo Acoustics |
| PLZT | : | Lanthanum Lead Zirconate Titanate |
| PMN-PT | : | Lead Magnesium Nitrate-Lead Titanate |
| PTD | : | Photo Thermal Deflection |
| PVA | : | Polyvinyl Alcohol |
| PZT | : | Lead Zirconate Titanate |

| | | |
|---|---|---|
| RE | : | Rare earth |
| S/cm | : | Siemens/cm |
| SEM | : | Scanning Electron Microscopy |
| SHS | : | Self-propagated High-temperature Synthesis |
| $\sigma_e$ | : | Conductivity |
| SOFC | : | Solid oxide fuel cells |
| SS | : | Solid State |
| T | : | Tesla |
| tan $\delta$ | : | loss factor (dissipation factor) |
| Tc | : | Curie temperature |
| TCC | : | Temperature Coefficient of Capacitance |
| TCRF | : | Temperature Coefficient of Resonance Frequency |
| TEM | : | Transmission Electron Microscopy |
| TGA | : | Thermogravimetric Analysis |
| VHF | : | Very High Frequency |
| XRD | : | X-ray Diffractometer |
| XRF | : | X-ray Fluorescence Spectrometer |

# CONTENTS

CHAPTER 4

# SYNTHESIS AND CHARACTERISATION OF RARE EARTH TITANATES, $RE_2Ti_2O_7$

CHAPTER 6

## SYNTHESIS AND CHARACTERISATION OF MIXED RARE EARTH TITANATES (RE, RE')$Ti_2O_7$

# GENERAL INTRODUCTION

K.R. Dayas “Self propagated high temperature synthesis of electroceramic rare earth titanates and their characterisation ” Thesis. Department of Chemistry, University of Calicut, 2006

# CHAPTER 1

# GENERAL INTRODUCTION

## Traditional and Advanced Ceramic Materials

Among the materials known to mankind, ceramics occupies an important position by its own command in the life of human beings. "The great ceramist" moulded man from clay minerals and blew the breath of life through his nostrils and then endowed him with the power to rule the "earth". Man, a product of the Creator, continues to imitate the very art of shaping ceramics to his needs, to build palaces on the earth, to cook food in ceramic vessels, to serve the dishes in ceramic plates and to travel along the brick-laid pavements, and roads. In his efforts, man has learned to make attractive potteries, porcelain articles, refractories, bricks and tiles. He has also developed new types of products like abrasives, cements, glass, enamels and so on. In the modern era, ceramists have added more of scientific flavour to the ceramic technology and opened up new vistas of application for ceramic products. They have brought out several new classes of ceramics for typical functional applications such as magnetic ceramics, electrooptic ceramics, electronic ceramics, ferroelectrics, piezoelectrics, superconductors, nuclear fuels, and so on.

The basic characteristics of ceramics have been totally transformed to produce materials with altogether different properties. Thus, several high insulating ceramics have been converted to better conductors than the metallic conductors, even to a level of high Tc superconducting oxide ceramics of the type YBaCuO with zero resistivity.[1-4] The high opaque nature of ceramics have been changed to the electrooptic PLZT devices.[5-9] The characteristic brittleness, the main identity of ceramics, has been changed to suitable ceramic composites that find uses even as ceramic automobile engines.[5,6,9,10]

In the art of producing ceramics, the building blocks, the tiny particles of the oxides, or other compounds are blended and consolidated to shapes and then heated to melting or near melting temperatures to produce a strong ceramic body. In producing ceramic powders technological advancements have made great leaps and helped to bring down the size of particles. The micron level sized powders give way to sub micron size particles which in turn are replaced by nanometer sized and sub nanometer sized particles which are effectively nothing but a conglomeration of a few atoms or molecules of the constituent elements or compounds. The great advantage of nanoparticles is that the ceramic products formed from such materials can conveniently be sintered at substantially lower temperatures, even 200 $^0$C lower than the usual sintering temperatures.

The processing techniques of producing ceramic powders have also made great strides in their own right by way of the development of energy efficient methods to synthesize phase pure compounds. The latest methods such as alkoxide method, sol-gel techniques, hydrothermal processing, micro emulsion methods, self-propagated-high temperature synthesis (SHS), etc. are some of the low temperature methods to produce functional ceramic powders. Among these, the SHS method is very simple and cost effective technique to synthesize phase pure nanosized ceramic products which are attracting worldwide attention in high-tech ceramics.

The present investigation is aimed **at a multifocused approach for process and product developments. The major objectives of the investigation are:**

**(a) to synthesize advanced ceramics such as rare earth titanates of different structural modifications like monoclinic and cubic $RE_2Ti_2O_7$, orthorhombic $RE_2TiO_5$ and monoclinic or cubic mixed**

**rare earth titanates $(RE,RE')Ti_2O_7$ by the cost effective method namely SHS method,**

(b) **to synthesize phase pure rare earth titanates by SHS method using new types activators instead of conventional organic activators,**

(c) **to make low temperature sinterable nanosized powders of the rare earth titanates,**

(d) **to make ceramic dielectrics having stable high permittivity characteristics in a wide range of frequencies (100 Hz to 10 MHz) having good temperature stabilities in the dielectric properties in the usual device application ranges and to have dielectrics with very low loss tangent (dissipation factor) in the entire frequency range,**

(e) **to develop a useful ceramic material having very low thermal diffusivity property that can have applications in protective thermal barrier coatings.**

Therefore, some of the salient features of ceramic materials pertinent to the present investigation are presented here.

**Classification of ceramics**

Ceramics can be defined as solid components that are formed by the application of heat and pressure[8,10] in the following elemental combinations:

i) comprising at least one metal and one non metal (e.g. Metal oxides: MgO, $ZrO_2$; metal borides: $ZrB_2$; carbides: TiC, WC; nitrides: AlN, etc.)

ii) two nonmetals (e.g. oxides: $SiO_2$; nitrides: BN; carbides: SiC, $B_4C$, etc and

iii) one or more metals and one or more non metals (e.g. $BaTiO_3$, $YBa_2Cu_3O_7$, $Ti_3SiC_2$, SiAlON, etc.)

Thus ceramics include a wide spectrum of traditional materials such as pottery, porcelain, refractories, structural clay products, abrasives, porcelain enamels, cements, glass[8,10-15] and the advanced products like magnetic materials,[5-9] ferroelectrics,[5-9] single crystals,[8] glass-ceramics,[8,16] piezoceramics,[5-9,17] electrooptics,[5-7,9] ceramic superconductors,[1-4] etc. Many industries dependent on ceramic products, e.g. refractories are basic component of metallurgical industry, abrasives are essential requirement for mechanical and automobile industries, glass products are largely required in automobile industry, architectural, electronic and electrical industries. In various forms, ceramics are employed in almost all industries utilizing their characteristic electrical, mechanical, thermal and structural properties.

The basic characteristic of ceramics is their brittleness compared to the deforming nature of metals. Shaping of ceramics generally follow a different route starting from the powders, consolidation and firing to the desired shape.

Ceramics can broadly be classified[8] into (a) Traditional ceramics and (b) Advanced ceramics. Important aspects of these two classes are briefly discussed below.

**Traditional ceramics**

Our ancestors had well appreciated the importance of certain earthy materials such as clays that are easily mouldable into different shapes that upon heating become rigid and strong. One of the fascinating endeavours of ancient civilizations was the moulding of appliances for practical uses and shaping beautiful articles for aesthetic pleasure from certain muds, clays, etc.

During the industrial revolution, structural clay products such as bricks and other heat resistant refractory materials and similar electrical insulators were developed in large scale to meet their demands in diverse fields. Most of these traditional ceramics were silicate based porous structures that are quite coarse, non uniform and multiphase. These silicate based ceramic products were usually prepared by mixing clays and feldspars followed by forming either by slip casting or on a potters wheel, firing in a flame kiln to sinter and finally glazing to get good appearance.

**Advanced ceramics**

Modern developments in ceramic products are mainly based on non-silicate and much more sophisticated materials such as binary oxides, carbides, perovskites and also certain completely synthetic materials. Such materials are referred as advanced ceramics.[5-9,18,19] There are several advantages for these, over traditional ceramics and they are further classified on the basis of their chemical composition and specific functional applications.[5,6,9,20,21] Typical classes of ceramic materials based on chemical composition are briefly mentioned below.

**Pure oxide ceramics**: Apart from conventional applications, several pure oxide ceramics are found to have interesting electrical and refractory properties suitable for use as substrates in integrated circuits and high temperature insulation fibreboards.[22] Commonly used oxides are alumina, zirconia, thoria, beryllia, magnesia, spinel [$MgAl_2O_4$], forsterite [$Mg_2SiO_4$], etc.

**Ceramic nitrides**: Ceramic nitrides like aluminium nitride [AlN], silicon-aluminium-oxygen-nitride [SiAlON], boron nitride [BN] are developed for special applications.[23-29] AlN is used as a refractory for melting aluminium

metal, SiAlON as refractories and potential gas turbine components, BN is high temperature refractory material and also as a good abrasive.[25-30]

**Ceramic carbides**: The best known in this category is silicon carbide [SiC], a common abrasive material and used in a number of fields such as, making grinding wheels,[29,31-35] high temperature saggers, etc..

**Ceramic borides**: Ceramic borides possess high temperature strength and oxidation resistance[29-36] and as a result borides such as $TiB_2$, FeB, CrB, etc. have use as hard materials.

**Functional ceramics**

Examples of some of the important functional ceramics are given below.

**Nuclear fuels**: The oxide ceramic $UO_2$ is widely used as nuclear fuel because of its ability to maintain the fuel characteristics even after long continued use in nuclear reactors.[20,21]

**Electrooptic ceramics**: The electrooptical characteristic of transforming the electrical signals to optical signals and vice versa exhibited by ceramic materials such as lithium niobate [$LiNbO_3$], lanthanum modified lead zirconate titanate [PLZT], etc., are utilized in different electrooptic devices.[5-7,19]

**Magnetic ceramics**: Ceramic magnets like ferrite magnets: $SmCo_5$, $Sm_2Co_{17}$, NdFeB are widely used as magnetic memory units in computers.[5-7,9] Their electrical properties are utilized in high frequency microwave electronic applications.[5-7,9]

**Single crystals**: Different single crystals are synthesized artificially, either to replace the natural crystals or to extract their peculiar properties.[8] For example, single crystals of ruby and garnet are used as laser crystals.[8]

**Nonsilicate glasses**: These glasses are useful for IR transmission. Certain non-silicate glasses have special optical properties and can function as semi-conducting devices.[10,38-41]

**Ferroelectric ceramics**: The high dielectric constants of ceramic titanates like barium titanate [$BaTiO_3$] make them highly useful in electronic industry for manufacturing ceramic capacitors.[5-9,42,43] Other alkaline earth titanates like $SrTiO_3$, $MgTiO_3$, $PbTiO_3$, etc. are also used in electronic industry.[43]

**Piezoelectric ceramics**: Lead zirconate titanate [PZT] exhibits good piezoelectric properties of transforming electrical energy to mechanical energy and vice versa and find applications in transducers, buzzers, actuators, etc.[5-7,9,17]

**Relaxor ferroelectric ceramics**: The best known example in this category is the mixed metal oxide ceramic, lead magnesium niobate-lead titanate [PMN-PT], which is found to have very high permittivity value of about 30,000 and it produces a strain 0.1 %, on application of electrical energy. Therefore such materials are used as electrostrictive actuators[5,6,9] and as high value ceramic capacitors.[5,6,9] They are also made in multilayer structures to suit low voltage applications.

**Methods of synthesis of ceramics**

Conventional ceramics including refractories are generally made by crushing, grinding, sieving and physical mixing of the raw materials, whereas for producing 'advanced ceramics' or 'high performance ceramics', chemically homogenous submicron particles (even nano particles) of highly reactive ceramic powders are essential to ensure products having minimum porosity, high density, and controlled microstructure. In the solid state reaction at high temperatures, the constituent oxides, carbonates, hydroxides, oxalates, etc. are intimately mixed by ball milling and the mix is then calcined

in air at temperatures 1000 $^0$C and above. Since several phases are likely to form during the process, repeated sintering and milling is required to get phase pure products. Ceramic powder synthesis continues to modernize with the introduction of new techniques to improve the fine particle sizes (nano-particle range), low temperatures of formation, uniform size distributions and high powder purity. The conventional methods of synthesis of ceramic powder have been advantageously replaced by several new methods.[5-9,44-46] Different methods reported for the production of advanced ceramic powders are mentioned below.

| **Solid state technique** | **Solution technique** | **Vapour–phase technique** |
|---|---|---|
| a) Solid decomposition<br><br>b) Solid state reaction at high temperatures<br><br>c) Self propagated high temp. synthesis(SHS method)<br><br>d) Pechini method | *a) Precipitation-Filtration*<br>(i) Co-precipitation<br>(ii) Forced hydrolysis<br>(iii)Alkoxide hydrolysis<br>(iv) Hydrothermal precipitation<br>*b) Solvent vapourization*<br>(i) Simple evapouration<br>(ii) Spray drying<br>(iii )Spray roasting<br>(iv) Freeze drying<br>(v) Emulsion drying<br>*c) Liquid drying*<br>*d) Sol-gel* | *a)Vapourization-condensation*<br>*b)Vapour decomposition*<br>*c)Vapour-vapour reaction*<br>(i) Conventionally heated<br>(ii)Plasma heated<br>(iii)Laser heated<br>*d)Vapour-liquid reaction*<br>*e)Vapour- solid reaction* |

Among these some of the important and frequently employed synthetic methods are briefly discussed below.

**Alkoxide process**: The alkoxides (ethoxide, propoxide, etc) of constituent metals in alcohols are refluxed and then decomposed by hydrolysis in $CO_2$ free atmosphere. The hydrated compound thus formed is dried in vacuum or inert atmosphere at around 50 $^0$C. Different alkoxides and suitable solvents are employed in this process and by controlling the concentration of reactants,

the temperature of reaction, hydrolysis can be performed to produce particles of desired fine sizes.[49-53] Because of the high cost of the reactants, the alkoxide process is not employed in large-scale production of ceramics. Nanosized (5-15 nm) $BaTiO_3$ has been prepared by this method.[49-51,54]

**Sol-gel method**: In this technique, a sol of the reactants is initially prepared and then subjected to gelation to form the products. For example, in the synthesis of PZT powder by the sol-gel process, a mixture of methanolic solution of lead acetate, Zr-isopropoxide, Ti-ethoxide and a complexing agent (acetic acid or acetylacetone) are mixed by stirring. The complexing agent retards hydrolysis and condensation of alkoxides. By adding water to this mixture a low viscosity gel is obtained which on drying at 110 $^0$C yields the precursor powder. By calcining the precursor powder at about 650 $^0$C polycrystalline phase pure PZT material of APS 300 nm can be obtained. Alternatively, addition of acetone (in place of water) to the sol of Zr-isopropoxide, Ti-ethoxide and Pb-acetate yields fine precursor powder of size about 100 nm, which can be dried and calcined to form phase pure PZT powder.[48,54] Sol-gel synthesis using cheaper reagents such as nitrates, halides of metals are also known.[48]

**Solid state methods**

This is the most widely used technique for the synthesis of both traditional and advanced ceramic materials. In the case of traditional ceramics, where phase purity and structural specifications are not generally specified, sintering of the constituent precursor materials such as oxides, carbonates, silicates, etc. through conventional techniques are only required.[8,48] Pyrolysis of complex compounds such as metal oxalates, citrates, catecholates, etc have also been reported as good starting materials for the preparation of ceramic powders such as $BaTiO_3$. However, in recent years, the solid state route of synthesis of ceramic materials were extensively modified to get phase pure

materials having desired properties and applications. Thus several methods were developed for the synthesis of various advanced and functional ceramic materials through solid state sintering techniques. Of these, perhaps the most important is the Self propagated High temperature Synthesis (SHS method). Although, in the literature, different groups of researchers in this area referred this method in different ways such as combustion method, propellant method, etc., the basic chemical principles involved are the same.

Since in the present investigation the SHS method was successfully adopted for the synthesis of phase pure rare earth titanates, some of the important characteristics of the method are outlined below.

**Self Propagated High Temperature Synthesis**

The term "Self propagated High temperature Synthesis" (SHS), was coined by Merzhanov et al. in 1972, for the process of combustion synthesis of refractory inorganic compounds[56-65] such as borides, carbides, silicides, nitrides, oxides, sulphides, phosphides, hydrides, etc. As early as in 1825, Berzelius reported the preparation of zirconium oxide from amorphous zirconium metal by heating to temperatures below redness. Moissan (1892) observed the formation of titanium nitride from titanium metal powder by heating to 800 $^{o}$C in nitrogen gas, which showed vivid incandescence during the reaction.[66,67] A similar incandescent reaction during the synthesis of cerium nitrate from cerium metal in nitrogen stream was reported by Muthumann and Kraft.[56,83]

Compared to other types of reactions, including the conventional methods, SHS offers a highly cost effective method for the manufacture of ceramics[67-80] due to several factors such as (1) Utilization of reaction heat generated during the reaction instead of external power, (2) High combustion temperature and burning velocity, (3) Simplicity of experimental set up and

(4) High quality of the products. In general, SHS is a material and energy saving process and can be used for net-shape production of finished machine parts. The worldwide importance of SHS research is evident from the regular international symposia on SHS since 1991 and publication from 1992 onwards.

Self-propagated high temperature synthesis (SHS) also known as autocombustion, is an important technique widely used for the synthesis of a variety of oxides for different applications. This method possess several advantages over other methods such as: i) the reagents are simple compounds, ii) no special equipments are required, and iii) powder agglomeration is limited. The method uses the energy produced by the exothermic decomposition of a redox mixture of a metal salt usually metal nitrates with an organic compound like urea, alanine, glycine, etc. as activator. In the combustion mixture, the nitrates and the activator behave like conventional 'oxidants' and 'fuels'. The reaction is usually carried out by dissolving metal nitrates and fuels in a minimum amount of water in a pyrex beaker and heating the mixture to evapourate off the water. The resulting viscous liquid foams, ignites, and undergoes self-sustained combustion, producing ashes containing the oxide product.[68,81,82] During the combustion, exothermic redox reactions associated with nitrate decomposition and fuel oxidation take place. Gases such as $N_2$, $H_2O$ and $CO_2$ evolve favouring the formation of fine particle ashes within a few minutes. The properties of the final product (particle size, surface area and porosity) depend on the method of combustion. The liberation of gases favours the desegregation of the products (increases the porosity) and heat dissipation (inhibits the sintering of the products). Exothermicity of combustion is controlled by the nature of the fuel and the oxidizer to fuel ratio. The reaction paths for synthesis have been described in the literature.[67-71,83-88]

The combustion reaction occurs spontaneously by utilizing the energy released during the exothermic fuel oxidation reaction. Due to the profuse liberation of gases, instant flame is formed which can have temperatures of more than 2000 °C, a stage at which self propagated high temperature attains.[84-90] During the SHS reaction, the reactants undergo dehydration, the fuel melts, disperses and decomposes with evolution of gases so that the product froaths and swells to a foam-like structure and readily starts glowing with instant flame to form the ceramic powders.

The combustion reaction initiates at the sample surface when a heated wire, electric spark, laser beam, etc. induces a heat flux, then the reaction proceeds spontaneously and rapidly.[66-72] The rate of SHS process depends on the exothermic nature of the reaction as well as the mode of heat supplied/received by the system, state of aggregation of reactants, kinetics of phase/structure transformations,[85-92] etc.

The products formed in SHS reactions may be ordinary loose powders, particle agglomerates, foams, cakes, ingots, films, whiskers, fibres and crystals.[69-72] Products formed under optimum conditions are of green composition and contain only traces of unreacted reactants or contaminats.[73,81,87] The grain size depends on rate of cooling and kinetics of crystallization. The products can have porosities in the range of zero (compact materials) and 90-95% (foam materials). A range of products like refractory compounds, inorganic composites (ceramics, cermets, composite materials, etc.); organic compounds (piperazine malonate, quinhydrone, etc.), polymers by frontal polymerization have been made by SHS method.[55,84]

The SHS reaction is similar to the well known Thermite process developed by Goldschmidt in 1895, for the reduction of metallic compounds,[55,84] at specified sites. Goldschmidt used ignition powders (barium peroxide and aluminium) or burning magnesium strip (as fuels) to

initiate the reaction. Once it started, it propagated rapidly throughout the mass. High heats of reaction evolved, (the temperature as high as 3000 °C in 60 seconds) helped the metals such as Al to melt. Vladimir Hlavacek suggested that Goldschmidt deserves the credit for the discovery of Self Propagating reactions of solid-solid non-catalytic systems.[55] Several such SHS reactions were reported.

Chyi-Ching Hwang et al. have reported a method for synthesis of ceramic oxide powders of ferrites, superconductors, varistors, etc., using the metal nitrates as oxidants in presence of organic compounds, like glycine, urea, citric acid, alanine, etc. which act as fuel for the combustion reaction and observed that the powders formed can be sintered at lower temperatures to get ferrite structures.[93]

Steffano Polizi et al. synthesized lanthanide doped $Y_2O_3$ from wet precursors by the so called propellant synthesis method using aqueous solution containing glycine [$NH_2CH_2COOH$] and metal nitrate.[94] This method is different from self-propagating high temperature synthesis of solid-state reactants. By the propellant synthesis method he could produce doped Yttria of open, sponge-like microstructure of large surface area particles. The powder samples were highly porous fractal aggregates of nanocrystallites with an average size of 20 to 50 nm. He suggested a fractal structure for the product on the basis of TEM analysis.

Open polymeric like microstructures are formed by means of a fast cluster-cluster aggregation process. This may be a possible growth mechanism during the combustion or propellant synthesis, which are typically very fast and non-equilibrium processes.

The SHS method of making materials has the advantages on the control of reaction rate, temperature and the microstructure of resultant

product.[62,63,69,70,83,86] The researchers applied external magnetic field during the SHS reaction to form ferrites to get controlled magnetic structures. SHS products find extensive applications[85,86] in mechanical engineering, metallurgy, chemical industry, electrical and electronic engineering, aerospace industry, building industry, medicine, scientific instruments, etc.

Perhaps the most important and interesting aspects of the SHS reaction is the conversion of a simple metallic compound such as metal nitrate into a highly useful ceramic material of desired properties.[95] Common organic compounds such as urea, glycine, alanine etc. are used as activators (fuels) through a cost effective method. Thus, numerous metal oxide ceramics have been prepared by the SHS method. However, no reports exist on the synthesis of phase pure rare earth titanates by the SHS method using ammonium acetate as the activator.

Rare earth titanates are generally prepared by sintering the constituent oxides at high temperatures.[162] But phase pure materials are seldom obtained even by the SHS method using organic fuels such as urea, glycine, etc. Therefore, development of new methods are essential for the synthesis of phase pure crystalline rare earth titanates having desired physico-chemical properties. **The present investigation has been so designed to provide some breakthrough in this direction. Instead of the organic fuels such as urea, in the present study, an inorganic compound itself like ammonium acetate was used as fuel for the SHS reaction. The product obtained on characterization revealed that the method is very effective in the synthesis of phase pure rare earth titanates.**

# RARE EARTH TITANATES A REVIEW

K.R. Dayas “Self propagated high temperature synthesis of electroceramic rare earth titanates and their characterisation ” Thesis. Department of Chemistry, University of Calicut, 2006

# CHAPTER 2

# RARE EARTH TITANATES - A REVIEW

## Introduction

The term rare earths was coined to those elements of the 4f block of the periodic table from $^{57}$Ln to $^{71}$Lu mainly because of their extraction from certain (**rare**) oxide (**earth**) minerals.[96,97] In fact, they are more abundant in the earth crust than gold, silver, mercury, tungsten, etc. Rare earth elements never found as the free metals in the Earth's crust. Pure minerals of individual rare earths do not exist in nature; all their minerals contain mixtures of the rare-earth elements. Promethium has no stable isotopes and is never found in the Earth's crust. The fission products formed in nuclear reactors are found to contain small amounts of Promethium.[98,99] One of the main commercial sources of light rare-earth elements is monazite, which is orthophosphates of lanthanides and thorium. Because of the similarities in properties due to lanthanide contraction, rare earth elements are considered together for almost all physical and chemical studies.

Rare Earths and their compounds find applications in metallurgy,[100] petroleum cracking catalysis,[100] ceramic and glass industries,[97] electronics,[97] optoelectronics,[100] superconductivity,[100] computers,[96] permanent magnets,[96,98,101] alloys, hydrogen storage and transport, rechargeable hydride batteries, space applications,[100] etc. Cerium and erbium are used in high performance alloys,[96] neodymium, holmium and dysprosium are employed for laser crystals, samarium for high performance strong permanent magnets,[96,101] ytterbium and terbium are applied in magnetic bubble and magnetooptic devices to store computer data[96,100] and europium functions as red phosphor in colour television screens.[96] The trichromatic fluorescent lamps made from rare earths such as Eu, Tb as activators and Y, La, Gd as hosts, consume less power (about five times less) than conventional types.[100] Gd is used for detection of tumors, cancer by mammography.[100]

Ceramic oxides such as LaBaCuO, YBaCuO, $EuBa_2Cu_3O_{6+\delta}$ etc. are used as high Tc superconductors.[1-4] Nd-Fe-B magnets are largely used in Magnetic Resonance Imaging (MRI).[101]

Stabilized zirconia containing yttrium oxide is extensively used as oxygen sensors to monitor and control combustion reactions with optimum process conditions.[100] Yttrium oxide/Zirconium oxide on controlled processing can perform as artificial diamonds, the cheap alternative for real diamonds.[100] Cerium oxide is widely used in glass industry for polishing, decolourising or colouring glass compositions.[100] Praseodymium doped zirconium silicate is the yellow colouring agent in glazed tiles.[100]

Ferroelectric polycrystalline barium titanate suitably doped with Dy, Si and Nb functions as Grain Boundary Barrier Layer (GBBL) capacitors with extremely high capacitance values.[102] When the piezoelectric material (PZT) is modified by inclusion of La, it becomes highly transparent PLZT material of high transparency and can be used in electrooptics as optical shutters, memory display devices,[102] etc. Certain pervoskite oxides like $(RE)MO_3$ (where RE – La to Gd and M = Cr, Mn, Fe, Co) mixed with transition metals exhibit alcohol sensing characteristics and are used as breath analysers for detecting alcohol consumed drivers.[102]

Lanthanum modified lead titanate ceramics have better stability and are suitable for very high frequency (VHF) resonators.[102] By adjusting La content, a temperature coefficient of resonance frequency (TCRF) value near zero can be produced.[102] Europium doped $YVO_4$ or $Y_2O_2S$ are used as red phosphor in colour TV picture tubes.[102]

Yttria stabilized zirconia generally functions as electrolyte for oxygen ion at high temperatures in solid oxide fuel cells, which convert chemical energy to electrical energy.[102-112] For the purpose of electrode contacts Sr

doped $LaMnO_3$ or $PrMnO_3$ are used as air electrodes and for interconnects Mg doped $LaCrO_3$.[102-104,113] Lanthanum chromite ($LaCrO_3$) is an extremely good refractory material of melting point >2400 °C. It has an electrical conductivity >100 $\Omega^{-1}m^{-1}$ above 300 °C, and find application such as hot electrode for Magneto-Hydro-Dynamic (MHD) power generation and as high temperature heating elements.[102,104]

**Rare earth titanates**

Among the transition metal oxides, the highest melting and most stable are those of the titanium group: $TiO_2$, $ZrO_2$ and $HfO_2$. These oxides have many applications, for example $TiO_2$ is used as a white pigment, $ZrO_2$ as solid electrolytes and as high melting materials.[102,105-113] Although these oxides are not used primarily as hard materials they are quite hard. $TiO_2$ occurs as a mineral in three well known modifications: rutile, anatase and brookite. Of these rutile is the most important white pigment available. It has the highest density of the three forms and is the most stable. On heating, both anatase and brookite irreversibly transform to rutile.[238]

In all the three modifications, titanium atoms have somewhat distorted octahedral oxygen coordination and the oxygen atoms have a trigonal, more or less planar titanium environment.[239]

Generally, rare earth oxides are of the type $Ln_2O_3$ derived from the formal $Ln^{3+}$ oxidation state. However, due to the typical stability of the empty, half-filled or fully-filled 4f orbitals electronic configuration $Ce^{4+}$ with $[Xe]4f^06s^0$, $Eu^{2+}$ with $[Xe]4f^76s^0$ and $Yb^{2+}$ with $[Xe]4f^{14}6s^0$ can form stable oxides $CeO_2$, EuO and YbO respectively. It has also been observed that praseodymium forms $PrO_2$, a brown black powder of density 6.82 g/cc that transforms to $Pr_6O_{11}$ at 350 °C and terbium forms $Tb_4O_7$ of dark-brown or black solid in appearance are stable.[116]

Synthesis and characterisation of rare earth titanates were first reported in the 1950s. Since then numerous papers appeared in the general and patent literature on various aspects of different rare earth titanates including the phase diagrams of rare earth oxide-$TiO_2$. The phase diagrams of the systems are briefly discussed below.

## Phase diagram of $RE_2O_3$-$TiO_2$

The Phase diagram for the Rare earth oxide-Titanium oxide indicates formation of the common titanates and some additional phases of metastable compounds. In many cases, the intermediate compositions, solid solutions of different products are found to exist at different temperature along with the formation of eutectic solutions at low temperatures. $RE_2O_3$-$TiO_2$ systems for RE = La, Pr, Nd, Sm, Gd , Dy, Lu, and Y are described below.

**Lanthanum Titanate**: The phase diagram of $La_2O_3$ – $TiO_2$ showed the formation of five different lanthanum[117-121] titanates (Fig. 2.1). Characteristic structural properties of these compounds are given in table 2.1. In addition another phase of composition $La_4Ti_3O_{12}$ was also observed.

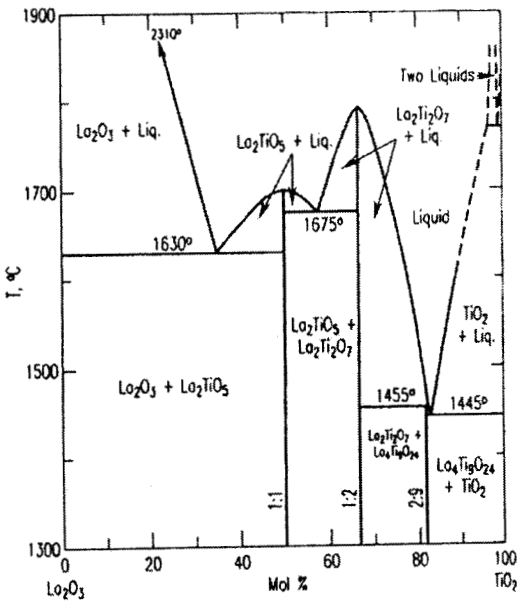


**Fig. 2.1 Phase diagram of $La_2O_3$-$TiO_2$ system**

**Table 2.1. Characteristic structural properties of Lanthanum titanate**

| Structural properties | | Compound | | | | |
|---|---|---|---|---|---|---|
| | | $La_2TiO_5$ | $La_2Ti_2O_7$ | $La_4Ti_9O_{24}$ | $La_2(TiO_3)_3$ | $LaTiO_3$ |
| Structure | | Ortho-rhombic | Mono-clinic | Ortho-rhombic | Ortho-rhombic | Cubic |
| Space group | | (O) | P21 | (O) | (O) | (O) |
| Axes | a | 10.970 | 13.015 | 35.410 | 4.0710 | 3.920 |
| | b | 11.370 | 5.5456 | 14.140 | 4.082 | 3.920 |
| | c | 3.9370 | 7.8170 | 14.580 | 8.010 | 3.920 |
| Angles | $\alpha$ | 90 | 90 | 90 | 90 | 90 |
| | $\beta$ | 90 | 98.64 | 90 | 90 | 90 |
| | $\gamma$ | 90 | 90 | 90 | 90 | 90 |
| Z | | 4 | 4 | 16 | 1 | 1 |
| Unit Cell Vol. $(A^o)^3$ | | 491.06 | 557.80 | 7300.17 | 133.11 | 60.24 |
| Theoretical Density (g/cc) | | 5.448 | 5.782 | 4.992 | 4.727 | 6.473 |

**$LaTiO_x$ system:** The compound, $LaTiO_x$, with 'x' from 3.0 to 3.10 range exhibited weak ferromagnetic semiconducting characteristics[123] in the temperature range of –125 °C to –270 °C; from –125 °C to 0 °C exhibited the semiconducting properties and x > 3.25 to 3.50 were found to be semiconducting in nature as given in Fig. 2.2.

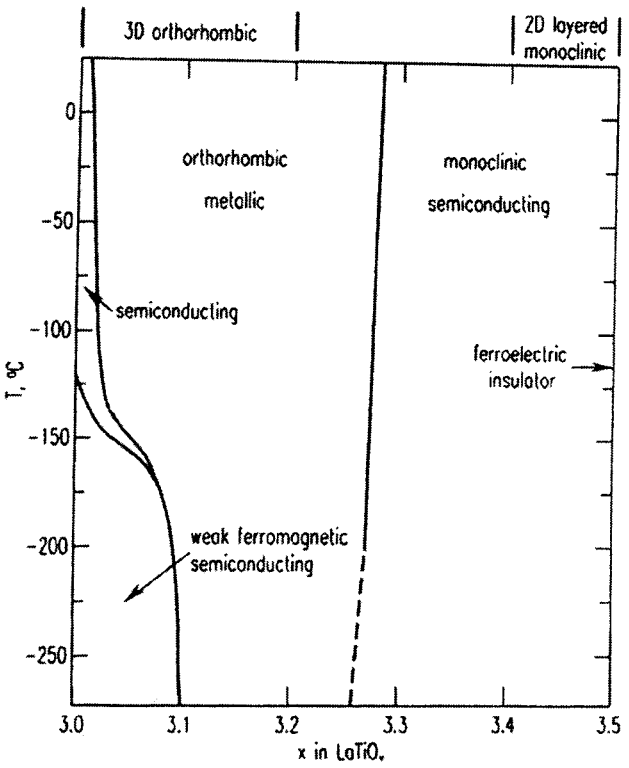


**Fig. 2.2. Effect of oxygen stoichiometry on the conduction nature of LaTiOx (3.0 > x < 3.5) system**

**Praseodymium Titanate:** The $Pr_2O_3$-$TiO_2$ system has three different titanates[124-127] $Pr_2Ti_2O_7$, $Pr_4Ti_9O_{24}$, and $PrTiO_3$. Among this the $Pr_2Ti_2O_7$ exhibits polymorphic transformation to the crystalline modifications monoclinic and orthorhombic. The structural parameters are given in table 2.2.

**Table 2.2. Structural parameters of praseodymium titanate**

| Structural properties | | Compound | | | |
|---|---|---|---|---|---|
| | | $Pr_2Ti_2O_7$ | $Pr_2Ti_2O_7$ | $Pr_4Ti_9O_{24}$ | $PrTiO_3$ |
| Structure | | Mono-clinic | Ortho-rhombic | Ortho-rhombic | Ortho-rhombic |
| Space group | | (O) | Pna21 | Fddd | Pbnm |
| Axes | a | 13.023 | 25.760 | 14.508 | 5.5530 |
| | b | 5.4970 | 7.7300 | 35.374 | 5.622 |
| | c | 7.7130 | 5.4900 | 14.022 | 7.8330 |
| Angles | α | 90 | 90 | 90 | 90 |
| | β | 98.51 | 90 | 90 | 90 |
| | γ | 90 | 90 | 90 | 90 |
| Z | | 4 | 8 | 16 | 4 |
| Unit Cell Vol. $(A^o)^3$ | | 546.07 | 1093.20 | 7196.17 | 244.54 |
| Theoretical Density (g/cc) | | 5.956 | 5.950 | 5.090 | 6.432 |

**Neodymium Titanate**: In the phase diagram of $Nd_2O_3$-$TiO_2$ system formulation of different compositions of neodymium titanates[128-135] such as $Nd_2TiO_5$, $Nd_2Ti_2O_7$ and $Nd_4Ti_9O_{24}$ were observed (Fig. 2.3). Pt-Rh quenching furnace used above 1600 °C in argon. Structural characteristics of these phases are given in table 2.3.

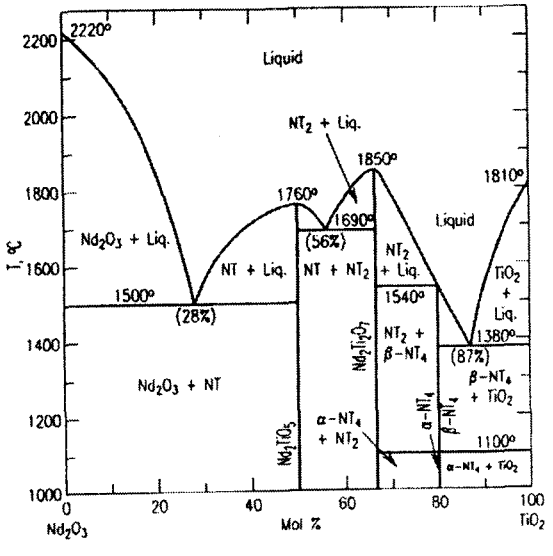


**Fig. 2.3. Phase diagram of $Nd_2O_3$-$TiO_2$ system**

**Table 2.3. Structural parameters of neodymium titanate**

| Structural properties | | Compound | | | | |
|---|---|---|---|---|---|---|
| | | $Nd_2TiO_5$ | $Nd_2Ti_2O_7$ | $Nd_2Ti_4O_{11}$ | $Nd_4Ti_9O_{24}$ | $NdTiO_3$ |
| Structure | | Ortho-rhombic | Mono-clinic | Ortho-rhombic | Ortho-rhombic | Ortho-rhombic |
| Space group | | Pnam | P21 | (O) | Fddd | Pbnam |
| Axes | a | 10.725 | 13.008 | 6.570 | 14.475 | 5.5080 |
| | b | 11.341 | 5.4648 | 6.700 | 35.304 | 5.5820 |
| | c | 3.8457 | 7.6790 | 9.6400 | 13.996 | 7.7990 |
| Angles | α | 90 | 90 | 90 | 90 | 90 |
| | β | 90 | 98.56 | 90 | 90 | 90 |
| | γ | 90 | 90 | 90 | 90 | 90 |
| Z | | 4 | 4 | 2 | 16 | 4 |
| Unit Cell Vol. $(A^o)^3$ | | 46.75 | 539.79 | 424.34 | 7152.31 | 239.79 |
| Theoretical Density (g/cc) | | 5.913 | 6.107 | 5.135 | 5.171 | 6.652 |

**Samarium Titanate:**

The phase diagram of $Sm_2O_3$-$TiO_2$ is given in figure 2.4. Structural characteristics of different samarium titanates[143] formed are brought out in table 2.4. Samarium titanates, also prepared by the coprecipitation from hydrochloric acid solutions of $TiCl_4$ and $Sm_2O_3$ using ammonium hydroxide as precipitating agent, calcined at 900 °C indicated the formation of two crystalline compounds:[136-142] $Sm_2TiO_5$ (melt at 1825 °C, with decomposition) and $Sm_2Ti_2O_7$.

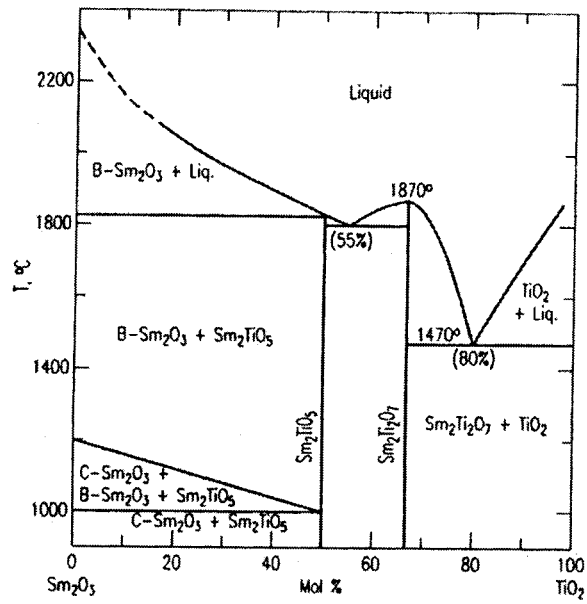


**Fig.2.4. Phase diagram of $Sm_2O_3$-$TiO_2$ system**

**Table 2.4. Structural parameters of samarium titanates**

| Structural properties | | Compound | | | | | |
|---|---|---|---|---|---|---|---|
| | | $Sm_2TiO_5$ | $Sm_2TiO_5$ | $Sm_2Ti_2O_7$ | $Sm_2Ti_2O_7$ | $Sm_4Ti_3O_{12}$ | $SmTiO_3$ |
| Structure | | Ortho-rhombic | Hexa-gonal | Cubic | Ortho-rhombic | Mono-clinic | Ortho-rhombic |
| Space group | | Pnam | (O) | (O) | Cmc21 | (O) | (O) |
| Axes | a | 10.590 | 3.7150 | 10.230 | 3.8062 | 3.7440 | 5.4680 |
| | b | 3.7920 | 3.7150 | 10.2300 | 25.6942 | 11.870 | 5.6650 |
| | c | 11.350 | 11.749 | 10.230 | 5.4190 | 7.4800 | 7.7370 |
| Angles | $\alpha$ | 90 | 90 | 90 | 90 | 90 | 90 |
| | $\beta$ | 90 | 90 | 90 | 90 | 120 | 90 |
| | $\gamma$ | 90 | 120 | 90 | 90 | 90 | 90 |
| Z | | 4 | 1 | 8 | 4 | 1 | 4 |
| Unitcell Vol $(A^o)^3$ | | 455.79 | 140.43 | 1070.6 | 529.96 | 287.88 | 239.66 |
| Theo.Density,g/cc | | 6.247 | 5.069 | 6.311 | 6.374 | 5.406 | 6.826 |

**Gadolinium Titanate**: The phase diagram of $Gd_2O_3$-$TiO_2$ system reveals the formation of two stable compounds namely $Gd_2TiO_5$ (1:1) melting at about 1775 °C and $Gd_2Ti_2O_7$ (1:2) melting at 1820 °C. For the $Gd_2TiO_5$ (1:1), there are two different forms[144-147] namely the L-1:1, the low form and H-1:1 the high form. The low form is found at lower temperature regions while the high form is present in the high temperature regions. Another crystalline modification of composition $GdTiO_3$ was also observed in the phase diagram (Fig. 2.5). Details of different crystalline structures are given in table 2.5.

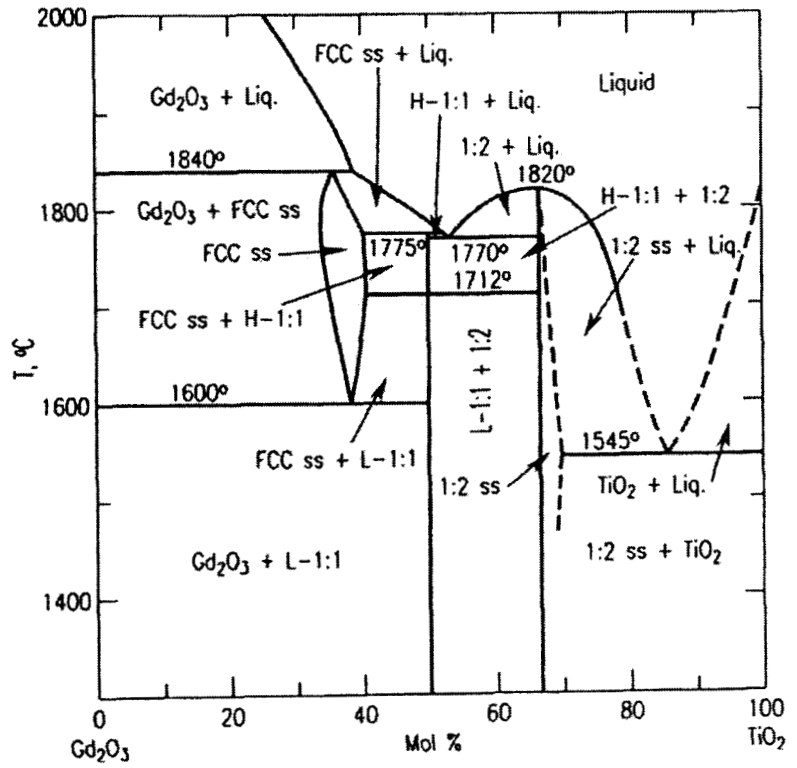


**Fig. 2.5. Phase diagram of $Gd_2O_3$-$TiO_2$ system**

**Table 2.5. Structural parameters of Gadolinium titanates**

| Structural properties | | Compound | | | |
|---|---|---|---|---|---|
| | | $Gd_2TiO5$ | $Gd_2TiO5$ | $Gd_2Ti_2O_7$ | $GdTiO_3$ |
| Structure | | Hexa-gonal | Ortho-rhombic | Cubic | Ortho-rhombic |
| Space group | | (O) | Pnam | Fd3m | Pbnm |
| Axes | a | 3.668 | 10.4788 | 10.1860 | 5.4060 |
| | b | 3.668 | 11.3280 | 10.1860 | 5.7010 |
| | c | 11.908 | 3.7547 | 10.1860 | 7.6790 |
| Angles | α | 90 | 90 | 90 | 90 |
| | β | 90 | 90 | 90 | 90 |
| | γ | 120 | 90 | 90 | 90 |
| Z | | 1 | 4 | 8 | 4 |
| Unit Cell Vol. $(A^o)^3$ | | 138.75 | 445.70 | 1056.84 | 236.66 |
| Theor. Density (g/cc) | | 5.295 | 6.593 | 6.565 | 7.105 |

**Dysprosium Titanate**: Formation of two different phases were reported in the phase diagram (Fig. 2.6) of $Dy_2O_3$-$TiO_2$ having the composition $Dy_2TiO_5$ and $Dy_2Ti_2O_7$. Though $Dy_2TiO_5$ have three different crystalline modifications namely orthorhombic, hexagonal and cubic $Dy_2Ti_2O_7$ exist only in the cubic structure.[148-152] The crystal structure characteristics of these are given in table 2.6.

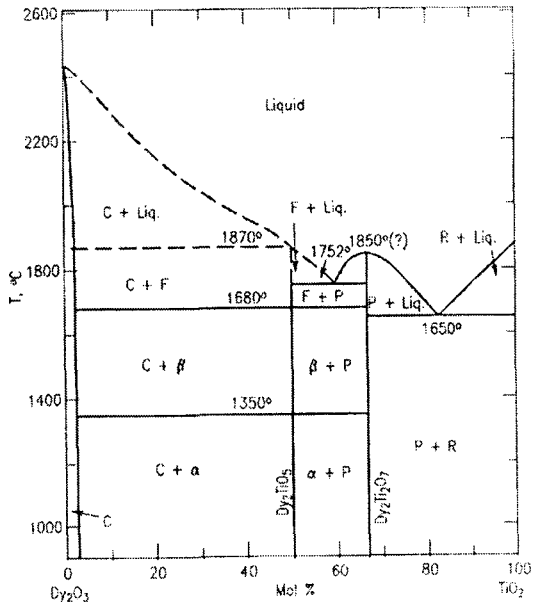


**Fig. 2-6 Phase diagram of $Dy_2O_3$-$TiO_2$ system**

**Table 2.6. Structural parameters of dysprosium titanates**

| Structural properties | | Compound | | | |
|---|---|---|---|---|---|
| | | $Dy_2TiO_5$ | $Dy_2TiO_5$ | $Dy_2TiO_5$ | $Dy_2Ti_2O_7$ |
| Structure | | Orthorhombic | Hexagonal | Cubic | Cubic |
| Space group | | Pnam | (O) | Fd3m | Fd3m |
| Axes | a | 10.490 | 3.6260 | 10.300 | 10.106 |
| | b | 11.2600 | 3.6260 | 10.3000 | 10.1060 |
| | c | 3.7000 | 11.799 | 10.300 | 10.106 |
| Angles | α | 90 | 90 | 90 | 90 |
| | β | 90 | 90 | 90 | 90 |
| | γ | 90 | 120 | 90 | 90 |
| Z | | 4 | 1 | 11 | 8 |
| Unit Cell Vol. $(A^o)^3$ | | 437.03 | 134.35 | 1092.73 | 1032.14 |
| Theor.Density (g/cc) | | 6.884 | 5.598 | 7.343 | 6.857 |

**Yttrium Titanate**: The phase diagram of $Y_2O_3$-$TiO_2$ system (Fig. 2.7) constructed from the co-precipitation of $YCl_3$ and $TiCl_4$, followed by sintering yielded two distinct phases,[153-158] $Y_2TiO_5$ (melting at 1520 °C) and $Y_2Ti_2O_7$ (melting at 1580 °C). Crystalline modifications of $Y_2TiO_5$ (orthorhombic and hexagonal); the cubic structure of $Y_2Ti_2O_7$ and orthorhombic $YTiO_3$ were confirmed. The structural details of these samarium titanate are given in table 2.7.

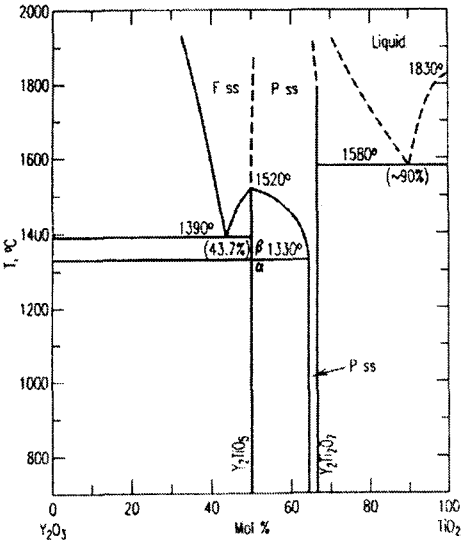


**Fig. 2.7. Phase diagram of $Y_2O_3$-$TiO_2$ system**

**Table 2.7. Structural parameters of yttrium titanates**

| Structural properties | | Compound | | | |
|---|---|---|---|---|---|
| | | $Y_2TiO_5$ | $Y_2TiO_5$ | $Y_2Ti_2O_7$ | YTiO3 |
| Structure | | Ortho-rhombic | Hexagonal | Cubic | Ortho-rhombic |
| Space group | | Pnam | (O) | Fd3m | (O) |
| Axes | a | 10.3330 | 3.6140 | 10.0947 | 5.3270 |
| | b | 11.1810 | 3.6140 | 10.0947 | 5.6180 |
| | c | 3.6992 | 1.840 | 10.0947 | 7.5910 |
| Angles | α | 90 | 90 | 90 | 90 |
| | β | 90 | 90 | 90 | 90 |
| | γ | 90 | 120 | 90 | 90 |
| Z | | 4 | 1 | 8 | 4 |
| Unit Cell Vol. $(A^o)^3$ | | 427.38 | 133.92 | 1028.68 | 227.18 |
| Theoretical Density (g/cc) | | 4.751 | 3.790 | 4.980 | 5.403 |

**Lutetium Titanate**: Formation of two well defined phases of composition $Lu_2TiO_5$ and $Lu_2Ti_2O_7$ were reported in the $Lu_2O_3$-$TiO_2$ system. The $Lu_2TiO_5$ (1:1) unlike titanates of other lanthanides does not show polymorphism.[159] Its fluorite type solid solution melts with decomposition at 2100 °C; whereas the 1:2 compound $Lu_2Ti_2O_7$ melts congruently at 1990 °C.

**Synthesis of rare earth titanates**

The rare earth-transition metal compound oxides have been synthesized by the solid-state reaction between their constituent oxides at very high temperatures.[160-162] The compound oxides can also be synthesized at

slightly lower temperatures by the solid-state reaction between the carbonates, hydroxides, oxalates, etc., as one of the constituents and the other in its oxide form.[160-162]

After reaction, the products are ground to fine particles by ball milling and then consolidating to the required shapes and sintering to obtain the desired components. In the recent techniques, to bring down the sintering temperatures for component formation, very fine particles of titanates are produced by several methods like: Sol-gel method,[163] alkoxide route,[47-53] complex oxalate method,[164] hydrothermal route,[165-169] spray pyrolysis technique,[48] Pechini method,[48] Self Propagated High Temperature Synthesis,[48] etc.

**Structure of Rare Earth Titanates**

Formation of rare earth-titanium oxides of different stoichiometry are well known. Of these $A_2Ti_2O_7$ and $A_2TiO_5$ where A is a trivalent rare earth ion are the most important. Generally $A_2Ti_2O_7$ have pyrochlore structures analogous to modified cubic fluorite structure.[160,161,170,171]

The general formula $A_2B_2O_7$ of oxide pyrochlore need to be correctly written as $A_2B_2O_6O$. The space group of this structure is Fd3m, with unit cell containing eight molecules and four crystallographically non equivalent sites.[162,172,173] L. Minervini and R.W. Grimes[172,174] suggested special position for the ions like 'A' at '16d', B at '16c', O at '48f' and O at '8b'. Some authors denote slight different positions like A at '16c', 'B' at '16d', O at '48f' and O at '8a'. In such cases the crystal is termed to have ordered defective fluorite structure. In defective fluorites, seven oxygen atoms are tetrahedrally coordinated by four random cations and evenly distributed over eight equivalent sites. The pyrochlore structure differs in which the six oxygen atoms occupy the '48f' sites, surrounded by two A and two B cations while the

seventh oxygen atom occupies the 8b site and is surrounded by four A cations. The remaining unoccupied '8a' site is surrounded by B cations.[172]

**Properties and applications of rare earth titanates**

**Magnetic properties:** In $RE_2Ti_2O_7$ the different rare earth ions on a pyrochlore lattice exhibits typical magnetic properties, e.g., $Er_2Ti_2O_7$ and $Gd_2Ti_2O_7$ order below 2 K in complex antiferromagnetic structures[173,175] and some Gd moments may remain paramagnetic below ordering transition. $Ho_2Ti_2O_7$ and $Dy_2Ti_2O_7$ are 'spin ices' with strong single ion anisotropy,[171,176-178] whereas $Tb_2Ti_2O_7$ remains as 'spin liquid' down to 0.07K. S.W. Han et al. attribute an ideal disorder free pyrochlore lattice for $Tb_2Ti_2O_7$ within the experimental error, as the system was remaining in a dynamic, frustrated spin state to the lowest observed temperature.[177,179-181] For $Gd_2Ti_2O_7$, it was found to obey the Curie-Weiss behaviour in the range 10-300K when the d.c susceptibility was measured at an applied field of 0.01T vs temperature. A transition to long-range antiferromagnetic order was noticed[177] at about 2K when the a.c susceptibility was measured down to 0.3K.

Though ferromagnets are generally unfrustrated in nature, recently Harris et al. discovered frustration in the ferromagnet, $Ho_2Ti_2O_7$. No magnetic ordering was observed down to 0.05K. They described this phenomenon is due to strong single-ion anisotropy.[182] The spin arrangements in each tetrahedron are two pointing into and two out similar to ice rules of proton ordering in 'ice model'. The spins may be due to large magnetic moments of $Ho^{3+}$ ions.[183,184]

Normally $Gd_2Ti_2O_7$ is an electronic conductor but a small ionic conduction takes place at elevated oxygen partial pressures and low temperatures.[185-189] The mixed ionic-electronic conduction (MIEC) becomes prominent when $Gd_2Ti_2O_7$ is preferentially doped with donor/acceptor

impurities like Ru, Mn, etc. that makes it attractive candidates for solid-state ionic devices like fuel cells and chemical sensors.[187]

Dan Goldschmidt and Harry L. Tuller describes a small-polaron conduction mechanism in $Y_2Ti_2O_7$ as a result of an extremely strong electron-phonon(e-$\phi$) interaction so that in reduced $Y_2Ti_2O_7$ the dc drift mobility is very low and thermally active over large temperature ranges.[190]

The pyrochlore structure of $Y_2Ti_2O_7$ possess a large unit cell of eight formula units than the other $RE_2Ti_2O_7$ pyrochlore, the arrangement of oxygen ions in the unit cell is such that one-seventh of the ions are relatively free to move, as they do not participate in the network forming $TiO_6$ polyhedra. The large unit cell accommodates large vacancy concentrations without affecting stability of the compound and offers large ionic conductivity for the material.[190,191]

**Dielectric properties**: Usually titanates are employed as dielectric material for the production of capacitors and microwave dielectrics.[192-197] While the alkaline earth titanates, $MgTiO_3$, $CaTiO_3$, $SrTiO_3$ and $BaTiO_3$ possess very high dielectric constant values with a sharp peak at their ferroelectric Curie temperatures,[16,198] e.g., barium titanate has a dielectric constant of 10,000 to 15,000 at 125 °C. The rare earth titanates are found to have low dielectric constant values which remains almost constant with temperature changes. This peculiar property makes the rare earth titanates and their doped compositions to be attractive candidates for microwave applications as resonators,[199-205] etc.

Titanates are used as major ingredient in ceramic capacitor formulations.[193-198,206] The high permittivity of titanates and other ferroelectric materials have the advantage of obtaining high capacitance values for small volume of material. Advantageously ceramic titanates

generally have low loss factor (tan δ). Increasing the area of dielectric material and decreasing its thickness, high capacitance can be obtained for a given material.[16] This principle is employed in the production of ceramic multilayer chip capacitors of layer thickness 10μ and number of layers more than 100.

**Electrooptic applications**: When lead zirconate titanate (PZT) is modified by the inclusion of lanthanum oxide in it to form PLZT, the material transforms from opaque to transparent.[5,6,9] The high optical quality of PLZT is obtained through controlled material processing. The presence of impurities and residual pores in the sintered bodies reduce the optical qualities and also reduce the anisotropy of crystal lattices. Ferroelectric devices for optoelectronics demand good transparency coupled with low driving voltage. The devices made are memory display devices, real time graphic displays, analog space modulators, etc., whereas the largest application of PLZT being optical shutters.[5-9,43]

**Dielectric resonators**: Lead titanate is considered as a stable piezoelectric material for high frequency and high temperature applications.[5-9,43] The La modified $PbTiO_3$ ceramics have better properties and are suitable for Very High Frequency (VHF) resonators.[5-9,43] By controlling the concentration of La in $PbTiO_3$ it is possible to achieve temperature coefficient of resonance frequency (TCRF) nearer to zero. Compositions like $BaO\text{-}PbO\text{-}Nd_2O_3\text{-}TiO_2$ and $(Ba,Sr)O\text{-}Sm_2O_3\text{-}TiO_2$ were developed by Wakino et al.[5,6,9] found to have reasonably high dielectric constants in the range 70 to 90 with very low TCRF, almost near to zero. A typical composition, $0.15\ (Ba_{0.95}Sr_{0.05})O\text{-}0.15(Sm_2O_3)0.7(TiO_2)$ was deveoped by Nishigaki et al.[5,6,9] having a zero TCRF value. Dielectric resonators are applied in producing microwave devices such as band pass filters, band stop filters and frequency stabilization of solid-state oscillators.[5,6,9]

As potential hosts for actinides in radioactive waste ceramics as an ionic conductors in industrial field, rare earth titanates and zirconates are being widely used.[240]

**Electrical conductivity**: Gadolinium titanates are useful materials for electrochemical devices[187-191] such as SOFC, as it exhibits ion conductivities when doped with calcia. When processed under reducing conditions it becomes electronic conductor due to the change in oxidation state of $Ti^{4+}$ ions to $Ti^{3+}$ ions. Thus Mixed Ionic Electronic Conduction (MIEC) is achieved under anodic conditions.

Appropriately doped gadolinium titanate can be employed as electrolyte and electrode in SOFC having the advantage of similar chemical, mechanical and thermal properties and high compatibility for the system.[187-191] The Ca doped (acceptor) gadolinium titanate is found to have high ionic conductivity of the order of $\geq 10^{-2}$ S/cm at 1000 °C, with negligible electronic conductivity over wide temperature range and oxygen partial pressure, whereas Mo containing gadolinium titanate $[Gd_2(Ti_{1-y}Mo_y)_2O_7]$ is a good anode material for SOFC applications with electrical conductivities of $\sigma_e > 10$ S/cm for compositions with y = 0.5. The system $Gd_2Mo_2O_7$ is found to exhibit very high electrical conductivities, similar to metals, in the order of $10^2$ S/cm at room temperature.[186,188,191]

Lanthanum titanate, in the pyrochlore structure, $La_2Ti_2O_7$ or in the perovskite modification, $La_{2/3}TiO_3$ conducts photocurrent in the UV region due to the charge transfer between oxygen ions and titanium or lanthanum ions.[207-209] Some important applications of pyrochlore are fluorescence centers, catalyts, host phase in nuclear waste control, as electrolyte and as conducting electrodes in solid oxide fuel cells.[210-219]

**Other applications**: Optical wave guiding properties were demonstrated for thin films of lanthanum titanate that was deposited by laser (Excimer Ultraviolet) ablation of potassium lanthanum titanate on substrates like silica-coated silicon and fused silica.[209,220] The deposited films are colourless and transparent with a refractive index of 1.917 (for TE nodes at 632.8).

In intelligent gas turbine engines, for controlling its functions piezoelectric actuators and sensors that work at high temperatures like 1000 to 2500 °F are required. Ordinary piezoeletric materials are found unsuitable as they can work only at low temperatures of 300 to 400 °F. Whereas Lanthanum titanate exhibits piezoelectric properties at very high temperatures[219,220] as it has an extraordinary high Tc of 1500 °C and can be conveniently used above 1000°C. Advantageously, lanthanum titanate was found to sustain very high-applied fields from 0.1 V/cm to 80 kV/cm without dielectric break down.

Single crystals of dysporisum titanate ($Dy_2Ti_2O_7$) exhibit optical properties when the far infrared rays fall on it at different temperatures.[221] Seven phonon modes were identified at frequencies below 1000 $cm^{-1}$. The optical conductivity spectra indicates that both the Born effective charges an the static optical permittivity values increase with decreasing temperature.[221] Similarly the phonon line width narrowing at a phonon mode shift with decreasing temperature are also observed.

Xiao Qiang Liu et al. observed the effect of neodymium titanate ($Nd_2Ti_2O_7$) addition on the increase of fracture toughness of zirconia.[222] The addition of $Nd_2Ti_2O_7$ to 8 mol % yttria doped fully stabilized zirconia (8Y-FSZ) improved the mirostructure and mechanical property like fracture toughness of the resultant ceramic. $Nd_2Ti_2O_7$ co-existed as a secondary phase in the stabilized zirconia matrix.[222]

The low temperature firing neodymium titanate has been found extremely suitable for the production of Multi Layer Ceramic Chip Capacitors (MLCCs). It enables the use of low cost internal electrode material like 70Ag/30Pd in place of the costliest electrode materials of pure Pd or Pt. The low firing electrode is compatible with the dielectric neodymium titanate.

As control rods in controlling the safe limits of nuclear reactions taking place in thermal reactors, $Dy_2TiO_5$ materials are employed.[223] The fluorite phase of $Dy_2TiO_5$ was found to have lowest in-service irradiation swelling characteristics as control rod elements.

# MATERIALS, METHODS AND INSTRUMENTS

K.R. Dayas “Self propagated high temperature synthesis of electroceramic rare earth titanates and their characterisation ” Thesis. Department of Chemistry, University of Calicut, 2006

# CHAPTER 3

# MATERIALS, METHODS AND INSTRUMENTS

Various materials used for the synthesis, different experimental methods adopted, various equipments employed for characterization in the present investigation are described in this section.

## MATERIALS

All the rare earth oxides ($Ln_2O_3$) (assay > 99 %)were procured from **Indian Rare Earths Limited**, Kerala, India.

The titanium dioxide, $TiO_2$: (assay = 99.00 %, mol. wt.= 79.88) used was obtained from Merck India Limited.

All the rare earth oxides and $TiO_2$ were quantitatively analyzed (for assessing its purity levels) using XRF spectrometer. Samples for XRF were prepared as follows. The oxides were first dried in an air oven at 120 $^0$C and a definite amount was thoroughly mixed with 'Hoechst wax'. The powder mixture was compacted to discs of 50 mm ∅ and around 2mm thickness. The analysis results obtained are given below in table 3.1.

Other reagents are:

Nitric acid, $HNO_3$ (assay: 69.00 %), Merck India;
Urea, $H_2N$-CO-$NH_2$ (assay: 99.00 %), Qualigens, India;
Ammonium Acetate, $CH_3$-COO-($NH_4$) (assay: 98.00 %) Qualigens, India
Poly vinyl alcohol, (Mol. Wt.~1,25,000, assay = 98.50%) S.D. Fine-Chem. Limited, India

**Table 3.1. Results of assay (by XRF) of rare earth oxides and $TiO_2$**

| % by wt. of oxide | Rare earth oxides | | | | | | | |
|---|---|---|---|---|---|---|---|---|
| | **$La_2O_3$** | **$Pr_6O_{11}$** | **$Nd_2O_3$** | **$Sm_2O_3$** | **$Gd_2O_3$** | **$Dy_2O_3$** | **$Y_2O_3$** | **$TiO_2$** |
| $Al_2O_3$ | ..... | 0.138 | 0.072 | ..... | ..... | ..... | ..... | 0.083 |
| $SiO_2$ | 0.185 | 0.442 | 0.388 | 0.348 | ..... | ..... | 0.333 | 0.340 |
| $SO_3$ | 0.035 | 0.039 | ..... | ..... | ..... | ..... | ..... | 0.090 |
| $K_2O$ | ..... | ..... | ..... | ..... | ..... | ..... | ..... | 0.232 |
| CaO | ..... | 0.166 | ..... | 0.144 | 0.051 | 0.064 | ..... | 0.026 |
| **$TiO_2$** | ..... | ..... | ..... | ..... | ..... | ..... | ..... | **98.81** |
| $ZrO_2$ | ..... | ..... | ..... | ..... | ..... | ..... | ..... | 0.027 |
| $Nb_2O_5$ | ..... | ..... | ..... | ..... | ..... | ..... | ..... | 0.397 |
| $Ta_2O_5$ | ..... | ..... | ..... | ..... | ..... | 0.344 | ..... | ..... |
| ZnO | ..... | ..... | ..... | 0.474 | ..... | ..... | ..... | ..... |
| $Eu_2O_3$ | ..... | ..... | ..... | 0.207 | ..... | ..... | ..... | ..... |
| $Fe_2O_3$ | ..... | ..... | 0.104 | ..... | ..... | ..... | 0.035 | ..... |
| $GeO_2$ | ..... | ..... | ..... | ..... | ..... | ..... | 0.083 | ..... |
| MgO | ..... | ..... | 0.492 | ..... | ..... | ..... | ..... | ..... |
| MnO | ..... | ..... | 0.352 | ..... | ..... | ..... | ..... | ..... |
| PdO | ..... | ..... | ..... | ..... | 0.755 | ..... | ..... | ..... |
| **$La_2O_3$** | **99.780** | 0.470 | ..... | ..... | ..... | ..... | ..... | ..... |
| **$Pr_6O_{11}$** | ..... | **98.745** | ..... | ..... | ..... | ..... | ..... | ..... |
| **$Nd_2O_3$** | ..... | ..... | **98.592** | ..... | ..... | ..... | ..... | ..... |
| **$Sm_2O_3$** | ..... | ..... | ..... | **98.827** | ..... | ..... | ..... | ..... |
| **$Gd_2O_3$** | ..... | ..... | ..... | ..... | **99.194** | ..... | ..... | ..... |
| **$Dy_2O_3$** | ..... | ..... | ..... | ..... | ..... | **99.692** | 0.576 | ..... |
| **$Y_2O_3$** | ..... | ..... | ..... | ..... | ..... | ..... | **98.973** | ..... |

## METHODS AND INSTRUMENTS

Details of the different instruments employed and characterization methods adopted and its application for property evaluation of the product formed are briefly mentioned below.

### X-ray diffraction (XRD)

X-ray diffraction is a powerful technique for characterization and fingerprinting of crystalline substances [The Bruker AXS 5005 XRD machine with Cu $K_\alpha$ ($\lambda$ = 1.5418Å) radiation was used for evaluating the products synthesized in this study]. The principle of XRD is based on Bragg equation, $n\lambda = 2d \sin\theta$. An XRD spectrum indicates positions of different peaks according to the 'd'-spacing or Bragg angle, '$\theta$' and have peak intensities characteristic of the crystalline nature of the substance. Generally, positions of the peaks of a pure crystalline material is fixed but there could be variations in intensities of peaks depending on the preparation method and conditions. Standard XRD patterns of various substances are available as powder diffraction files known as ICDD files. One of the two indexing methods can be employed for comparison of standards for checking phase purity. In the 'Hanawalt index' the eight most intense lines are compared but in the 'Fink index' the first eight lines of longest 'd', spacing in the powder XRD pattern are matched. The usual practice in characterizing a new crystalline material is to compare the XRD peaks with the available standard XRD peaks. In the present investigation all XRD spectral peaks are discussed after comparison with the standard XRD data files.

The unit cell parameters like co-ordinate axes: a, b, c and angles : $\alpha$, $\beta$, $\gamma$ of the crystalline material decides the position of 'd'- spacing in the XRD spectrum; these values are determined from the single crystals of the substances. By assigning the Miller indices (hkl) to the powder patterns and

applying a least square minimization procedure, values of unit cell parameters can be obtained to an accuracy level of five significant figures.[241]

The XRD can also be utilized for very fine particle size measurements of APS < 200 nm.[241] Usually the breadth of the peaks are finite but in the case of very fine particles, there is a phenomenon of peak broadening with decreasing the size of particles. The high temperature X-ray diffraction enables the measurements of thermal expansion coefficients by measuring the change in unit cell parameters. Phases and polymorphic phase transformations taking place at high temperatures can be detected by high temperature XRD.[241]

**Scanning Electron Microscopy (SEM)**

Electron microscopy can provide wide magnifications helpful for structural studies of substances. SEM functions as an instrument working on the reflection mode. The samples are to be coated with fine films of metals to prevent charge build up on the surface to be measured. SEM covers the range between optical microscope and TEM and usually has the range from $10^{-2}$ μ to $10^{2}$ μ (i.e. 10 nm to 100 μm). In the SEM, the electron beam from the gun focuses on a small point of about 50 to 100 Å and then it scans systematically over the surface of the sample similar to the TV screen. The secondary electrons emitted from the surface of the samples are used to build the image of the surface on the screen. SEM is useful for studies of particle size, shape, texture, surface details, etc.; when attached to energy dispersive X-ray systems, known as SEM EDAX it is possible to carry out quantitative elemental analysis of the surface scanned. A JEOL JSM-840A SEM at IISc, Bangalore was used for SEM microstructure measurements.

## FTIR and Raman Spectroscopy

IR and Raman spectra are very much useful for identification of functional groups of organic molecules, and also in the characterization of inorganic solids.[243-244] Intense IR and Raman peaks are obtained for covalently bonded linkages like hydroxyl groups, trapped water, oxy anions-carbonate, nitrate, sulphates etc. Laser Raman spectroscopy can also be used to identify different polymorphs of a material, e.g. the two polymorphs of silica namely quartz and cristobalite are found to have three different sharp peaks, e.g. (a) quartz: 464, 208 and 128 (b) cristobalite: 416, 228 and 116. The Raman spectra were recorded using the Bruker, Germany make FT-Raman, model IFS66V/FRA- 106, available at SAIF, Chennai. The FTIR, Thermo-Nicolet Avatar 370 at SAIF, Kochi and the FTIR 8400S-CE,Shimadzu make at Sree Vyasa NSS College, Thrissur, Kerala were employed for studies.

## Thermal Analysis

By the thermal analysis, it is possible to detect the physical and chemical changes of solids with temperature, such as enthalpy, heat capacity, mass and coefficient of thermal expansion, phase transitions, thermal decompositions, etc. TGA and DTA can be done in different atmospheres such as air, oxygen, nitrogen, carbon dioxide, argon, vacuum etc., to study the effect of thermal changes in presence of gases.

The differential thermal analysis (DTA) measures the difference in temperatures ($\Delta T$) between the sample and an inert reference material with increasing temperature; DTA therefore detects changes in heat content of the sample. In DTA measurement, temperature of the sample and the reference material continues to be the same until some thermal event such as melting, decomposition or change in crystal structure occurs in the sample. Temperature of the sample lags behind that of reference material if an

endothermic change takes place and the temperature of the sample leads the reference material if an exothermic change occurs.

Compared to TGA, DTA results are more useful. TGA detects only the changes in weight with temperature, while DTA detects such changes and also those changes where there is no change in weight but only change in heat content, e.g. polymorphic transitions. The TG/DTA of Perkin Elmer make Pyris Diamond model equipment was used for the TG-DTA data of the samples.

**X-ray Fluorescence Analysis**

Elemental compositions of the starting materials and the products were quantitatively analyzed using XRF. The Philips PW 2400 model sequential wavelength dispersive X-ray Fluorescence spectrometer was used for the analysis.

When high-energy electrons or X-rays bombards on the samples, electrons from the innermost shells are ejected. Electrons from the outer shells jump to occupy the vacant positions and in the process, releases excess energy, characteristic of the element, in the form of electromagnetic radiation. Each element has its own characteristic X-ray peaks in the XRF spectrum. The prominent lines for low atomic number elements (upto atomic number 60) are the 'K' lines ($K_\alpha$, $K_\beta$) while for heavier elements (atomic number > 60) the L lines ($L_\alpha$, $L_\beta$). Positions of peaks in the spectrum depend on the difference in energy between electron levels, which in turn depends on the atomic number of the element. Moseley, in 1913 showed the relation between atomic number (Z) and reciprocal wavelength ($1/\lambda$) for each of the element,

$$C/\lambda = a\,(Z-\sigma)^2$$

where a = Proportionality constant

$\sigma$ = Constant whose value depends on spectral series.

In a XRF spectrum, the position of peaks ($2\theta$ values) corresponds to specific elements and intensity of the peak corresponds to its concentration. By comparing the intensities of the known standards with unknown samples, it is possible to quantitatively analyze samples containing several elements.[241]

Both wavelength dispersive type and energy dispersive type XRF spectrometers are widely used for both qualitative and quantitative analyses.[241,247] In the former type X-rays produced from X-ray tubes are used to bombard on the samples while in the latter case radiations from radioactive sources, e.g. $Am^{241}$ are used to excite the samples. X-rays are photons of high energy and short wavelengths (tenths of angstroms to several angstroms).

If the short wave length cut off ($\lambda_0$) value of an element is lower than its 'K' absorption edge, then it is possible to excite K lines for that element. '$\lambda_0$' is independent of target element but depends only upon the voltage across the X-ray tube. At '$\lambda_0$', all of the energy of the electron is converted, at one impact, to a photon. The relationship between tube voltage and $\lambda_0$ is given by the Duane-Hunt equation[241]

$$\lambda_0 = \frac{hC}{eV} = \frac{12{,}400}{V}$$

where $h = 6.626 \times 10^{-27}$ erg.sec (Planck's Constant)

$C = 3 \times 10^{10}$ cm/sec (velocity of light)

$e = 1.6022 \times 10^{-19}$ coulomb (Energy of electron)

An increase in tube voltage, V, results in (i) an increase in energy emitted and (ii) movement of spectral distribution towards shorter

wavelengths. Thus, using a high voltage X-ray tube, it is possible to analyze heavy elements with much precision.

**BET Surface Area Analyser**

The surface area of the particles was measured using the Quanta chrome Nova model 1200 BET analyzer. After measuring the surface area using the Brunauer-Emett-Teller (BET) method,[242,245,246] using nitrogen gas as the adsorbent to fill in the empty space in the packed sample powder, the average particle size of rare earth titanate powders were calculated using the empirical relation[242]

$$S = \frac{3}{\rho r} \quad \text{or} \quad 2r = \frac{6}{\rho S}$$

where r = radius of particle
S = surface area ($m^2/g$)
$\rho$ = density (g/cc)

**Gain phase Analyser**

The dielectric properties such as permittivity and dissipation factor of all the sintered samples at different frequencies from 100 Hz to 10 MHz and varying temperatures from 20 $^0$C to 120 $^0$C were measured using Agilent make Gain phase analyzer model 4294 A. The principle of dielectric property measurement is that, the equipment measures the impedance of the device under test by measuring vector voltage to current ratio. The impedance of the DUT is determined (auto-balancing-bridge method) by the vector ratio between the voltage across the DUT and the current flowing through it. The parameters such as L,C and R are derived mathematically from the measured impedance value.[6]

**Reflectance spectra**

Electron absorption spectroscopy gives information about the characteristic wavelength over which the samples absorb. For opaque

samples, usually reflection spectra are taken and the valleys indicate the strongly absorbing regions.

The reflectance spectra of the samples were recorded in the range 200-800 nm, using the Jasco V-570 (UV/VIS/IR) spectrophotometer.

**Fluorescence spectra**

Fluorescence spectra were recorded on a Varian spectrophotofluorometer (Cary eclipse EL 0602-341) at ISP, CUSAT. The emission spectra were recorded at different excitation energies as determined from the reflectance spectra.

**Photo Acoustic studies**

The term photoacoustic effect (PA) usually refers to the generation of acoustic waves by a sample as a result of interaction with modulated electromagnetic radiation. It can be used to measure the thermal and elastic properties of materials like thermal diffusivity. It can also be used to detect cracks and other defects in ceramics, rubber, etc.[224-229]

Intensity modulation of the light source is a necessary requirement for the production of PA signal as it is the periodic heating and cooling of the sample, following absorption, which induces the measurable acoustic signal. The absorbed optical energy, which ultimately causes the photoacoustic signal, is that fraction of the total absorbed energy, which is converted to heat via non-radiative de-excitation processes in the sample. Though Alexander Graham Bell discovered,[224-226] the PA effect as early as in 1880, the versatility of PA technique has paved way to several innovative experiments only after the advent of high power lasers, sensitive detection schemes and data acquisition systems.[225-228]

The experimental method is rather simple. When a solid sample placed inside an airtight cavity is irradiated with a modulated optical radiation, the energy liberated through non-radiative channels will result in the generation of thermal waves within the sample. The thermal waves diffuse through the sample to the gas in the cavity and will produce periodic pressure fluctuations in the cavity. This pressure variation can be detected using a microphone kept inside the cavity.[223-229] The experimental set up is shown in the figure 3-1.

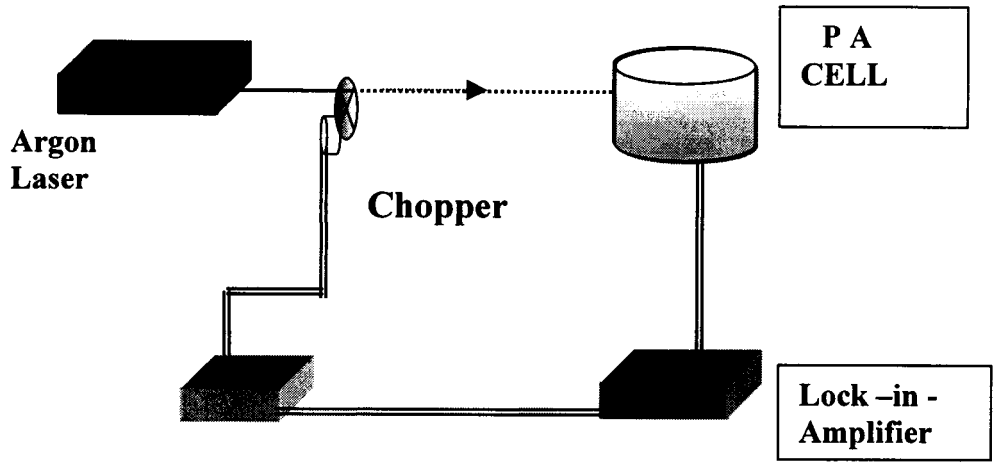


**Fig. 3.1. Schematic diagram of a PA experimental set up**

Optical radiation from an argon ion laser at 488 nm, 20 mW (cw, Liconix 5300) was the source of excitation. It's intensity was modulated using a mechanical chopper (Stanford Research Systems SR 540) before it reaches the sample. Detection of the PA signal was made using a sensitive electret microphone (Knowles BT 1754). The phase and amplitude of the PA signal was measured using a dual phase lock-in-amplifier (Stanford Research Systems SR 830). The PA signal amplitude and phase was recorded as a function of frequency and plotted. From this data, thermal diffusivity can be calculated using the following theory. Rosencwaig and Gersho[227-229] observed that, the pressure variation at the front surface of an optically thick sample

depends on its thermal diffusivity. At higher modulation frequencies, the sample becomes thermally thick, so that the PA signal becomes

$$Q_{th} = \frac{\gamma P_0 I_0 (\alpha_g \alpha_s)^{1/2} e^{-l_s \sqrt{\pi f / \alpha_s}}}{\pi T_0 l_g k_s f} e^{j(\omega t - \pi/2 - l_s a_s)}$$

where $\gamma$ is the ratio of specific heat capacities of air; $P_0$ is the pressure at the ambient temperature $T_0$; f is the modulation frequency; $I_0$ is the incident beam intensity; $l_i$, $k_i$, $\alpha_i$ are the thickness, thermal conductivity and thermal diffusivity of the medium i, where i=g (gas), s (sample).

The amplitude of the PA signal varies as $(1/f)\exp(b\sqrt{f})$ where $b = l_s\sqrt{\pi/\alpha_s}$ whereas phase decreases linearly with $\sqrt{f}$, namely $\Phi_{th} = -\pi/2 - b\sqrt{f}$.

PA can provide information on optical absorption because of the detection of a signal, which is directly proportional to thermal energy induced by the absorbed photons. PTD technique is one of the simplest and popular approaches for thermal characterization of materials. The PTD signal as a function of pump-probe offset allows point by point scanning over the surface, thermal diffusivity can be studied by this method. The same laser source and lock-in-amplifier can be used in PTD method. The pump beam is focused using a convex lens of focal length 20 cm before it strikes the sample. The incident radiation is chopped at 10 Hz so that $\omega\tau << 1$ where $\tau$ is the recombination time of photo excited carriers. Under such experimental conditions, only pure thermal wave component dominates in the heat transport mechanism. The sample is placed at the bottom of a quartz cuvette containing $CCl_4$ as the coupling medium. The probe laser beam used for the present studies is a He-Ne laser (633 nm, 4 Mw Uniphase). A position

sensitive quadrant detector is used to measure the deflection of the probe beam.

**Thermal diffusivity**

Thermal diffusivity is an important thermo physical parameter, which essentially determines the diffusion of heat through a sample. The inverse of thermal diffusivity is a measure of time required to establish thermal equilibrium in a system for which a transient temperature change has occurred.[230-237] The basic law defining the propagation of heat in a one-dimensional homogeneous solid is

$$\frac{\partial Q}{\partial t} = -kA\frac{\partial T}{\partial x} \qquad (1)$$

The above equation is known as Fourier equation.[233-236] Equation (1) implies that the quantity of heat $dQ$ conducted in the x-direction of a uniform solid in time $dt$ is equal to the product of the conducting area $A$ normal to the flow path, the temperature gradient $dT/dx$ along this path, and the thermal conductivity $k$ of the conducting material. Formal definition of thermal diffusivity arises when deriving an expression for a transient temperature field in a conducting solid from the Fourier equation. The equation describing the temperature field in a homogeneous, linear conducting solid with no internal heat source is,

$$\nabla^2 T = \frac{1}{\alpha}\frac{\partial T}{\partial t} \qquad (2)$$

where the thermal diffusivity $\alpha$ is given by

$$\alpha = \frac{k}{\rho C} \qquad (3)$$

where $k$ is the thermal conductivity, $\rho$ is the density and $C$ is the specific heat capacity of the material. The thermal diffusivity $\alpha$ is usually expressed in $cm^2/s$.

Rare earth titanates have a number of applications as discussed in **chapter 2**. Most of these applications are dependent on phase purity, stoichiometry, particle size, surface area and various physico-chemical and structural parameters. These properties are highly dependent on nature of the starting materials, method of preparation and experimental conditions employed. Thus optimization of synthetic parameters have considerable importance on the properties of rare earth titanates. In this study rare earth titanates of the following six rare earth elements were only considered: La, Pr, Nd, Sm, Gd and Dy. Since many of the properties of Y resemble lanthanides yttrium titanates were also included. In the present investigation, both solid state method and SHS methods were attempted for the preparation of rare earth titanates. In the SHS methods, different rare earth titanates were prepared by using one of the widely employed activator for the SHS reaction namely urea (organic fuel). A new activator ammonium acetate was successfully employed in the present investigation as an inorganic fuel for the synthesis of rare earth titanates by SHS route. Characterization of the products obtained from different methods revealed that their structure and properties are highly dependent on the experimental conditions employed for the synthesis. Thus the synthetic details on the different methods and the characterization of the products obtained are presented separately in different sections, as below.

**Section 1** : Solid state synthesis and characterisation of rare earth titanates using $RE_2O_3$ and $TiO_2$.

**Section 2** : Preparation of rare earth titanates from $RE_2O_3$ and $TiO_2$ by SHS method using urea as the activator and their characterisation.

**Section 3** : Synthesis of rare earth titanates $RE_2Ti_2O_7$ from rare earth nitrates, $RE(NO_3)_3$ and $TiO_2$ by SHS method using urea as the activator and their characterisation.

**Section 4** : Synthesis of rare earth titanates $RE_2Ti_2O_7$ from rare earth nitrates $RE(NO_3)_3$ and $TiO_2$ using ammonium acetate as the activator and their characterisation.

# SYNTHESIS AND CHARACTERISATION OF RARE EARTH TITANATES, $RE_2Ti_20_7$

K.R. Dayas "Self propagated high temperature synthesis of electroceramic rare earth titanates and their characterisation " Thesis. Department of Chemistry, University of Calicut, 2006

CHAPTER 4

# SYNTHESIS AND CHARACTERIZATION OF RARE EARTH TITANATES, $RE_2Ti_2O_7$

## SECTION 1

# SOLID STATE SYNTHESIS AND CHARACTERISATION OF RARE EARTH TITANATES, USING $RE_2O_3$ AND $TiO_2$

## EXPERIMENTAL

Direct reaction between different rare earth oxides and titanium dioxide were conducted at temperatures of 1350 $^0$C, 1400 $^0$C, 1450 $^0$C, 1500 $^0$C and 1550 $^0$C for the preparation of the rare earth titanates. For this, $TiO_2$ (3.1952 g, 0.04 mol) and $RE_2O_3$ (0.02 mol) were mixed homogenously in presence of isopropanol (15 to 20 ml) and dried (although different solvents including water or acetone were used, better homogeneity of the mix was observed in isopropanol). To this, required amount of 5 % aqueous solution of PVA was added to ensure 1.5 % solid PVA in the mix (after drying). PVA was used for better adherence of the material during the preparation of green discs for sintering. The bindered material of dough like consistency was then dried, crushed and granulated by passing through 50 MPI sieve and then again sieved through 200 MPI sieve to remove the very fine powders in order to prevent layer formation during disc compaction. The granules were compacted in hydraulic press at a pressure of 3 to 5 tons per square inch to discs of 6 mm ∅ and about 1 mm thickness. These discs were loaded over the surface of stabilized zirconia setter powder spread on high alumina sintering trays and then sintered at the peak temperatures by adopting a bell shaped heating-cooling profile with an intermediate soaking at 600 $^0$C in order to expel completely the organic part. A high temperature soaking for 2 h duration was also given in the heating cycle as shown in Fig. 4.1. Thus five set of samples of each $RE_2O_3$ were prepared at different peak temperatures of 1350 $^0$C, 1400 $^0$C, 1450 $^0$C, 1500 $^0$C and 1550 $^0$C.

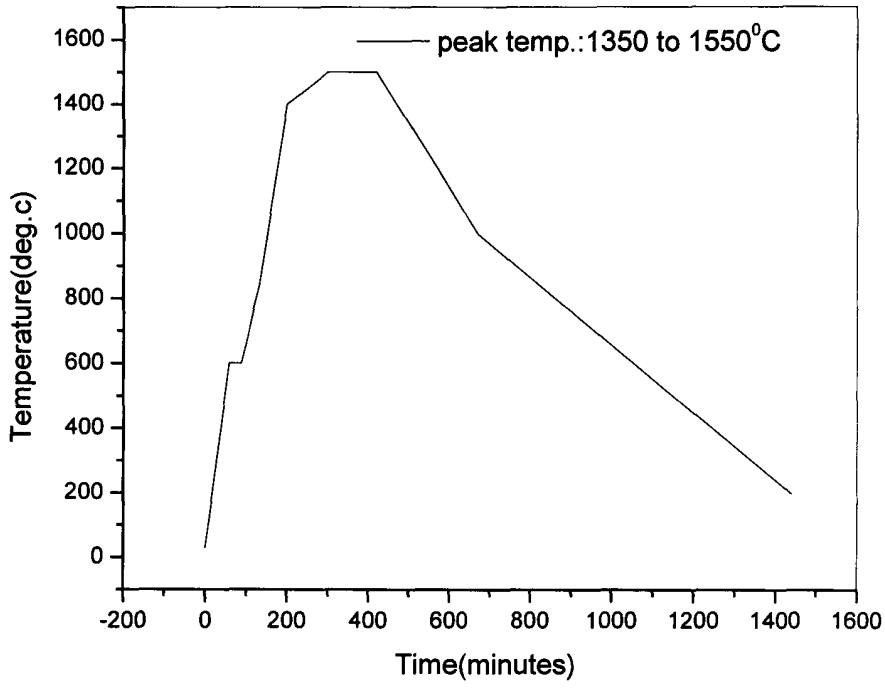


**Fig. 4.1. Sintering temperature vs time profile**

**For recording XRD spectra** samples of the sintered discs were cleaned and crushed in an agate mortar to fine powder. Sintered density by dimensional measurements and also by Archimedes' principle was determined with the cleaned discs.

**Samples for measuring dielectric properties were prepared as follows.** Silver electrodes were fixed on the surfaces of the sintered discs by applying silver paste on both sides, drying at 120 $^0$C for 30 minutes and then curing the film electrodes at 760 $^0$C peak temperature by following a bell shaped heating–cooling profile of 30 minutes from room temperature through peak temperature to room temperature in a conveyor belt furnace of drying zone 200 $^0$C and preheating zone of 400 $^0$C. Over the silvered surfaces tinned copper wires were attached by dip soldering in a solder bath at a temperature of 215 $^0$C, dipping for about 1 to 2 seconds. A 60/40 Pb/Sn solder containing

2 % silver was used as solder bath. Prior to soldering, the surface was cleaned by dipping the discs in a flux bath of tartaric acid to increase the surface contact angle of the solder with silvered surfaces of the discs. Using isopropyl alcohol, the soldered discs were cleaned. It was then dried for 10 minutes at 120 $^0$C in an air oven. The lead attached components are then encapsulated by epoxy resin. For this, the component was heated to 100 $^0$C, and while hot it was dipped in the epoxy powder for 1 second and then heated to 100 $^0$C for 15 minutes. The process was repeated 3 to 4 times to get a smooth coating of epoxy over the component.

The capacitance value and loss factor (tan $\delta$) of the components were measured at different frequencies continuously from 100Hz to 10 MHz using an Agilent Gain phase Analyzer HP- 4294 A. The permittivity values were then calculated from the equation

$$C = \frac{\epsilon_0 \epsilon_r A}{t} \quad \text{or } K = \frac{C.t.10000}{0.0885\ A}$$

where '$\epsilon_0$' is the permittivity of air and $\epsilon_r$ is the permittivity of the dielectric, K = dielectric constant, C = capacitance (in nF) 'A' area of plate (in mm$^2$) and 't' thickness of the dielectric (in mm). The permittivity values and loss factor were continuously plotted against the corresponding frequencies

## RESULTS AND DISCUSSION

The rare earth titanates obtained were characterized using various physico-chemical techniques and the results are discussed below.

### Elemental analysis

The titanium and rare earth percentages of the rare earth titanates analyzed by XRF are given in table 4.1. The data conform to the composition of $RE_2Ti_2O_7$ of all the samples prepared.

**Table 4.1. Elemental percentage of $RE_2Ti_2O_7$ by XRF**

| $RE_2Ti_2O_7$ where RE = | % RE | | % Ti | |
|---|---|---|---|---|
| | Found for the product | Calculated | Found for the product | Calculated |
| La | 57.85 | 57.21 | 19.58 | 19.73 |
| Pr | 57.32 | 57.56 | 19.63 | 19.57 |
| Nd | 58.42 | 58.13 | 19.19 | 19.30 |
| Sm | 59.31 | 59.13 | 19.11 | 18.84 |
| Gd | 61.11 | 60.21 | 18.06 | 18.34 |
| Dy | 60.75 | 61.00 | 17.63 | 17.98 |
| Y | 46.75 | 46.11 | 25.23 | 24.84 |

## Physical characteristics

An interesting observation in the case of the rare earth titanates formed by the method is that their colour is dependent on the sintering temperature (thermochromic property) as the temperature increases the colour changes as given in table 4.2. The colour changes of the sintered discs with temperature is photographed and exhibited as figure 4.2.

| RE | Sintering temperature, $^0$C | | | |
|---|---|---|---|---|
| | 1400 | 1450 | 1500 | 1550 |
| La |  |  |  |  |
| Pr |  |  |  |  |
| Nd |  |  |  |  |
| Sm |  |  |  |  |
| Gd |  |  | 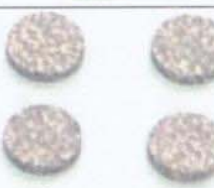 |  |
| Dy |  |  |  |  |
| Y |  |  |  |  |

**Fig. 4.2 COLOUR AND APPEARANCE OF $RE_2Ti_2O_7$ SINTERED AT DIFFERENT TEMPERATURES**

**Table 4.2. Colour change with temperature of sintering of $RE_2Ti_2O_7$**

| Sl. No | $RE_2Ti_2O_7$ | Colour before sintering | Colour at the sintering temperature | | |
|---|---|---|---|---|---|
| | | | 1350 $^0$C - 1400 $^0$C | 1400 $^0$C - 1500 $^0$C | Above 1500 $^0$C |
| 1 | $La_2Ti_2O_7$ | White | Light rose | Yellow | Golden cream |
| 2 | $Pr_2Ti_2O_7$ | Black | Yellow | Green | Dung green |
| 3 | $Nd_2Ti_2O_7$ | Light rose | Brown | Brown | Brown |
| 4 | $Sm_2Ti_2O_7$ | White | Cream | Yellow | Golden cream |
| 5 | $Gd_2Ti_2O_7$ | White | Light rose | Off white | Brown |
| 6 | $Dy_2Ti_2O_7$ | White | White | White | Brown |
| 7 | $Y_2Ti_2O_7$ | White | Off white | Off white | Slate colour |

The densities of discs sintered at different temperatures from 1350 $^0$C to 1550 $^0$C (50 $^0$C intervals) were measured and the values are given in table 4.3. The data clearly shows that titanates of Y, Sm, Gd and Dy were having highest density values when sintered at 1550 $^0$C; while in the case of La, Pr and Nd highest density values were obtained at a sintering temperature of 1450 $^0$C.

**Table 4.3. Density of $RE_2Ti_2O_7$ at different sintering temperatures**

| RE in $RE_2Ti_2O_7$ | Theoretical density (g/cc) | Density (g/cc) of samples sintered at different temperatures, $^0C$ | | | | |
|---|---|---|---|---|---|---|
| | | **1350** | **1400** | **1450** | **1500** | **1550** |
| **La** | **5.78** | 3.12 | 3.08 | 4.19 | 4.16 | 4.01 |
| **Pr** | **5.95** | 3.10 | 3.20 | 4.23 | 4.15 | 3.89 |
| **Nd** | **6.11** | 4.67 | 4.65 | 4.79 | --- | 4.22 |
| **Sm** | **6.31** | 4.35 | 5.05 | 5.02 | 5.03 | 5.11 |
| **Gd** | **6.56** | 3.17 | 3.43 | 3.76 | 3.91 | 4.16 |
| **Dy** | **6.86** | 3.25 | 3.43 | 3.57 | 3.77 | 4.08 |
| **Y** | **4.98** | 2.35 | 2.42 | 2.53 | 2.69 | 2.95 |

From the table, it is evident that sintering of the rare earth titanates upto 1550 $^0C$ did not yield products having densities close to the calculated theoretical densities.

**XRD Data**

The XRD patterns of rare earth titanates sintered at 1450 $^0C$ indicates that the compounds are not sufficiently phase pure. Typical XRD spectra of the compounds $La_2Ti_2O_7$, $Pr_2Ti_2O_7$, $Nd_2Ti_2O_7$ and $Sm_2Ti_2O_7$ are given in figures 4.3 to 4.6. A comparison of the spectra with the respective standard ICDD spectra of the rare earth titanates of composition, $RE_2Ti_2O_7$ revealed that many of the peaks exactly match with the standard data. Thus the several characteristic peaks of standard cubic $Sm_2Ti_2O_7$ are present in the spectrum of the compound prepared (fig. 4.6). There are several other peaks that are not matching well with the standard peaks of $Sm_2Ti_2O_7$. Similarly the XRD spectra of La, Pr and Nd titanates displayed several peaks that correspond to

the monoclinic structure of the compounds. In these cases also, perfect agreement with the standard ICDD XRD patterns were not observed. Thus it can be concluded that direct reaction of $RE_2O_3$ and $TiO_2$ may not yield phase pure $RE_2Ti_2O_7$. Since the compounds synthesized by the solid state reaction of the oxide constituents were not sufficiently phase pure, further characterizations were not carried out.

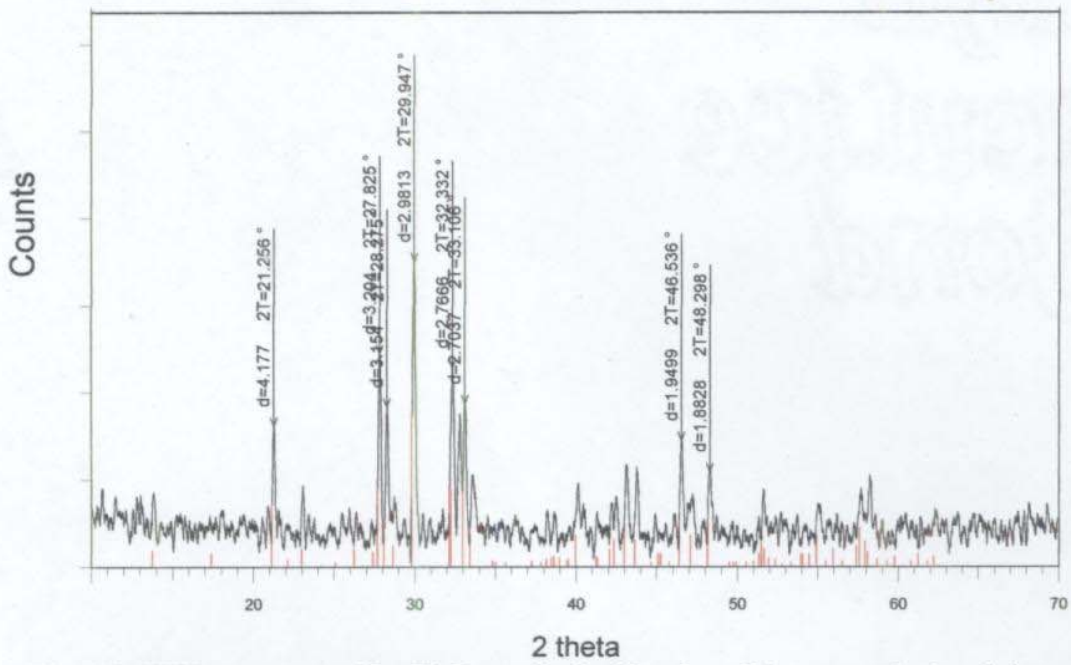


**Fig. 4.3. XRD spectrum of $La_2Ti_2O_7$ synthesized by the solid state method and sintered at 1450 $^0$C (Match ICDD 28.0517, Monodinic, $La_2Ti_2O_7$, shown in red colour)**

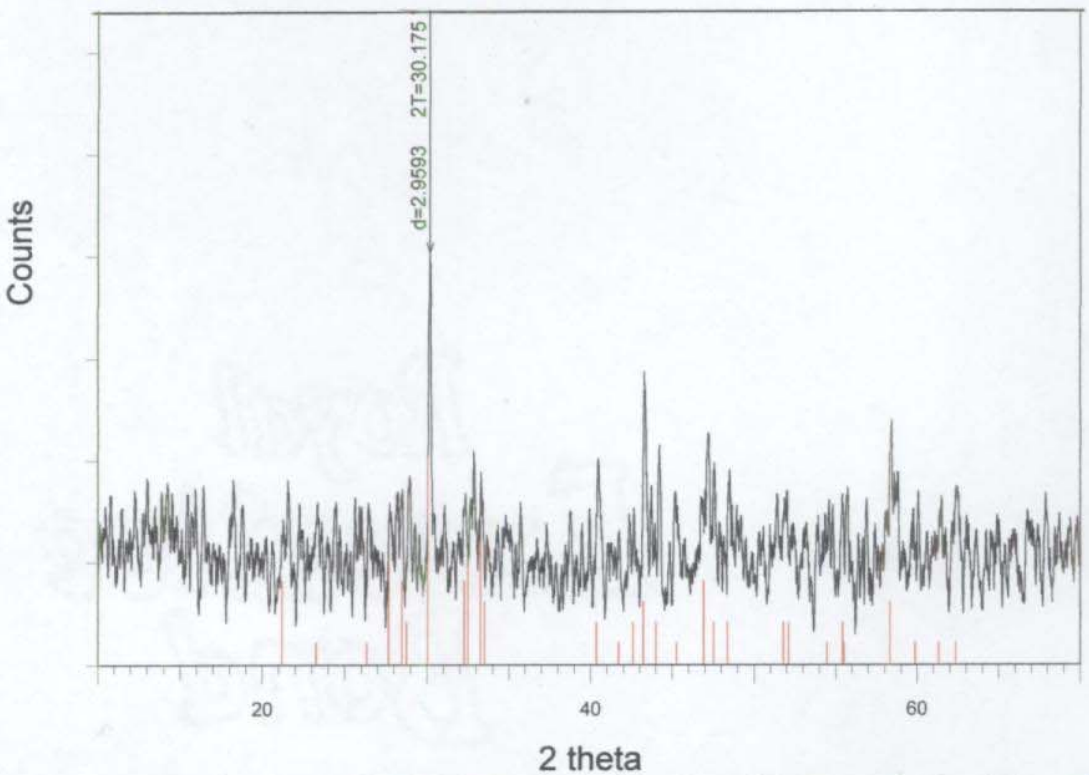


**Fig. 4.4. XRD Spectrum of $Pr_2Ti_2O_7$ synthesized by the solid state method and sintered at 1450 $^0$C (Match ICDD 35-0267, monocline, $Pr_2Ti_2O_7$ shown in red colour)**

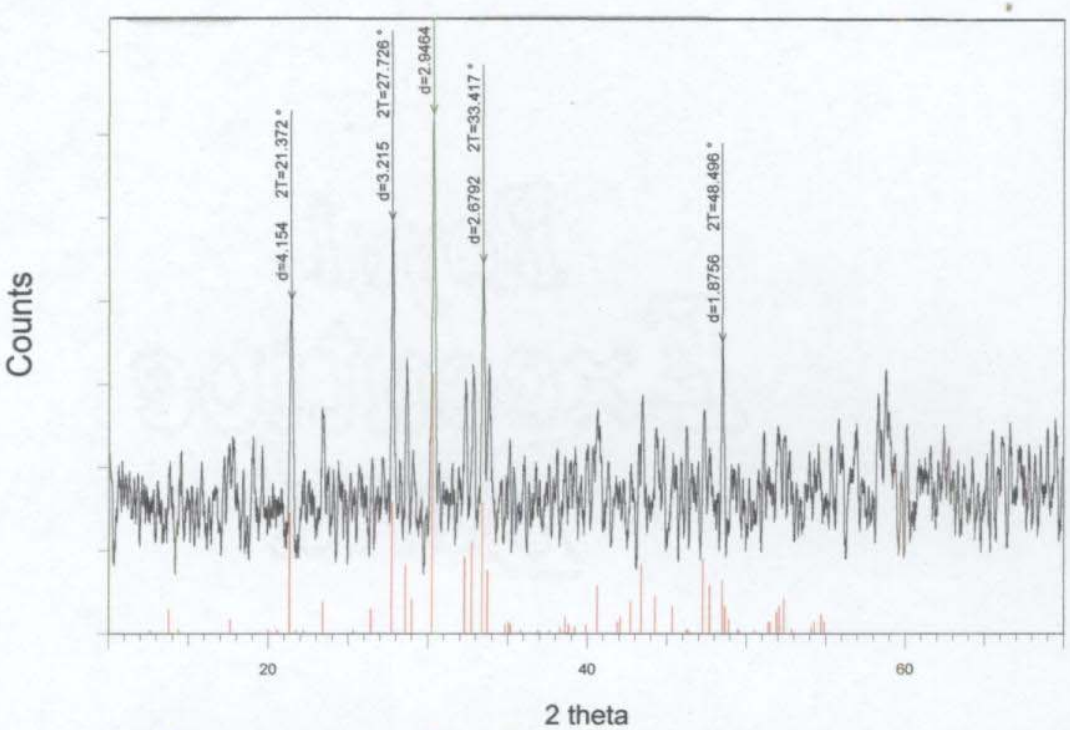


**Fig. 4.5. XRD spectrum of $Nd_2Ti_2O_7$ synthesized by the solid state method and sintered at 1450 $^0$C (Match ICDD 33.0492 monoclinic, $Nd_2Ti_2O_7$, shown in red colour)**

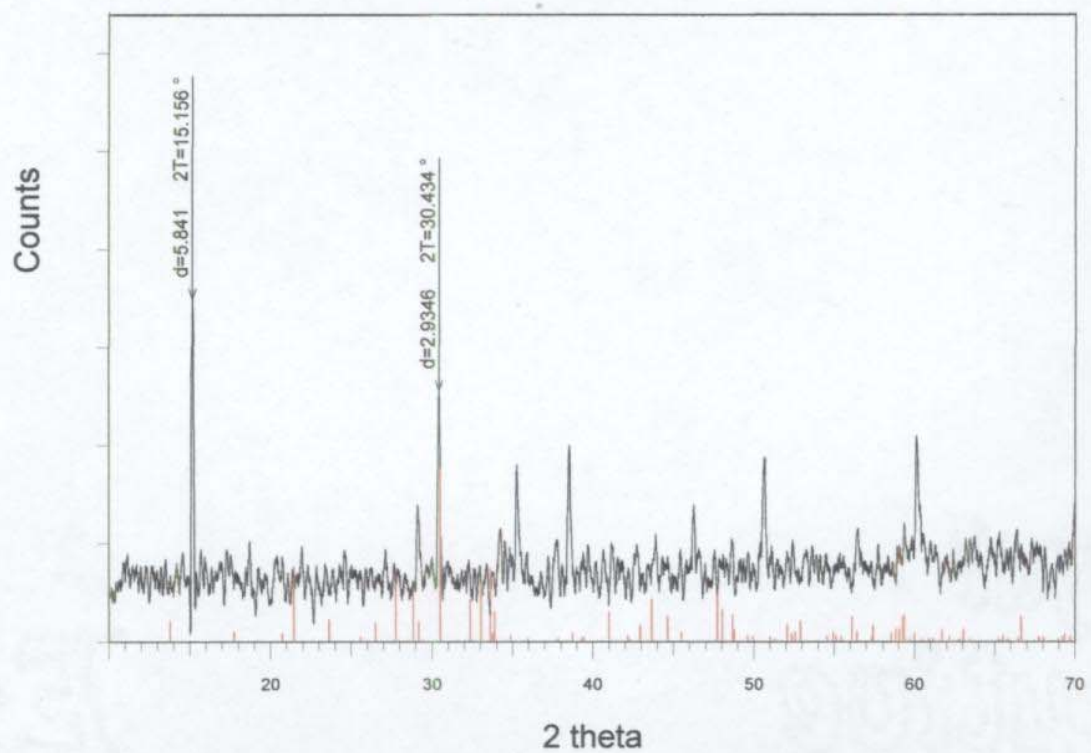


**Fig. 4.6. XRD spectra of $Sm_2Ti_2O_7$ synthesized by the solid state method and sintered at 1450 $^0$C (Match ICDD 16.400 cubic, $Sm_2Ti_2O_7$, shown in red colour)**

## SECTION 2

# PREPARATION OF RARE EARTH TITANATES ($RE_2Ti_2O_7$) FROM $RE_2O_3$ AND $TiO_2$ BY SHS METHOD USING UREA AS THE ACTIVATOR AND THEIR CHARACTERISATION

## EXPERIMENTAL

Direct reaction between $RE_2O_3$ and $TiO_2$ were performed by the SHS method using the organic fuel, urea, as the activator for the reaction as detailed below. Rare earth oxides, $RE_2O_3$ (RE = Sm, Dy and Y) 0.01 mol, $TiO_2$ (0.02 mol) and urea (0.05 mol) were taken in a glass beaker and heated on an electric Bunsen. When urea starts melting the reactants were stirred well. As the reaction proceeds dense white fumes were liberated. However no SHS reaction was observed. The product formed was characterized by XRD.

## RESULTS AND DISCUSSION

**Elemental analysis:** The titanium and rare earth percentages of the rare earth titanates analyzed by XRF are given in table 4.4. The data almost conform to the composition of $RE_2Ti_2O_7$ of all the samples prepared

**Table 4.4. Elemental percentage of $RE_2Ti_2O_7$ by XRF**

| $RE_2Ti_2O_7$ where RE = | % RE | | % Ti | |
|---|---|---|---|---|
| | Found for the product | Calculated | Found for the product | Calculated |
| Sm | 58.84 | 59.13 | 19.23 | 18.84 |
| Dy | 60.55 | 61.00 | 18.11 | 17.98 |
| Y | 45.76 | 46.11 | 25.13 | 24.84 |

**XRD Data**

The XRD spectra of the powders prepared as such and also calcined at temperatures: 600 $^0$C, 800 $^0$C and 1000 $^0$C revealed that the products are not phase pure. A comparison of the peaks with the standard peaks of $RE_2Ti_2O_7$ showed several peaks due to other compounds which are marked by indexing the corresponding peaks of the compounds (Fig. 4.7 to 4.9). However many characteristic peaks of $RE_2Ti_2O_7$ with high intensity are present in the spectra as revealed from a comparison with standard XRD patterns. Since the products contain several phases further characterisation of the materials were not attempted.

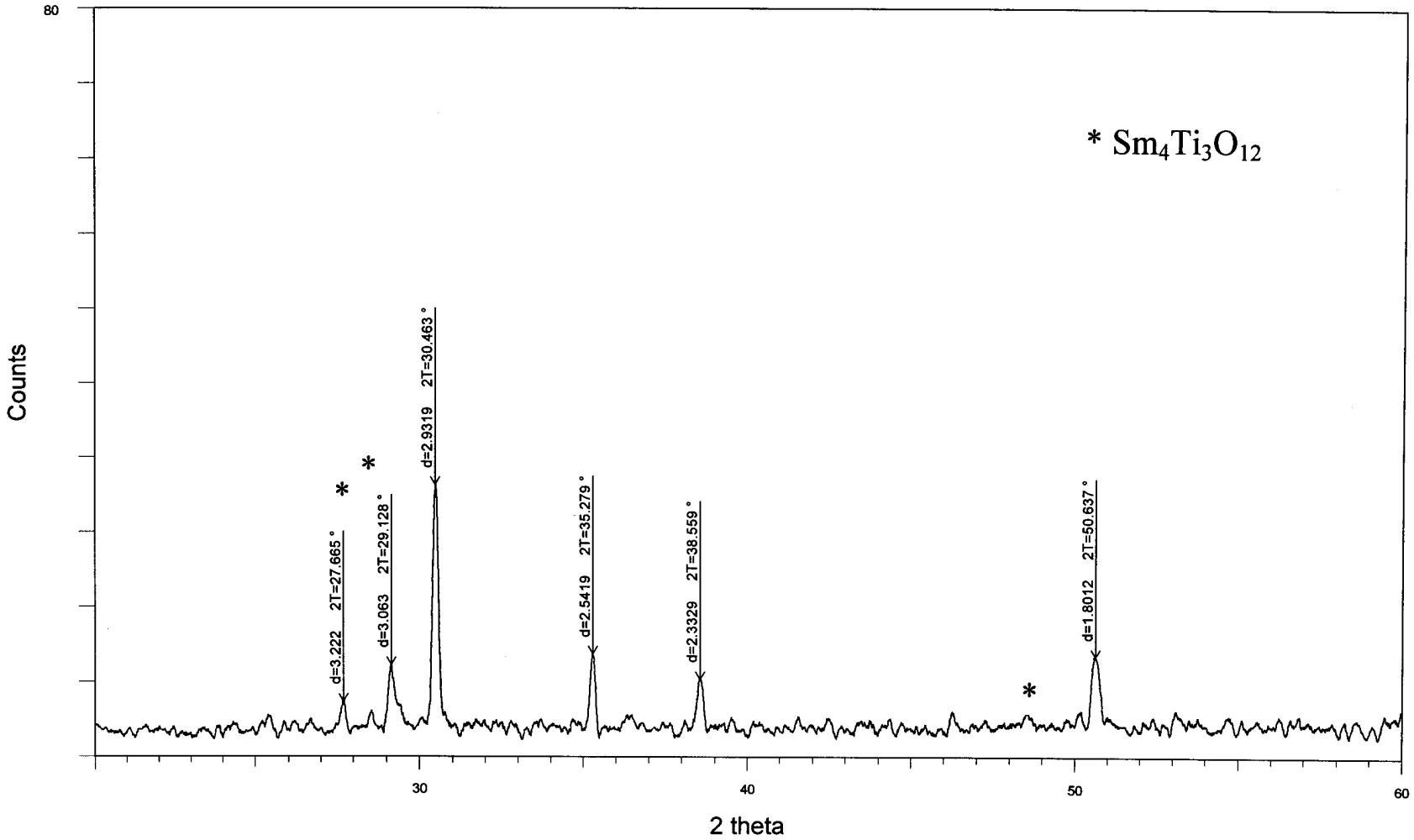


**Fig. 4.7. XRD spectrum of samarium titanate prepared by SHS reaction between oxides of Sm and Ti in presence of urea as activator**

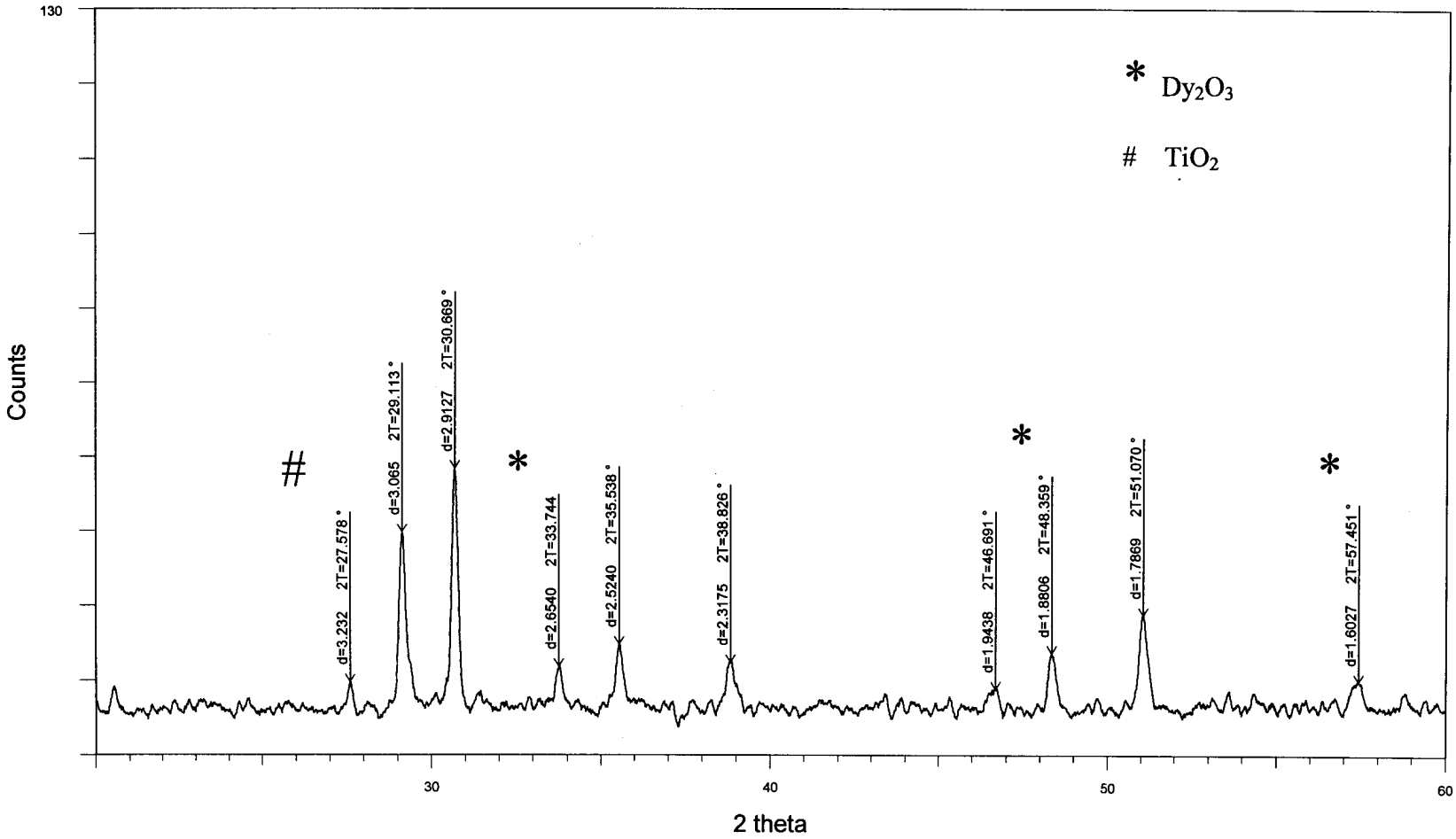


**Fig. 4.8. XRD spectrum of Dysprosium titanate prepared by SHS reaction between oxides of Dy and Ti in presence of urea as activator**

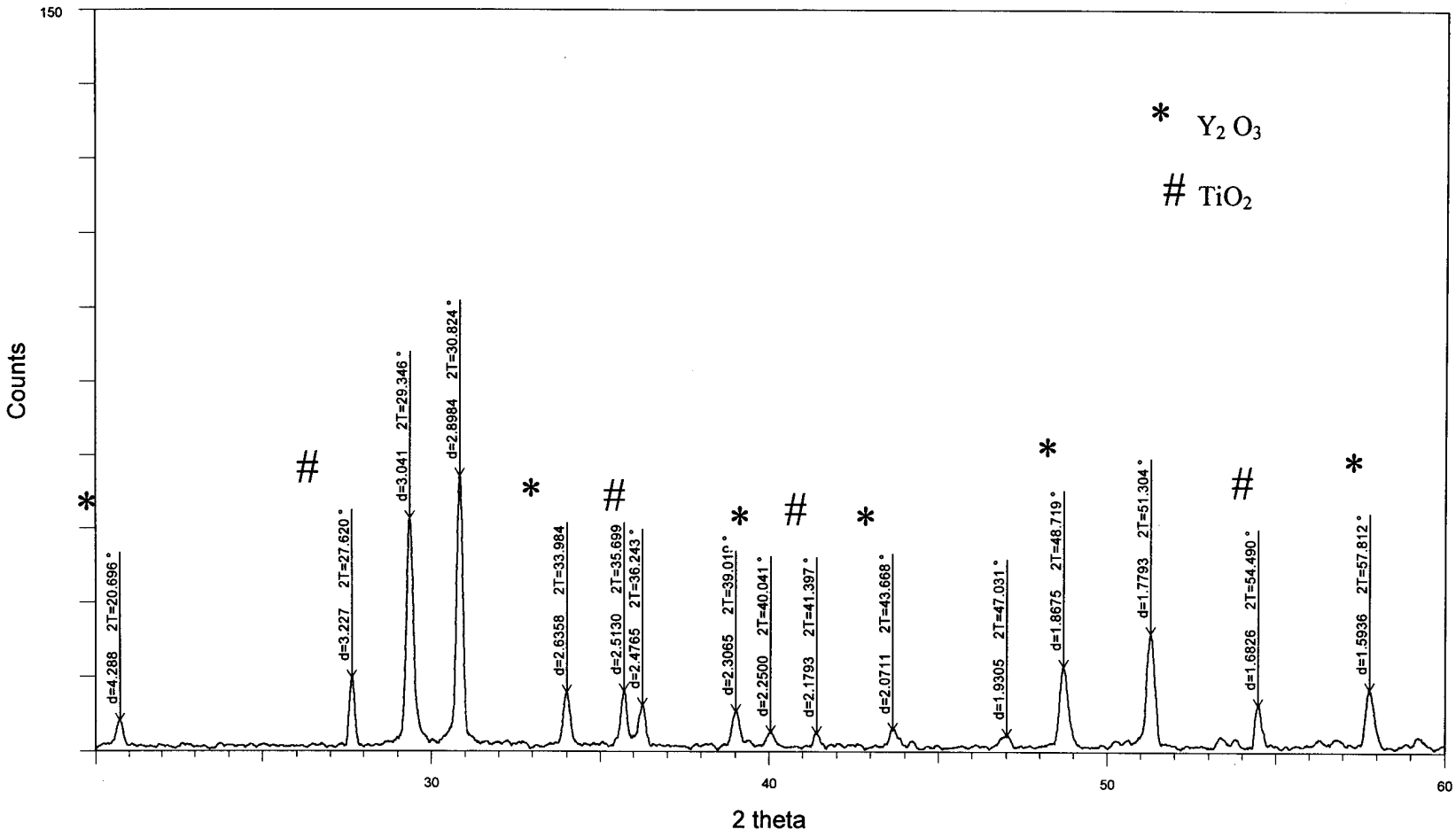


**Fig. 4.9. XRD of Yttrium titanate prepared by SHS reaction between oxides of Y and Ti in presence of urea as activator**

## SECTION 3

# SYNTHESIS OF RARE EARTH TITANATES $RE_2Ti_2O_7$ FROM RARE EARTH NITRATES, $RE(NO_3)_3$ AND $TiO_2$ BY SHS METHOD USING UREA AS THE ACTIVATOR AND THEIR CHARACTERISATION

## EXPERIMENTAL

Rare earth oxides are generally more stable and less reactive compared to their salts such as nitrates, halides, etc. Therefore, rare earth nitrates were employed for the synthesis of phase pure titanates. The rare earth oxides: $La_2O_3$, $Pr_6O_{11}$, $Nd_2O_3$, $Sm_2O_3$, $Gd_2O_3$, $Dy_2O_3$ and $Y_2O_3$ were converted to rare earth nitrates as follows. The rare earth oxide (0.02 mol) was dissolved in hot 1:1 $HNO_3$. The solution was slowly heated on a boiling water bath to remove the excess acid, if any, and evaporated to get the dry rare earth nitrate. To this $TiO_2$ (3.1952 g, 0.04 mol) and urea (4.60 g, 0.16 mol) were added and heated on an electric Bunsen and the contents in the beaker were thoroughly mixed by stirring. As the temperature increases urea melts and starts decomposing with the evolution of ammonia. When the temperature reaches ~350 $^0$C copious brown fumes of oxides of nitrogen start evolving. At this stage a spontaneous incandescent reaction takes place vigorously with bright flame along with evolution of large amounts of gases. The content of the vessel froaths up to a highly porous network of foam like structure, which almost fills the reaction vessel and gradually the flame subsides. The highly porous product formed was cooled to room temperature and characterized by various physico-chemical techniques.

## RESULTS AND DISCUSSION

During the SHS reaction, initially the organic fuel, namely urea do not get dispersed readily with the crystalline rare earth nitrates. However, on

heating the reactants, urea starts melting and allow dispersion of the rare earth nitrates and titanium dioxide. It requires constant stirring of the thick slurry of the reactants even at higher temperatures to get a homogenous dispersion of the nitrate and $TiO_2$ to ensure good SHS reaction. If the dispersion is not proper the SHS reaction was found to take place at different locations in the vessel at slightly different intervals; as if intermittent reactions are taking place instead of a complete reaction. This generally affects the overall efficiency of the SHS reaction to yield phase pure $RE_2Ti_2O_7$. Thorough mixing of the reactants during the reaction is necessary for the formation of phase pure product.

**Elemental analysis**

The titanium and rare earth percentages of the rare earth titanates analyzed by XRF are given in table 4.5. The data conform to the composition of $RE_2Ti_2O_7$ of all the samples prepared

**Table 4.5. Elemental analysis data of $RE_2Ti_2O_7$**

| $RE_2Ti_2O_7$ where RE= | % RE | | % Ti | |
|---|---|---|---|---|
| | Found for the product | Calculated | Found for the product | Calculated |
| La | 57.135 | 57.21 | 19.685 | 19.73 |
| Pr | 57.498 | 57.56 | 19.549 | 19.57 |
| Nd | 58.058 | 58.13 | 19.297 | 19.30 |
| Sm | 58.987 | 59.13 | 18.785 | 18.84 |
| Gd | 60.198 | 60.21 | 18.296 | 18.34 |
| Dy | 60.596 | 61.00 | 17.884 | 17.98 |
| Y | 45.981 | 46.11 | 24.789 | 24.84 |

**XRD Data**

The XRD spectra of the SHS powders obtained in the as such form and also after calcination at different temperatures from 600 $^0$C and 1200 $^0$C were recorded. The XRD of as such SHS powder showed the amorphous or microcrystalline nature of the products. However the crystallinity gradually improves on calcination at different temperatures and at 1200 $^0$C, transformed to 100 per cent phase pure crystalline material. The XRD spectra of all the compounds calcined at 1200 $^0$C are given in figures 4.10 to 4.16. The peaks in the spectra of $RE_2Ti_2O_7$, where RE = La, Pr and Nd match exactly with the peaks of the standard monoclinic $RE_2Ti_2O_7$; whereas the spectra of Sm, Gd, Dy and Y agree well with standard cubic $RE_2Ti_2O_7$.

Since 100% phase pure $RE_2Ti_2O_7$ were obtained by the method presented in section 4, further physico-chemical studies of the rare earth titanate considered in this section were not carried out.

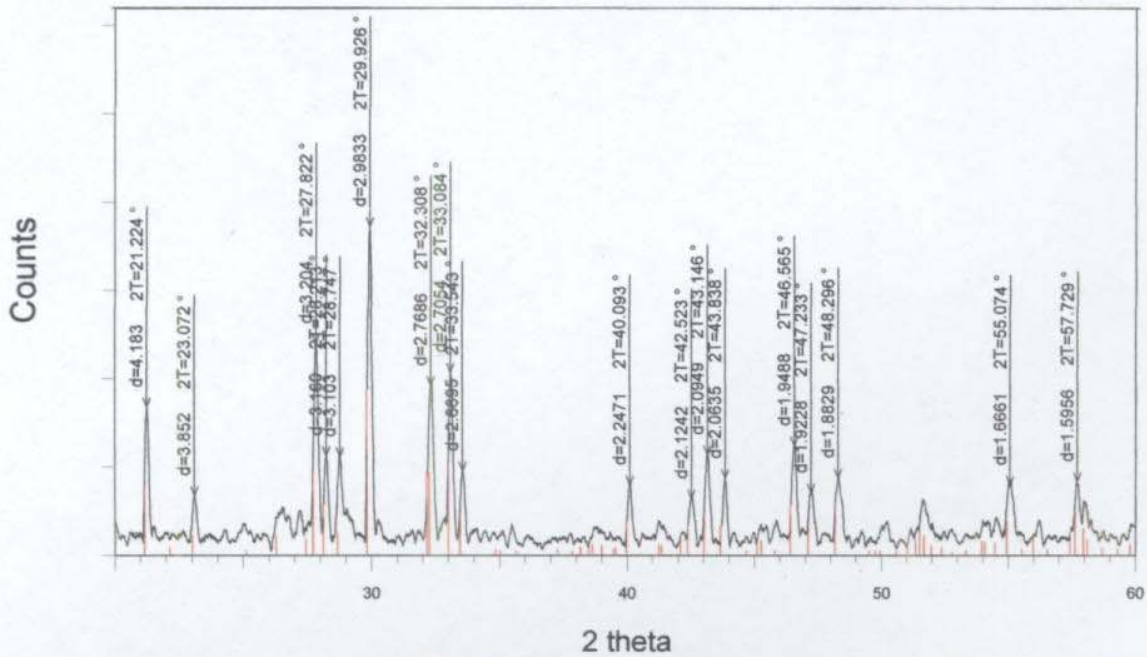


**Fig. 4.10. XRD spectrum of $La_2Ti_2O_7$ synthesized by SHS-urea method and calcined at 1200 $^0$C (Match ICDD 28-0517 monoclinic $La_2Ti_2O_7$)**

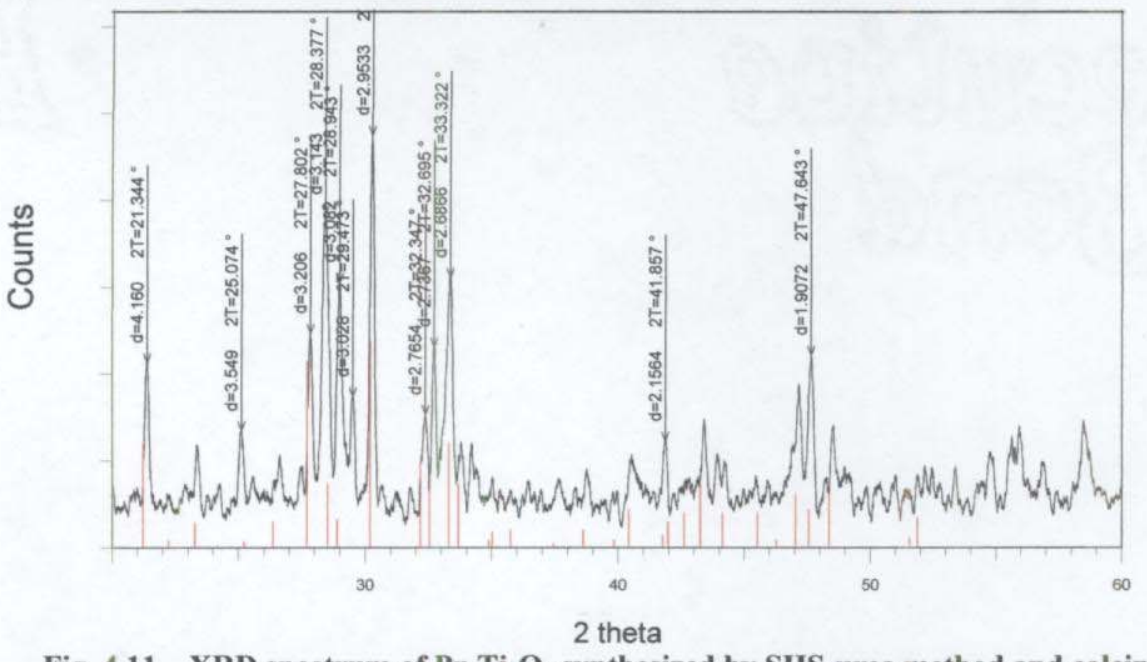


**Fig. 4.11. XRD spectrum of $Pr_2Ti_2O_7$ synthesized by SHS-urea method and calcined at 1200 $^0$C (Match ICDD 35-0267 monoclinic $Pr_2Ti_2O_7$)**

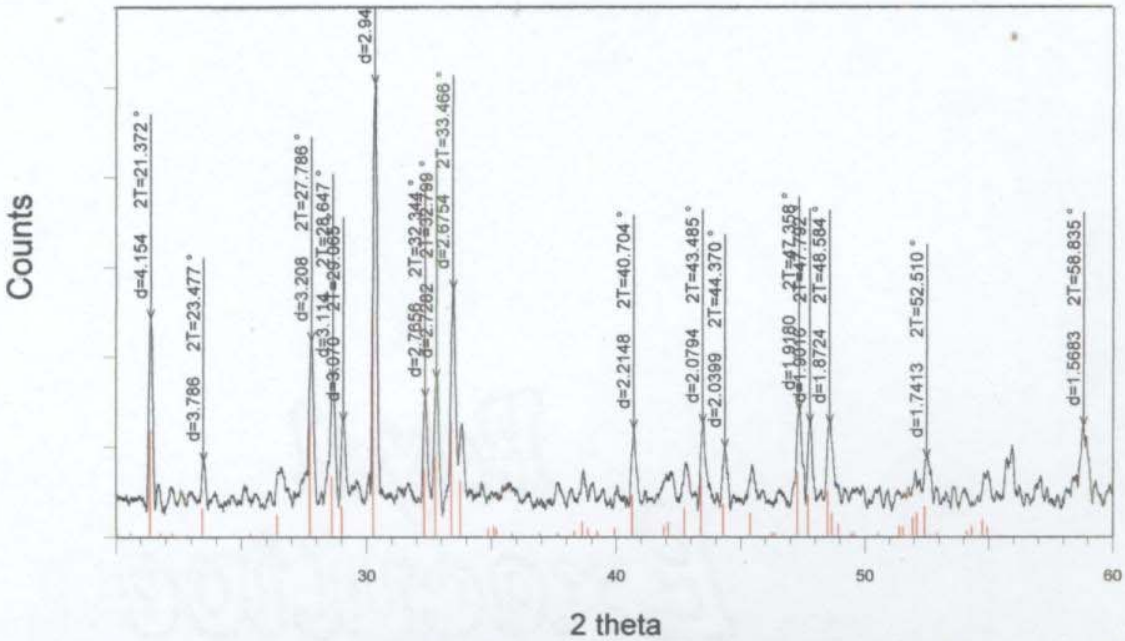


**Fig. 4.12. XRD spectrum of $Nd_2Ti_2O_7$ synthesized by SHS-urea method and calcined at 1200 $^0$C (Match ICDD 33-0942 monoclinic $Nd_2Ti_2O_7$)**

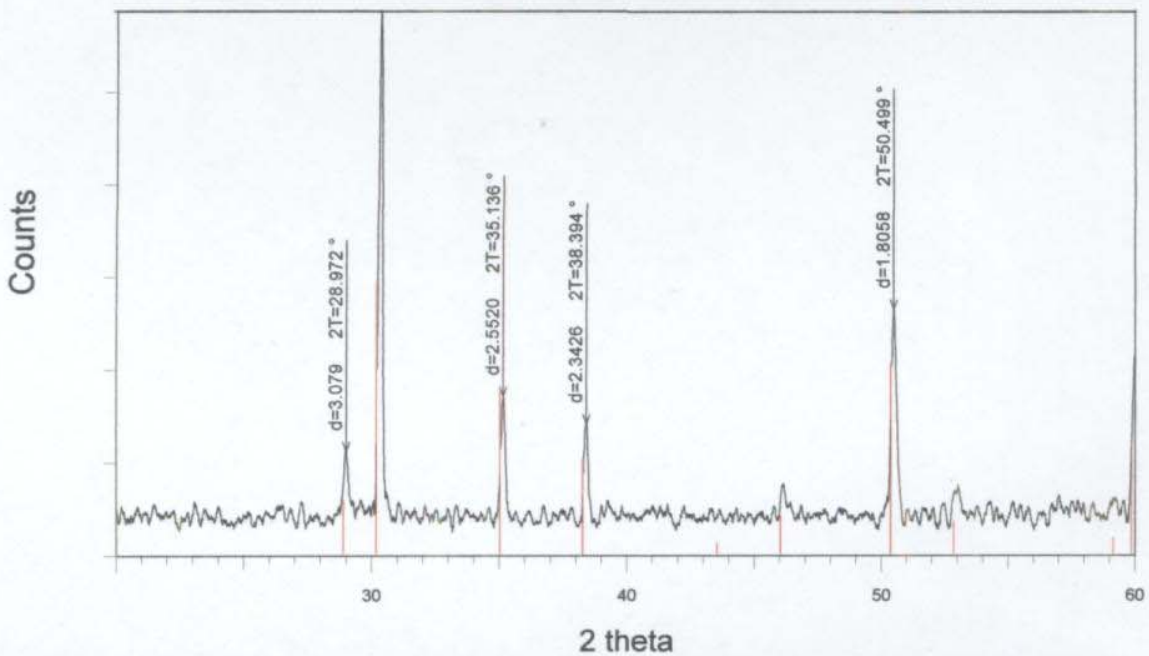


**Fig. 4.13. XRD spectrum of $Sm_2Ti_2O_7$ synthesized by SHS-urea method and calcined at 1200 $^0$C (Match ICDD 16-400 cubic $Sm_2Ti_2O_7$)**

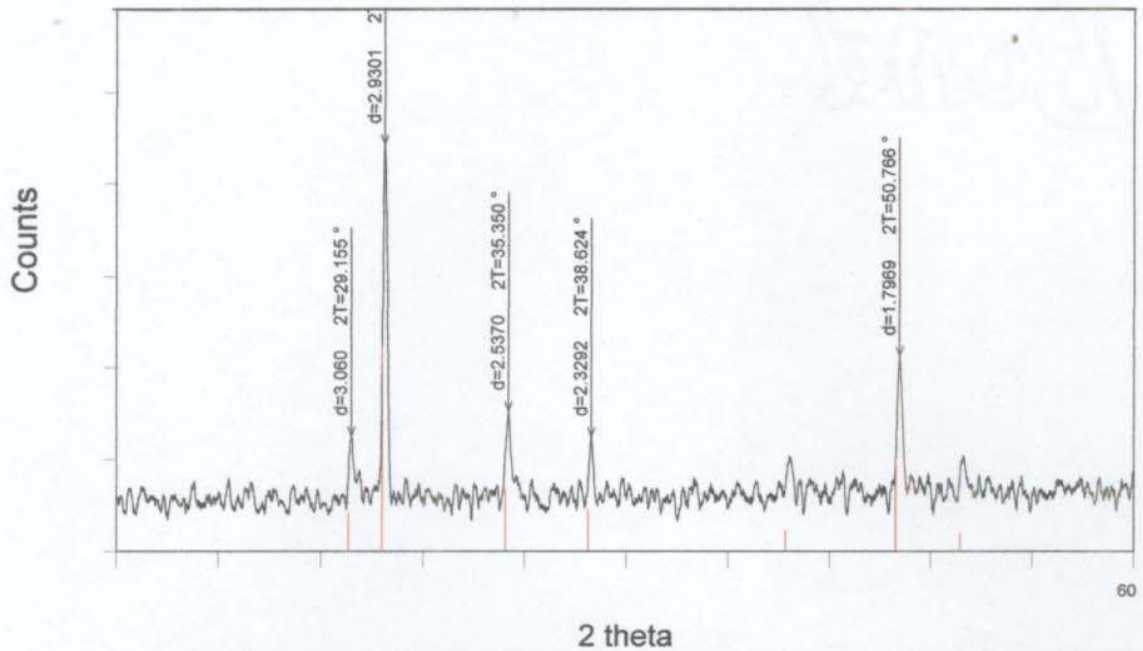


**Fig. 4.14. XRD spectrum of $Gd_2Ti_2O_7$ synthesized by SHS-urea method and calcined at 1200 $^0$C (Match ICDD 23-0259 cubic $Gd_2Ti_2O_7$)**

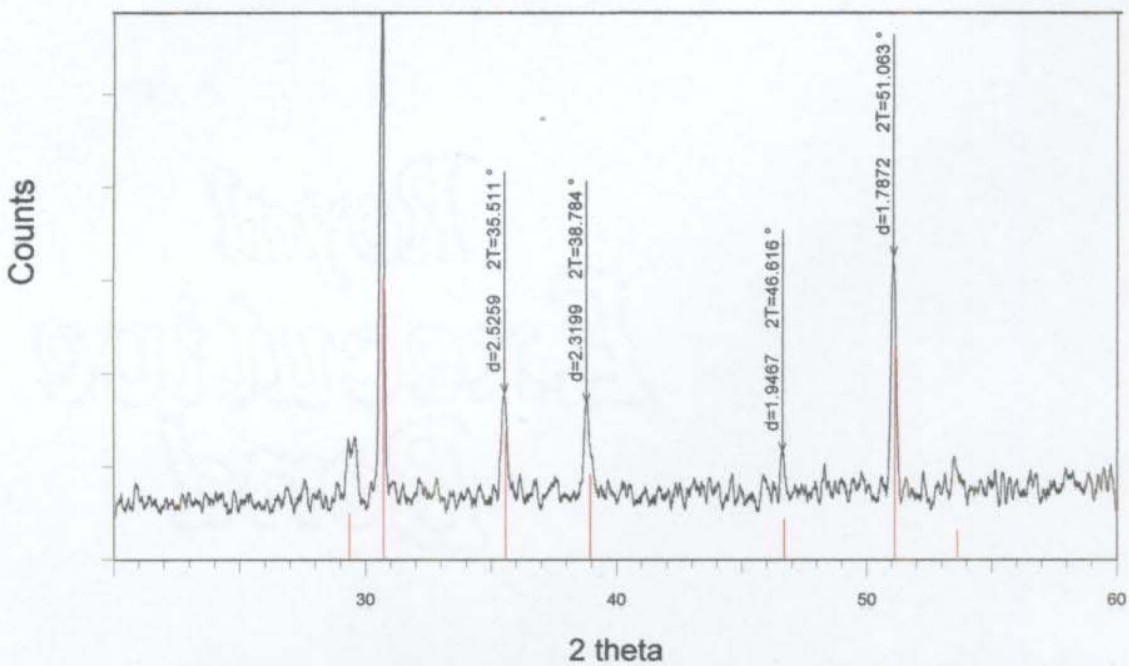


**Fig. 4.15. XRD spectrum of $Dy_2Ti_2O_7$ synthesized by SHS-urea method and calcined at 1200 $^0$C (Match ICDD 17-0453 cubic $Dy_2Ti_2O_7$)**

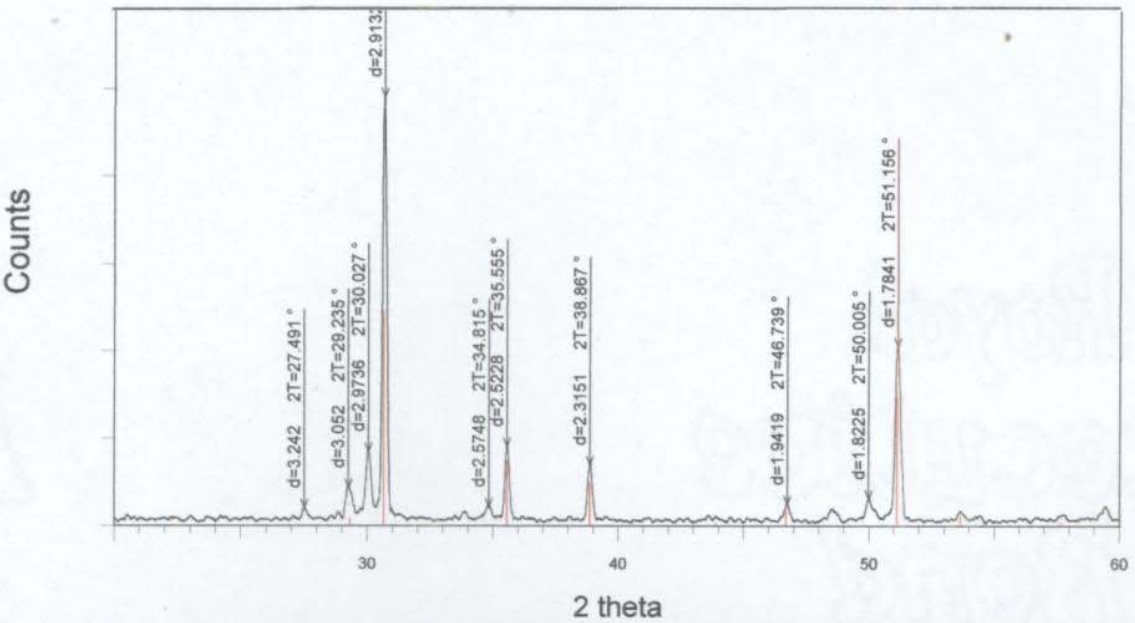


**Fig. 4.16. XRD spectrum of $Y_2Ti_2O_7$ synthesized by SHS-urea method and calcined at 1200 $^0$C (Match ICDD 42-0413 cubic $Y_2Ti_2O_7$)**

## SECTION 4

# SYNTHESIS OF RARE EARTH TITANATES FROM RARE EARTH NITRATES, $RE(NO_3)_3$ AND $TiO_2$ BY SHS METHOD USING AMMONIUM ACETATE AS THE ACTIVATOR AND THEIR CHARACTERISATION

Phase pure crystalline $RE_2Ti_2O_7$ can be prepared by SHS reaction between $RE(NO_3)_3$ and $TiO_2$ in presence of urea as discussed in **section 3**; however a more efficient and convenient SHS method for the preparation of phase pure $RE_2Ti_2O_7$ has been developed in the investigation by employing ammonium acetate instead of urea in the SHS reaction activator. Experimental details and characteristics of the product are discussed in this section.

## EXPERIMENTAL

Rare earth nitrates, $RE(NO_3)_3$, were prepared from $RE_2O_3$ as described in **section 3**. The rare earth nitrates of La, Pr, Nd, Sm, Gd, Dy and Y were used in the SHS reaction. The procedural details are given below. Rare earth nitrates (0.04 mol) and the 'inorganic fuel' namely ammonium acetate (0.20 mol) were dissolved in water (~100ml) to get a clear solution. To this 0.04 mol of $TiO_2$ was added and vigorously stirred to keep the fine particles of $TiO_2$ in suspension. The mixture was evaporated slowly on a boiling water bath to remove the water content. The dry product was then heated on an electric Bunsen. As the temperature was gradually increased, initially small amounts of fumes were liberated from the reactants, at ~350 $^0$C brown fumes start evolving from the mixture and an incandescent reaction set in with smoke and flame in the vessel with a bright glow. Due to the evolution of large amounts of gases, the mixture froths almost filling the vessel with foam like porous network of particles of the products formed. Appearance of the

reactions at different stages of a typical experiment are shown in the photograph given in figure 4-17.

The SHS powder synthesized in this technique is very fluffy in nature. At the peak of the SHS reaction, the products being very light and fine it starts flying fast out of the reaction vessel; the tendency for flying out is accelerated by the liberation of hot gases at this stage. It requires a typical set up to be attached at the mouth of the reaction vessel to collect the flying off particles also, which leaves the vessel like burning of 'fireworks flower pots'. A conical shaped wide collector was placed at the mouth of the reaction vessel and collected the flying particles.

## RESULTS AND DISCUSSION

In the case of inorganic fuel (ammonium acetate) activated SHS reactions better homogeneity of the reactants has been ensured at the beginning stage of the reaction. In this method the rare earth nitrates and ammonium acetate were dissolved in water to form a clear solution. The titanium dioxide added to this solution gets totally dispersed in the solution uniformly wetted by the other reagents. This homogenous dispersion of reactants has greatly influenced the SHS reaction to perform efficiently to produce phase pure $RE_2Ti_2O_7$ compared to the product formed in the SHS reaction activated by the organic fuel, urea.

### Elemental analysis

The titanium and rare earth percentages of the rare earth titanates analyzed by XRF are given in table 4.6. The data conform to the composition of $RE_2Ti_2O_7$ of all the samples prepared.

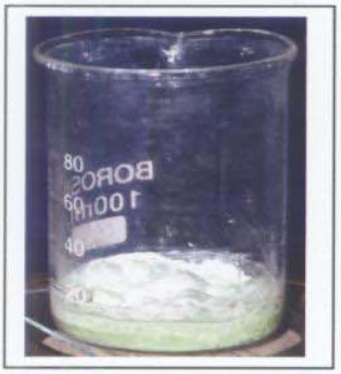

REACTANTS

DIFFERENT STAGES OF REACTION

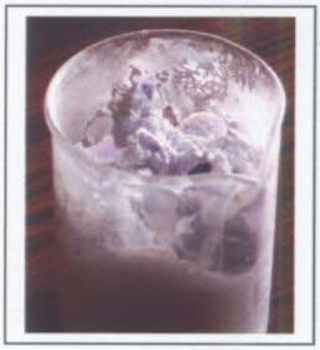

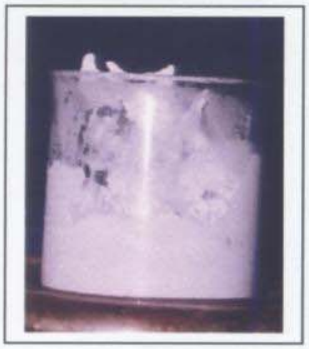

PRODUCT
(APS ~ 50to 70 nm)

Fig. 4.17 APPEARANCE OF THE SHS REACTION AT DIFFERENT STAGES

**Table 4.6. Elemental Percentage of $RE_2Ti_2O_7$**

| $RE_2Ti_2O_7$ where RE= | % RE | | % Ti | |
|---|---|---|---|---|
| | Found for the product | Calculated | Found for the product | Calculated |
| La | 57.135 | 57.21 | 19.685 | 19.73 |
| Pr | 57.498 | 57.56 | 19.549 | 19.57 |
| Nd | 58.058 | 58.13 | 19.297 | 19.30 |
| Sm | 58.987 | 59.13 | 18.785 | 18.84 |
| Gd | 60.198 | 60.21 | 18.296 | 18.34 |
| Dy | 60.596 | 61.00 | 17.884 | 17.98 |
| Y | 45.981 | 46.11 | 24.789 | 24.84 |

The characteristics of the nanosized SHS powders of different compounds, which were synthesized by SHS-ammonium acetate (AA) method, were studied by various physico-chemical methods. For the SHS powder the physical characteristics like BET surface area and the average particle size, the SEM micro structural studies, thermal properties such as TG, DTG and DTA, XRD spectra etc. were studied. After calcining the SHS powders at different temperatures (600 $^0$C to 1200 $^0$C) the XRD spectra, FT IR and Laser Raman spectra were also taken. For the discs sintered at different sintering temperatures from 1375 $^0$C to 1575 $^0$C, the dielectric properties, and its variation with frequencies (from 100 Hz to 10 MHz) and temperatures (from 20 $^0$C to 120 $^0$C); optical properties such as fluorescence, absorbance and photoacoustic were studied. These studies showed that La, Pr and Nd formed monoclinic $RE_2Ti_2O_7$ and Sm, Gd, Dy and Y formed cubic structure. Therefore details on structural characterisation and properties are discussed separately as two subsections.

## SECTION - 4A

## MONOCLINIC $RE_2Ti_2O_7$

### TG-DTA analysis

The thermograms and DTA curves of the three rare earth titanates are given in figures 4.18 to 4.23. The weight loss/gain at different temperatures are presented in table 4.7. The data show that the weight loss in the case of $La_2Ti_2O_7$ and $Nd_2Ti_2O_7$ upto a temperature of ~750 $^0$C is ~10 % and slight increase in weight above 750 $^0$C (However, in the case of $Pr_2Ti_2O_7$, a weight loss of 3.73 % at ~450 $^0$C and only 12.7 % upto ~1400 $^0$C)

**Table 4.7. TG data of the SHS powders of Monoclinic $RE_2Ti_2O_7$[RE=La ,Pr ,Nd]**

| $RE_2Ti_2O_7$ | Atmosphere | Weight Loss (%) | Temp. ($^0$C) | Weight Gain (%) | Temp. ($^0$C) |
|---|---|---|---|---|---|
| $La_2Ti_2O_7$ | Nitrogen | 10.5 | 750 | 1.4 | 1326 |
| $Pr_2Ti_2O_7$ | Oxygen | 12.7 | 1414 | ----- | ----- |
| $Nd_2Ti_2O_7$ | Nitrogen | 8.1 | 760 | 10.0 | 1411 |

The DTA data of all the SHS powder (table 4.8) indicate two distinct regions in the curve correspond to exothermic and endothermic changes. The exothermic maxima are in the range 555 $^0$C to 675 $^0$C and the endothermic behavior between 1043 $^0$C to 1220 $^0$C. The peak heights (table 4.8) in the exothermic region were lower compared to the endothermic region.

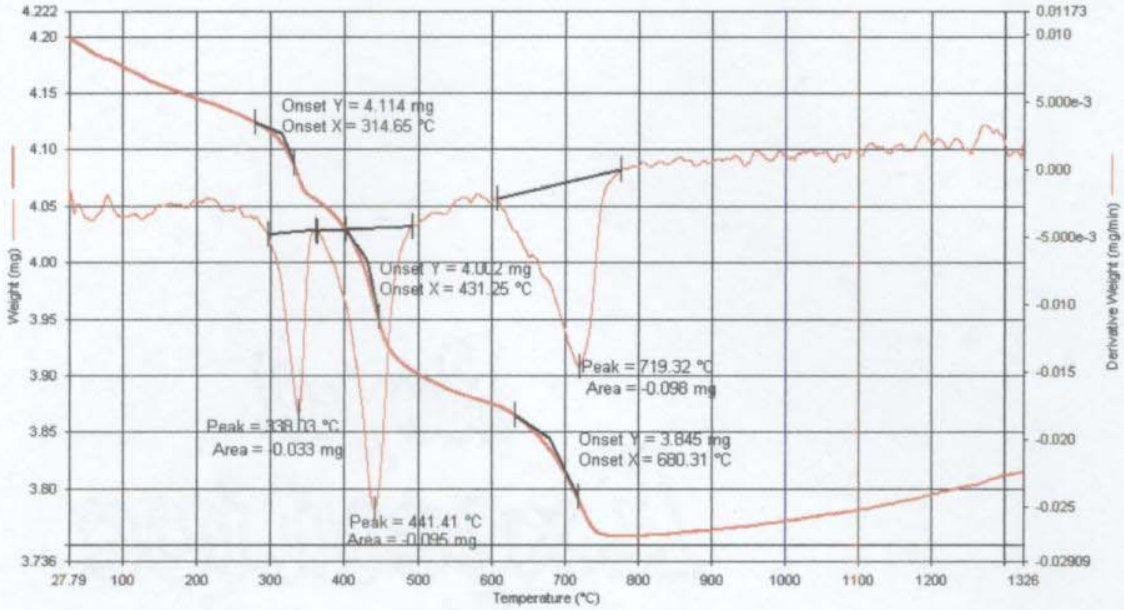


**Fig. 4.18. TG-DTG (Nitrogen atm.) of $La_2Ti_2O_7$ synthesized by SHS-AA method**

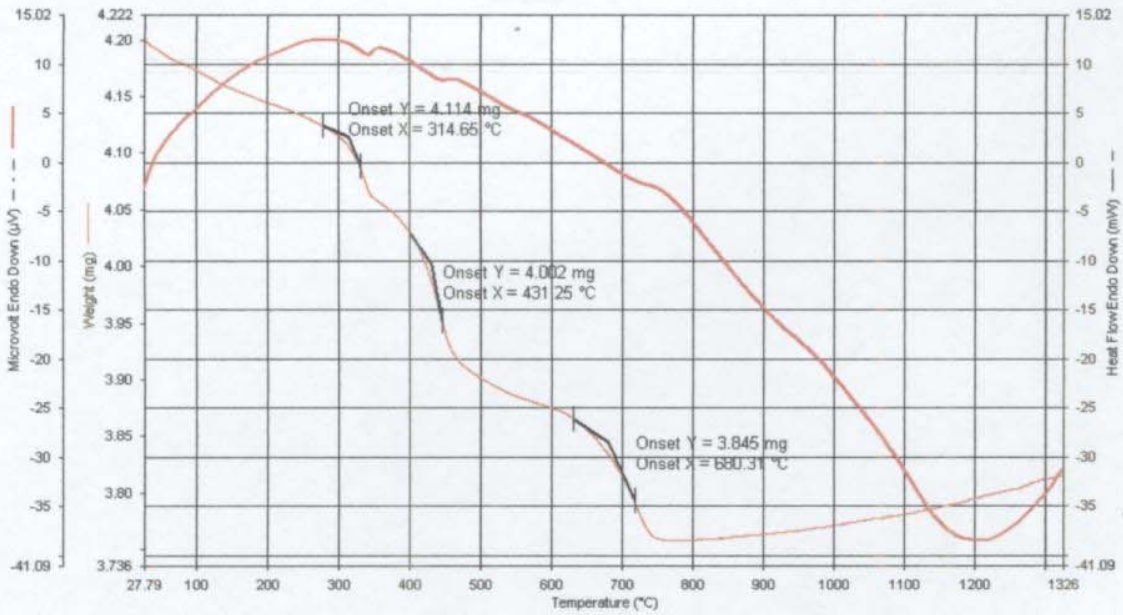


**Fig. 4.19. TG-DTA (Nitrogen atm.) of $La_2Ti_2O_7$ synthesized by SHS-AA method**

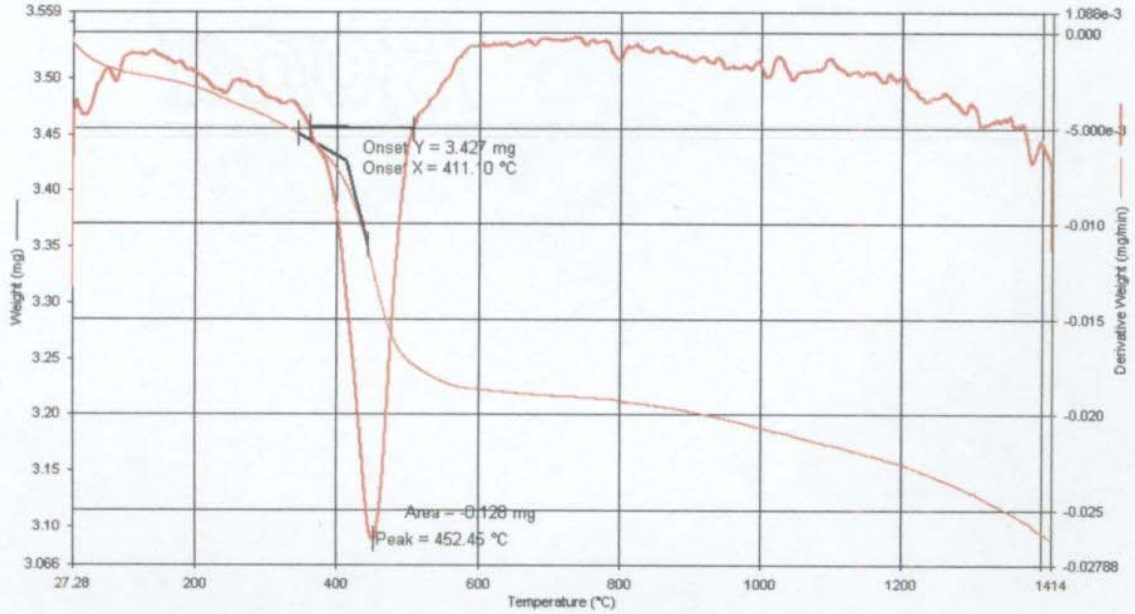


**Fig. 4.20. TG-DTG (Oxygen atm.) of $Pr_2Ti_2O_7$ synthesized by SHS-AA method**

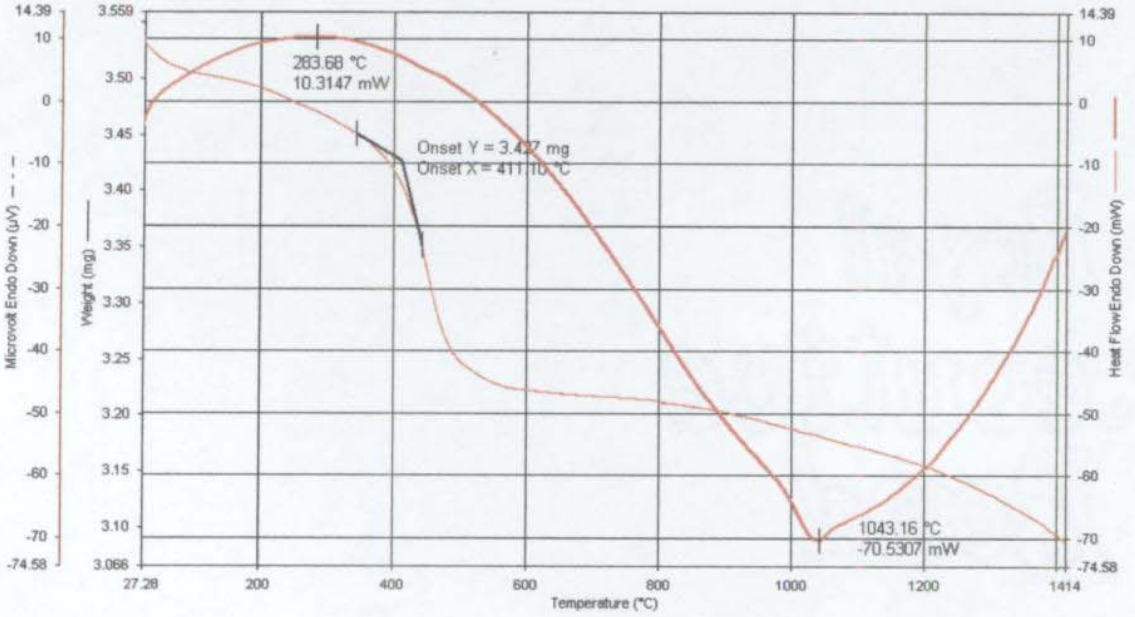


**Fig. 4.21. TG-DTA (Oxygen atm.) of $Pr_2Ti_2O_7$ synthesized by SHS-AA method**

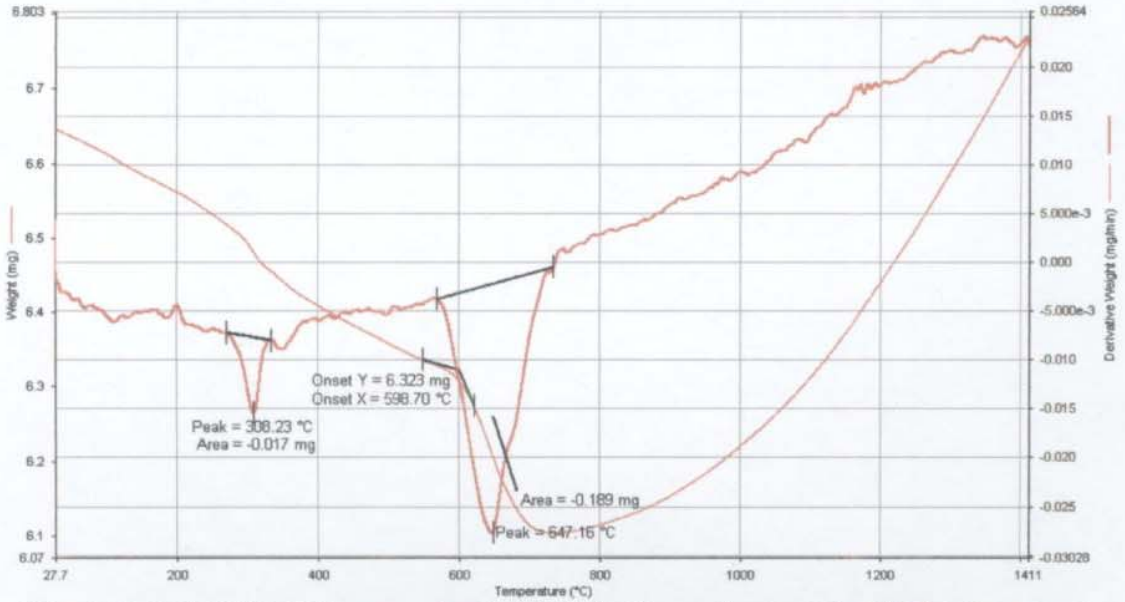


**Fig. 4.22. TG-DTG (Nitrogen atm.) of $Nd_2Ti_2O_7$ synthesized by SHS-AA method**

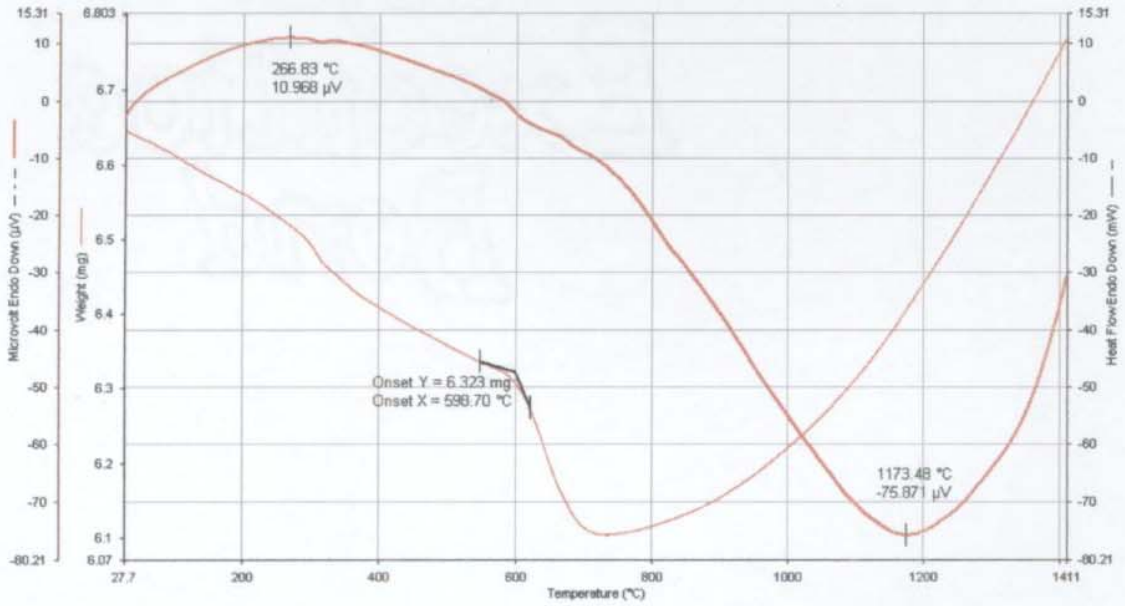


**Fig. 4.23. TG-DTA (Nitrogen atm.) of $Nd_2Ti_2O_7$ synthesized by SHS-AA method**

**Table 4.8. DTA data of the SHS powders of Monoclinic $RE_2Ti_2O_7$ [RE=La, Pr, Nd]**

| $RE_2Ti_2O_7$ (atmosphere) | Temp maxima | | Peak Values of reaction | | | |
|---|---|---|---|---|---|---|
| | | | Exothermic | | Endothermic | |
| | Exothermic ($^0$C) | Endothermic ($^0$C) | Value ($\mu$V) | Temp. ($^0$C) | Value ($\mu$V) | Temp. ($^0$C) |
| $La_2Ti_2O_7$ ($N_2$) | 675 | 1326 | 12.600 | 275.00 | -38.50 | 1220.0 |
| $Pr_2Ti_2O_7$ ($O_2$) | 555 | 1414 | 10.315 | 283.68 | -70.53 | 1043.2 |
| $Nd_2Ti_2O_7$ ($N_2$) | 580 | 1411 | 10.968 | 266.83 | -75.87 | 1173.0 |

The TG and DTA data indicates that characteristic transition takes place in the SHS material at higher temperatures and become phase pure at 1200 $^0$C. This has also been evident from the XRD patterns of the samples obtained at higher temperatures. The XRD patterns of all the three compounds obtained after calcination at 1200 $^0$C matches well with standard monoclinic rare earth titanates.

## XRD CRYSTAL STRUCTURE STUDIES

The XRD spectra of the three monoclinic rare earth titanates obtained by the SHS method and also calcined at 600 $^0$, 800 $^0$, 1000 $^0$ and 1200 $^0$C are given in figures 4.24 to 4.26. The XRD data can conveniently be explained by considering the three rare earth titanates separately.

**(a) XRD of Lanthanum titanate, $La_2Ti_2O_7$ :** XRD pattern of the SHS powder of $La_2Ti_2O_7$ shows the material is microcrystalline in nature. Upon calcining at higher temperatures, the material improves its crystallinity and becomes phase pure monoclinic structure of lanthanum titanate, $La_2Ti_2O_7$ (ICDD: 28-517).

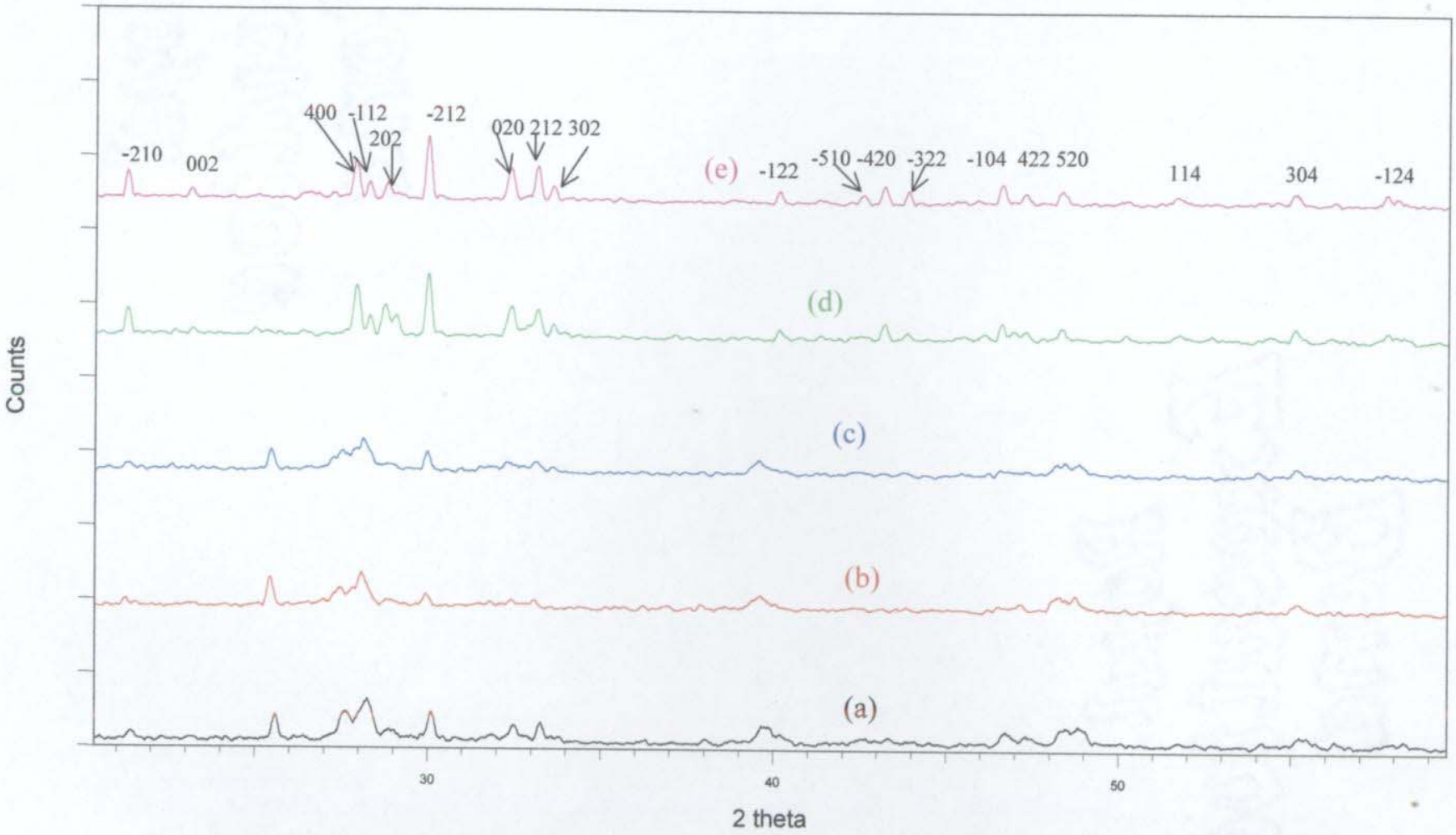


**Fig. 4.24. XRD patterns of $La_2Ti_2O_7$ (a) SHS powder-before calcination and calcined at (b) 600 $^0$C (c) 800 $^0$C (d) 1000 $^0$C and at (e) 1200 $^0$C (Match ICDD 28-0517 monoclinic $La_2Ti_2O_7$)**

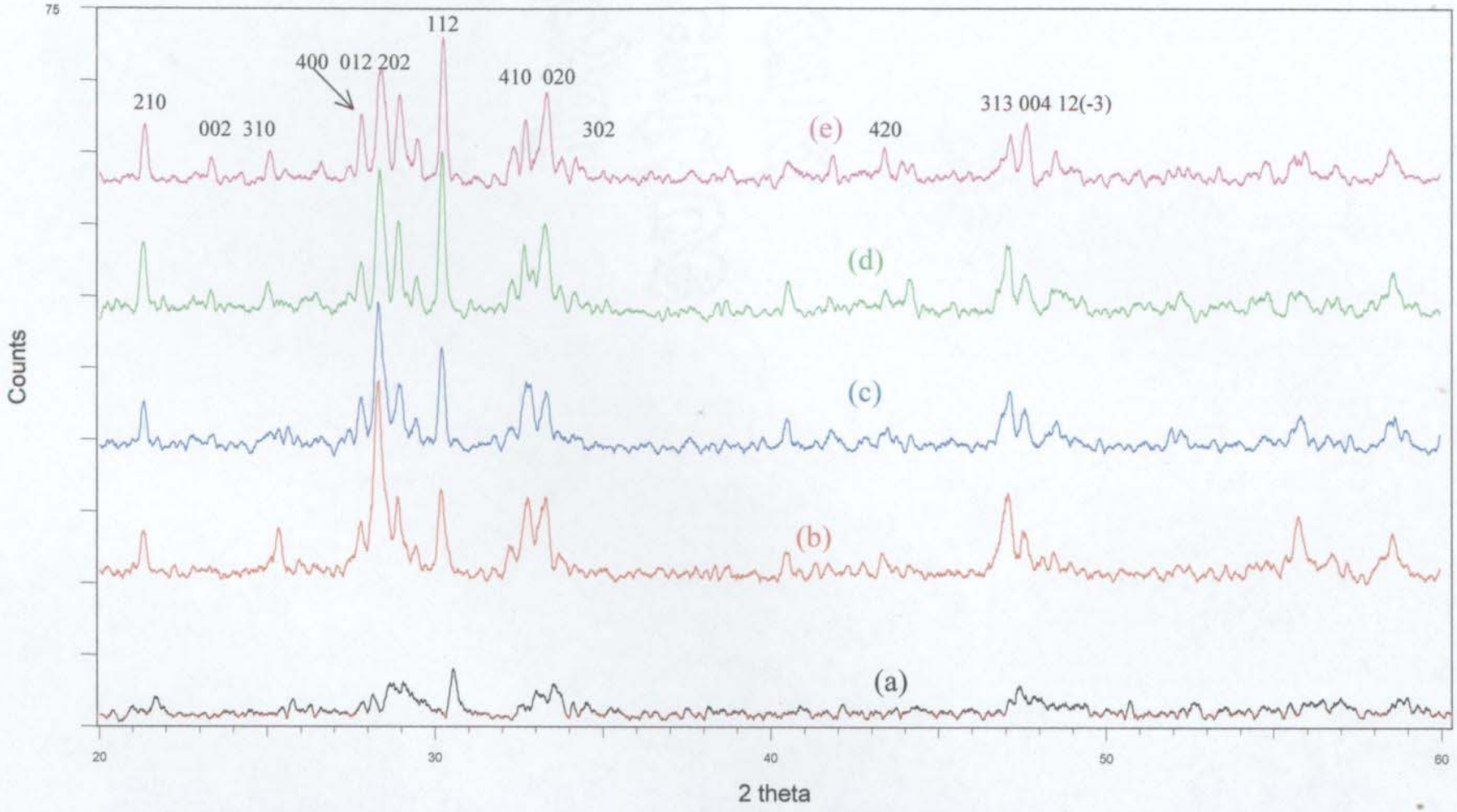


**Fig. 4.25. XRD patterns of $Pr_2Ti_2O_7$ (a) SHS powder-before calcination and calcined at (b) 600 $^0$C (c) 800 $^0$C (d) 1000 $^0$C and at (e) 1200 $^0$C (Match ICDD 35-0267 monoclinic $Pr_2Ti_2O_7$)**

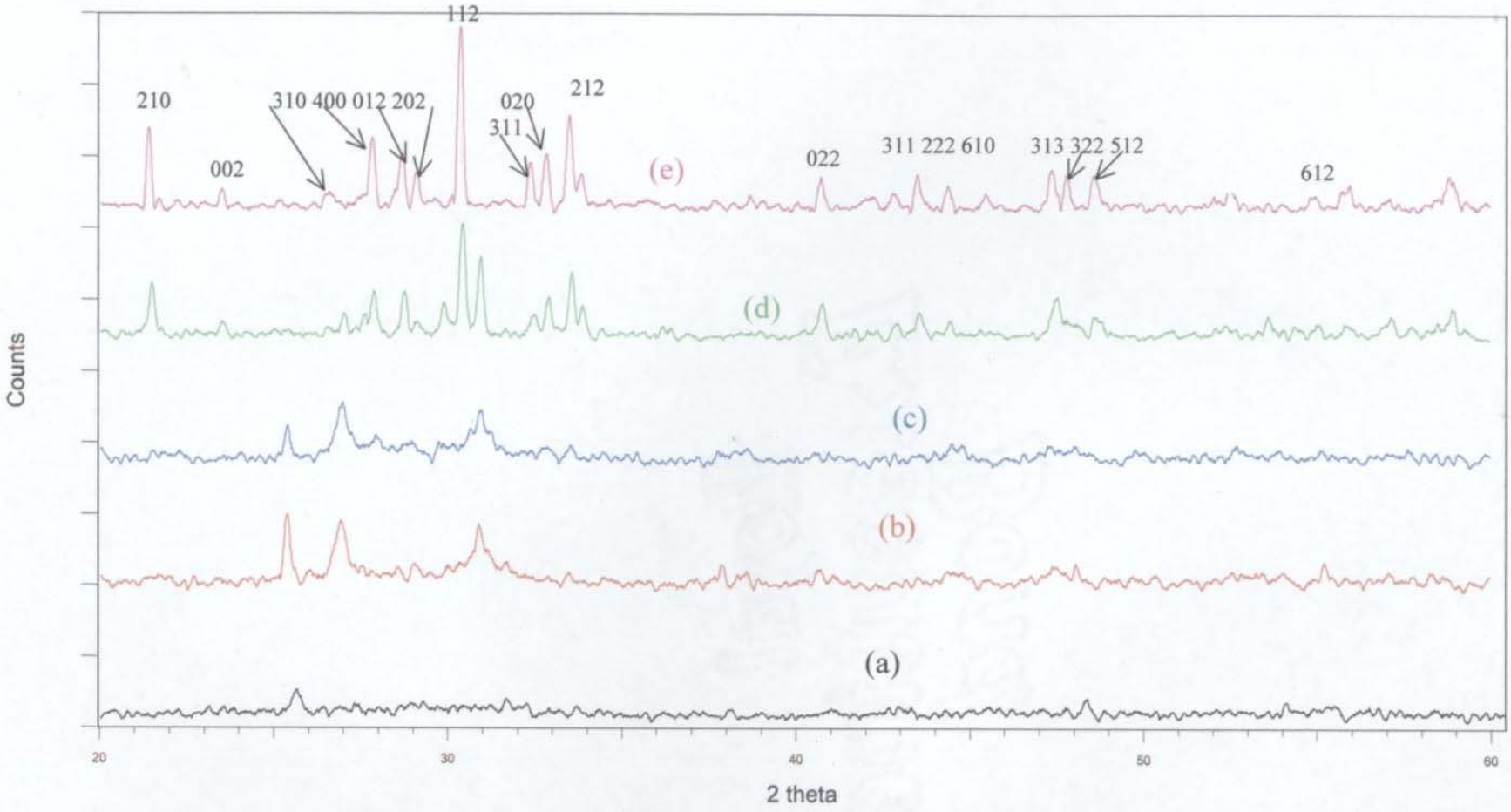


**Fig. 4.26. XRD patterns of $Nd_2Ti_2O_7$ (a) SHS powder-before calcination and calcined at (b) 600 $^0$C (c) 800 $^0$C (d) 1000 $^0$C and at (e) 1200 $^0$C (Match ICDD 33-0942 monoclinic $Nd_2Ti_2O_7$)**

**(b) XRD of Praseodymium titanate, $Pr_2Ti_2O_7$ :** The XRD of $Pr_2Ti_2O_7$ before calcination shows an amorphous/ microcrystalline nature with no characteristic peaks. However, the XRD spectrum recorded of samples calcined at temperatures 600 $^0$C, 800 $^0$C,1000 $^0$C and 1200 $^0$C showed the formation of well defined crystalline form above 1000 $^0$C. At 1200 $^0$C the powder becomes 100 % monoclinic structure (ICDD: 35-267).

**(c) XRD of Neodymium titanate, $Nd_2Ti_2O_7$ :** The XRD spectrum of $Nd_2Ti_2O_7$ obtained indicated that the material was amorphous/microcrystalline in nature. Upon calcining the powder acquire crystalline nature. The XRD spectrum of the sample calcined at 1200 $^0$C showed the presence of 100 % monoclinic structure of $Nd_2Ti_2O_7$ (ICDD: 33-492).

**FT IR and Raman spectral studies**

As the rare earth titanates are compound oxides of $RE_2O_3$ and $TiO_2$ their vibrational spectra due to the inter-atomic bonding will be largely dependent on the spectral behavior of both $RE_2O_3$ and $TiO_2$. It is well known that $TiO_2$ transforms from its anatase phase to the rutile phase on heating the material above 700$^0$C. The $TiO_2$ used in the present study was also heated to 1200 $^0$C along with the SHS powders and confirmed its formation of rutile, $TiO_2$ by taking XRD spectra of the resultant powder.

The characteristic peaks[243,244] for rutile, $TiO_2$, in the IR and Raman spectra are at positions as given in the table below.

| Raman mode | IR mode |
|---|---|
| $A_{1g}$ : 612 $cm^{-1}$($\nu_S$ Ti-O) | A2u<br>TO : 167 $cm^{-1}$<br>LO : 811 $cm^{-1}$ |
| B1g : 143 $cm^{-1}$ | Eu<br>TO : 500 $cm^{-1}$ |
| B2g : 826 $cm^{-1}$ | LO : 806 $cm^{-1}$<br>TO : 388 $cm^{-1}$ |
| Eg : 447 $cm^{-1}$ ($\nu$as Ti-O) | LO : 458 $cm^{-1}$<br>TO : 183 $cm^{-1}$<br>LO : 373 $cm^{-1}$ |

The oxides of rare earths, $RE_2O_3$ with the bixbyte structure are reported[244] to have the following spectral bands. Because of the complex nature of the unit cell of the $RE_2O_3$ structure no specific assignments of these bands were reported.

| $RE_2O_3$ | A | B | C | D | E | F | G | H | I |
|---|---|---|---|---|---|---|---|---|---|
| $Gd_2O_3$ | 535 | 440 | 391 | 355 | 318 | 302 | 280 | 130 | 124 |
| $Dy_2O_3$ | 550 | 460 | 410 | 372 | 328 | 315 | 291 | 132 | 125 |
| $Y_2O_3$ | 561 | 468 | 405 | 391 | 343 | --- | 312 | --- | 120 |

The FT-IR spectra recorded of the monoclinic $RE_2Ti_2O_7$ calcined at $1200^0$C in the region 400-1000 $cm^{-1}$ are given in fig. 4.27. A comparison of the reported spectral data of rutile, $TiO_2$ and the $RE_2O_3$ with the spectra of the rare earth titanates revealed that significant differences exist in the spectra of $RE_2Ti_2O_7$ in terms of the number and positions of the vibrations. Several new vibrations appeared in the spectra of $RE_2Ti_2O_7$ and bands due to various Ti-O and RE-O vibrations changed appreciably.

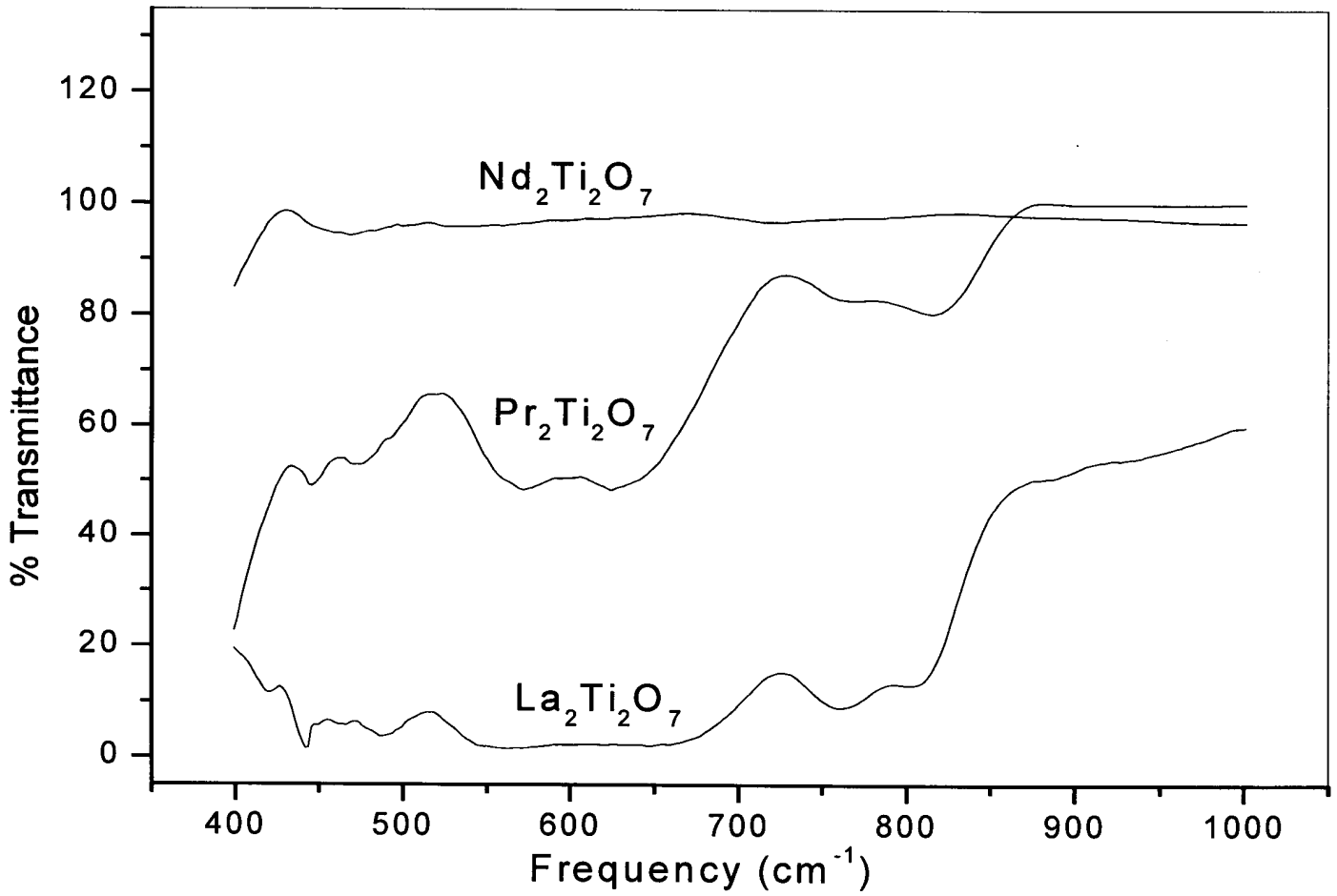


**Fig. 4.27. FTIR spectra of monoclinic $RE_2Ti_2O_7$ synthesized by SHS method and calcined at 1200°C (400-1000 $cm^{-1}$)**

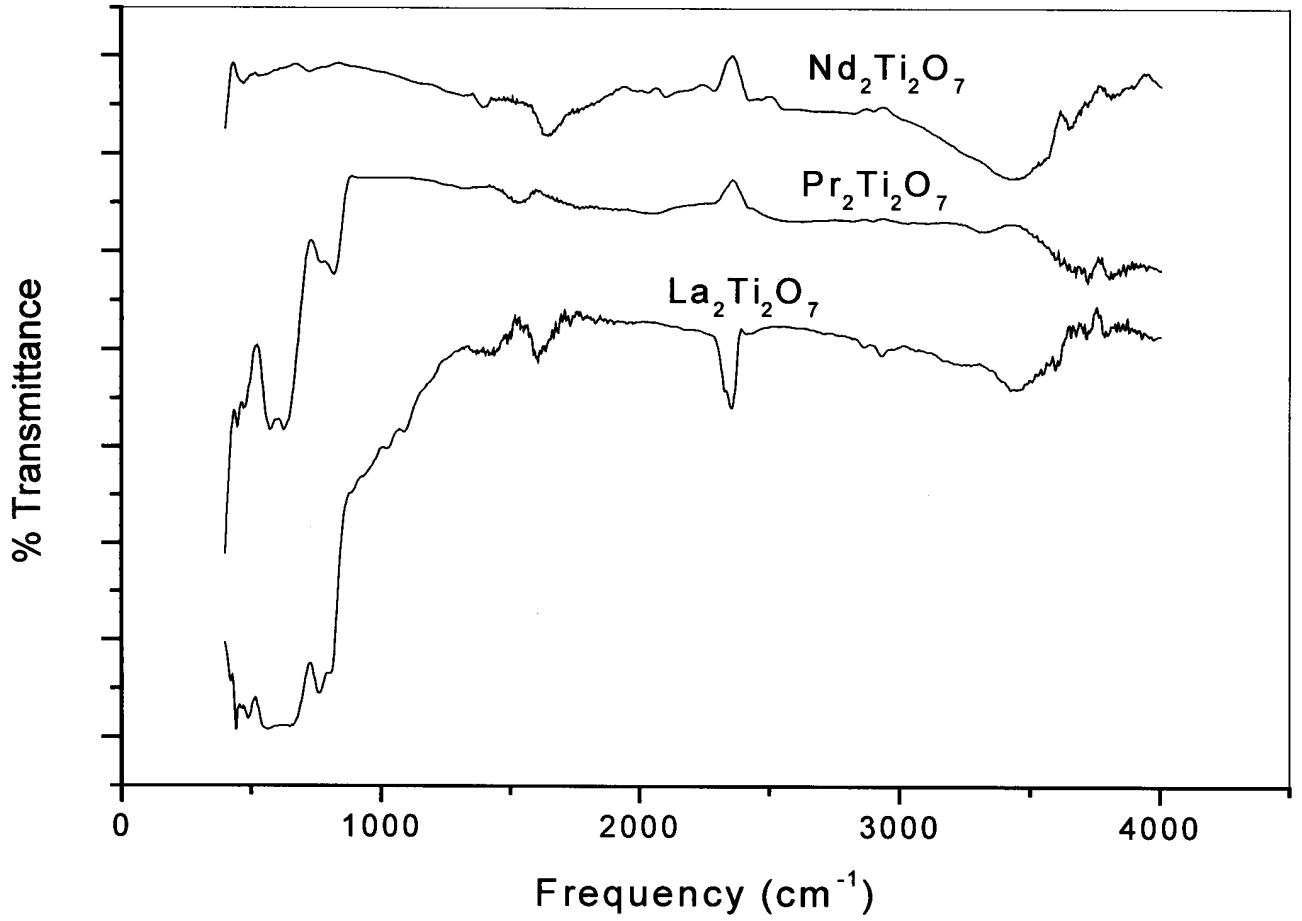


**Fig. 4.28. FTIR spectra of monoclinic $RE_2Ti_2O_7$ synthesized by SHS method and calcined at 1200°C (400-4000 $cm^{-1}$)**

The FTIR spectral bands in the frequency region of interest: 400 to 1000 $cm^{-1}$ is given in table 4.9.

**Table 4.9. Characteristic FT-IR bands of monoclinic $RE_2Ti_2O_7$ in the range of 400 to 1000 $cm^{-1}$**

| $La_2Ti_2O_7$ | $Pr_2Ti_2O_7$ | $Nd_2Ti_2O_7$ | Probable Assignments |
|---|---|---|---|
| 804 m | 814 w | | $A_{2u}$-LO of $TiO_2$ (811)<br>$E_u$-LO of $TiO_2$ (806) |
| 760 m | 766 w<br>625 m | 720 mbr | |
| 561 sbr | 571 m | 525 mbr | |
| 488 s<br>467 m<br>442 s<br>420 m | 471 m<br>446 m | 469 s | $E_u$-LO of $TiO_2$ (458)<br>RE-O(B) |
| w = weak; m = medium; s = strong; br = broad | | | |

The spectral data in the region 1000 to 4000 $cm^{-1}$ (Fig. 4.28) exhibit several weak absorptions. Since the spectra were recorded after calcining the samples at 1200 $^0C$ the presence of X-H vibrations such as O-H, N-H, C-H etc. characteristic of this region cannot be expected. Therefore those weak absorptions may be due to overtones and combinational bands of the compounds

**Laser Raman spectra** of the three monoclinic rare earth titanates calcined at 1200$^0C$ were recorded in the region 400 to 4000 $cm^{-1}$. The spectra in the region of interest 400 to 1000 $cm^{-1}$ is also shown in fig 4.29.

**Table 4.10. Important Raman spectral bands of the monoclinic $RE_2Ti_2O_7$**

| $La_2Ti_2O_7$ | $Pr_2Ti_2O_7$ | $Nd_2Ti_2O_7$ | Probable Assignments |
|---|---|---|---|
| 884 w | 816 s | 824 m | $B_2g$ $TiO_2$(826) |
| 804 m<br>729 w<br>654 w | 796 s | 794 m<br>684 wbr | |
| 615 m | 608 w | 614 m | $A_1g$ $TiO_2$(612) |
| 567 w<br>529 w | 580 w<br>552 w<br>472 m | 574 m | RE-O(A) |
| 456 m<br>412 m | 464 m | 440 m | Eg $TiO_2$(447) |
| 351 m | 360 s | 370 s<br>347 s | RE-O(D) |
| 248 s<br>163 vvs | 282 vvs<br>172 vs | 277 vs<br>172 vvs | RE-O(G)<br>RE-O |
| 124 m<br>61 mbr | | 124 s | RE-O(I) |

The important spectral bands and their probable assignments are given in table 4.10. The spectral data can conveniently be explained by considering the finger print region (50 to 1000 $cm^{-1}$). The spectral data in this region of all the compounds exhibited several characteristic absorptions.[243] From a comparison of typical bands of $TiO_2$ and $RE_2O_3$ several important conclusions can be derived. The $A_1g$ and Eg bands of $TiO_2$ shifted in the rare earth titanates. While the $A_1g$ band exhibited a marginal shift and the Eg band has shifted appreciably.

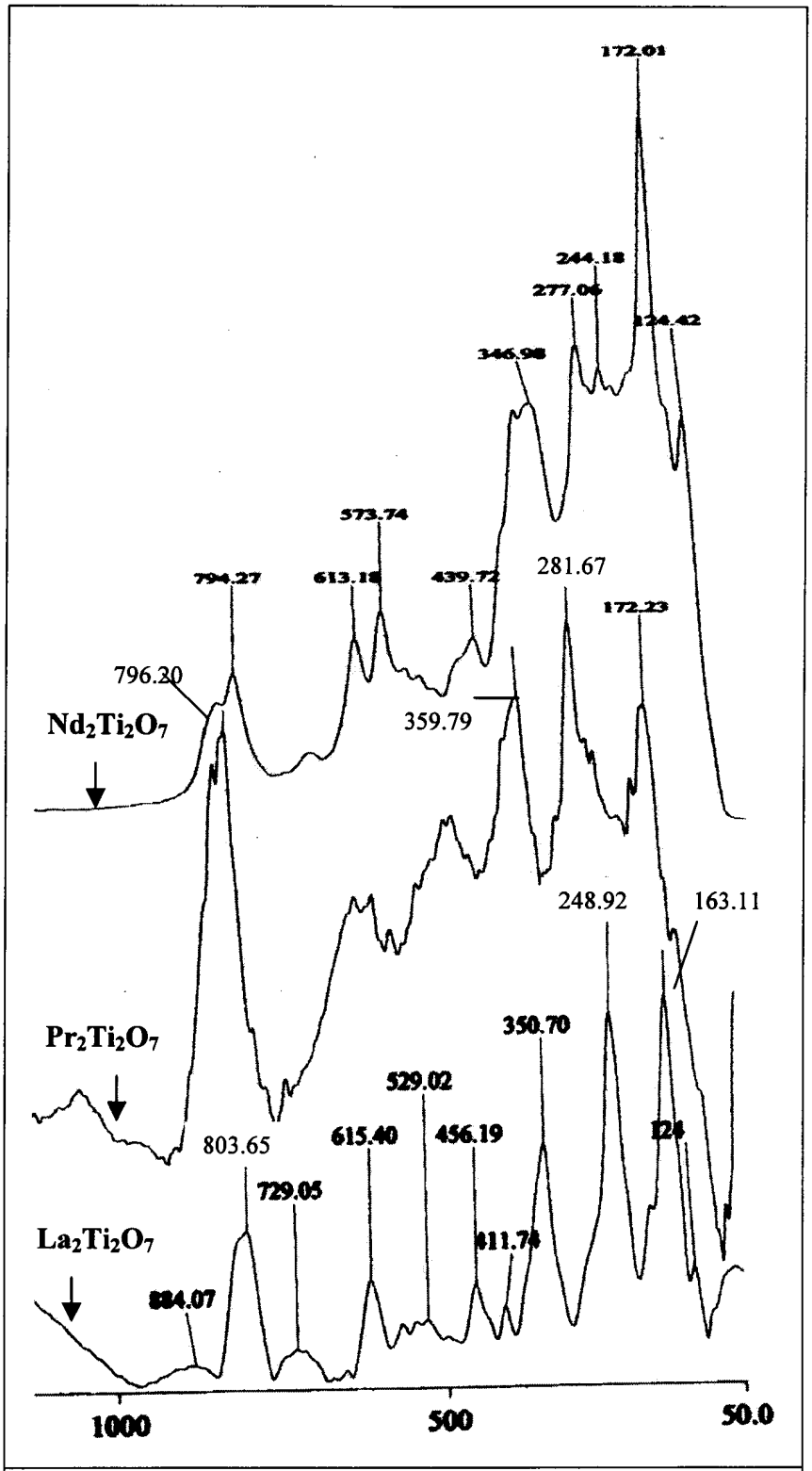


**Fig. 4.29. Raman spectra of the SHS powder of monoclinic $RE_2Ti_2O_7$ calcined at $1200^0C$**

Similarly the characteristic bands of the $RE_2O_3$ also shifted significantly in the $RE_2Ti_2O_7$ spectra. In addition several new bands appeared in the spectra of $RE_2Ti_2O_7$ presumably due to the compound formation and consequent phase changes and also the effect of ionic size, RE-O bond lengths, and strengths. The percentage shift in the Raman peaks of rare earth titanates with reference to the rutile characteristic peaks $A_1g$ and Eg are given in table 4.11.

**Table 4.11. Percentage shift in the Raman peaks of $RE_2Ti_2O_7$ compared to rutile peaks $A_1g$ and Eg**

| $RE_2Ti_2O_7$ | Wave number ($cm^{-1}$) and % shift | | | |
|---|---|---|---|---|
| | Equivalent to $A_1g$ (612) | | Equivalent to Eg (448) | |
| | Value | % Shift | Value | % Shift |
| $La_2Ti_2O_7$ | 615.40 | 0.56 | 456.19 | 1.83 |
| $Pr_2Ti_2O_7$ | 608.00 | -0.65 | 464.00 | 3.57 |
| $Nd_2Ti_2O_7$ | 613.18 | 0.19 | 439.72 | -1.85 |

**BET surface area analysis**

The surface area of the synthesized SHS powders of monoclinic pyrochlores: $La_2Ti_2O_7$, $Pr_2T\ i_2O_7$, and $Nd_2Ti_2O_7$ were measured by BET surface area method and the average particle size (APS) were calculated. The result showed that the La and Nd titanate have APS in the nanometer range.

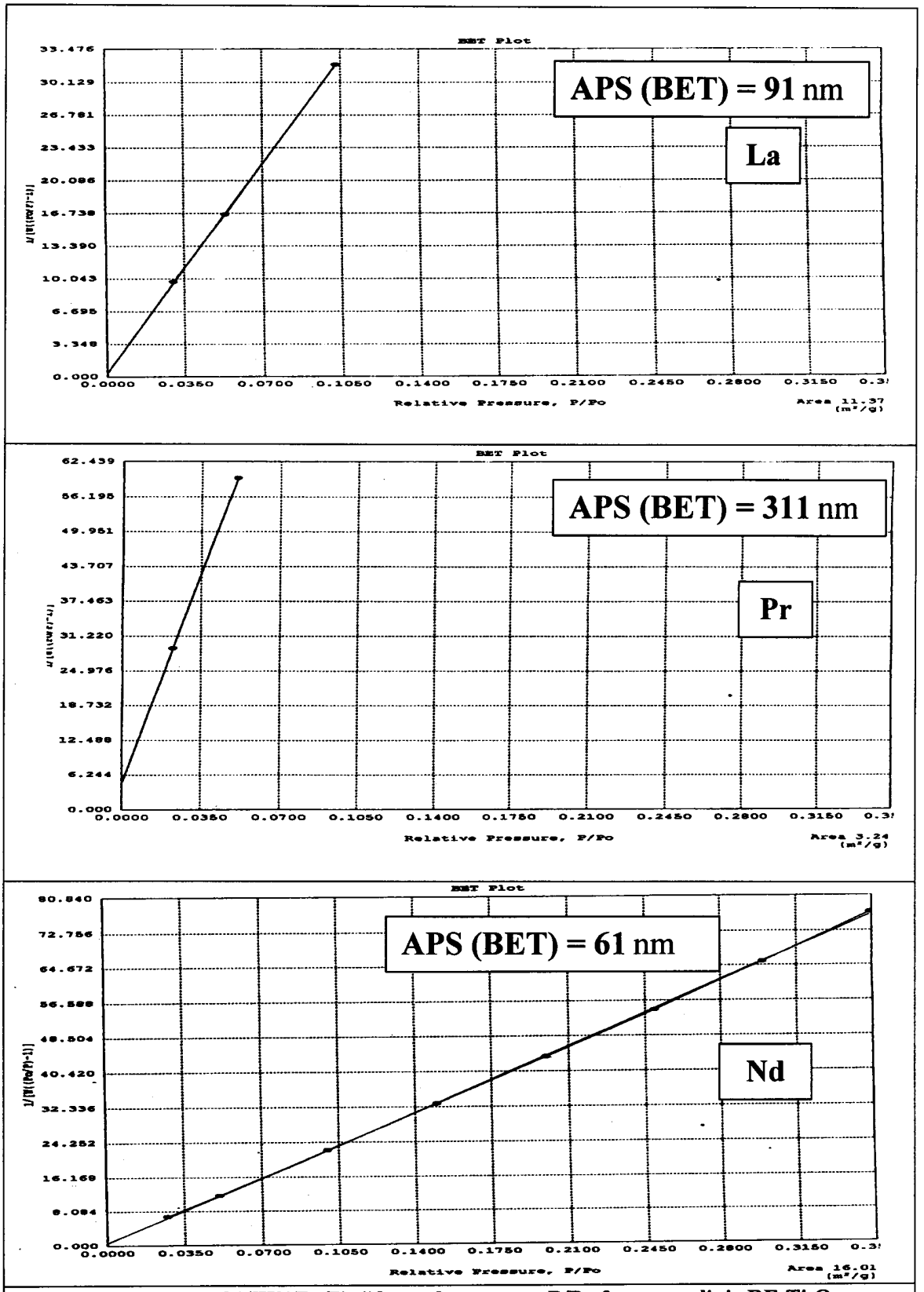


**Fig 4.30. BET plots of $1/[W((P_O/P)-1)]$ vs rel. pressure, $P/P_O$ for monoclinic $RE_2Ti_2O_7$**

The values are given in table 4.12. The BET plots of $1/[W((P_O/P)-1)]$ against relative pressure, $P/P_O$ for the three monoclinic rare earth titanates are given in figures 4.30.

**Table 4.12. BET Surface area & APS of monoclinic $RE_2Ti_2O_7$ synthesized by SHS method**

| $RE_2Ti_2O_7$ (RE = ) | Density (g/cc) | Surface area ($m^2/g$) | APS (nm) |
|---|---|---|---|
| La | 5.78 | 11.4 | 91 |
| Pr | 5.95 | 3.24 | 311 |
| Nd | 6.11 | 16.01 | 61 |

**SEM microstructures**

The SHS powders are generally very fluffy in nature with sponge like interconnected porous network, which can easily be smashed to particles of very fine size of the order of <100 nm. The SEM microstructures of the monoclinic rare earth titanates are shown in fig: 4-31.

The SEM photographs showed very fine sizes of the order of nanometer ranges of the powders. The $La_2Ti_2O7$ and $Nd_2Ti_2O_7$ powders appear to be free in nature with less interconnections of the powder particles compared to $Pr_2Ti_2O_7$ powders; which are not relatively free but remain loosely interconnected in a porous network which would lead to particles of lesser surface area and larger resultant particle sizes. This observation is in agreement with BET surface area measurements. The powder samples of $La_2Ti_2O_7$ and $Nd_2Ti_2O_7$ have lesser average particle sizes and more surface areas but $Pr_2Ti_2O_7$ is found to have only lesser surface area and hence larger particle size.

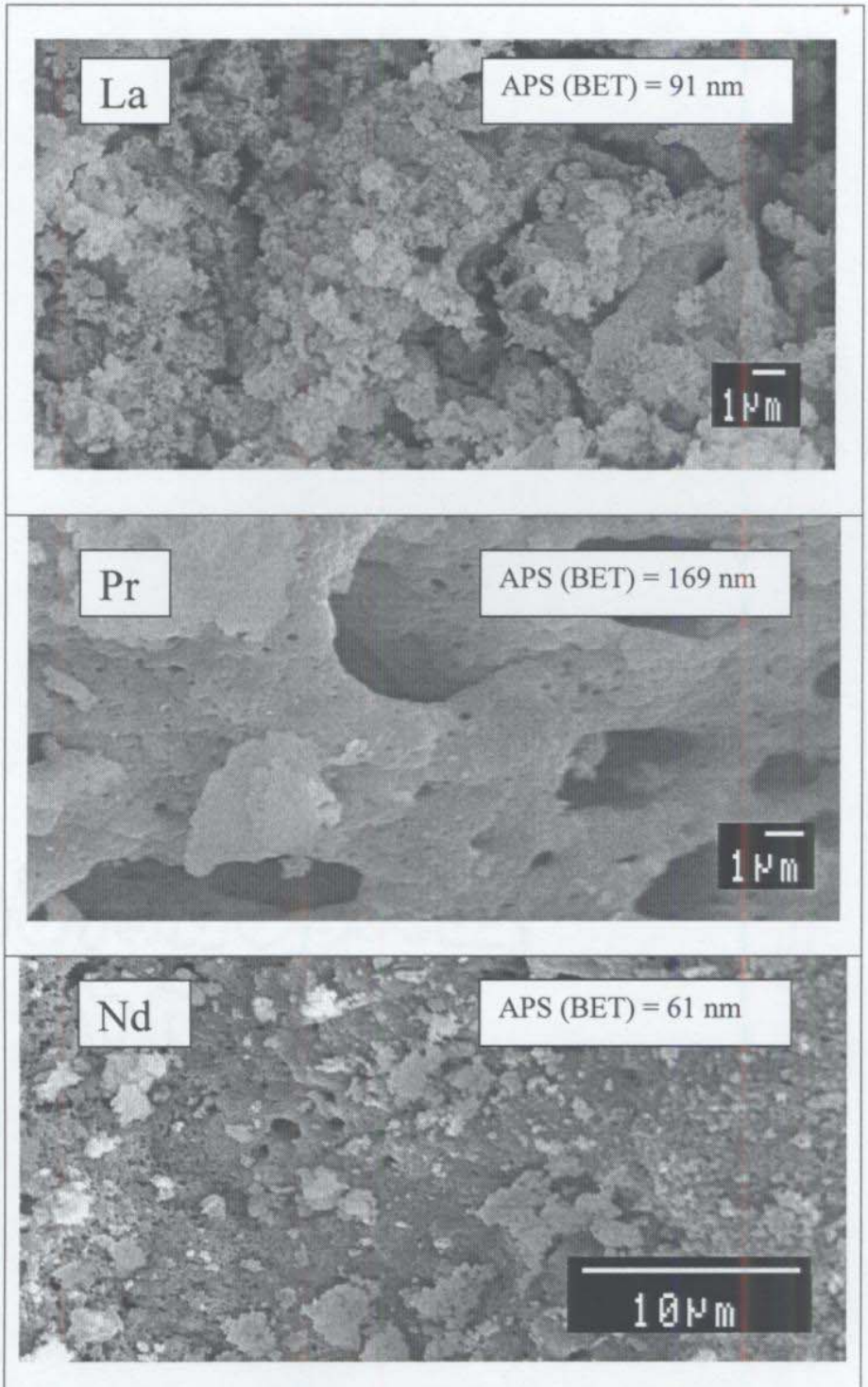


**Fig. 4.31. SEM microstructure of SHS powders of Monoclinic $RE_2Ti_2O_7$**

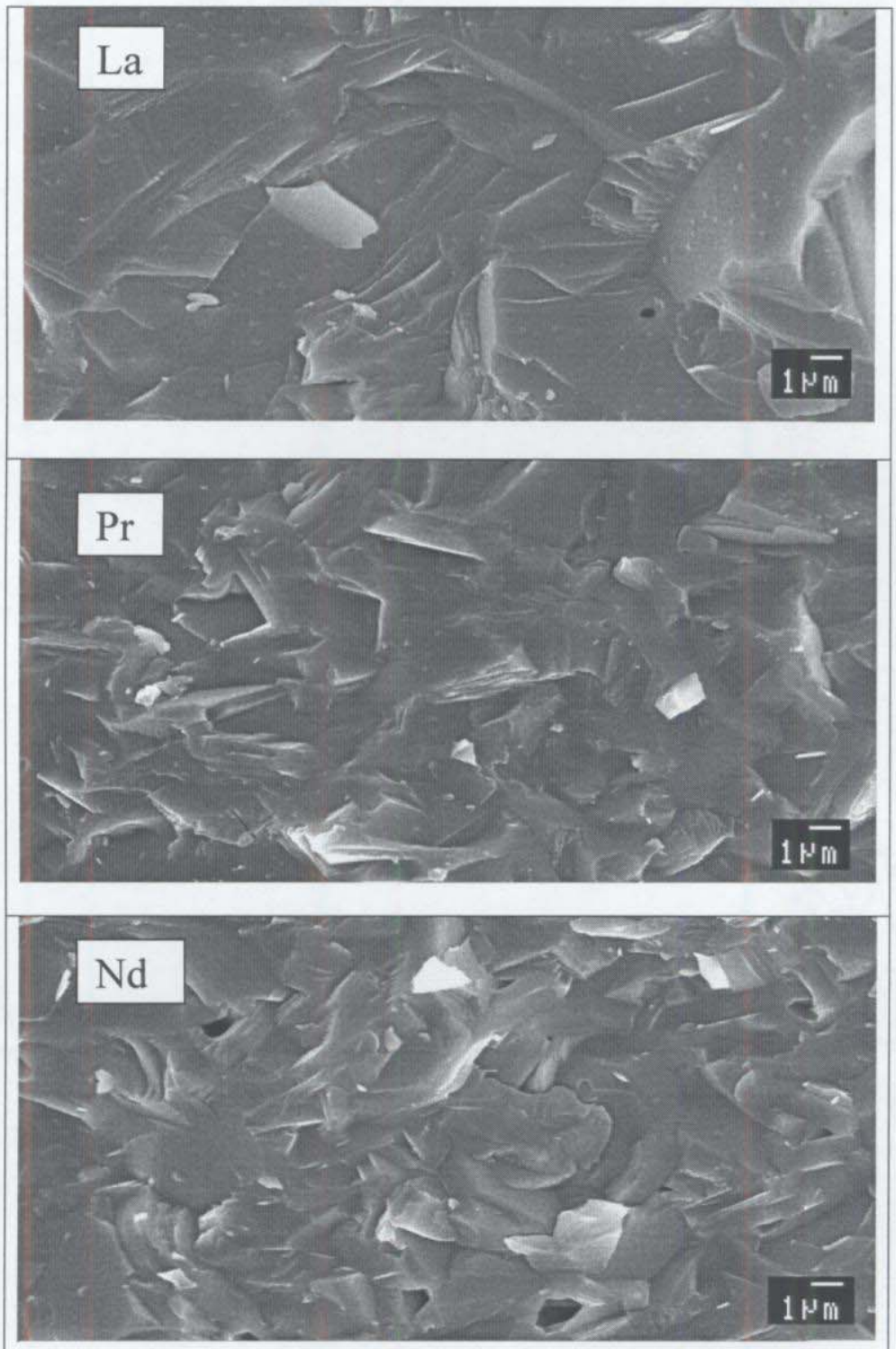


**Fig. 4.32. SEM of the cross section of sintered discs (at 1450 $^0$C) of monoclinic $RE_2Ti_2O_7$ made from SHS powders**

The SEM microstructure of the sintered (at 1450 $^0$C) monoclinic rare earth titanates exhibit a well sintered physical appearance for the broken cross-sectional structure for the discs. The grains are so smoothly interconnected with almost zero porosity and appear to be single domain in structure. The SEM microstructures of the cross sectional surfaces of the discs sintered at 1450 $^0$C are given figure 4.32.

**Dielectric properties**

The dielectric properties such as permittivity and dissipation factor of the rare earth titanates obtained by the solid state method and by the SHS method were measured in the frequency range 100 Hz to 10 MHz. In the case of samples synthesized by solid state method good data were obtained only in the case of $Pr_2Ti_2O_7$.

The changes in permittivity with frequency is shown in fig. 4.33 and the variation in dissipation factor with frequency in fig. 4.34 for the samples sintered at 1525 $^0$C and 1575 $^0$C. It is evident from fig. 4.34 that the dissipation factor approaches stable values in the higher frequency range above 10 kHz and it becomes highly stable. The change in permittivity with temperature (fig. 4.35) exhibited positive temperature coefficient of capacitance (TCC) with increasing temperature. To make it suitable for temperature stable dielectrics it is to be mixed with materials of negative TCC to form solid solutions.

Contrary to the behavior of other titanates, $Pr_2Ti_2O_7$ made by the solid-state route exhibited high permittivity values at lower frequencies compared to SHS material. e.g. at 1 MHz: 30.1(for solid-state:1525 $^0$C) and 40.2 (for SHS:1525 $^0$C). Similarly at 1 MHz 36.1, for solid-state and 41.0, for SHS, both sintered at 1575 $^0$C.

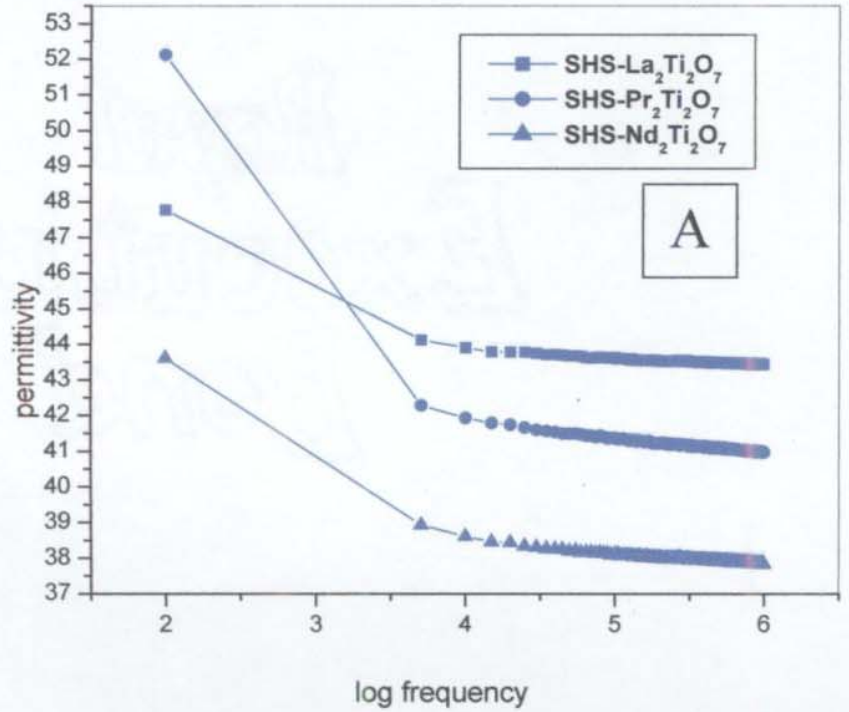


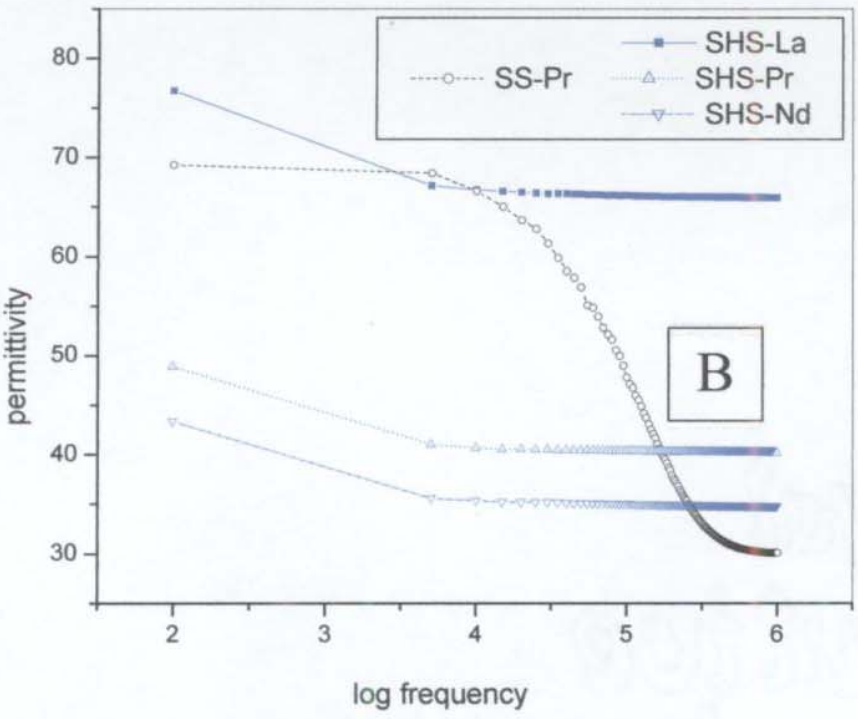


**Fig. 4.33. Changes in permittivity with frequency of monoclinic $RE_2Ti_2O_7$ sintered at(A)1575 $^0$C and (B)1525 $^0$C**

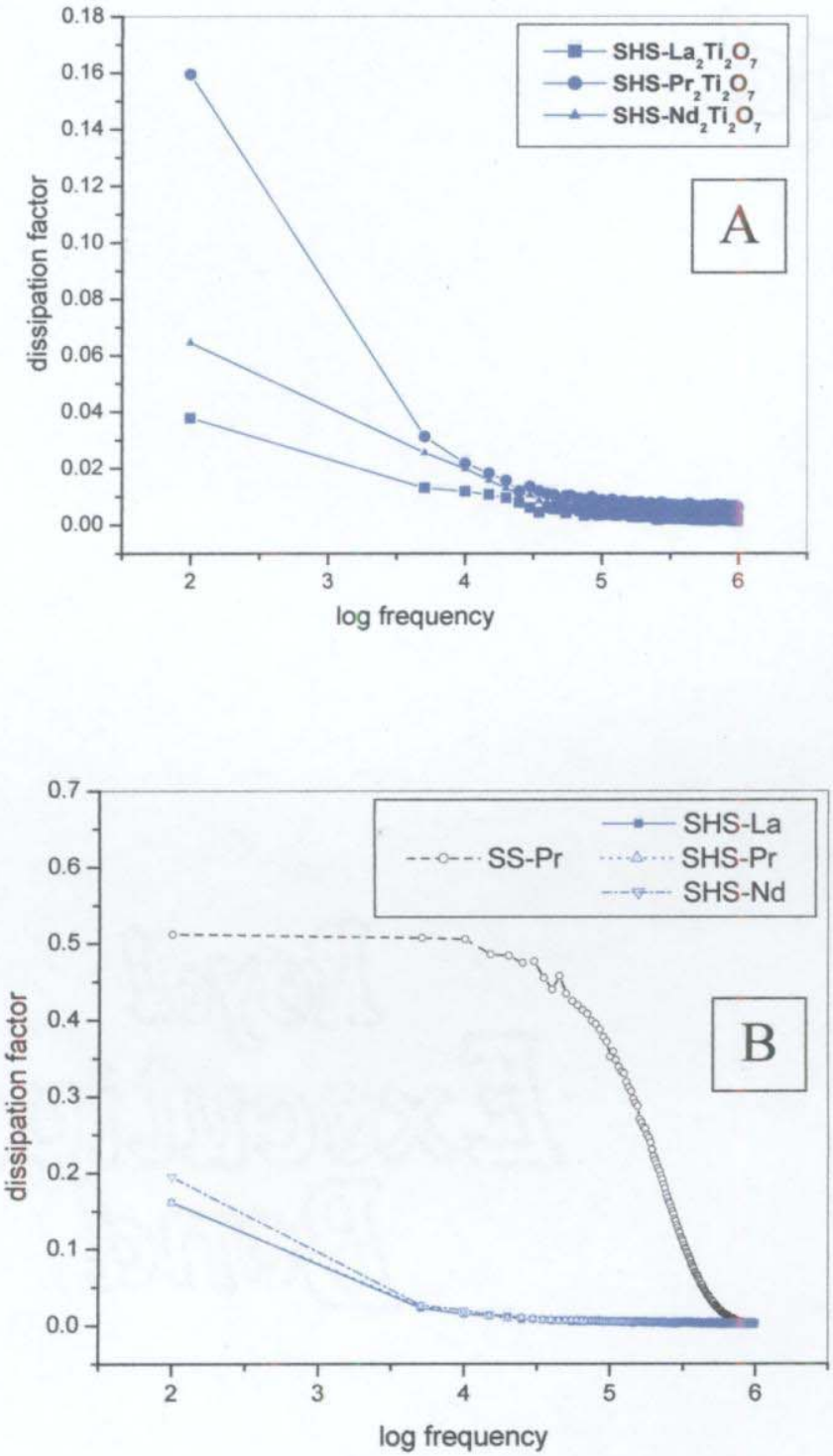


**Fig. 4.34. Changes in dissipation factor with frequency of monoclinic $RE_2Ti_2O_7$ sintered at(A)1575 $^0$C and (B)1525 $^0$C**

The dissipation factor values are high for solid-state samples. The values for samples sintered at 1525 $^0$C are 0.506 (at 10 KHz) and 0.352 (at 100 KHz) and for samples sintered at 1575 $^0$C are 0.272 (at 10 KHz) and 0.181 (at 100 KHz). The corresponding values for SHS samples sintered at 1525 $^0$C are 0.016 (at 10 KHz) and 0.004 (at 100 KHz), and for samples sintered at 1575 $^0$C are 0.022 (at 10 KHz) and 0.009 (at 100 KHz). At higher frequencies, 1 MHz and above, for both solid-state samples and SHS samples sintered at 1525 $^0$C or1575 $^0$C the dissipation factor values are in the range 0.002 to 0.006.

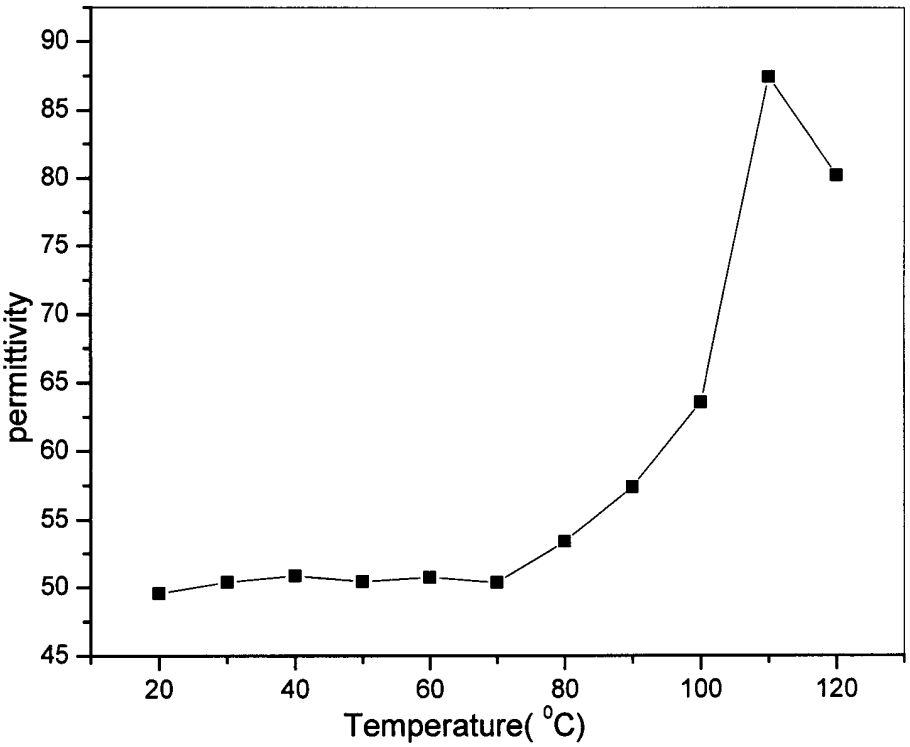


**Fig. 4.35. Changes in permitivity with temperature for the monoclinic, $La_2Ti_2O_7$ synthesized by SHS method**

Thus the rare earth titanates synthesized by SHS method exhibit good dielectric behavior with high permittivity values becoming stable in the higher frequency ranges compared to those made by the direct solid state method.

## SECTION 4B

## CUBIC $RE_2Ti_2O_7$

### TG-DTA analysis

The weight loss/gain obtained from the thermograms of $RE_2Ti_2O_7$, (where RE = Sm, Gd, Dy and Y) are given in table 4.13. Except $Sm_2Ti_2O_7$, all the others showed a weight loss less than 10 % upto 900 $^0$C. In the case of $Sm_2Ti_2O_7$, about 23 % loss in weight was observed at 715 $^0$C. Above 1100 $^0$C a slight increase in weight was observed probably due to phase transitions.

**Table 4.13. TG data of SHS powders of cubic $RE_2Ti_2O_7$ [where RE = Sm, Gd, Dy and Y]**

| Sample | Atmos-phere | wt. loss (%) | Temp. ($^0$C) | Wt. gain (%) | Temp. ($^0$C) |
|---|---|---|---|---|---|
| $Sm_2Ti_2O_7$ | Nitrogen | 23.3 | 715 | 4.4 | 1133 |
| $Gd_2Ti_2O_7$ | Nitrogen | 7.0 | 680 | 4.2 | 1349 |
| $Gd_2Ti_2O_7$ | Oxygen | 7.4 | 895 | 1.9 | 1417 |
| $Dy_2Ti_2O_7$ | Nitrogen | 4.7 | 700 | 6.1 | 1343 |
| $Y_2Ti_2O_7$ | Oxygen | 10.8 | 650 | 8.4 | 1367 |

The DTA curves of these compounds were found to have two distinct regions correspond to exothermic and endothermic changes, both in nitrogen and oxygen atmospheres. In all the cases except for $Sm_2Ti_2O_7$, the exothermic region of the curve commenced from 40 $^0$C and reached up to 525 to 665 $^0$C and the endothermic region of the curve started from this temperature and extended up to 1133 $^0$ to 1417$^0$C. But, for $Sm_2Ti_2O_7$ the exothermic region of

the curve started from 130 $^0$C extended up to 525 $^0$C and the endothermic region started from 525 $^0$C and it extended up to 1133 $^0$C only.

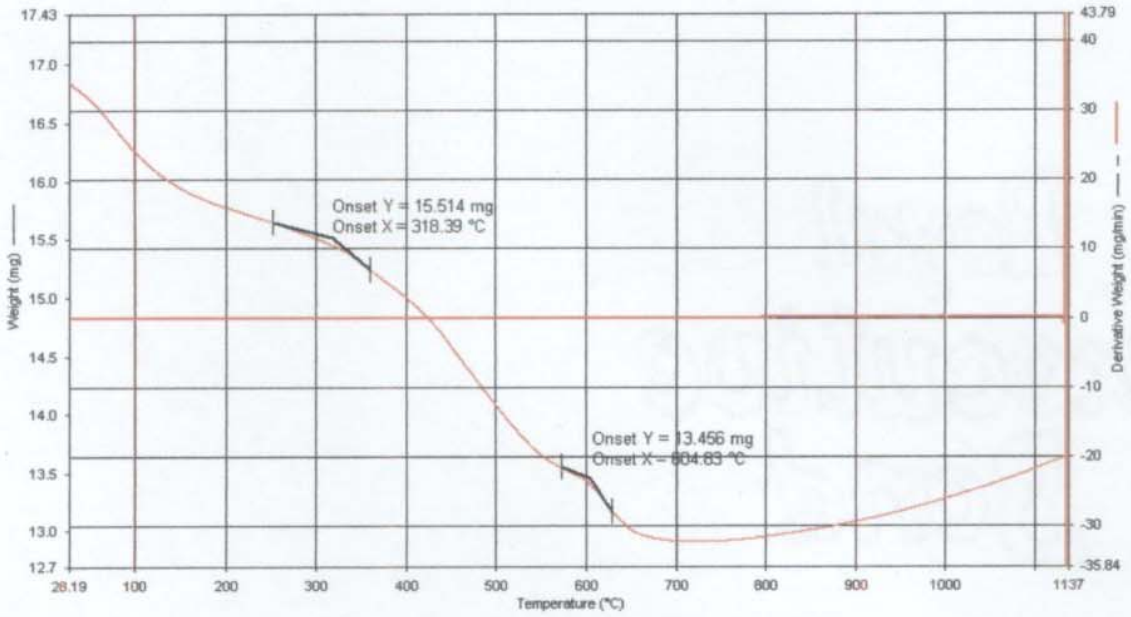


**Fig. 4.36. TG-DTG (Nitrogen atm.) of $Sm_2Ti_2O_7$ synthesized by SHS-AA method**

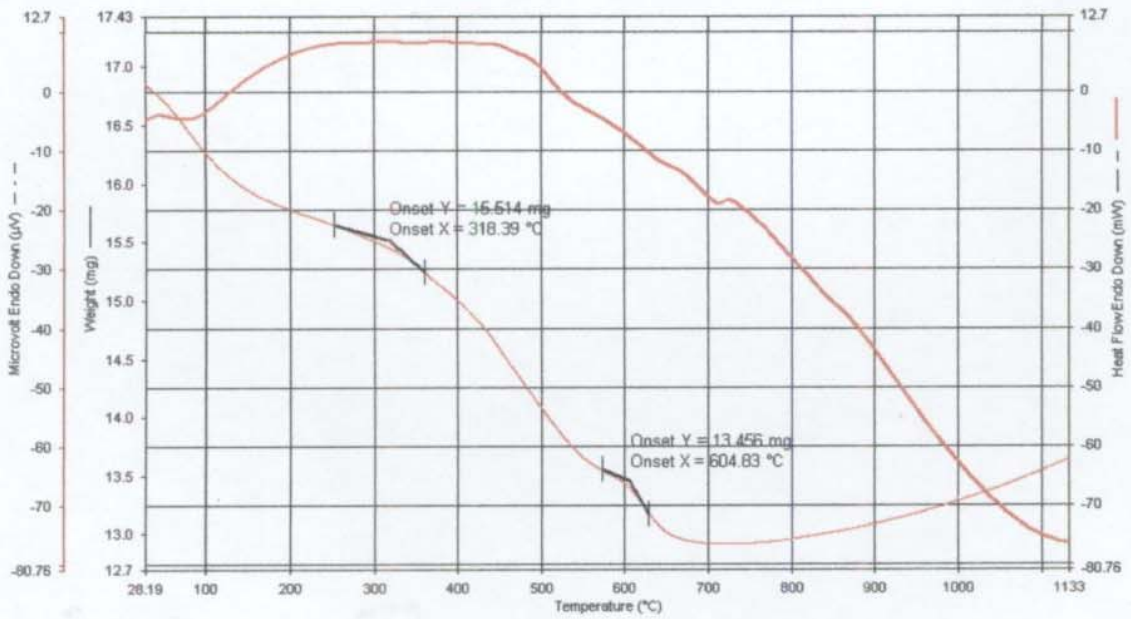


**Fig. 4.37. TG-DTA (Nitrogen atm.) of $Sm_2Ti_2O_7$ synthesized by SHS-AA method**

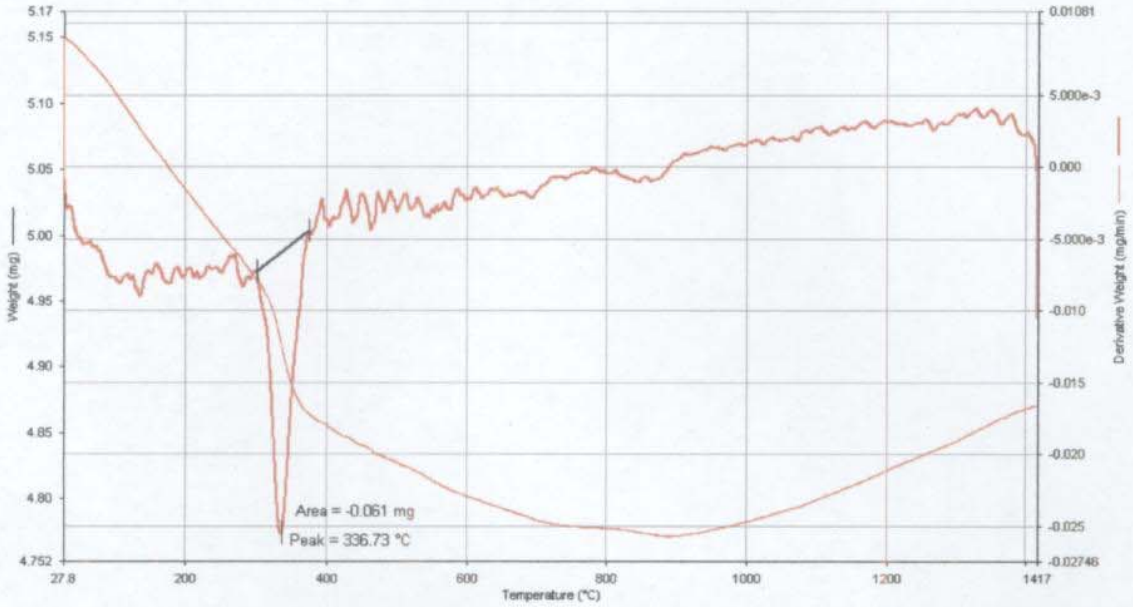


**Fig. 4.38. TG-DTG (Oxygen atm.) of $Gd_2Ti_2O_7$ synthesized by SHS-AA method**

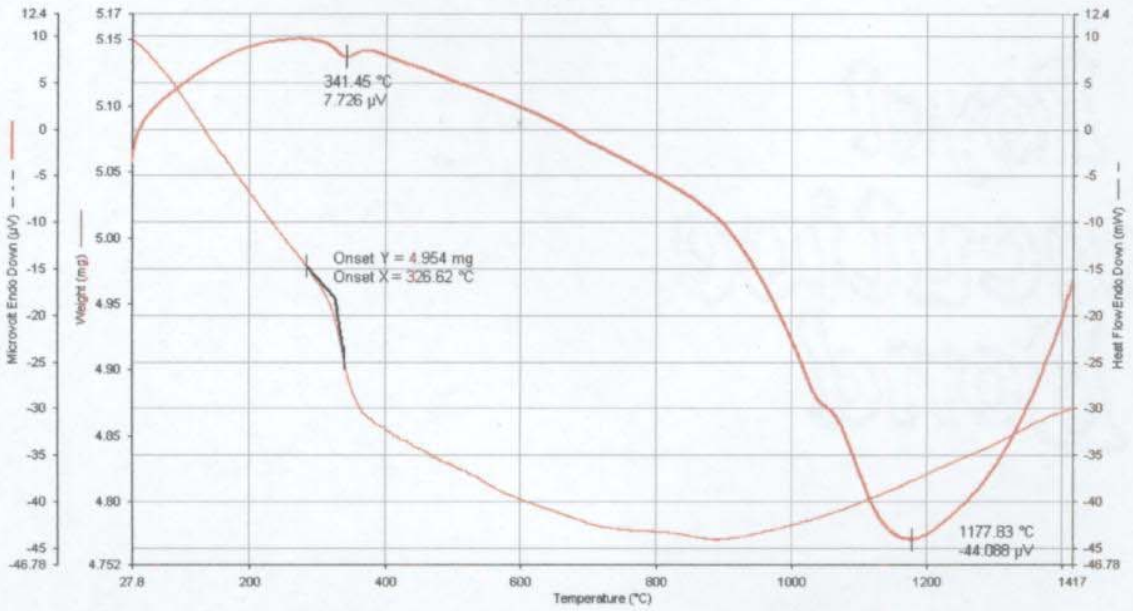


**Fig. 4.39. TG-DTA (Oxygen atm.) of $Gd_2Ti_2O_7$ synthesized by SHS-AA method**

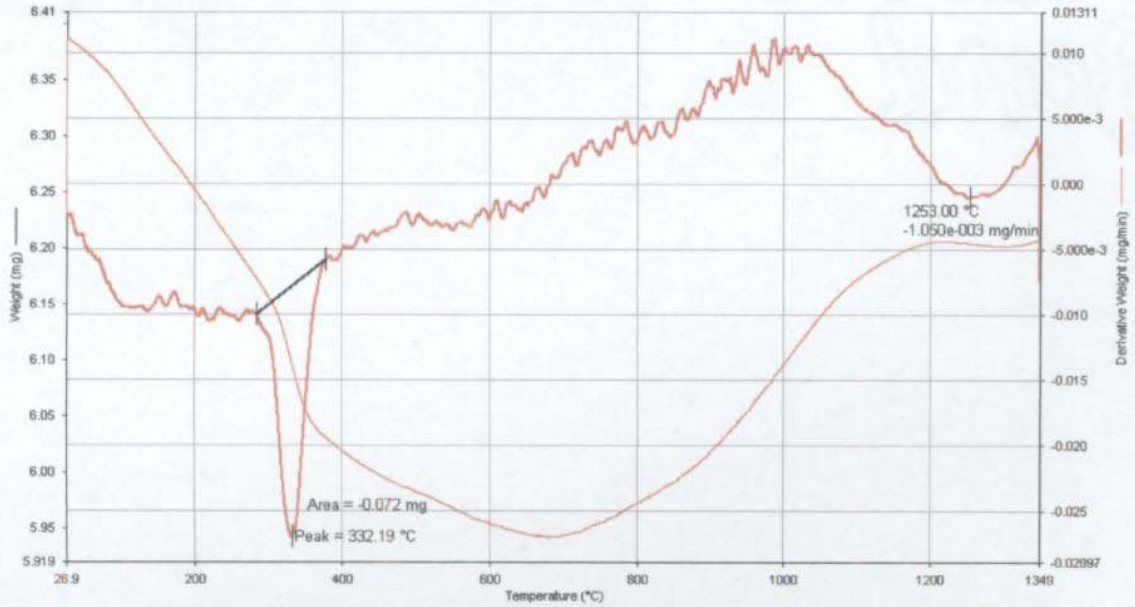


**Fig. 4.40. TG-DTG (Nitrogen atm.) of $Gd_2Ti_2O_7$ synthesized by SHS-AA method**

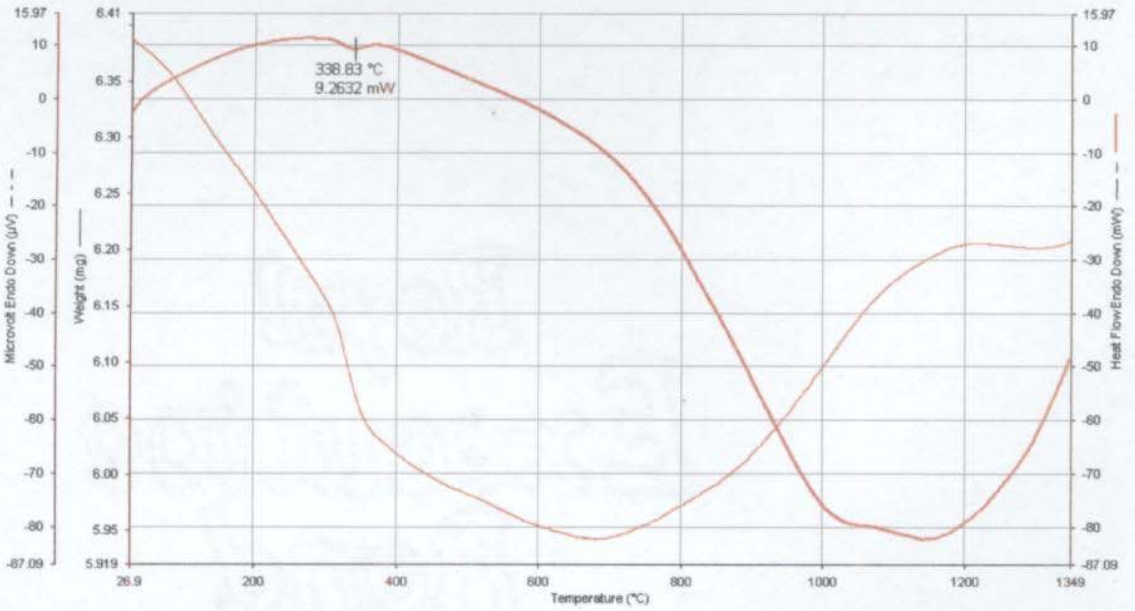


**Fig. 4.41. TG-DTA (Nitrogen atm.) of $Gd_2Ti_2O_7$ synthesized by SHS-AA method**

The exothermic peak heights were lower compared to the endothermic region (Table 4.14).

**Table 4.14. DTA data of SHS powders of cubic $RE_2Ti_2O_7$ [where RE = Sm, Gd, Dy and Y]**

| $RE_2Ti_2O_7$ (atmosphere) | Temp. maxima of reaction | | Peak Values of reaction | | | |
|---|---|---|---|---|---|---|
| | | | Exothermic | | Endothermic | |
| | Exothermic ($^0$C) | Endothermic ($^0$C) | Value ($\mu$V) | Temp. ($^0$C) | Value ($\mu$V) | Temp. ($^0$C) |
| $Sm_2Ti_2O_7$ ($N_2$) | 525 | 1133 | 08.000 | 300.00 | -76.70 | 1133.0 |
| $Gd_2Ti_2O_7$ ($N_2$) | 570 | 1349 | 09.263 | 338.83 | -82.00 | 1140.0 |
| $Gd_2Ti_2O_7$ ($O_2$) | 665 | 1417 | 07.726 | 341.45 | -44.00 | 1178.0 |
| $Dy_2Ti_2O_7$ ($N_2$) | 560 | 1343 | 11.536 | 298.17 | -51.96 | 1128.5 |
| $Y_2Ti_2O_7$ ($O_2$) | 535 | 1367 | 09.255 | 281.20 | -55.00 | 1100.0 |

In the TG-DTG & TG-DTA curves (fig. 4.36 to 4.45) the minimum weight observed in the temperature range 650 $^0$C to 895 $^0$C; in the DTA curves, the transition from exothermic region to endothermic region occur at 525 $^0$C to 665 $^0$C. This indicates that, typical transition takes place in the SHS material in the range of 530 $^0$C to 900 $^0$C. The changes in the crystalline structure found from XRD pattern of the SHS powders at temperatures of 600 $^0$, 800 $^0$, 1000 $^0$ and 1200 $^0$C also confirm the above transitions.

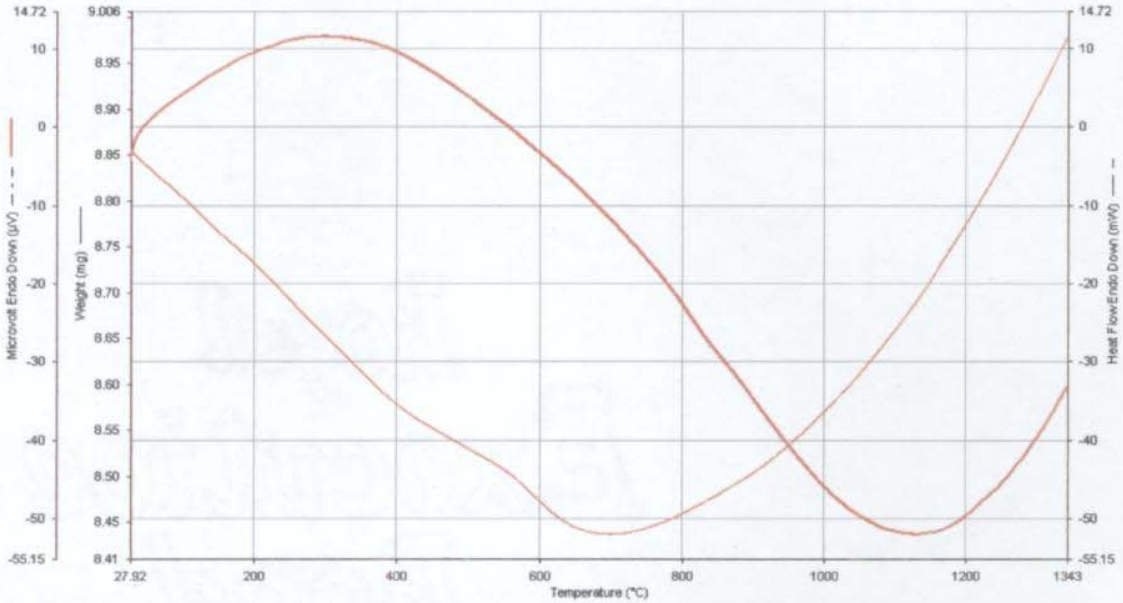


**Fig. 4.42. TG-DTA (Nitrogen atm.) of $Dy_2Ti_2O_7$ synthesized by SHS-AA method**

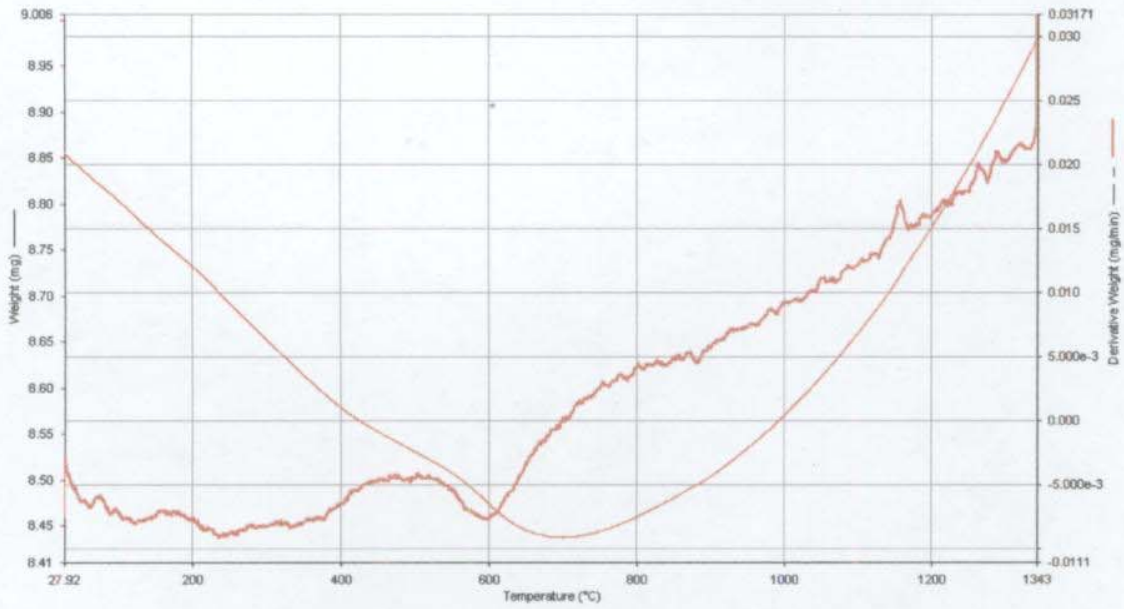


**Fig. 4.43. TG-DTG (Nitrogen atm.) of $Dy_2Ti_2O_7$ synthesized by SHS-AA method**

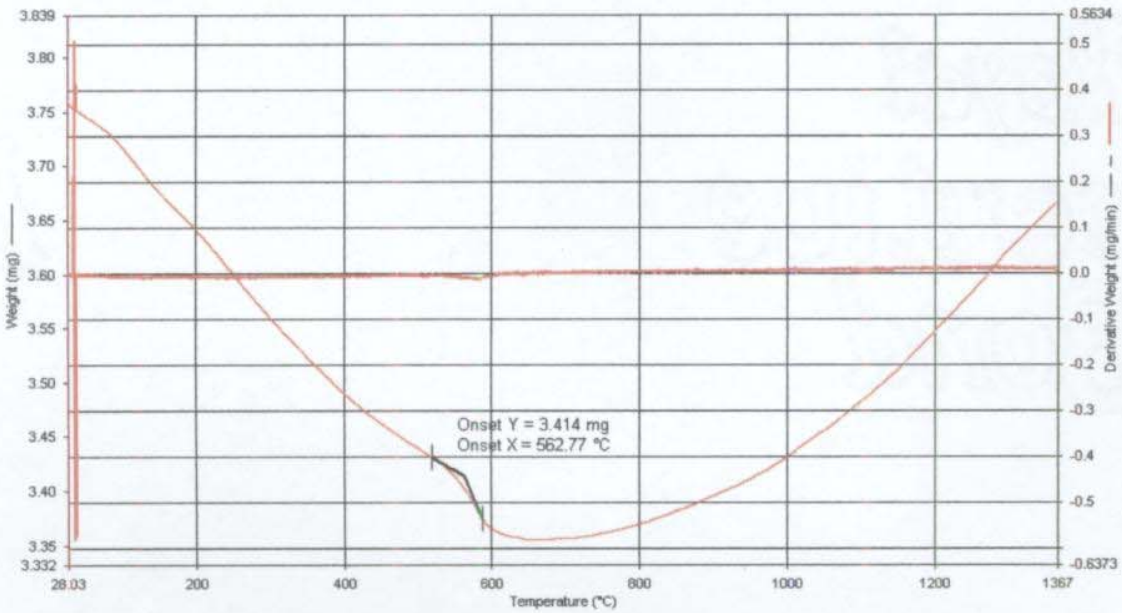


**Fig. 4.44. TG-DTG (Oxygen atm.) of $Y_2Ti_2O_7$ synthesized by SHS-AA method**

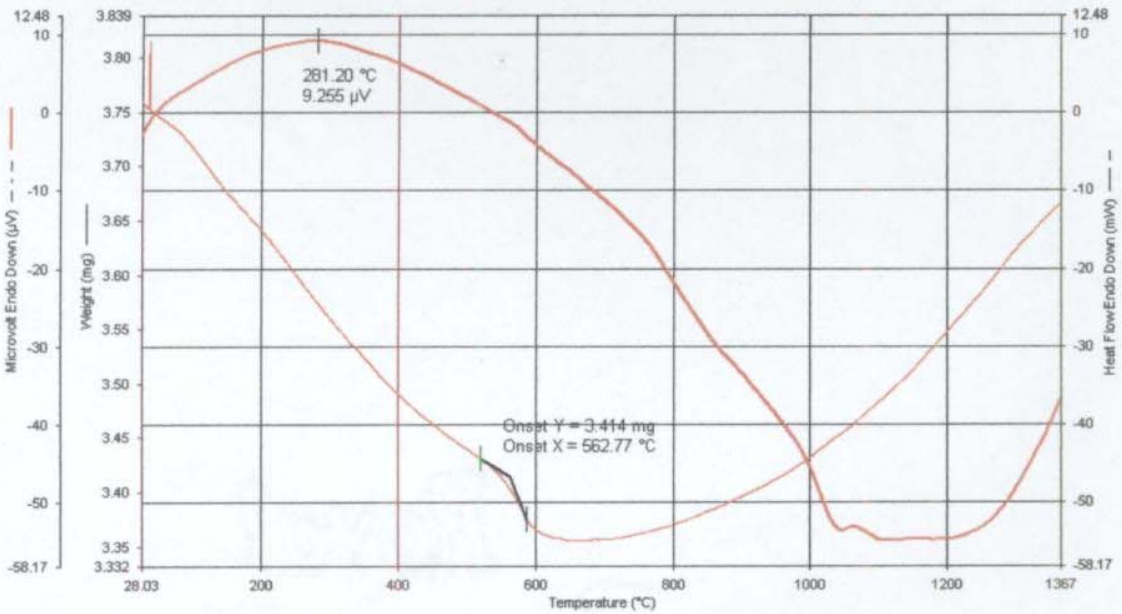


**Fig. 4.45. TG-DTA (Oxygen atm.) of $Y_2Ti_2O_7$ synthesized by SHS-AA method**

**XRD studies**

**Samarium titanate, $Sm_2Ti_2O_7$:** The SHS powder of $Sm_2Ti_2O_7$ appears to be microcrystalline in nature (XRD), but on calcination at temperatures $600^0$ to $1200^0$C, the crystallinity of the powder improves as shown in fig. 4.46. The (3 1 1) peak at d = 3.09, $2\theta = 29^0$, which was not present before calcination emerges on heating the sample above 600 $^0$C and becomes a well defined peak at 1200 $^0$C. The main peak (2 2 2) of the cubic form at d = 2.96, $2\theta = 30^0$ became prominent in the calcined material and assumed 100 % intensity at 1200 $^0$C. Similarly, all the major peaks (4 0 0) at d = 2.56, $2\theta = 35^0$ ; (4 4 0) at d = 1.81, $2\theta = 51^0$ ; and peak (3 3 1) at d = 2.35, $2\theta = 38^0$ which are absent initially becomes prominent in the XRD of powders calcined above 1000 $^0$C. At 1200 $^0$C, all the peaks found in the standard (ICDD: 16-400) appeared well defined and correspond to phase pure cubic crystalline $Sm_2Ti_2O_7$.

**Gadolinium titanate, $Gd_2Ti_2O_7$:** The XRD pattern of the SHS powder of $Gd_2Ti_2O_7$ obtained, showed its non- crystalline nature, but its crystallinity improved on calcination at higher temperatures, 600 $^0$ to 1200 $^0$C.It becomes a well defined crystalline material on calcination at $1200^0$C, matching with all peaks in the standard cubic $Gd_2Ti_2O_7$, ICDD:23-259 as given in fig. 4.47. The main peak (2 2 2), at d = 2.94,$2\theta = 31^0$ was absent in the SHS powder but it emerged and became prominent on calcination at 1000 $^0$C and 1200 $^0$C. Similarly other peaks such as (4 4 0) at d = 1.8, $2\theta = 51^0$ ; (4 0 0) at d = 2.5, $2\theta = 35^0$ ; and (3 3 1) at d = 2.4, $2\theta = 39^0$ which were absent in the SHS powder as well as in the material calcined upto $800^0$C emerged on calcination above 1000 $^0$C.

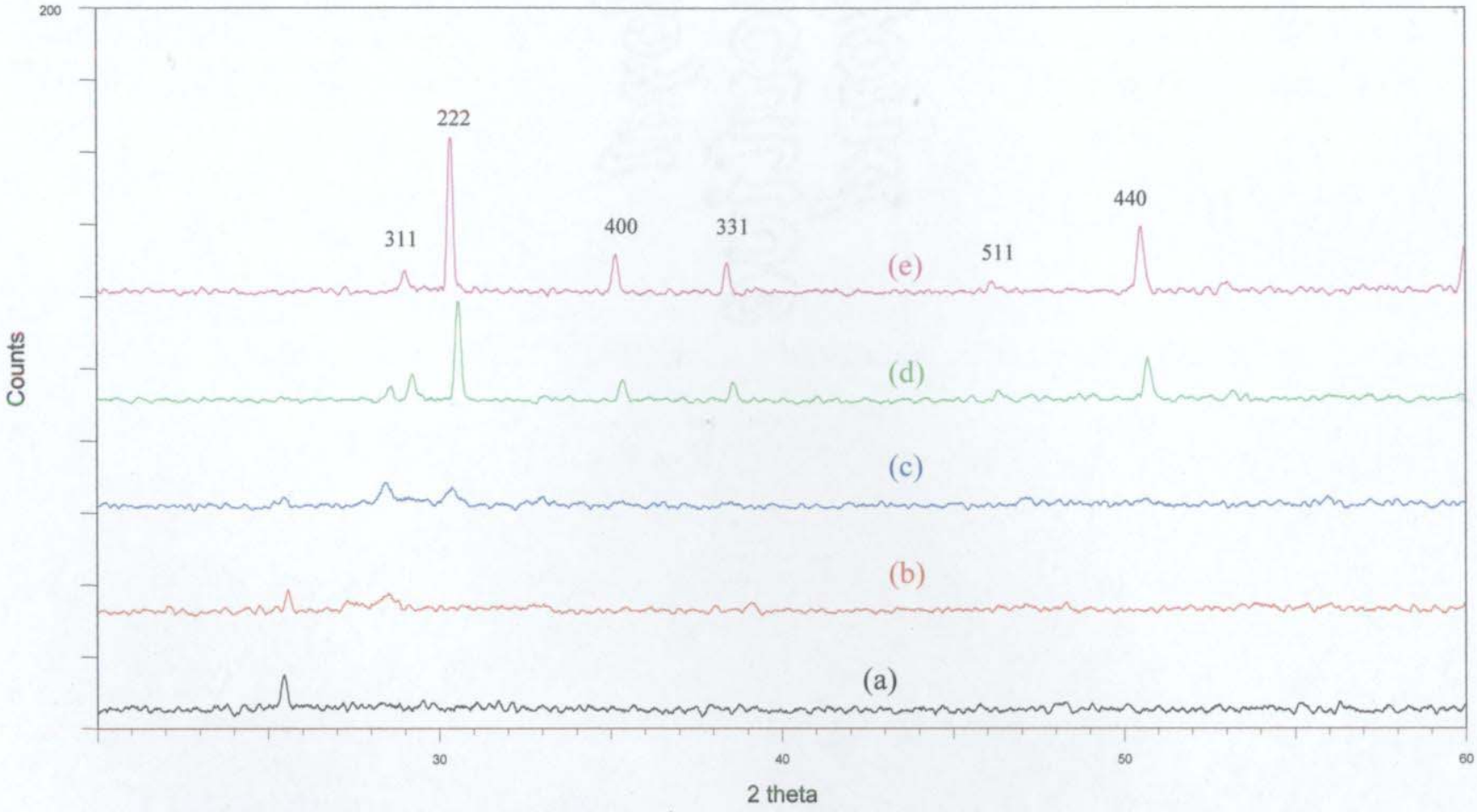


**Fig.4.46. XRD patterns of $Sm_2Ti_2O_7$ (a) SHS powder-before calcination, and calcined at (b) 600 $^0$C (c) 800 $^0$C (d) 1000 $^0$C and at (e) 1200 $^0$C (Match ICDD 16-0400 cubic $Sm_2Ti_2O_7$)**

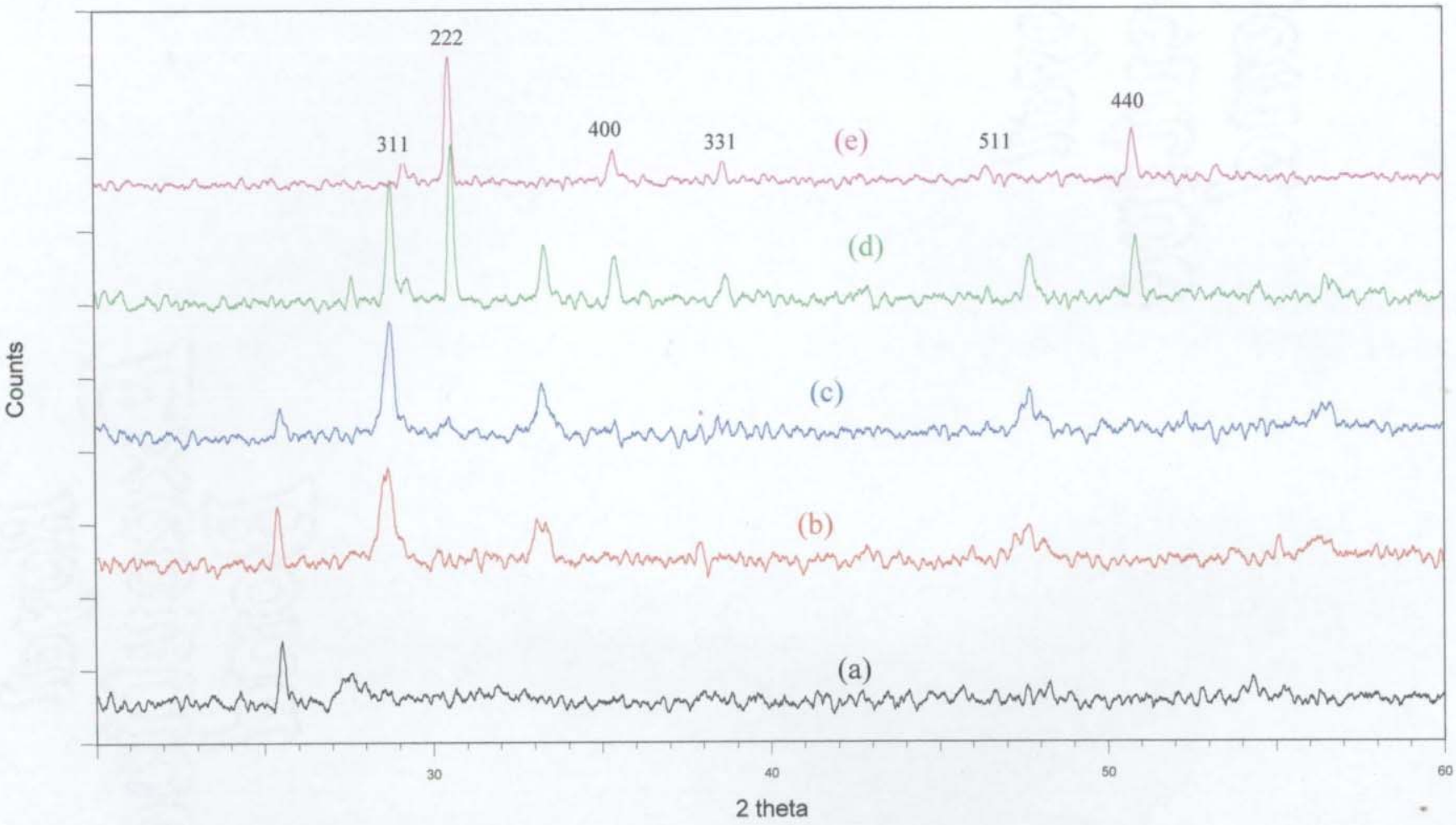


**Fig. 4.47. XRD patterns of $Gd_2Ti_2O_7$ (a) SHS powder-before calcination and calcined at (b) 600 $^0$C (c) 800 $^0$C (d) 1000 $^0$C and at (e) 1200 $^0$C (Match ICDD 23-0259 cubic $Gd_2Ti_2O_7$)**

**Dysprosium titanate, $Dy_2Ti_2O_7$:** The XRD pattern of the SHS powder displayed peaks characteristic of the cubic phase of $Dy_2Ti_2O_7$ even before calcination. However, the powder calcined at 1200 $^0$C showed perfect matching with the standard cubic $Dy_2Ti_2O_7$ ICDD: 17-453. The XRD spectra of cubic $Dy_2Ti_2O_7$ as such alongwith its different calcined forms are shown in fig. 4.48.

**Yttrium titanate, $Y_2Ti_2O_7$:** The $Y_2Ti_2O_7$ material synthesized by the SHS method shows a different set of peaks compared to the standard $Y_2Ti_2O_7$. A typical peak at d = 3.5, $2\theta$ = 25 $^0$, present in the SHS powder becomes prominent on calcination at 600 $^0$C to an intensity of the order of 100 % (This peak is not present in the standard). On calcination of the powder at higher temperatures, this peak gets suppressed and vanishes. The main peak, in the standard of 100 % intensity, at d = 2.9, $2\theta = 31^0$ which was absent in the SHS powder calcined upto 800 $^0$C, emerges at 1000 $^0$C and becomes the main peak (100% intensity) in the 1200 $^0$C calcined material as seen in fig. 4.49. Other prominent peaks, that is (4 4 0) at d = 1.8, $2\theta = 51^0$; (4 0 0) at d = 2.5, $2\theta = 36^0$; and (3 3 1) at d = 2.3, $2\theta$ = 39 $^0$ which are totally absent in the SHS powder becomes prominent on calcination at temperatures above 1000 $^0$C. The SHS powder calcined at 1200 $^0$C shows an XRD pattern that completely matches with the standard XRD of cubic $Y_2Ti_2O_7$ of ICDD: 42-413. Thus the XRD spectra of all the titanates considered in this section confirmed the formation of phase pure cubic $RE_2Ti_2O_7$

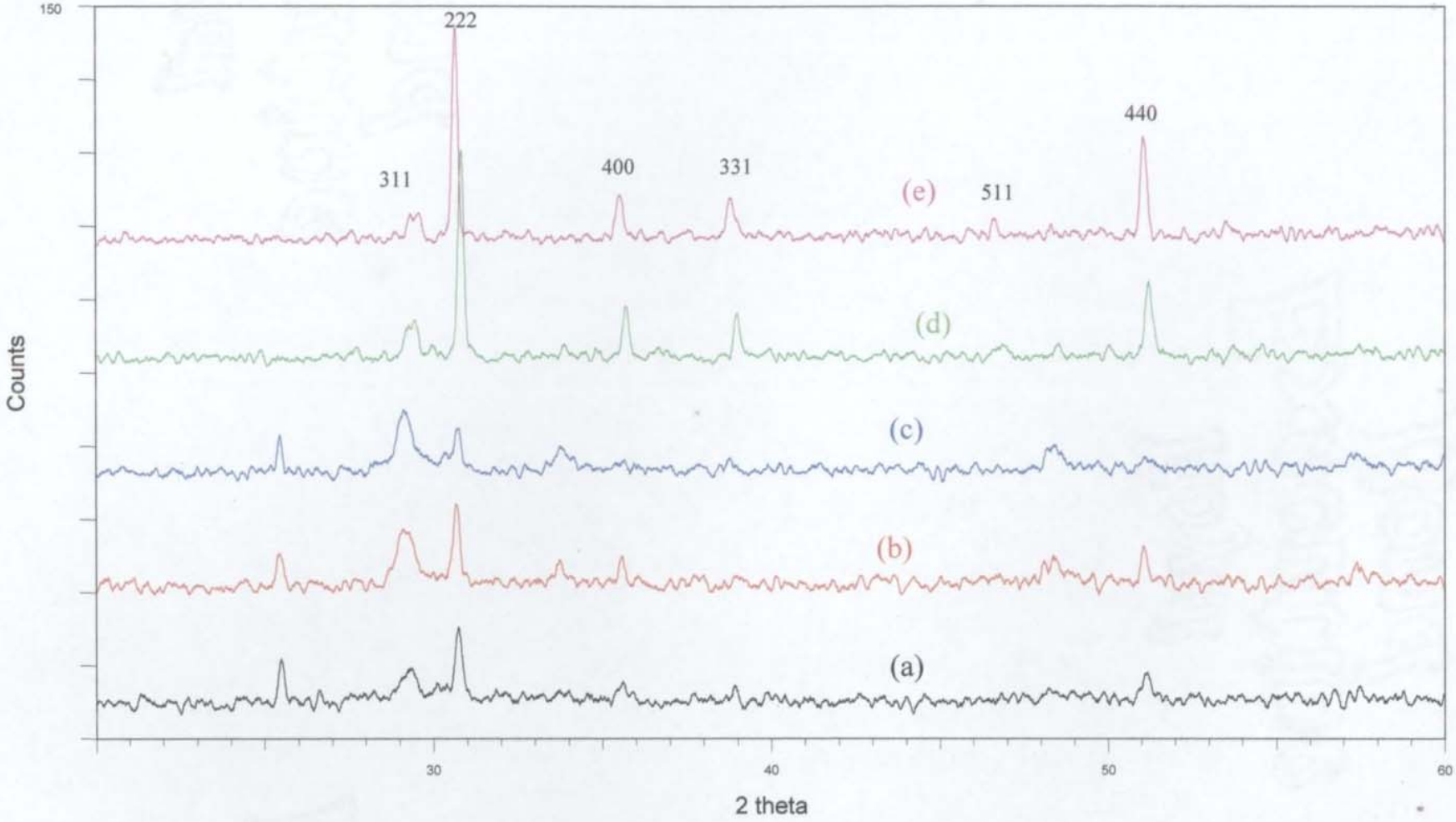


**Fig. 4.48. XRD patterns of $Dy_2Ti_2O_7$ (a) SHS powder-before calcination and calcined at (b) 600 $^0$C (c) 800 $^0$C (d) 1000 $^0$C and at (e) 1200 $^0$C (Match ICDD 17-0453 cubic $Dy_2Ti_2O_7$)**

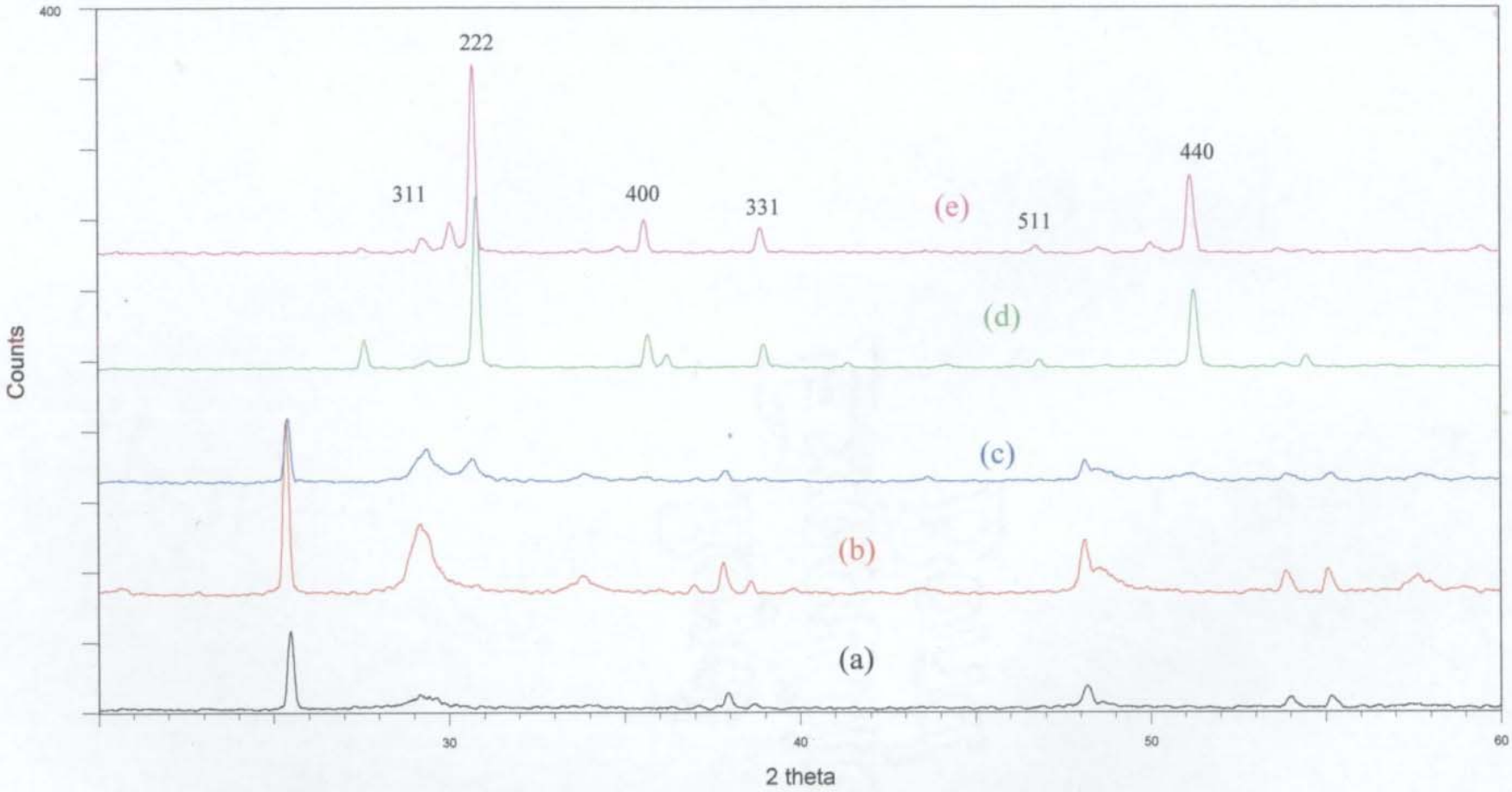


**Fig. 4.49. XRD patterns of $Y_2Ti_2O_7$ (a) SHS powder-before calcination and calcined at (b) 600 $^0$C (c) 800 $^0$C (d) 1000 $^0$C and at (e) 1200 $^0$C (Match ICDD 42-0413 cubic $Y_2Ti_2O_7$)**

**FTIR spectra**

The FTIR spectra of cubic, $RE_2Ti_2O_7$ calcined at $1200^0C$ in the region of 400 to 1000 $cm^{-1}$ are given in fig. 4.50. The spectral data clearly shows that the characteristic spectral bands of rutile, $TiO_2$ and the $RE_2O_3$ shifted significantly in the spectra of the rare earth titanates. Several new vibrations appeared in the spectra of $RE_2Ti_2O_7$ and bands due to various Ti-O and RE-O changed appreciably. The spectral data in the region 1000 to 4000 $cm^{-1}$ (Fig. 4.51) exhibit several weak absorptions. Since the samples are heated to 1200 $^0C$ the O-H, N-H, C-H etc vibrations cannot be expected. Hence, these weak absorptions may be due to overtones and combinational bands of the compounds

The FTIR spectral bands in the frequency region of interest: 400 to 1000 $cm^{-1}$ is given in table 4.15.

**Table 4.15. Characteristic FT-IR bands of cubic $RE_2Ti_2O_7$ in the range of 400 to 1000 $cm^{-1}$**

| $Sm_2Ti_2O_7$ | $Gd_2Ti_2O_7$ | $Dy_2Ti_2O_7$ | $Y_2Ti_2O_7$ | Probable Assignments |
|---|---|---|---|---|
| | | 937 vsbr | | |
| 841 m | 854 w | 835 sbr | | $A_{2u}$-LO of $TiO_2$ (811) |
| | | 793 sbr | | $E_u$-LO of $TiO_2$ (806) |
| 633 s | 669 m | 559 mbr | 681 m | |
| 588 vs | 644 m | | 644 m | |
| 544 vs | 615 m | | 615 m | |
| | 588 m | | 534 m | |
| | 548 s | | | |
| | 500 s | 493 w | | |
| 473 vvs | 476 vs | 474 w | 482 m | $E_u$-LO of $TiO_2$ (458) |
| 440 s | 444 m | | 463 vs | RE-O(B) |
| | 434 m | | 436 s | |
| | 417 m | | 413 m | |

w = weak; m = medium; s = strong vs = very strong; vvs = very very strong br = broad

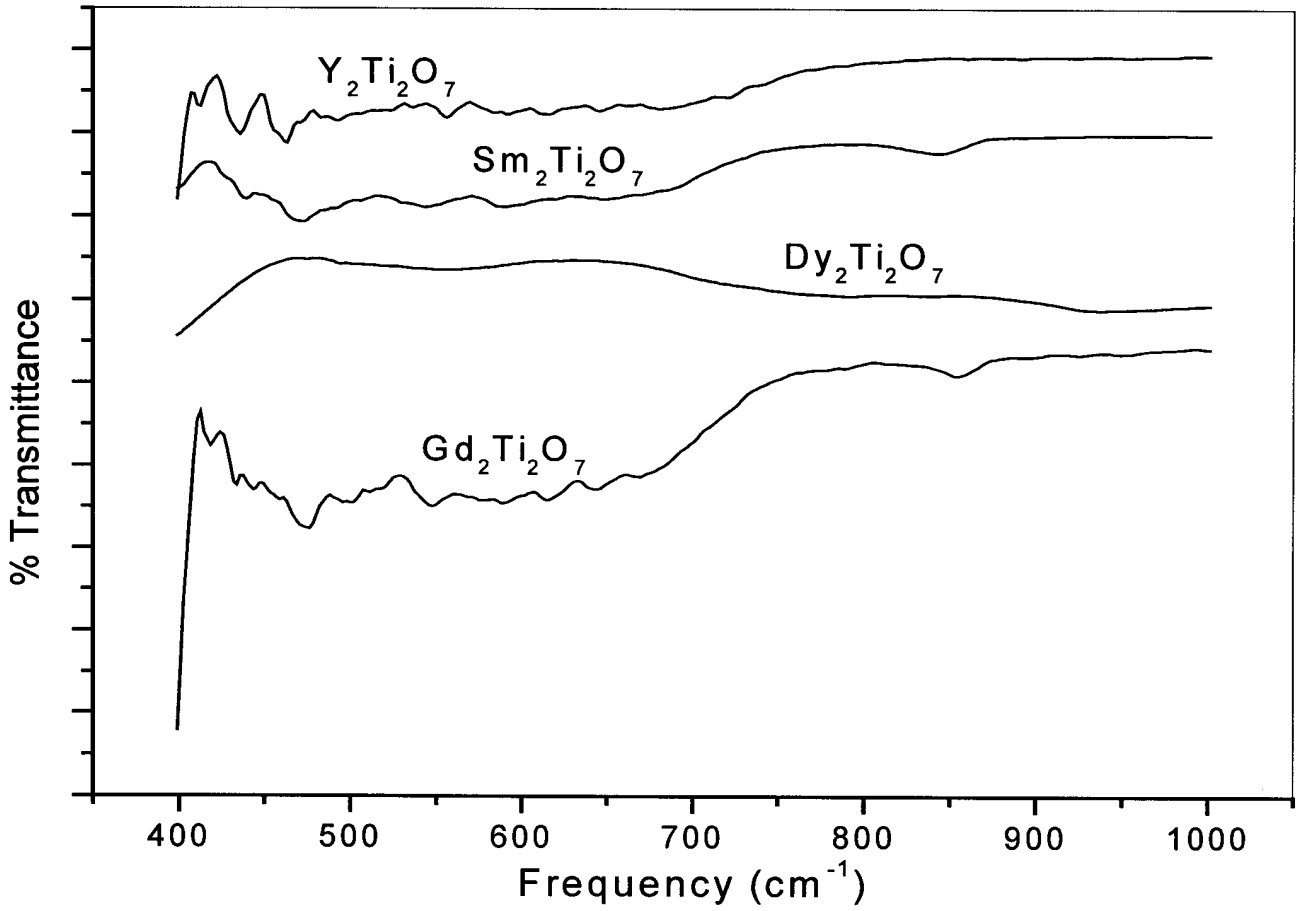


**Fig. 4.50. FTIR spectra of cubic $RE_2Ti_2O_7$ synthesized by SHS method and calcined at 1200°C (400-1000 $cm^{-1}$)**

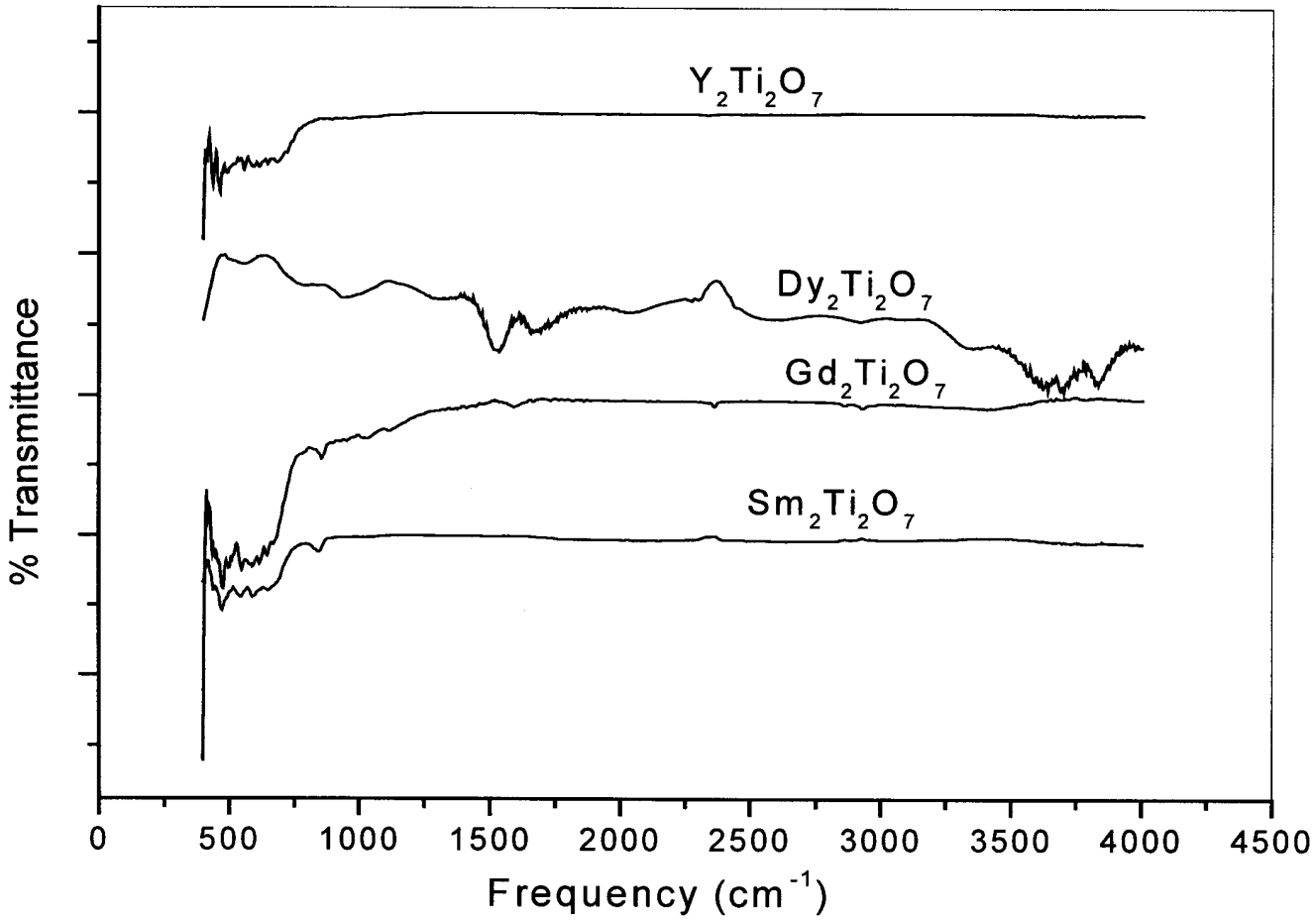


**Fig. 4.51. FTIR spectra of cubic $RE_2Ti_2O_7$ synthesized by SHS method and calcined at 1200°C (400-4000 $cm^{-1}$)**

**Laser Raman spectra**

Raman spectra of all the cubic rare earth titanates $RE_2Ti_2O_7$, (where RE = Sm, Gd, Dy and Y) synthesized by the SHS method and calcined at 1200 $^0C$ are given in fig. 4.52. The spectra were found to have the characteristic rutile reference peaks $A_1g$ (612 $cm^{-1}$) and Eg (448 $cm^{-1}$) bands at shifted positions. Important peaks and their probable assignments are given in table 4.16.

**Table 4.16. Raman spectral bands ($cm^{-1}$) for the cubic $RE_2Ti_2O_7$**

| $Sm_2Ti_2O_7$ | $Gd_2Ti_2O_7$ | $Dy_2Ti_2O_7$ | $Y_2Ti_2O_7$ | Probable Assignments |
|---|---|---|---|---|
| | 805 w | 808 w | | $B_2g$ $TiO_2$(826) |
| 795 m | 684 wbr | 698 w | 723 w | |
| 617 s | 619 s | 615 m | 627 m | $A_1g$ $TiO_2$(612) |
| 579 m | 527 s | 529 s | 540 s | RE-O(A) |
| 525 s | | | | |
| 454 s | 457 s | 455 m | 464 m | Eg $TiO_2$(447) |
| | 322 vvs | 316 vvs | 328 vvs | RE-O(D) |
| | 235 m | | | |

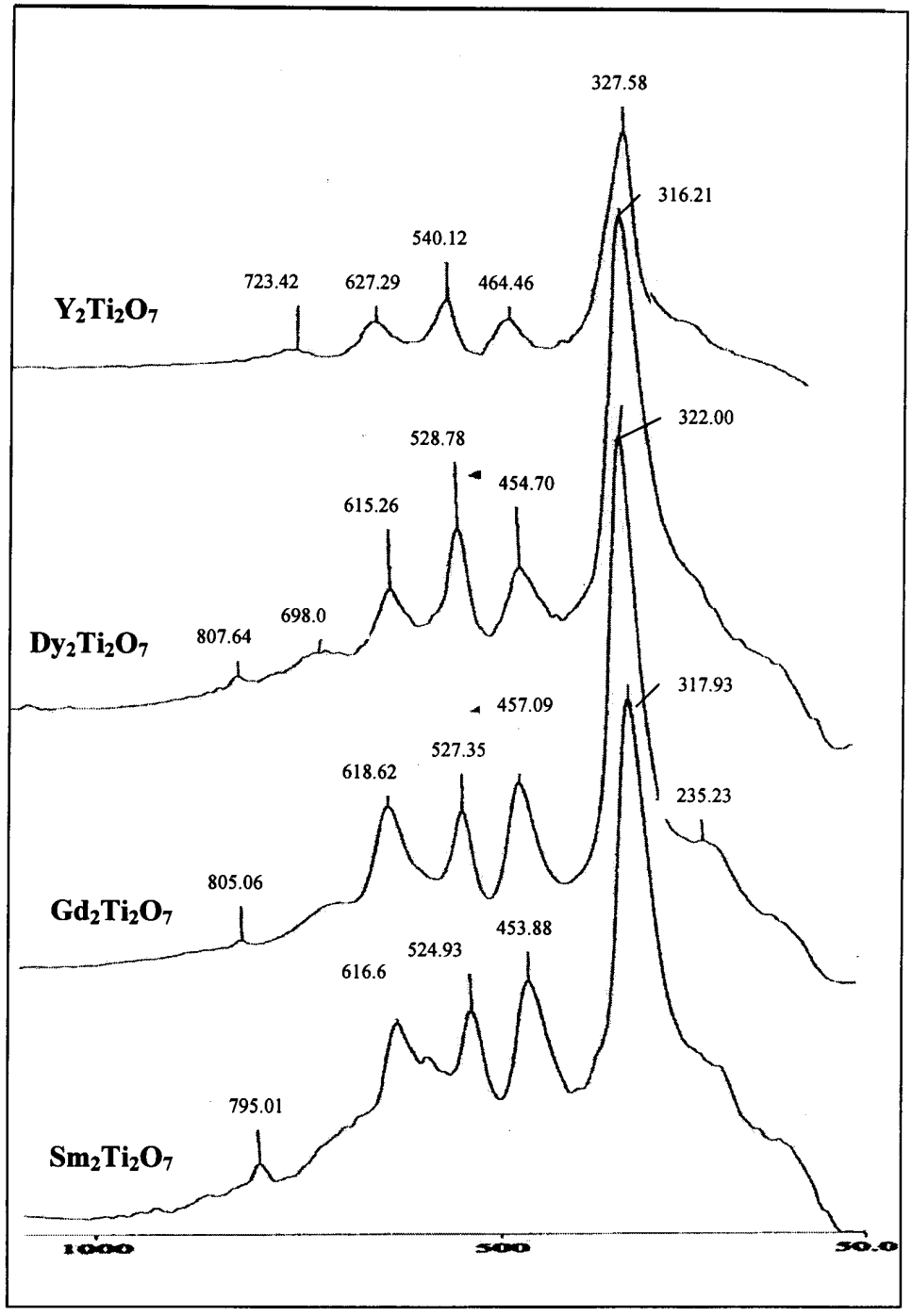


**Fig. 4.52. Raman spectra of the SHS powder of cubic $RE_2Ti_2O_7$ calcined at 1200°C**

**BET surface area analysis**

The surface area of all the cubic rare earth titanates, $RE_2Ti_2O_7$ (RE = Sm, Gd, Dy and Y) were measured using the BET surface area analyzer and from the data on density of the SHS powders, their average particle size were calculated as per the formula described in the section on monoclinic titanates. The values of surface area, and APS of the powders are given in table 4.17.

**Table 4.17. BET Surface area & APS of cubic $RE_2Ti_2O_7$ synthesized by SHS method**

| $RE_2Ti_2O_7$ (RE = ) | Density (g/cc) | Surface area ($m^2/g$) | APS (nm) |
|---|---|---|---|
| Sm | 6.311 | 11.71 | 81 |
| Gd | 6.56 | 13.67 | 67 |
| Dy | 6.86 | 2.882 | 303 |
| Y | 4.98 | 4.645 | 259 |

The BET plots of $1/[W((P_O/P)-1)]$ against relative pressure, $P/P_O$ for the four cubic rare earth titanates are given in figures 4.53 to 4.56. The data showed that the Sm and Gd titanates are nanosized particles.

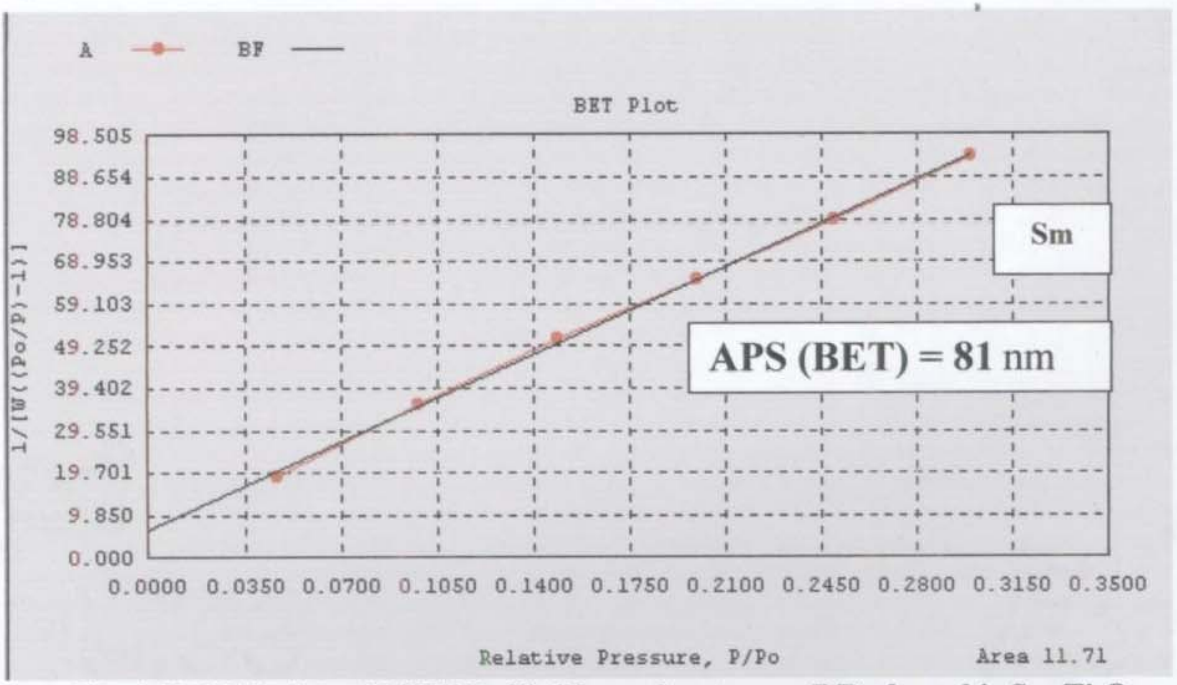


**Fig. 4.53. BET plots of $1/[W((P_O/P)-1)]$ vs rel. pressure, $P/P_O$ for cubic $Sm_2Ti_2O_7$**

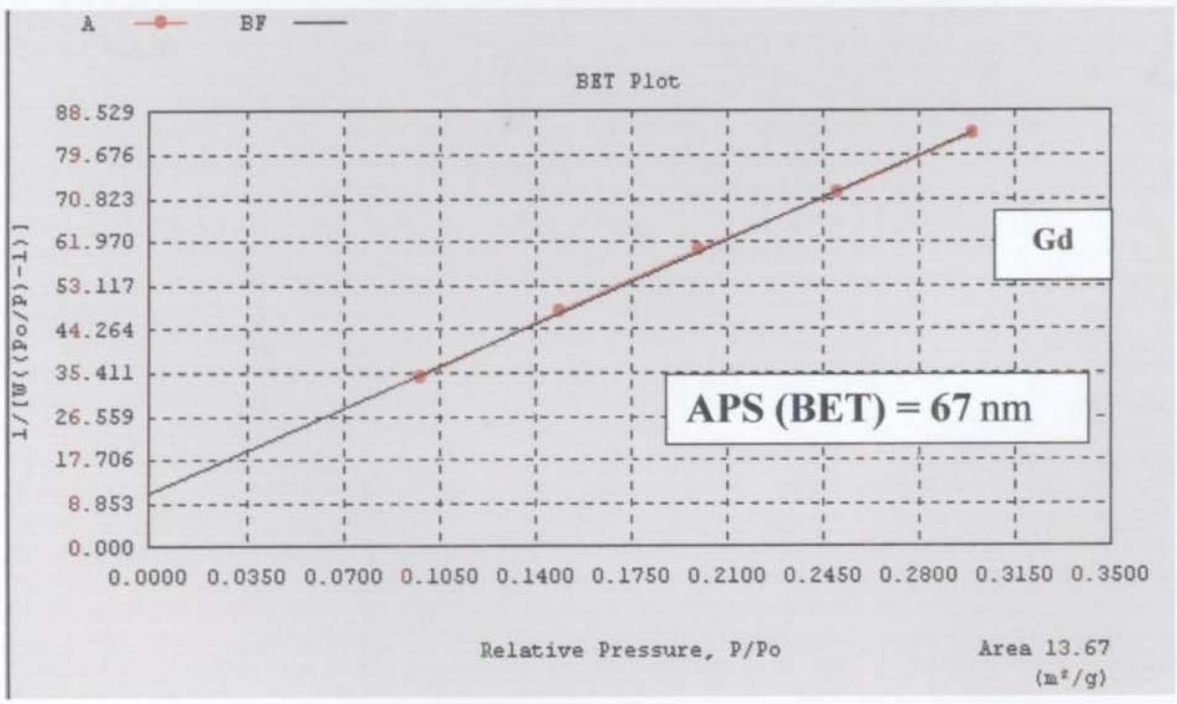


**Fig. 4.54. BET plots of $1/[W((P_O/P)-1)]$ vs rel. pressure, $P/P_O$ for cubic $Gd_2Ti_2O_7$**

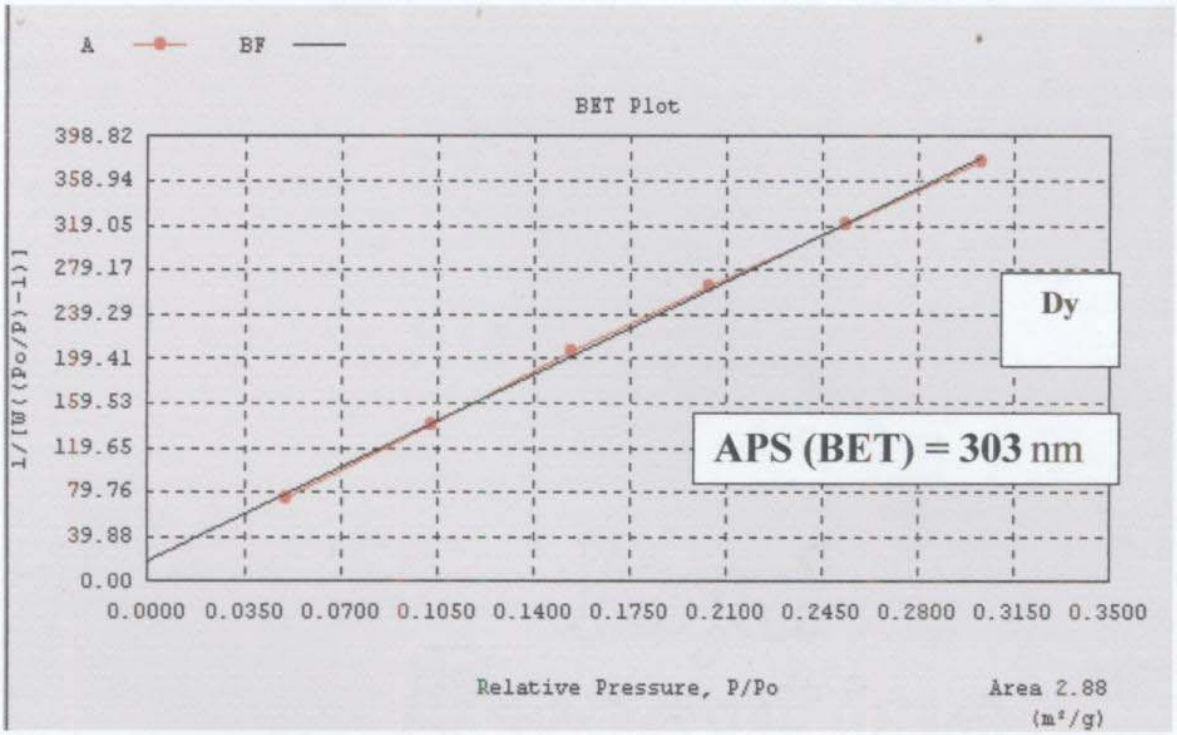


**Fig. 4.55. BET plots of 1/[W((P$_O$/P)-1)] vs rel. pressure, P/P$_O$ for cubic $Dy_2Ti_2O_7$**

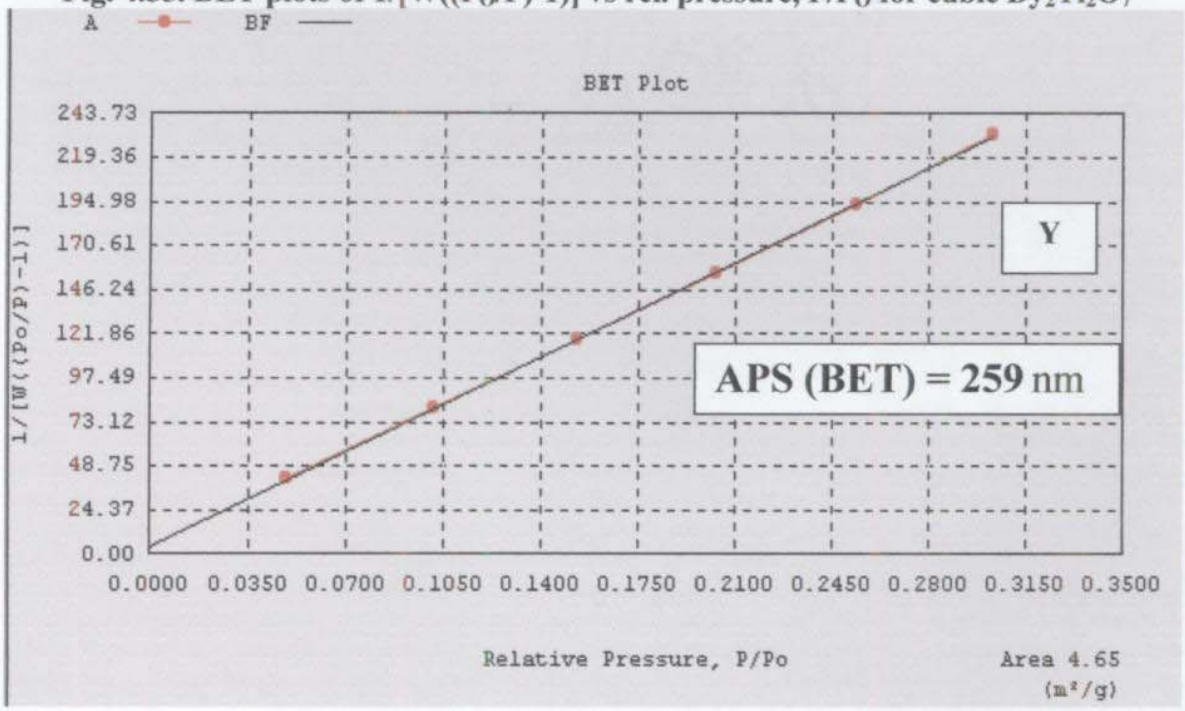


**Fig. 4.56. BET plots of 1/[W((P$_O$/P)-1)] vs rel. pressure, P/P$_O$ for cubic $Y_2Ti_2O_7$**

**SEM microstructures**

The SEM photographs of the compounds showed that the powders remain as interconnected network of porous structure and foam like appearance and very fine in size (< 100 nm) . The SEM microstructures are shown in figure 4.57.

The SEM of $Y_2Ti_2O_7$ and $Dy_2Ti_2O_7$ appear as a structure of interconnected powder particles in a porous network loosely holding the individual particles; but the SEM of $Gd_2Ti_2O_7$ and $Sm_2Ti_2O_7$ show loosely packed powders alongwith some particles, which remain, in a free state. From the physical appearance itself, it is indicative that the SHS powders of $Y_2Ti_2O_7$ and $Dy_2Ti_2O_7$ are having comparatively lower surface area and hence large particle size than the $Gd_2Ti_2O_7$ and $Sm_2Ti_2O_7$ powders. This observation is confirmed from the study of the surface area obtained of the SHS powders by BET method.

SEM microstructure of the sintered (1200 $^0$C) discs made from SHS powders of cubic crystalline rare earth titanate materials are shown in figure 4.58. A comparison with SEM structure of sintered monoclinic titanates revealed that the cubic form was not well sintered even at temperatures of 1450 $^0$C to 1500 $^0$C, unlike the monoclinic material. The size of the grains are larger for $Y_2Ti_2O_7$ with much porosity in their structure but for $Gd_2Ti_2O_7$ and $Dy_2Ti_2O_7$ the grains are smaller with less porosity. The $Dy_2Ti_2O_7$ samples have much adhesion between the grains and appear to be largely interconnected structure.

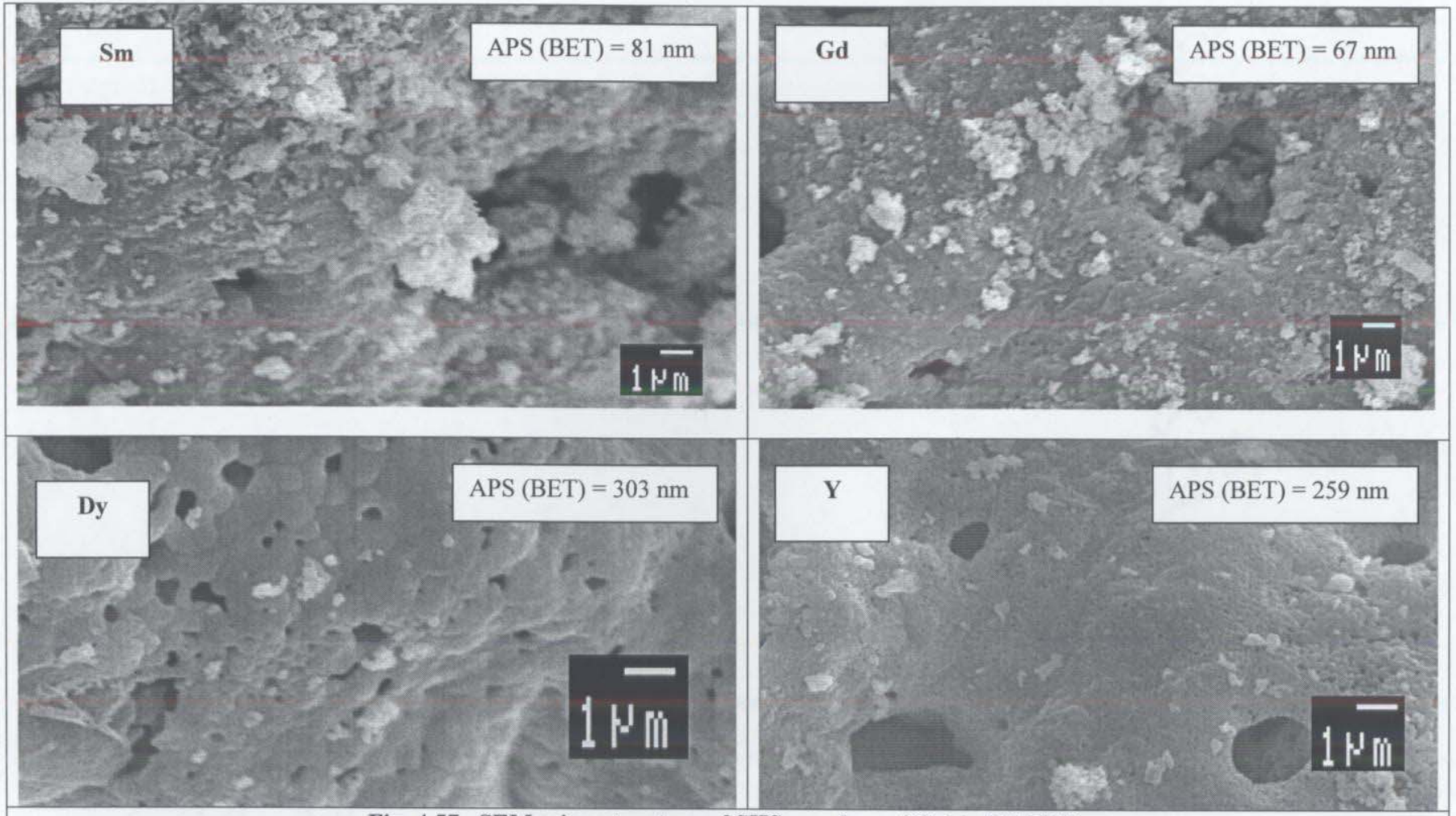


**Fig. 4.57. SEM microstructure of SHS powders of Cubic $RE_2Ti_2O_7$**

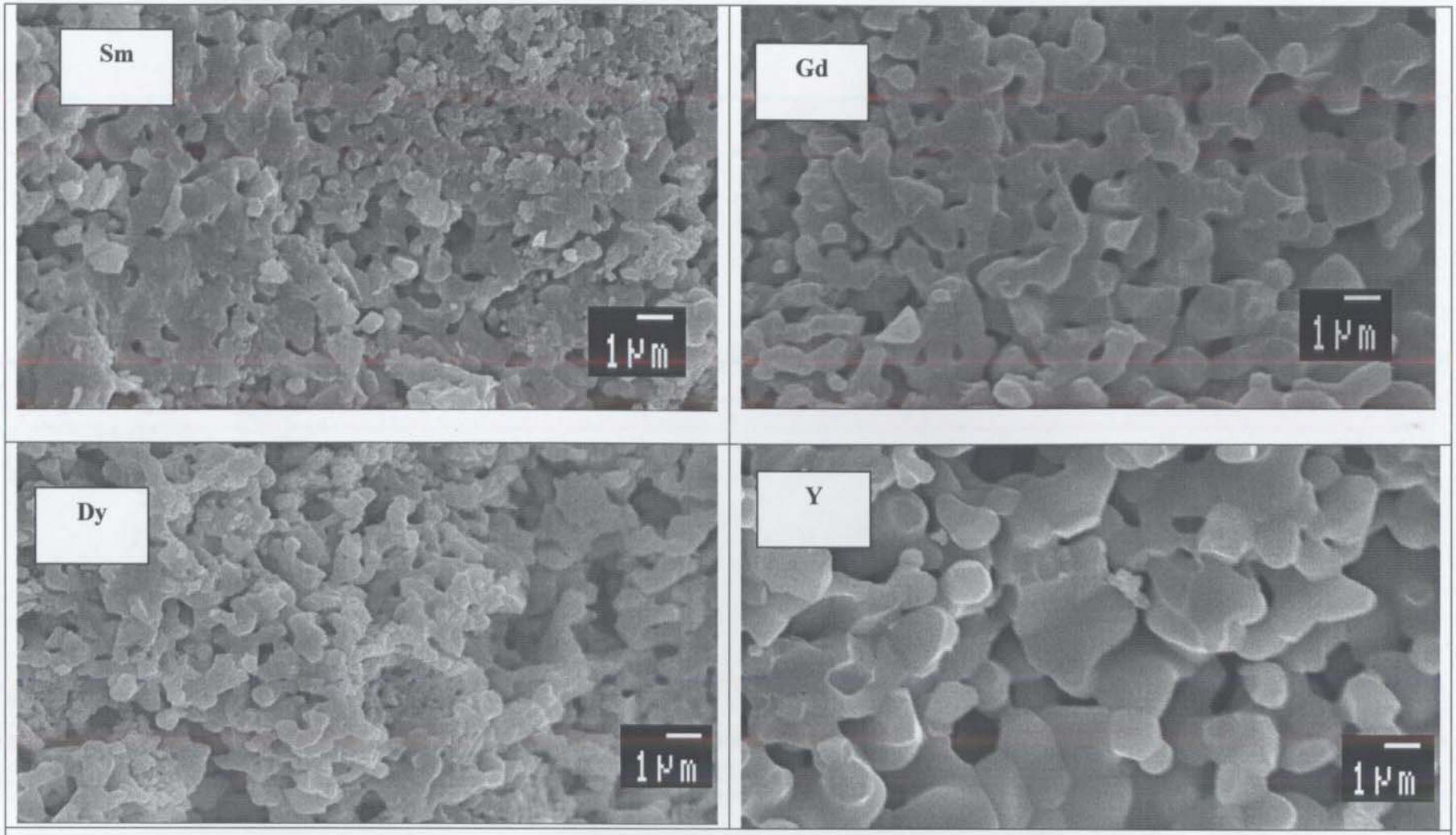


**Fig. 4.58. SEM of the cross section of sintered discs (at $1450^0$C ) of Cubic $RE_2Ti_2O_7$ made from SHS powders**

**Dielectric properties**

The permittivity values and dissipation factor obtained at different frequencies for the cubic rare earth titanates prepared by the solid state method and SHS method are presented graphically in figures 4.59 and 4.60. The measurements were made after sintering all the samples at 1525 $^0$C and 1575 $^0$C. In general, compounds synthesized by the SHS method exhibited high permittivity and low dissipation compared to the compounds from solid state method. The changes in permittivity with increasing temperature are shown in fig. 4.61. All the rare earth titanates generally exhibited a positive temperature coefficient of their permittivity values in the range from 20 $^0$C to 120 $^0$C.

**$Sm_2Ti_2O_7$:** The permittivity values show a regular decrease with increasing frequencies for the samples prepared by the SHS method and sintered at 1525 $^0$C and 1575 $^0$C, but for the samples made by the SHS method, the permittivity values remain almost constant at different frequencies. Eventhough, the dielectrics made by solid-state route show high values at low frequencies, their actual permittivity values at higher frequencies become lower than that of SHS samples.

**$Gd_2Ti_2O_7$:** While the permittivity values for the dielectrics made by the solid state route decrease with increasing frequencies, the dielectric made by SHS method remains almost constant at different frequencies. For $Gd_2Ti_2O_7$ samples made by either solid-state route or SHS and sintered at 1525 $^0$C or 1575 $^0$C, the dissipation factor at 1MHz is very low, in the range of 0.001 to 0.002 only.

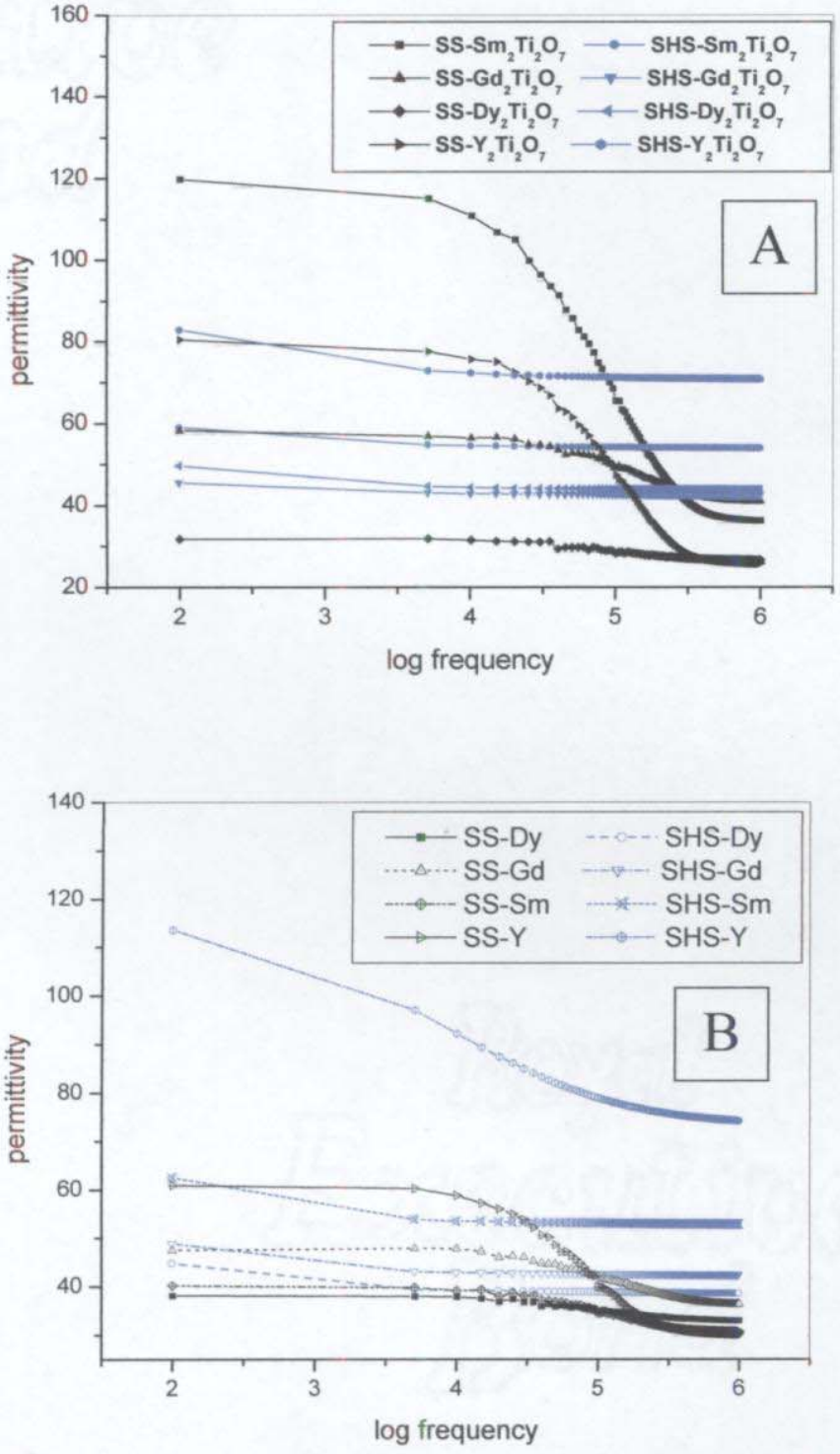


**Fig. 4.59. Changes in permittivity with frequency of cubic $RE_2Ti_2O_7$ sintered at(A)1575$^0$C and (B)1525$^0$C**

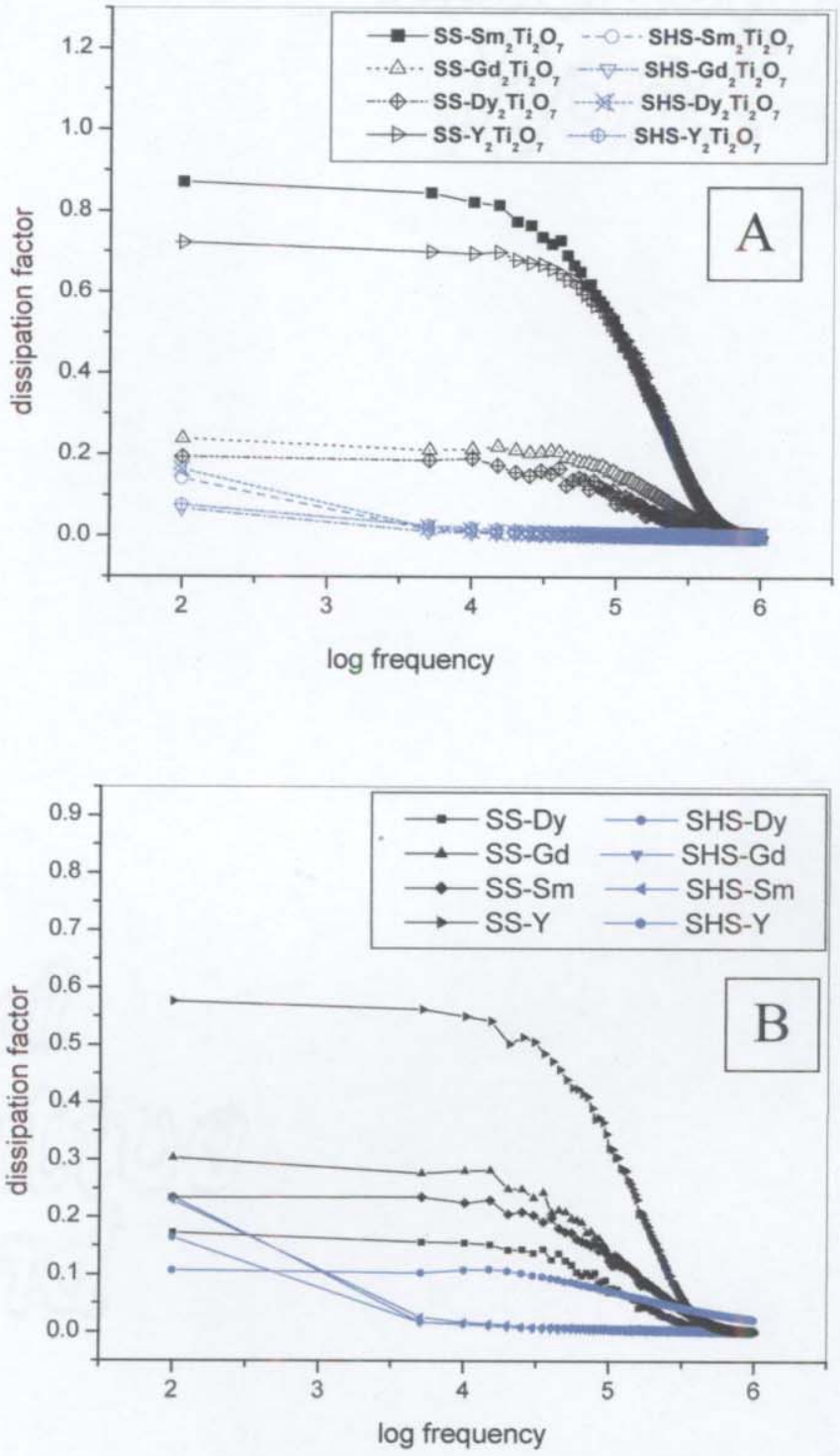


**Fig. 4.60. Changes in dissipation factor with frequency of cubic $RE_2Ti_2O_7$ sintered at (A)1575 $^0$C and (B)1525 $^0$C**

**$Dy_2Ti_2O_7$:** The $Dy_2Ti_2O_7$ samples made by SHS method are found to have higher permittivity values compared to the solid state samples at all frequencies of measurement, from 100Hz to 1 MHz. As in earlier cases, the solid state samples were found to show a decrease in permittivity with increasing frequency. At 1MHz both solid-state samples and SHS samples have very low dissipation factors of 0.001 to 0.004 whether sintered at 1525 $^0$C or 1575 $^0$C.

**$Y_2Ti_2O_7$:** Compared to the solid-state method the SHS samples of $Y_2Ti_2O_7$ exhibits very high permittivity values, e.g. at 1MHz 74.2 (for SHS) compared to 30.8 (for solid-state) for discs sintered at 1525 $^0$C and 70.9 (SHS) to 25.8 (solid state) at 1575 $^0$C. The permittivity values for solid-state samples decreased drastically with increasing frequencies. The dissipation factor values are very low for both types of samples.

Thus it appears that all the cubic rare earth titanates are good dielectrics suitable for high frequency applications.

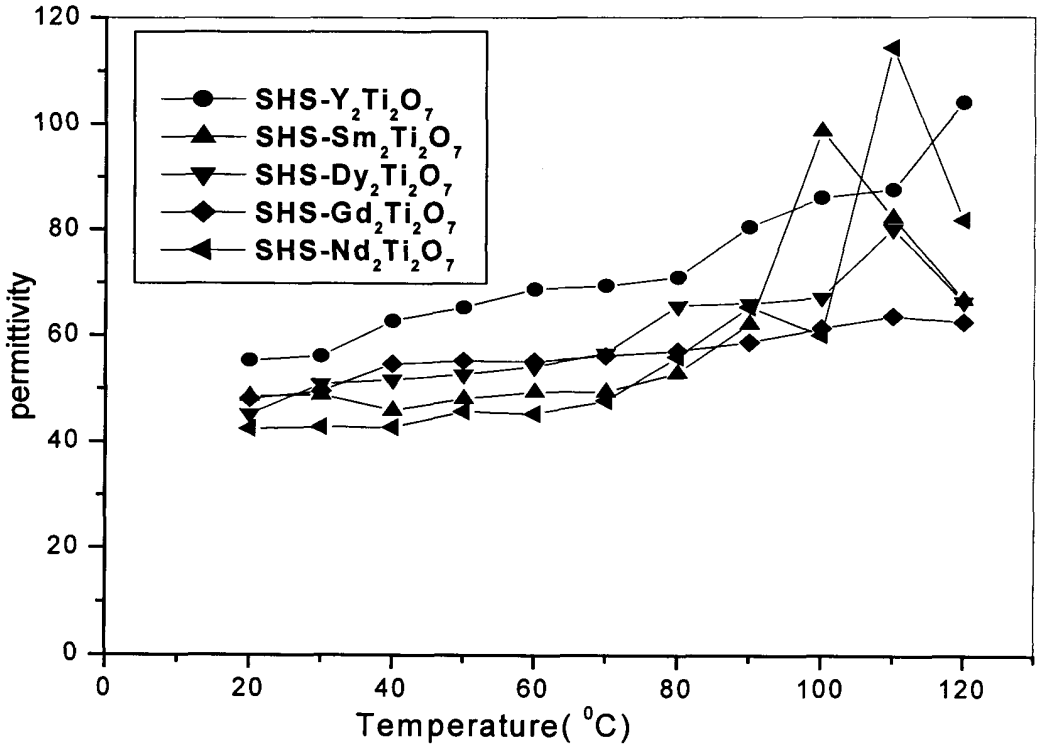


**Fig. 4-61. Changes in permittivity with temperature for the cubic $RE_2Ti_2O_7$ synthesized by SHS method**

## Optical properties

The thermal behavior of cubic rare earth titanates, $Sm_2Ti_2O_7$, $Dy_2Ti_2O_7$ and $Y_2Ti_2O_7$, synthesized by SHS method, were studied by photoacoustic (PA) technique. The variation of photoacoustic phase with square root of frequency is shown in fig. 4.62 and the changes in photothermal deflection (PTD) with the offset frequency is shown in fig. 4.63. From the slope of the plot, all the compounds are found to exhibit good thermal diffusivity.

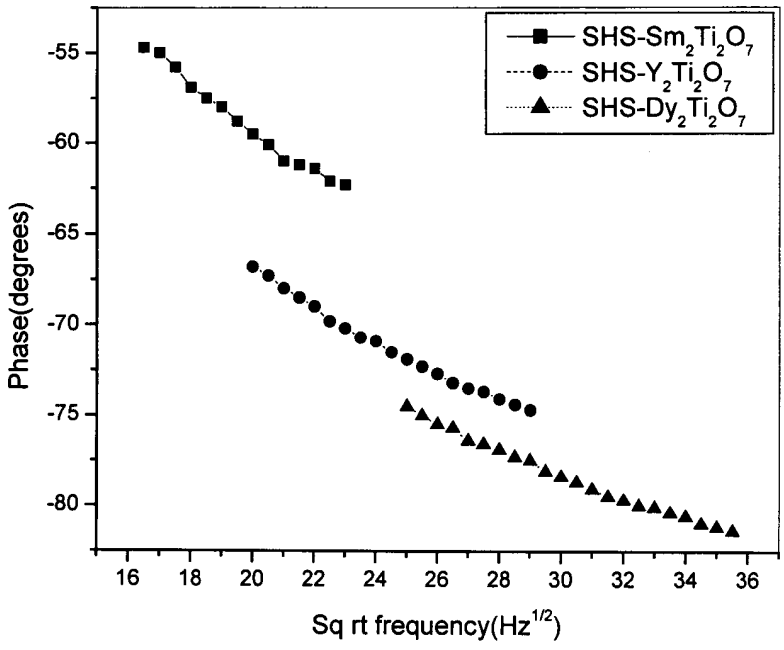


**Fig. 4.62. Variation of PA Phase with modulation frequency for Cubic rare earth titanates,$RE_2Ti_2O_7$**

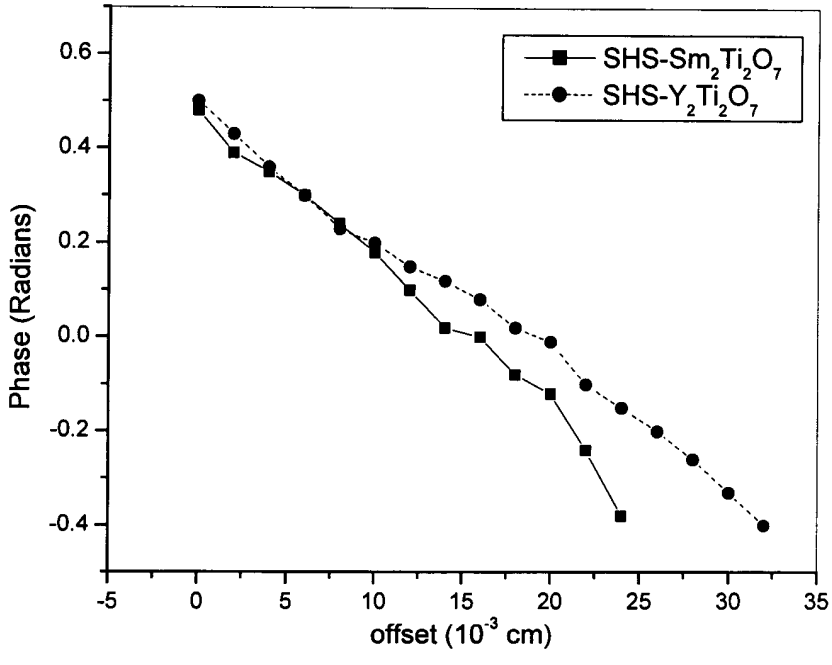


**Fig. 4.63. Variation of PTD Phase difference with offset frequency for Cubic rare earth titanates,$RE_2Ti_2O_7$**

Though the phase and amplitude of the PA signal contains clear signature of the thermal properties of the specimen, phase data is more reliable for open cell configuration, since the amplitude data depends on many external parameters such as, sample surface quality and detector response at different wavelengths. Thermal diffusivity of the samples are calculated from the slopes of the straight line graphs of PA Phase Vs square root of frequency and are tabulated in table 4.18.

**Table 4.18. Thermal diffusivity of rare earth titanates, $RE_2Ti_2O_7$ by PTD and PA techniques**

| $RE_2Ti_2O_7$ RE = | Sintering temperature ($^0C$) | Thickness of sample | $\alpha$ cm2/s(PTD) | $\alpha$ cm2/s(PA) |
|---|---|---|---|---|
| Sm | 1400 | 0.0853 | 0.0310 | 0.0317 |
| Dy | 1550 | 0.1092 | 0.0477 | 0.0480 |
| Y | 1550 | 0.1081 | ---- | 0.0795 |

## SUMMARY AND CONCLUSIONS

The study revealed that the formation structure and properties of the rare earth titanates of composition $RE_2Ti_2O_7$ are highly dependent on the nature of the starting materials and the method adopted for the synthesis. Thus, phase pure materials were not obtained by the solid state reaction between $RE_2O_3$ and $TiO_2$. Similarly, the reaction of $RE_2O_3$ and $TiO_2$ in presence of urea as SHS activator also failed to yield 100% phase pure products.

However, phase pure $RE_2Ti_2O_7$ were prepared by SHS method starting from $RE(NO_3)_3$ instead of $RE_2O_3$ using the common organic activator (fuel), urea and also using a new inorganic SHS fuel namely ammonium acetate. The

ceramic rare earth titanate obtained by using ammonium acetate were 100% phase pure. The La, Pr and Nd titanates were of monoclinic structure while the Sm, Gd, Dy and Y titanates were cubic. The APS (from BET analysis SEM microstructure) of most of compounds showed that the powders are nanosized.

The rare earth titanates synthesized by the SHS method, using ammonium acetate, exhibited good dielectric behaviour with high permittivity values. Stability at high frequencies, makes it suitable for high frequency applications. Similarly, the cubic rare earth titanates were found to exhibit good thermal diffusion, suitable for protective thermal barrier coating applications.

# SYNTHESIS AND CHARACTERISATION OF RARE EARTH TITANATES, $RE_2Ti0_5$

K.R. Dayas "Self propagated high temperature synthesis of electroceramic rare earth titanates and their characterisation " Thesis. Department of Chemistry, University of Calicut, 2006

CHAPTER 5

# SYNTHESIS AND CHARACTERIZATION OF RARE EARTH TITANATES, $RE_2TIO_5$

## EXPERIMENTAL

The rare earth titanates, $RE_2TiO_5$, were prepared by the direct solid state reaction between $TiO_2$ and $RE_2O_3$ and also by SHS reaction of $TiO_2$ and $RE(NO_3)_3$ in presence of ammonium acetate as activator. Experimental details are given below.

### A. Direct solid state reaction:

Titanium dioxide and $RE_2O_3$ (where RE = La, Pr, Nd, Sm, Gd, Dy and Y) in the 1:1 mol ratios were transferred to an agate vessel and homogeneously mixed in presence of isopropyl alcohol as the dispersion solvent and the solvent was evaporated off by placing in air oven at 120 $^0$C. The dried mass was then dispersed in a solution of 5 % polyvinyl alcohol in water to achieve a solid content of about 1.5 % PVA in the mix. It was then dried and granulated by passing through steel sieves and the sieve fraction between –50 MPI and +200 MPI of granules were taken and compacted at pressures of 3 to 5 tons per square inch to discs of dimensions around 10 mm diameter and 1.5 mm thickness. These discs were sintered at different peak temperatures: 1375 $^0$C, 1425 $^0$C, 1475 $^0$C, 1525 $^0$C and 1575 $^0$C. A bell shaped heating-cooling profile as described in the case of preparation of $RE_2Ti_2O_7$ was followed with different peak temperatures with a soaking for 2 h at the peak temperature.

## B. Preparation of $RE_2TiO_5$ by SHS reaction between $TiO_2$ and $RE(NO_3)_3$ using ammonium acetate as activator

The rare earth nitrates, $RE(NO_3)_3$ (where RE = La, Pr, Nd, Sm, Gd, Dy and Y) were prepared as discussed in **chapter 3**. To 0.04 mol of rare earth nitrate 0.24 mol ammonium acetate was added and dissolved in water to get a clear solution and to this 0.04 mol of $TiO_2$ was added and stirred well to keep the $TiO_2$ uniformally dispersed and to remain as a homogeneous suspension. The beaker was then placed in the heating cavity of an electric Bunsen and gradually heated. As the temperature increases initially water vapour leaves the vessel and the reactants become dry. On further heating copious white fumes evolve from the reactants and at ~ 400 $^0$C spontaneous evolution of gases takes place with the smell of ammonia followed by the brown gases of oxides of nitrogen. At this temperature a vigorous spontaneous incandescent reaction set in with bright flame along with evolution of large amounts of gases. The fluffy natured fine powder of the product flies out of the reaction vessel as if coming out from the 'firework flower pots'. A suitable set up of conical collector was placed at the mouth of the reaction vessel to collect the powder flying out of the reaction vessel. The highly porous product obtained was cooled and characterized as such and also after calcining at different temperatures.

A part of the SHS powder was converted to sintered discs of 10 mm diameter and 1.5 mm thickness as described in the solid-state route method and studied their dielectric properties.

## RESULTS AND DISCUSSION

**Elemental analysis:** The titanium and rare earth percentages of the rare earth titanates obtained were determined by XRF are given in table 5.1. The data conform to the composition of $RE_2TiO_5$ of all the samples prepared.

**Table 5.1. Percentage composition of $RE_2TiO_5$ by XRF**

| $RE_2TiO_5$ where RE = | % RE | | % Ti | |
|---|---|---|---|---|
| | Found for the product | Calculated | Found for the product | Calculated |
| La | 68.321 | 68.48 | 11.808 | 11.81 |
| Pr | 68.832 | 68.78 | 11.715 | 11.69 |
| Nd | 69.154 | 69.28 | 11.524 | 11.50 |
| Sm | 70.234 | 70.15 | 11.219 | 11.18 |
| Gd | 71.064 | 71.09 | 10.808 | 10.83 |
| Dy | 71.615 | 71.76 | 10.653 | 10.58 |
| Y | 58.227 | 58.16 | 15.837 | 15.67 |

**Physical characteristics**

The densification of rare earth titanates prepared by both solid state and SHS method measured after sintering at different temperatures are given in table 5.2. The data clearly show that the samples synthesized from SHS powders are comparatively denser than those made by the solid state route. Similarly the densification increases with increasing temperature and show maximum density at 1525 $^0$C. The densities of some of the compounds exhibited a decrease at 1575 $^0$C. The densities of products obtained by SHS method are more close to theoretical densities calculated for $RE_2TiO_5$ compared to that formed by solid state route. This indicates that compound formation is more facile in SHS method.

**Table 5.2. Density of $RE_2TiO_5$ samples synthesized by (a) Solid-state method and (b) SHS technique and sintered at different temperatures**

| Rare Earth | Method of synthesis | Densities (g/cc) of samples sintered at different temperatures, $^0$C | | | | | Theoretical density (g/cc) |
|---|---|---|---|---|---|---|---|
| | | 1375 | 1425 | 1475 | 1525 | 1575 | |
| Dy | (a) Solid state | 4.98 | 5.33 | 5.44 | 5.59 | 5.76 | **6.884** |
| | **(b) SHS** | **5.52** | **6.03** | **5.54** | **6.30** | **6.11** | |
| Gd | (a) Solid state | 4.73 | 5.05 | 5.24 | 5.39 | 5.28 | **6.593** |
| | **(b) SHS** | **5.13** | **5.73** | **5.73** | **5.83** | **5.74** | |
| Sm | (a) Solid state | 5.25 | 5.34 | 5.07 | 5.09 | 4.86 | **6.247** |
| | **(b) SHS** | **5.24** | **5.38** | **5.48** | **5.69** | **5.50** | |
| Nd | (a) Solid state | 3.58 | ----- | ------ | 3.86 | ------ | **5.913** |
| | **(b) SHS** | **4.75** | **5.06** | **5.09** | **5.12** | **5.16** | |
| Pr | (a) Solid state | 4.12 | 4.24 | 4.21 | 4.22 | 4.17 | **----** |
| | **(b) SHS** | **4.79** | **4.75** | **4.72** | **4.80** | **4.79** | |
| La | (a) Solid state | ---- | ----- | ------ | 3.75 | 3.78 | **5.448** |
| | **(b) SHS** | **3.72** | **-----** | **4.15** | **4.68** | **4.89** | |
| Y | (a) Solid state | 3.15 | 3.31 | 3.41 | 3.68 | 3.70 | **4.713** |
| | **(b) SHS** | **3.75** | **3.93** | **4.13** | **4.30** | **4.29** | |

**XRD crystal structure studies**

The XRD spectra of the products prepared by solid state revealed that the compounds are not phase pure and various peaks in the spectra are not matching with standard spectral peaks. Therefore the XRD data of the compounds obtained by the SHS method are only discussed here.

It has been reported that in general, as synthesized $RE_2TiO_5$, possess orthorhombic crystal structure. The XRD data obtained for the compounds

synthesized by SHS method and calcined at 1200 $^0$C and even 1300 $^0$C are given in figures 5.1 to 5.7. The observed peaks are not matching correctly with the standard JCPDS files of respective $RE_2TiO_5$ compounds of orthorhombic structures. The spectra were found to contain some additional peaks and hence it appears that the products formed by SHS method are not phase pure. However the spectra contained several peaks characteristic of the $RE_2O_3$ (indexed as '#' in the XRD spectra) and $RE_2Ti_2O_7$ (indexed as '*') and these peaks became prominent in the spectrum of the material calcined at 1300 $^0$C. Since these additional peaks are not well developed in the spectrum of the product before calcinations, it can be concluded that at higher temperatures the $RE_2TiO_5$ decomposes to $RE_2Ti_2O_7$ and $RE_2O_3$. A possible reaction path for this process is

$$2\ RE_2TiO_5 \rightarrow RE_2Ti_2O_7 + RE_2O_3.$$

A comparison of the XRD spectra of all the rare earth titanates revealed that the degree of decomposition is dependent on the nature of rare earths. The decomposition is the highest in the case of $Y_2TiO_5$ and lowest for $Dy_2TiO_5$ and the observed order is Y > La > Gd > Sm > Nd > Pr > Dy.

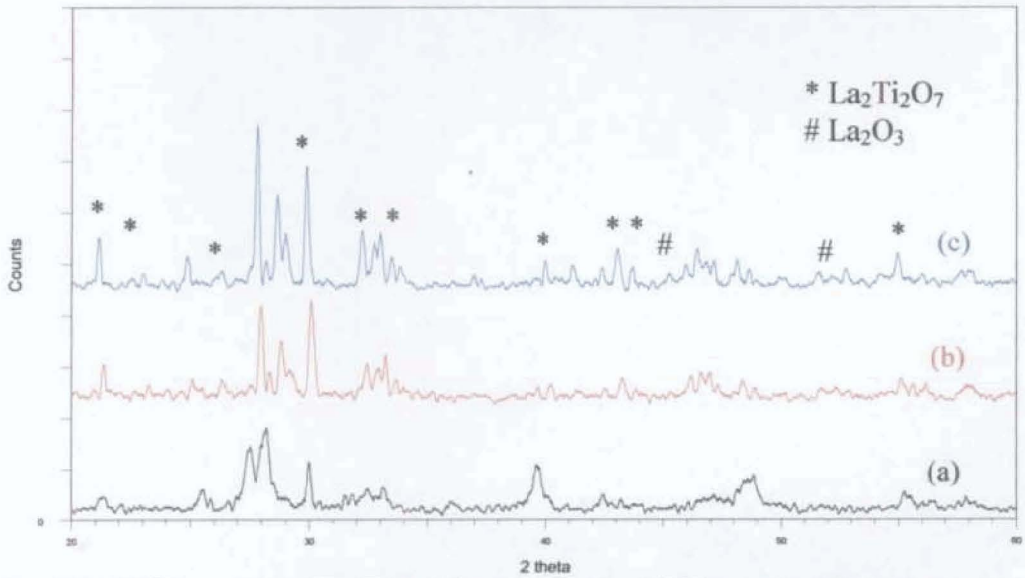


**Fig. 5.1. XRD spectra of $La_2TiO_5$ (a) as synthesised SHS powder at temperatures (b) calcined 1200 $^0$C and (c) 1300 $^0$C**

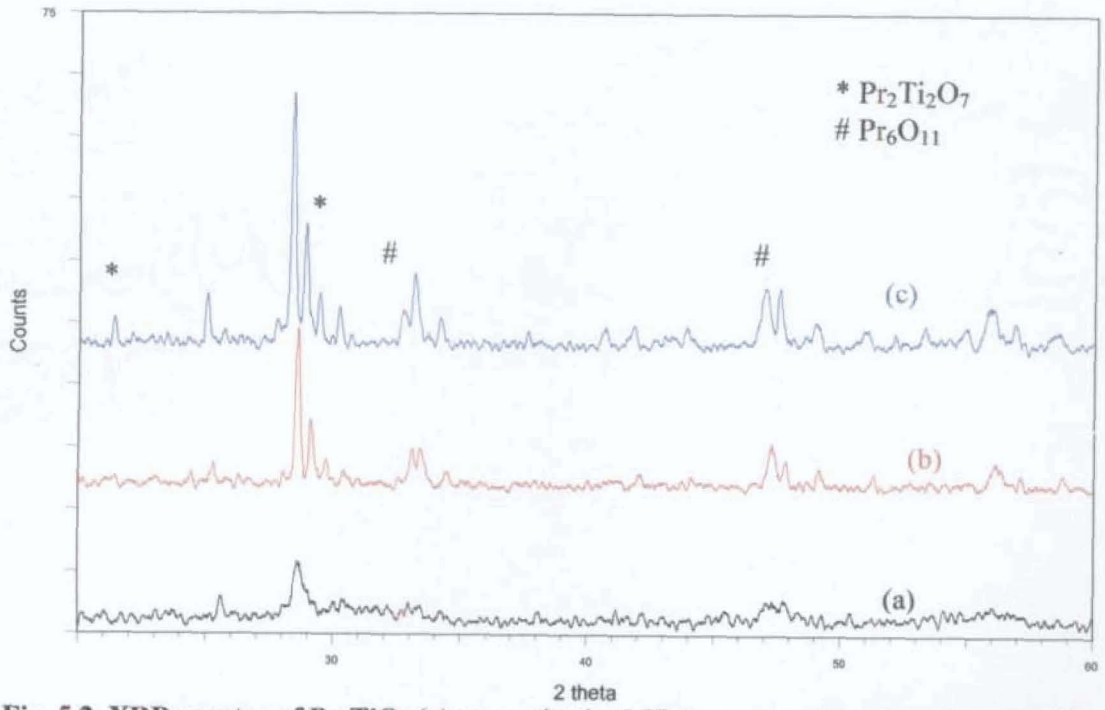


**Fig. 5.2. XRD spectra of $Pr_2TiO_5$ (a) as synthesised SHS powder (b) calcined at 1200 °C and (c) 1300 °C**

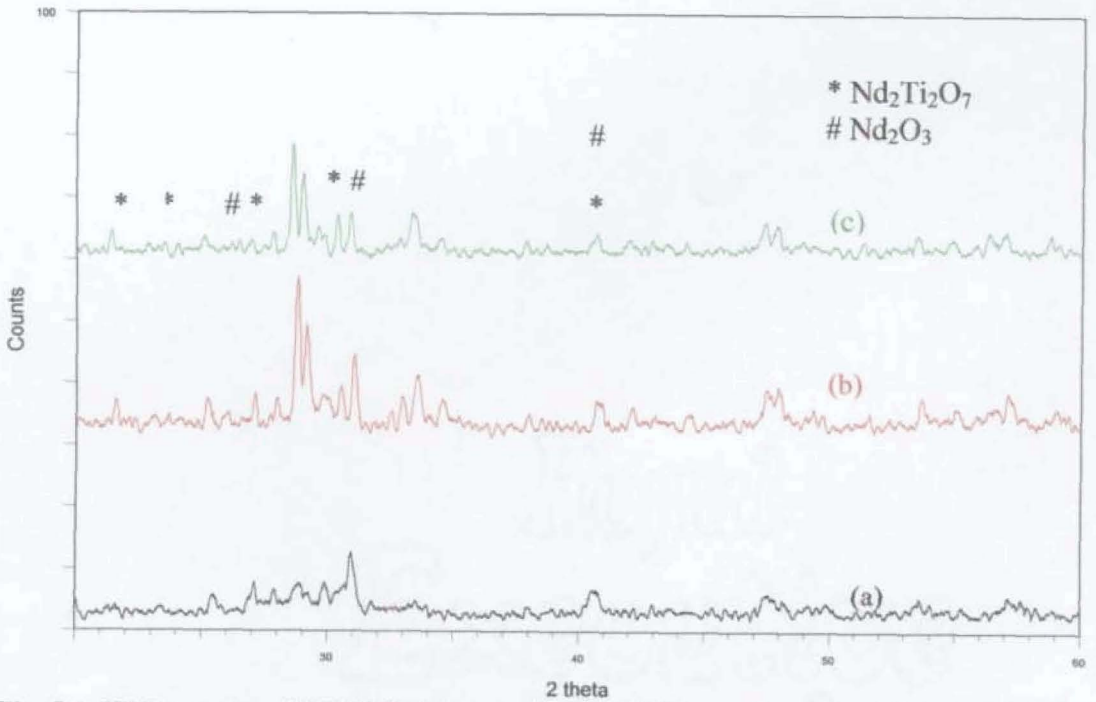


**Fig. 5.3. XRD spectra of $Nd_2TiO_5$ (a) as synthesised SHS powder (b) calcined at 1200 °C and (c) 1300 °C**

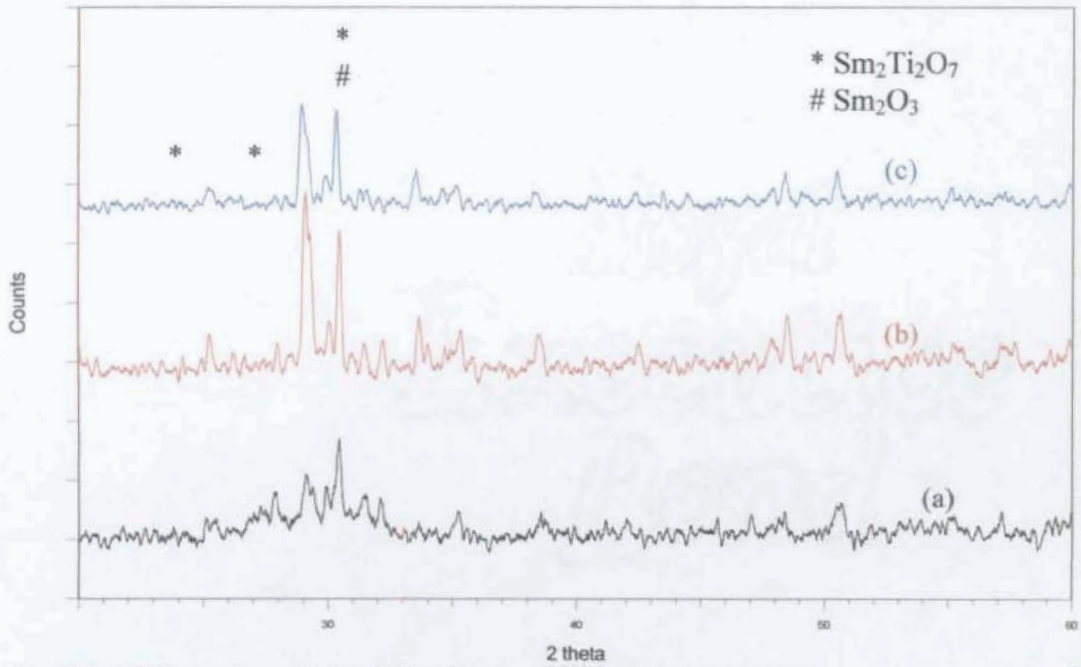


**Fig. 5.4. XRD spectra of $Sm_2TiO_5$ (a) as synthesised SHS powder (b) calcined at 1200 °C and (c) 1300 °C**

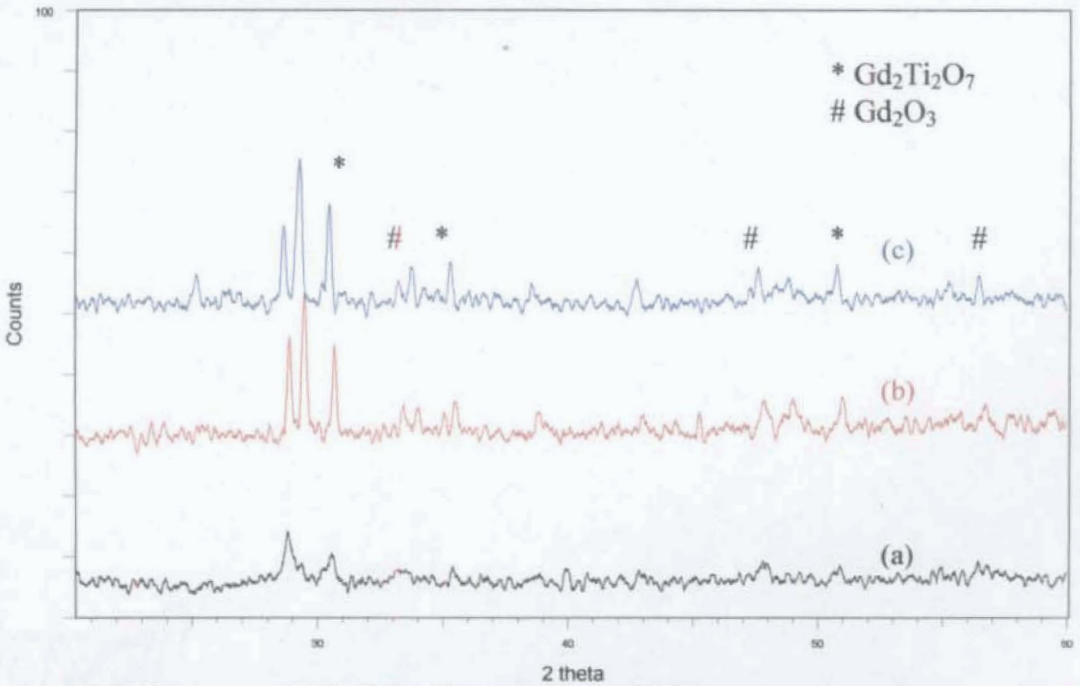


**Fig. 5.5. XRD spectra of $Gd_2TiO_5$ (a) as synthesised SHS powder (b) calcined at 1200 °C and (c) 1300 °C**

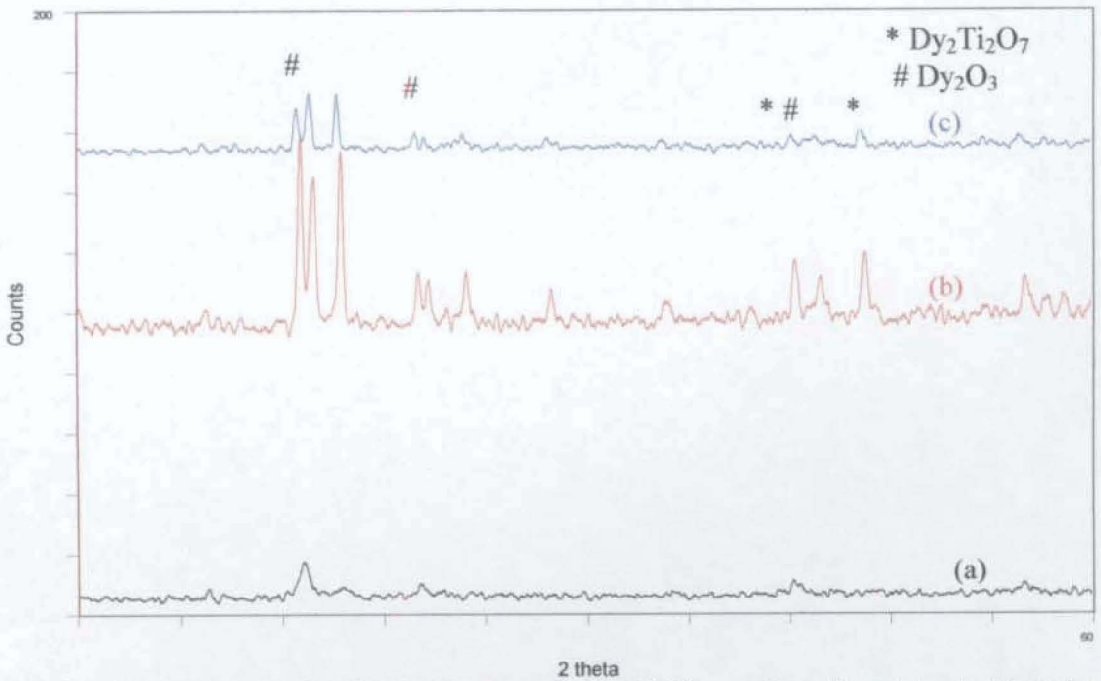


**Fig. 5.6. XRD spectra of $Dy_2TiO_5$ (a) as synthesised SHS powder (b) calcined at 1200 °C and (c) 1300 °C**

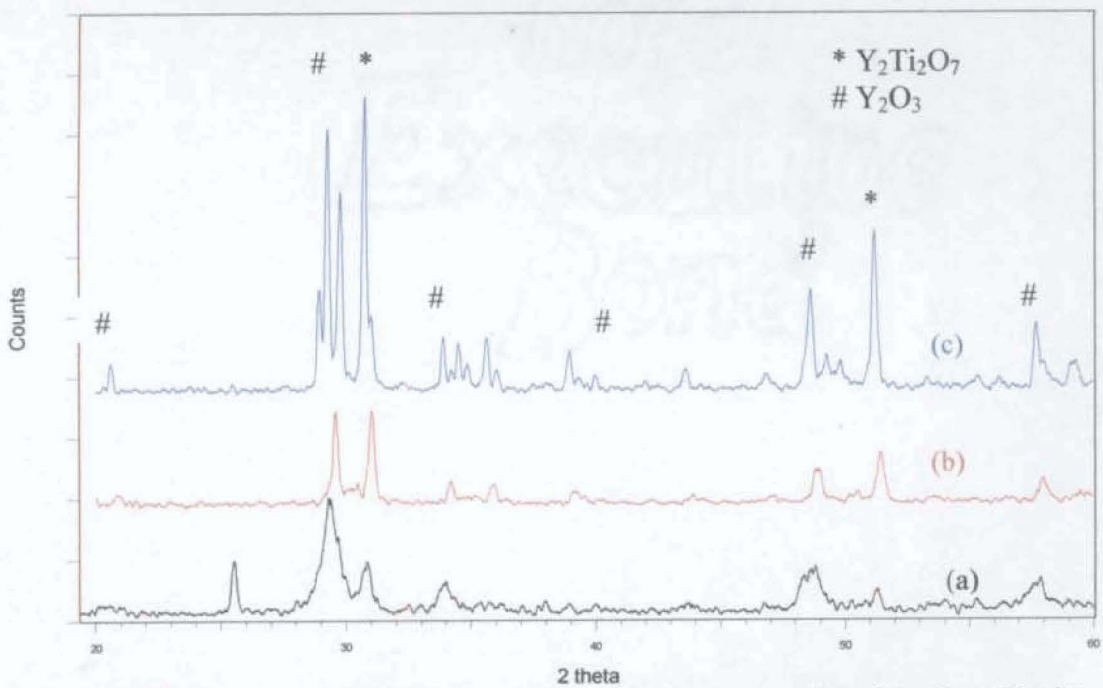


**Fig. 5.7. XRD spectra of $Y_2TiO_5$ (a) as synthesised SHS powder (b) calcined at 1200 °C and (c) 1300 °C**

**FTIR spectral studies**

The characteristic peaks for rutile ($TiO_2$), and the oxides of rare earths ($RE_2O_3$ with the bixbyte structure) in the IR and Raman spectra which are given under the "FTIR spectral studies of monoclinic pyrochlores, $RE_2Ti_2O_7$" in chapter 4 are used for comparison of FTIR spectral data of $RE_2TiO_5$ compounds.

The spectral bands of the compounds synthesized by the SHS method and the powder calcined at 1200 $^0$C in the range of wave number 400 to 1000 $cm^{-1}$ only have been considered for comparison.

**Table 5.3. Characteristic frequency of FT-IR peaks $RE_2TiO_5$ in the range 400 to 1000 $cm^{-1}$**

| $TiO_2/RE_2O_3$ Ref. peak | Characteristic bands of | | | | | |
|---|---|---|---|---|---|---|
| | $La_2TiO_5$ | $Pr_2TiO_5$ | $Sm_2TiO_5$ | $Gd_2TiO_5$ | $Dy_2TiO_5$ | $Y_2TiO_5$ |
| $A_{2u}$: LO | **810** | ------ | ------ | ------ | ------ | ------ |
| or $B_2g$ (rutile) | ------ | **822.6** | **836.8** | **846.9** | **853.6** | ------ |
| | **758.6** | **747.3** | ------ | ------ | ------ | ------ |
| $A_1g$ (rutile) | **623.9** | **610.9** | ------ | ------ | **617.2** | ------ |
| A (of $RE_2O_3$) | **579.4** | ------ | **584.2** | **599.5** | ------ | **566.1** |
| B (of $RE_2O_3$) | ------ | ------ | ------ | **472.0** | **477.9** | ------ |
| Eg (rutile) | **463.7** | **455.4** | **463.5** | **441.9** | ------ | **464.3** |

All the $RE_2TiO_5$ except the $Y_2TiO_5$ were found to have the $A_{2u}$: LO or $B_2g$ peak of rutile, with slight shift in position. Similarly the Eg peak of rutile also found at shifted positions in the titanates except $Dy_2TiO_5$.The FTIR spectra are shown in figures 5.8.

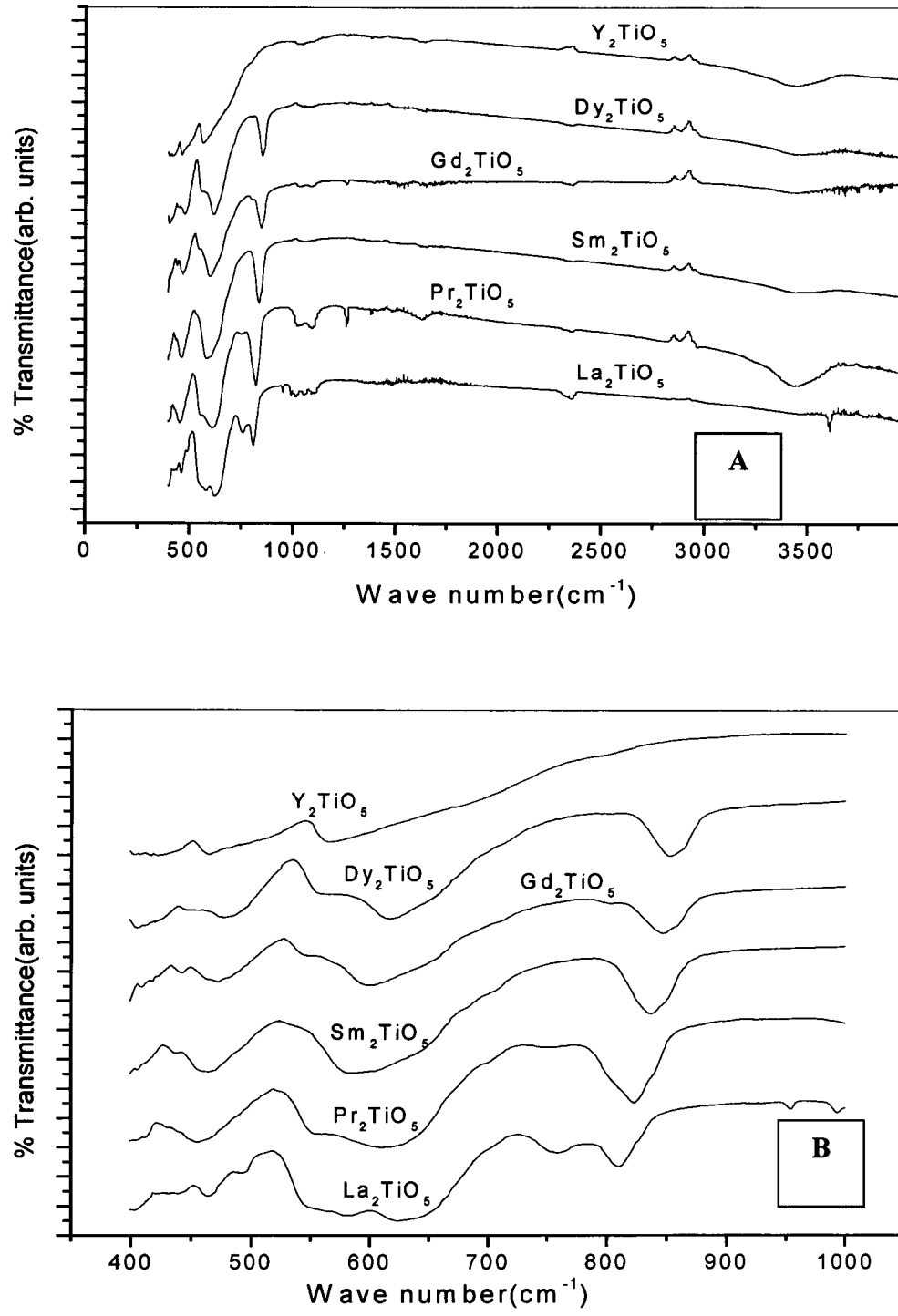


**Fig. 5.8. FTIR spectra of $RE_2TiO_5$ made by SHS method and calcined at 1200 $^0$C (A) 400-4000 & (B) 400-1000 cm$^{-1}$**

In order to get some information regarding the various reactions that are occurring during the SHS reaction, the IR spectrum of the SHS powder of $Sm_2TiO_5$ was compared with the IR spectra of the products formed at different stages of the reaction. These data were also compared with the spectra of the reactants – $TiO_2$, ammonium acetate and $Sm(NO)_3$ – used for the SHS reaction. All these spectra are brought out in figure 5.9.

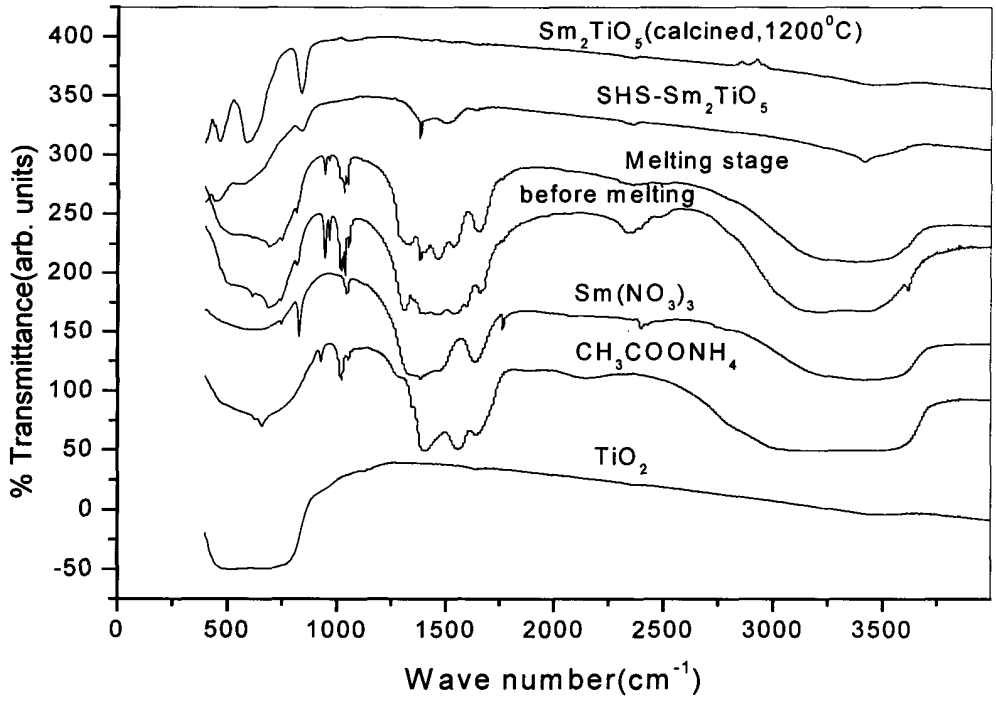


**Fig. 5.9. FTIR spectra of different stages of the intermediates, starting materials and the product in the synthesis of $Sm_2TiO_5$ by SHS method (A) 400-4000 & (B) 400-1000 $cm^{-1}$**

In the spectrum of the product recorded before the SHS reaction characteristic peaks of all the reactants are present. At the melting stage of the reaction also these bands are observed with considerable decrease in intensity. However, spectrum of the SHS powder obtained before calcination most of the

characteristic bands of the reactants disappeared and revealed the presence of certain new broad bands. Some of these broad bands transferred to sharp and intense peaks in the spectrum of the SHS powder calcined at 1200°C. These bands can be considered as due to the characteristic vibrations of the rare earth titanates.

**SEM microstructures**

The SEM pictures of powders synthesized by the SHS method showed that the material is very fluffy in nature with sponge like interconnected porous network and can easily be smashed to particles of very fine size of the order of <100 nm. The SEM microstructures of typical $RE_2TiO_5$ (RE = Nd, Sm) are shown in figs. 5.10 and 5.11.

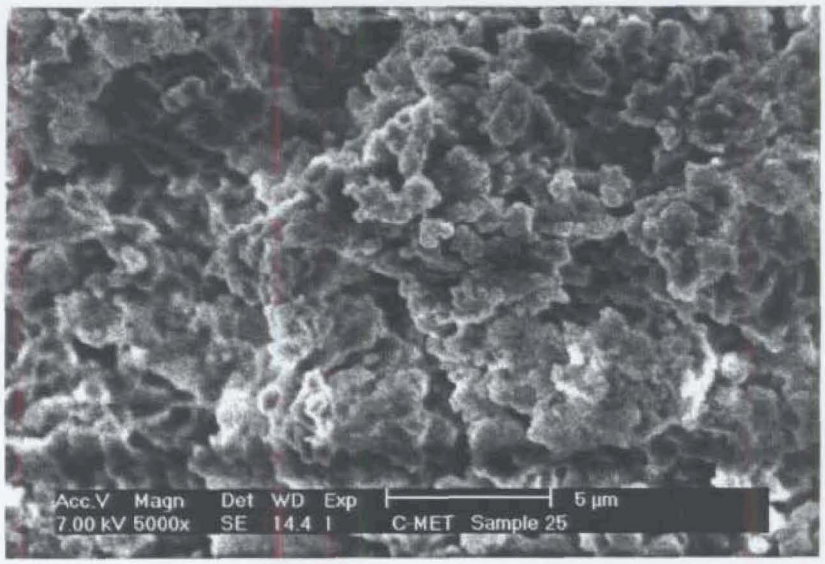


**Fig. 5.10. SEM of $Nd_2TiO_5$ Synthesized by SHS method**

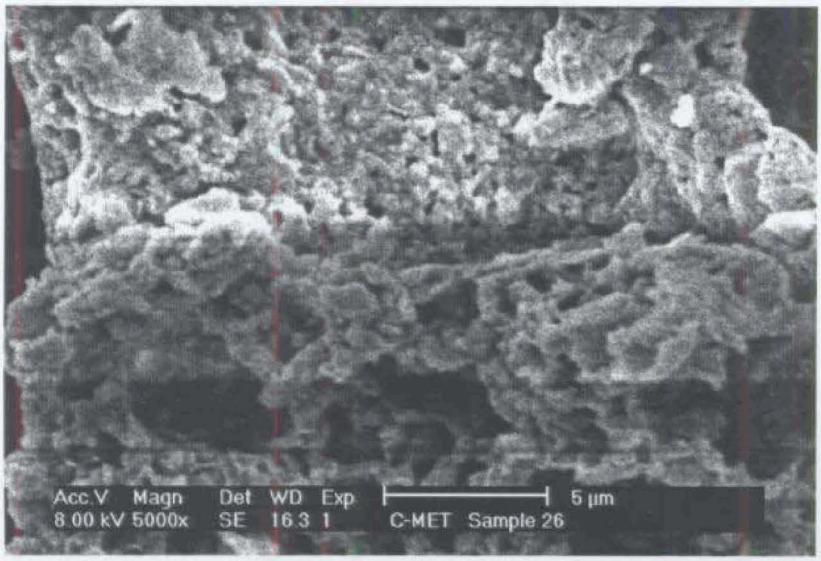


**Fig. 5.11. SEM of $Sm_2TiO_5$ Synthesized by SHS method**

**Dielectric properties**

The dielectric properties (permittivity and dissipation factor) of the compounds sintered at different temperatures were measured in the frequency range 100 Hz to 10 MHz. Reproducible values were obtained only in the case of samples sintered at 1525 $^0$C and 1575$^0$C.

The permittivity values of the $RE_2TiO_5$ (where RE = La, Pr, Nd, Sm, Gd, Dy and Y) are comparatively lower than the dielectric properties observed in the case of $RE_2Ti_2O_7$ compounds. The dielectric values are initially high at lower frequencies but become steady at frequencies above 1 kHz. The steady state permittivity values are compared for the samples made by both SHS route and solid-state method that were sintered at a peak temperatures, 1525 $^0$C and 1575 $^0$C. The permittivity values of $RE_2TiO_5$ prepared by the solid state and SHS methods at different frequencies are given graphically in figure 5.12. The values show that for $RE_2TiO_5$, whether it is synthesized by solid state method or by SHS technique and sintered at 1525 $^0$C or at 1575 $^0$C, the permittivity values do not differ much. But for La the

permittivity value for sample sintered at 1575 $^0$C is high for SHS route (34) compared to the solid-state method (16).

The dissipation factor values are slightly high for $RE_2TiO_5$ samples made by SHS method and solid-state route, but become lower for very high frequencies (Fig. 5.13). Thus the dielectric properties of compounds of $RE_2TiO_5$ are not desirable to be selected for such applications compared to the good dielectric properties of $RE_2Ti_2O_7$ compounds, which are having high permittivity and very low dissipation factor for the samples synthesized by SHS technique which make them attractive candidates for high frequency, microwave dielectric applications. The figures show that variation in permittivity and dissipation factor of samples with sintering temperatures is marginal, except in the case of $Pr_2TiO_5$. The most interesting observation is that the permittivity and dissipation factor of all the samples except Pr remain steady in the entire frequency range, a desired characteristic property of good dielectric for microwave applications. The $Pr_2TiO_5$ showed very high permittivity at low frequency and very low permittivity at high frequencies.

## SUMMARY AND CONCLUSIONS

Rare earth titanates of composition $RE_2TiO_5$ were prepared by solid state method using $RE_2O_3$ and $TiO_2$ and by SHS method using $RE(NO_3)_3$ and $TiO_2$ in presence of ammonium acetate as fuel. The crystalline nature of the materials obtained by the SHS method were indicated from XRD data. The SEM photoraphs showed their nano sized character. But at high temperatures (above 1000°C) the compounds transformed to $RE_2Ti_2O_7$ and $RE_2O_3$. The permitivity and dissipation factor showed that the materials are suitable as good dielectrics from microwave applications.

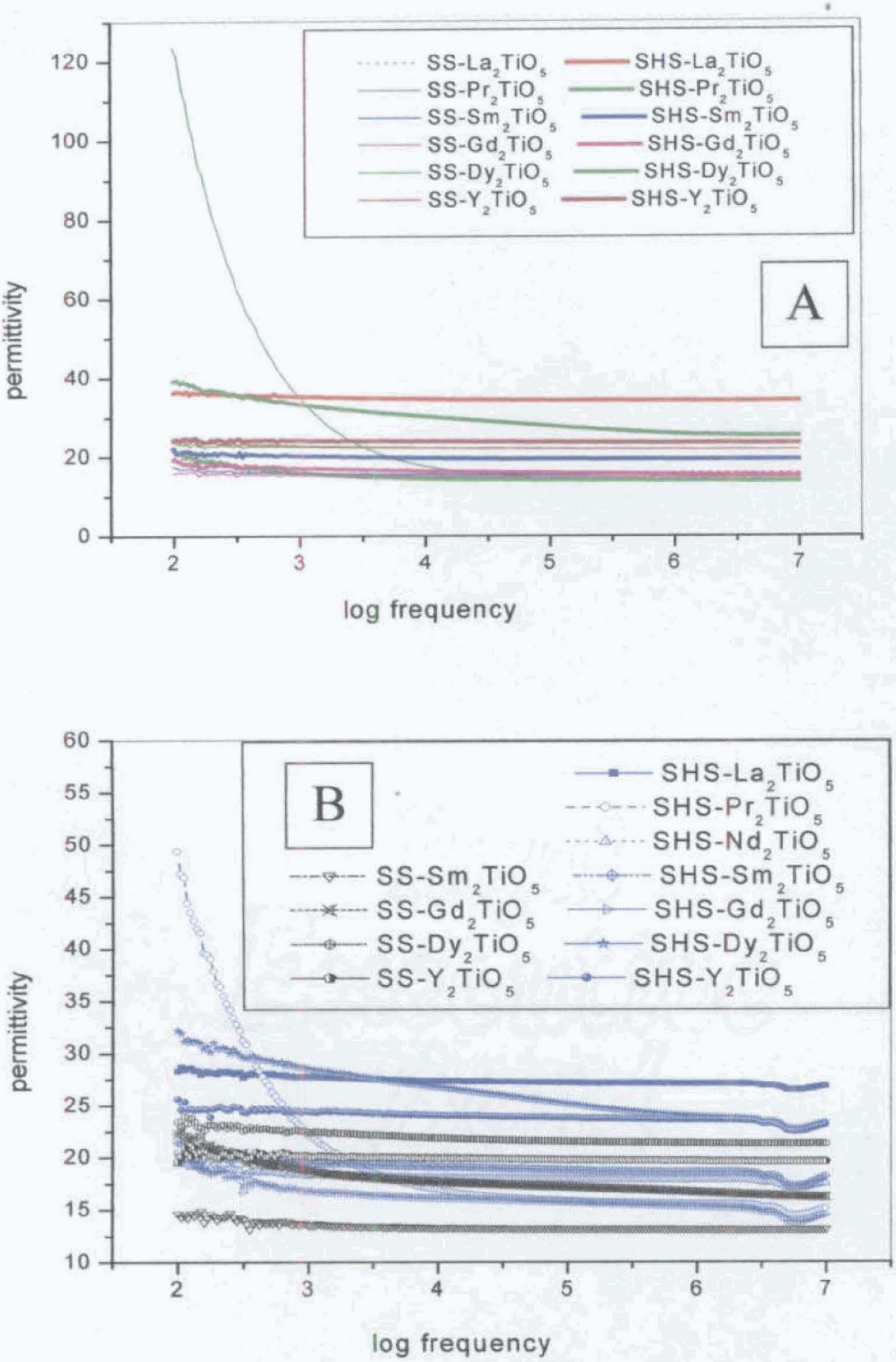


**Fig. 5.12. Changes in permittivity with frequency of $RE_2TiO_5$ samples sintered at (A)1575$^0$C and (B)1525$^0$C**

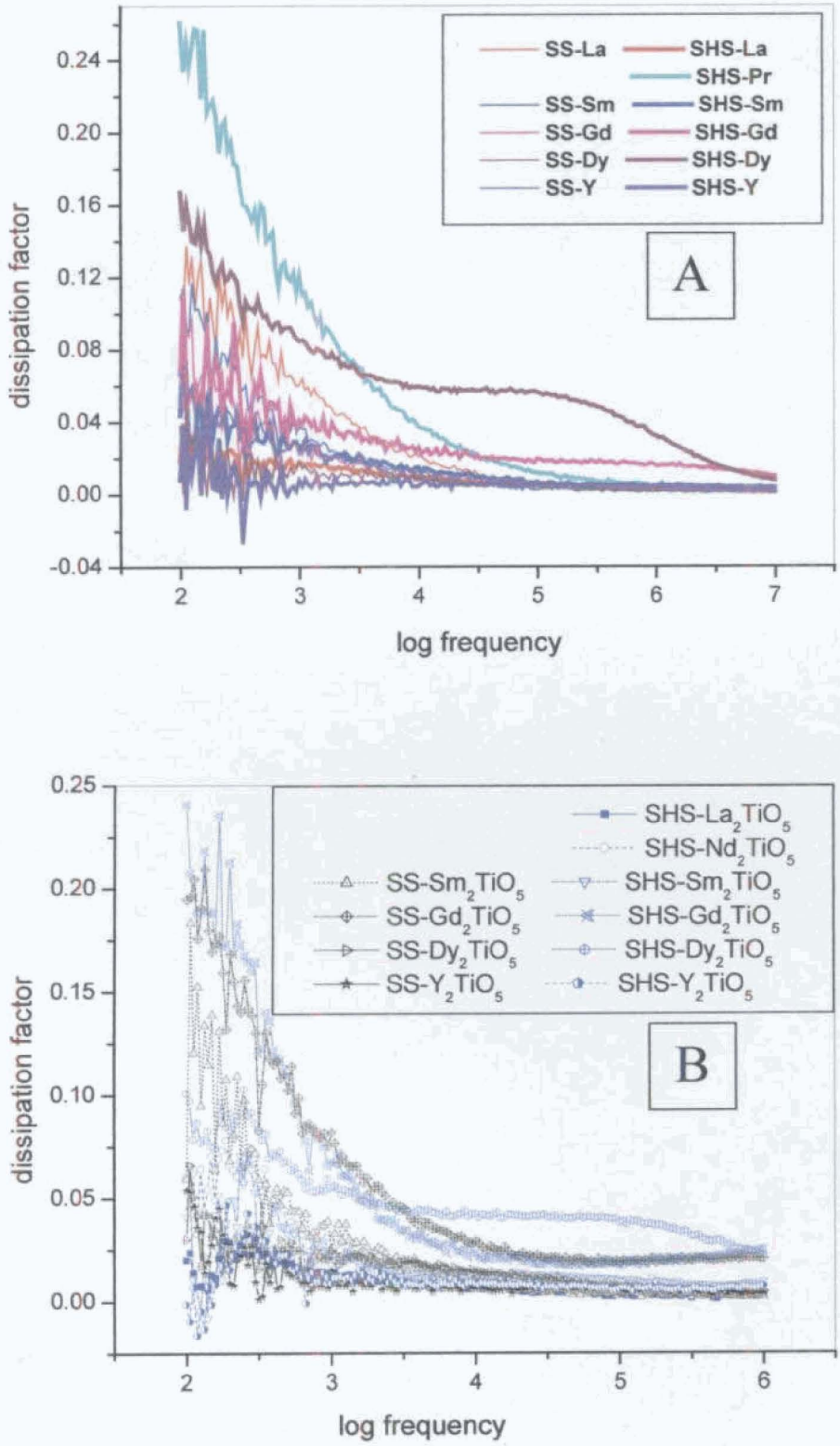


**Fig. 5.13. Changes in dissipation factor with frequency of $RE_2TiO_5$ samples sintered at (A)1575$^0$C and (B)1525$^0$C**

# SYNTHESIS AND CHARACTERISATION OF MIXED RARE EARTH TITANATES $(RE,RE')Ti_2O_7$

K.R. Dayas "Self propagated high temperature synthesis of electroceramic rare earth titanates and their characterisation " Thesis. Department of Chemistry, University of Calicut, 2006

# CHAPTER 6

# SYNTHESIS AND CHARACTERIZATION OF MIXED RARE EARTH TITANATES, $(RE,RE')Ti_2O_7$

## EXPERIMENTAL

The mixed rare earth titanates, $(RE,RE')Ti_2O_7$, were prepared by the direct solid state reaction between $TiO_2$ and the constituent $RE_2O_3$, $RE'_2O_3$ and also by SHS reaction of $TiO_2$ and the mixture of the rare earth nitrates, $RE(NO_3)_3$ and $RE'(NO_3)_3$, in presence of ammonium acetate as activator. Experimental details are given below.

### A. Direct Solid state reaction

Titanium dioxide and the mixture of $RE_2O_3 + RE'_2O_3$ (where RE, RE' = La-Pr, La-Nd, Pr-Nd, Sm-Gd, Sm-Dy, Sm-Y, Gd-Dy, Gd-Y, Dy-Y) in the 1:2 mol ratios (with the rare earths RE and RE' in equal molar ratios) were transferred to an agate vessel and homogeneously mixed in presence of isopropyl alcohol as the dispersion solvent and the solvent was evaporated off by placing in air oven at 120 $^0$C. The dried mass was then dispersed in a solution of 5 % polyvinyl alcohol in water to achieve a solid content of about 1.5 % PVA in the mix. It was then dried and granulated by passing through steel sieves and the sieve fraction between –50 MPI and +200 MPI of granules were taken and compacted, at pressures of 3 to 5 tons per square inch, to discs of dimensions around10 mm diameter and 1.5 mm thickness. These discs were sintered at different peak temperatures: 1375 $^0$C, 1425 $^0$C, 1475 $^0$C, 1525 $^0$C and 1575 $^0$C. A bell shaped heating-cooling profile as described in the case of preparation of $RE_2Ti_2O_7$ was followed with a soaking for 2 h at the peak temperature.

## B. Preparation of mixed rare earth titanates, $(RE,RE')Ti_2O_7$, by SHS reaction between $TiO_2$ and $RE(NO_3)_3$ using ammonium acetate as activator

The mixture of rare earth nitrates, $RE(NO_3)_3$ and $RE'(NO_3)_3$, in 1:1 ratio (where RE+RE' = La-Pr, La-Nd, Pr-Nd, Sm-Gd, Sm-Dy, Sm-Y, Gd-Dy, Gd-Y, Dy-Y) were prepared as discussed in chapter 3. To the mixture, containing 0.02 mol each of the rare earth nitrates, 0.24 mol ammonium acetate was added and diluted with water to get a clear solution. To this solution, 0.08 mol of $TiO_2$ was added and constantly stirred to keep the $TiO_2$ as a homogeneous suspension.

The beaker was heated in an electric Bunsen. As the temperature increases, initially water vapor leaves the vessel and the reactants become dry. On further heating copious white fumes evolve from the reactants and at the peak temperature (~ 400 $^0$C) spontaneous evolution of gases takes place with the smell of ammonia followed by the brown gases of oxides of nitrogen. At the peak temperature, a vigorous spontaneous incandescent reaction sets in with bright flame along with evolution of large amounts of gases. The fluffy natured fine powder of the product flies out of the reaction vessel as if coming out from the 'firework flower pots'. A suitable set up of conical collector was placed at the mouth of the reaction vessel to collect the powder flying out of the reaction vessel. The highly porous product obtained was cooled and characterized as such and also after calcining at different temperatures.

A part of the SHS powder was converted to sintered discs of 10 mm diameter and 1.5 mm thickness as described in the solid-state route method and studied their dielectric properties.

Using the sintered discs of mixed rare earth titanates, their reflectance spectra and photoacoustic response were studied. Optical radiation from an

argon ion laser at 488 nm, 20 mW (cw, Liconix 5300), intensity modulated by a chopper was used as the source of excitation and the PA signal was detected and measured using a sensitive microphone (Knowles BT 1754) and a lock in amplifier.

## RESULTS AND DISCUSSION

**Elemental analysis:** The percentage elemental composition of titanium and rare earths in the mixed rare earth titanates analyzed by XRF are given in table 6.1. The data conform to the composition of $(RE,RE')Ti_2O_7$ of all the samples prepared

**Table 6.1. Elemental composition of $(RE,RE')Ti_2O_7$ by XRF**

| $(RE,RE')Ti_2O_7$ where RE-RE'= | % RE | | % RE' | | % Ti | |
|---|---|---|---|---|---|---|
| | Found for the product | Calculated | Found for the product | Calculated | Found for the product | Calculated |
| **La-Pr** | 28.3 | 28.49 | 29.0 | 28.90 | 19.8 | 19.65 |
| **La-Nd** | 28.2 | 28.29 | 29.5 | 29.38 | 19.6 | 19.51 |
| **Pr-Nd** | 28.5 | 28.59 | 29.3 | 29.26 | 19.3 | 19.43 |
| **Sm-Gd** | 29.2 | 29.17 | 30.4 | 30.51 | 18.6 | 18.59 |
| **Sm-Dy** | 28.9 | 28.88 | 31.1 | 31.21 | 18.5 | 18.40 |
| **Sm-Y** | 33.5 | 33.63 | 20 | 19.89 | 21.5 | 21.43 |
| **Gd-Dy** | 29.9 | 29.81 | 30.6 | 30.80 | 18.2 | 18.16 |
| **Gd-Y** | 34.5 | 34.64 | 19.6 | 19.58 | 21.0 | 21.10 |
| **Dy-Y** | 35.5 | 35.39 | 19.4 | 19.36 | 21.0 | 20.86 |

**Physical characteristics**

The mixed rare earth titanates also exhibited change in colour discs with temperatures as given in table 6.2.

**Table 6.2. Variation of colour with temperature of $(RE,RE')Ti_2O_7$**

| Sl. No. | $(RE,RE')Ti_2O_7$ | Colour at the sintering temperature | | | | |
|---|---|---|---|---|---|---|
| | | 1375 $^0$C | 1425 $^0$C | 1475 $^0$C | 1525 $^0$C | 1575 $^0$C |
| 1 | $(La,Pr)Ti_2O_7$ | Light green | Dung green | Dung green | Light brown | Dark brown |
| 2 | $(La,Nd)Ti_2O_7$ | Light brown | Brown | Brown | Brown | Dark brown |
| 3 | $(Pr,Nd)Ti_2O_7$ | Brown | Brown | Brown | Dark brown | Dark brown |
| 4 | $(Sm,Gd)Ti_2O_7$ | Cream | Cream | Dark cream | Golden cream | Golden cream |
| 5 | $(Sm,Dy)Ti_2O_7$ | Golden cream | Golden cream | Golden cream | Golden cream | Golden cream |
| 6 | $(Sm,Y)Ti_2O_7$ | Cream | Cream | Cream | Golden cream | Golden cream |
| 7 | $(Gd,Dy)Ti_2O_7$ | Cream | Cream | Dark cream | Dark cream | Dark cream |
| 8 | $(Gd,Y)Ti_2O_7$ | Cream | Cream | Cream | Bright cream | Golden cream |
| 9 | $(Dy,Y)Ti_2O_7$ | Dull white | Cream | Cream | Cream | Dark cream |

**XRD studies Monoclinic mixed rare earth titanates, $(RE, RE')Ti_2O_7$**

The XRD patterns of the product showed that powders obtained from solid state method are not phase pure. Therefore, the XRD data of only products prepared by SHS method are discussed.

Among the mixed earth titanates synthesized, the XRD data showed that $(La,Pr)Ti_2O_7$; $(La,Nd)Ti_2O_7$ and $(Pr,Nd)Ti_2O_7$ are of monoclinic structure and all others are cubic structure. Therefore, the XRD data along with BET surface area analysis of the two types are discussed separately.

The XRD pattern of the SHS powder of the mixed rare earth titanate $(La,Pr)Ti_2O_7$ appears to be near microcrystalline in nature. On calcination at 1200 $^0$C all the characteristic peaks of the monoclinic crystalline material emerges (figure 6.1).

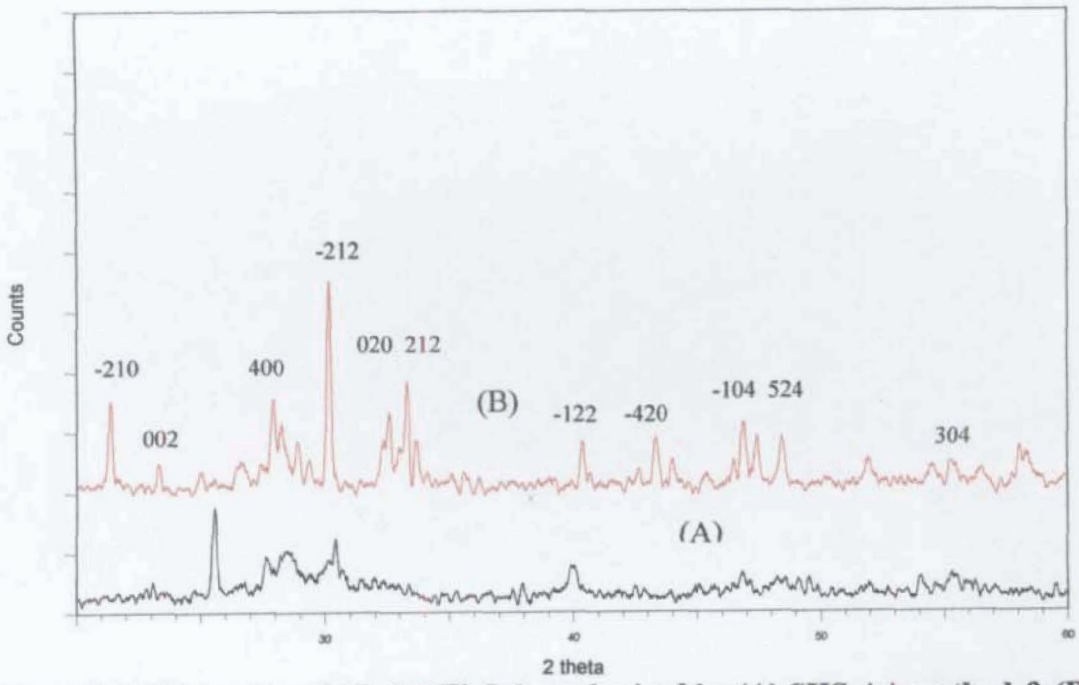


**Fig. 6.1. XRD spectra of [$(LaPr)Ti_2O_7$] synthesized by (A) SHS-AA method & (B) calcined at 1200 $^0$C-(Match JCPDS:35-267 $Pr_2Ti_2O_7$-Monoclinic)**

In the case of $(La, Nd)Ti_2O_7$ SHS powder, before calcination itself almost matches with the peaks present in the standards; but on calcining at 1200$^0$C the compound transforms to phase pure material (figure 6.2).

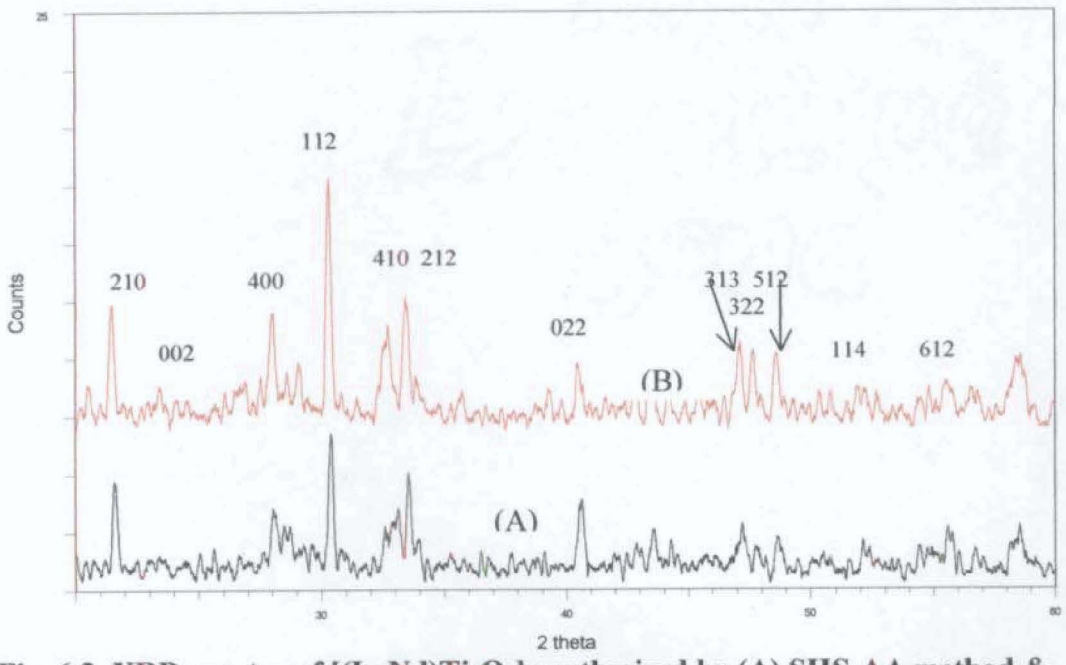


**Fig. 6.2. XRD spectra of [(LaNd)$Ti_2O_7$] synthesized by (A) SHS-AA method & (B) calcined at 1200$^0$C( Match JCPDS: 33-942 $Nd_2Ti_2O_7$-Monoclinic)**

Eventhough many peaks of the standard are present in the synthesized (Pr,Nd)$Ti_2O_7$ material, they are lower in intensities and appear as broad peaks. The calcined compound transforms to phase pure(figure 6.3).

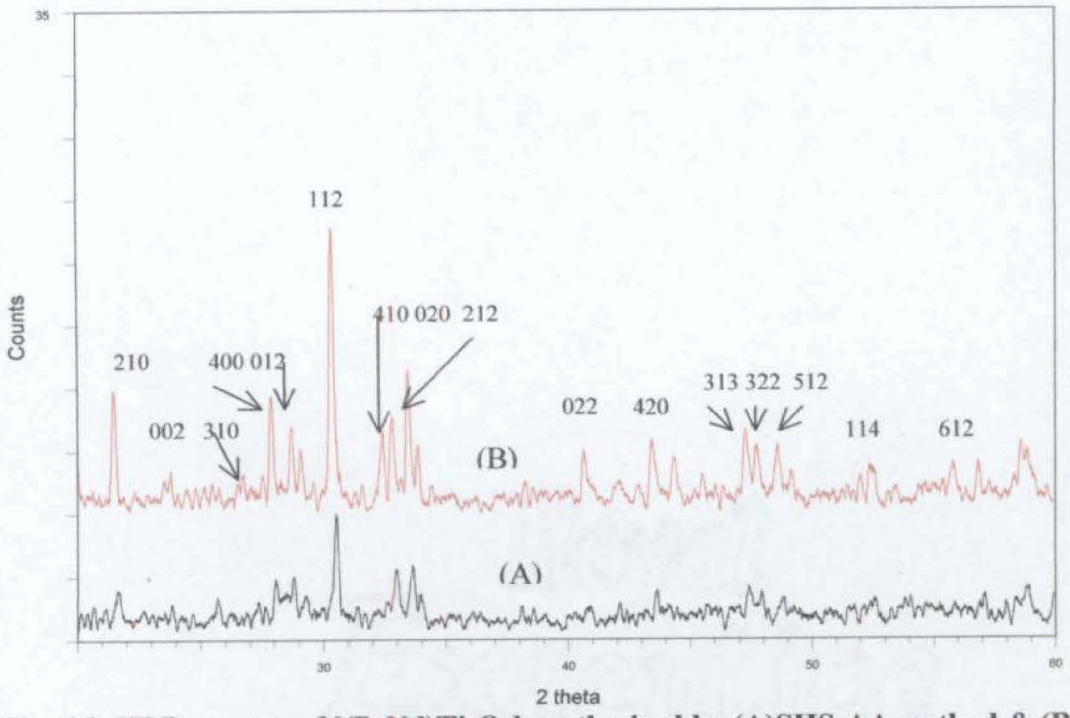


**Fig. 6.3. XRD spectra of [(PrNd)$Ti_2O_7$] synthesized by (A)SHS-AA method & (B) calcined at 1200$^0$C-(Match JCPDS:35-267 $Pr_2Ti_2O_7$-Monoclinic)**

**BET surface area analysis of monoclinic (RE, RE')$Ti_2O_7$**

The surface area of the SHS powders of monoclinic mixed rare earth titanates, (La,Pr)$Ti_2O_7$ and (La,Nd)$Ti_2O_7$ were measured and the average particle size (APS) were calculated from the empirical formula

$$2r = 6/\delta S$$

[where r = radius of the particle (microns), $\delta$ = density of the powder (g/cc) and S = surface area ($m^2/g$)]

The calculated values of APS are given in table 6.2.

**Table 6.2 BET surface area & APS of monoclinic mixed rare earth titanates, $(RE,RE')Ti_2O_7$, synthesized by SHS method**

| $(RE,RE')Ti_2O_7$ | Density(g/cc) | Surface area($m^2$/g) | APS(nm) |
|---|---|---|---|
| La-Pr | 5.865 | 15.54 | 66 |
| La-Nd | 5.947 | 1.58 | 638 |

The BET plots of $1/[W(P_O/P)-1]$ against relative pressure, $P/P_O$ of the two monoclinic mixed rare earth titanates are given in figure 6.4 & 6.5. The data suggest that the particle size of the mixed rare earth titanates even before any mechanical processing like milling, grinding etc. are in the nanometer range. The observed large particle size of $(La,Nd)Ti_2O_7$ may be due to agglomeration. However, nanoparticles can be prepared from the agglomerates by suitable mechanical processing.

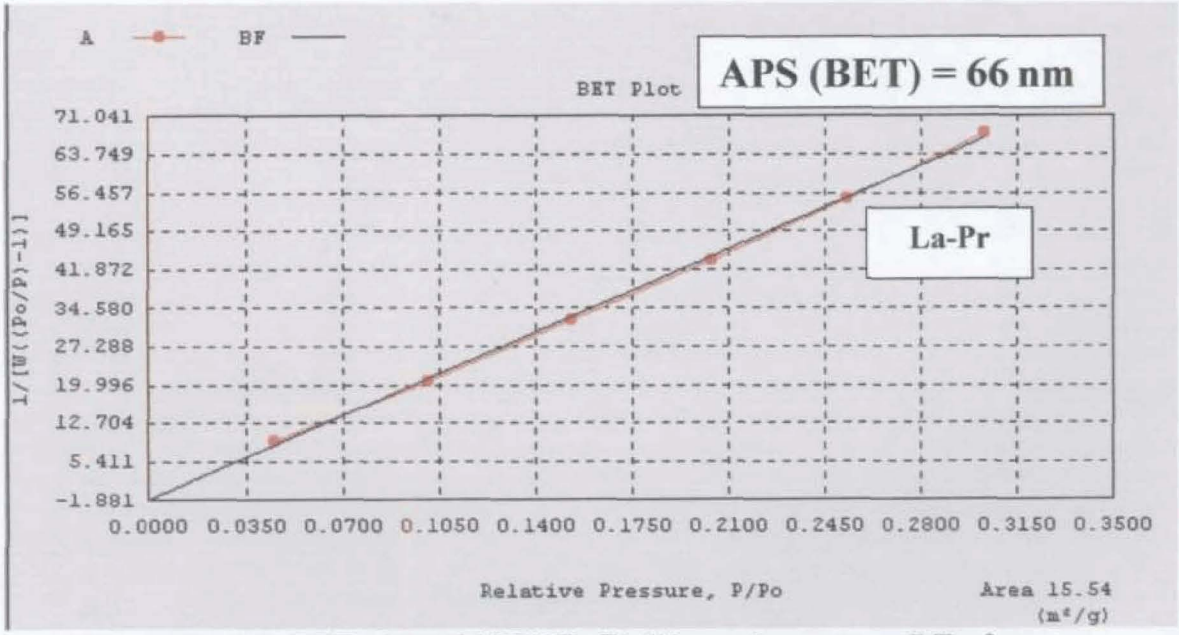


**Fig: 6.4. BET plots of $1/[W((P_O/P)-1)]$ vs rel. pressure, $P/P_O$ for monoclinic mixed rare earth titanates,$(La.Pr)Ti_2O_7$**

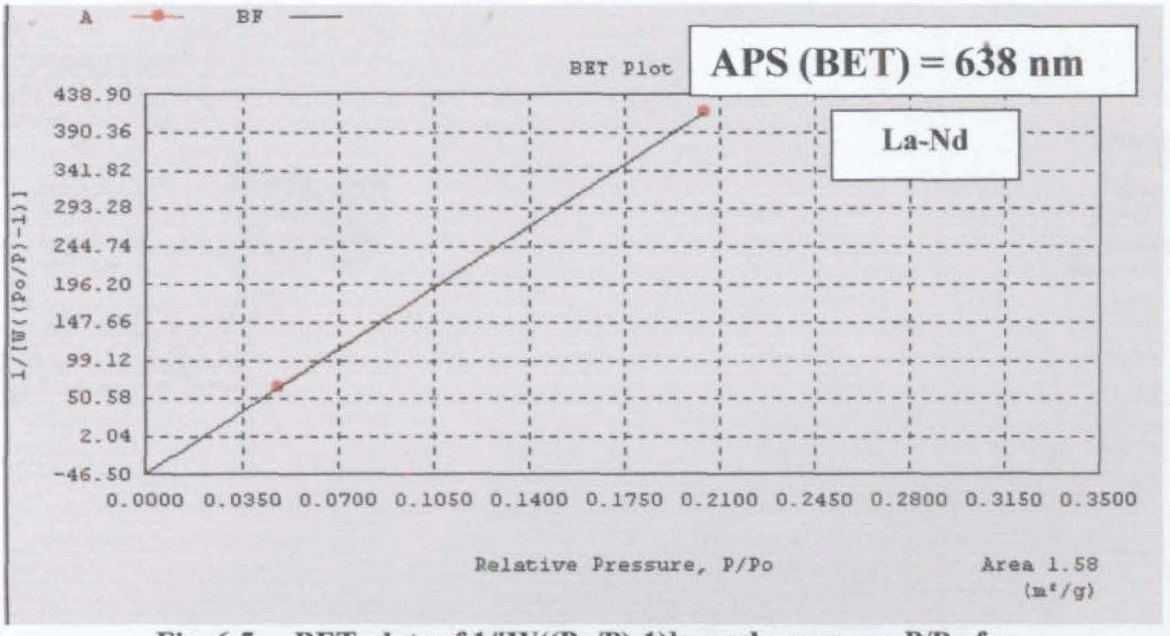


**Fig. 6.5. BET plots of $1/[W((P_O/P)-1)]$ vs rel. pressure, $P/P_O$ for monoclinic mixed rare earth titanates, $(La.Nd)Ti_2O_7$**

**XRD studies of cubic mixed rare earth titanates,$(RE,RE')Ti_2O_7$**

The mixed titanate $(Sm,Gd)Ti_2O_7$ in SHS powder form exhibits an XRD pattern having almost similar peaks as in the standard material of cubic structure but with lower intensities. On calcination at 1200 $^0$C, it gets transformed to phase pure material with the peaks in the standard matching with that of the calcined material, figure 6.6.

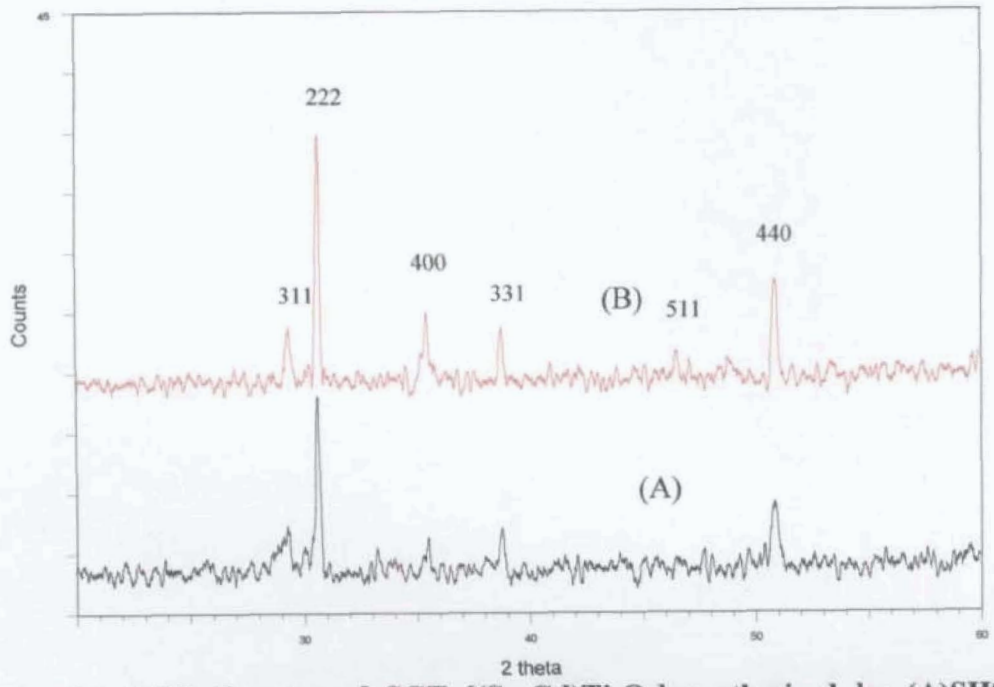


**Fig. 6.6. XRD Spectra of SGT [$(SmGd)Ti_2O_7$] synthesized by (A)SHS-AA method & (B) that calcined at 1200$^0$C [Match JCPDS: 23-259 $Gd_2Ti_2O_7$ (cubic)]**

The mixed titanate $(Sm,Dy)Ti_2O_7$ obtained by the SHS method appeared as a fluffy powder; it's XRD pattern exhibits broad peaks in the positions as in the standard material but with low intensities. The material on calcination at 1200 $^0$C gets transformed to phase pure with its peaks matching with the standard cubic RE titanates (figure 6.7).

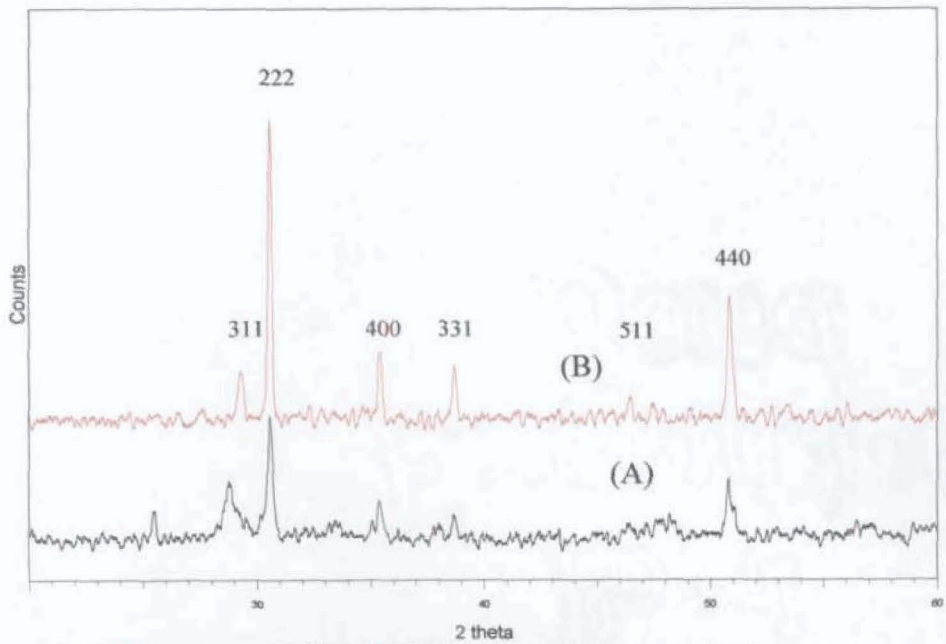


**Fig. 6.7. XRD spctra of [(SmDy)$Ti_2O_7$] synthesized by (A)SHS-AA method & (B) calcined at 1200$^0$C [Match JCPDS: 17-453 $Dy_2Ti_2O_7$ (cubic) & 16-400 $Sm_2Ti_2O_7$ (cubic)]**

The XRD pattern of the (Sm,Y)$Ti_2O_7$ have broad peaks of low intensities in the positions as in the standard material. But it becomes phase pure on calcination at 1200 $^0$C with matching peaks of the standard constituent RE titanates, figure 6.8.

The mixed titanate (Gd,Dy)$Ti_2O_7$ synthesized by the SHS method yielded fluffy products of the compound having less intense broad peaks at positions almost same as in the case of the standards. On calcination at 1200$^0$C the material turns to be phase pure (Fig: 6.9)

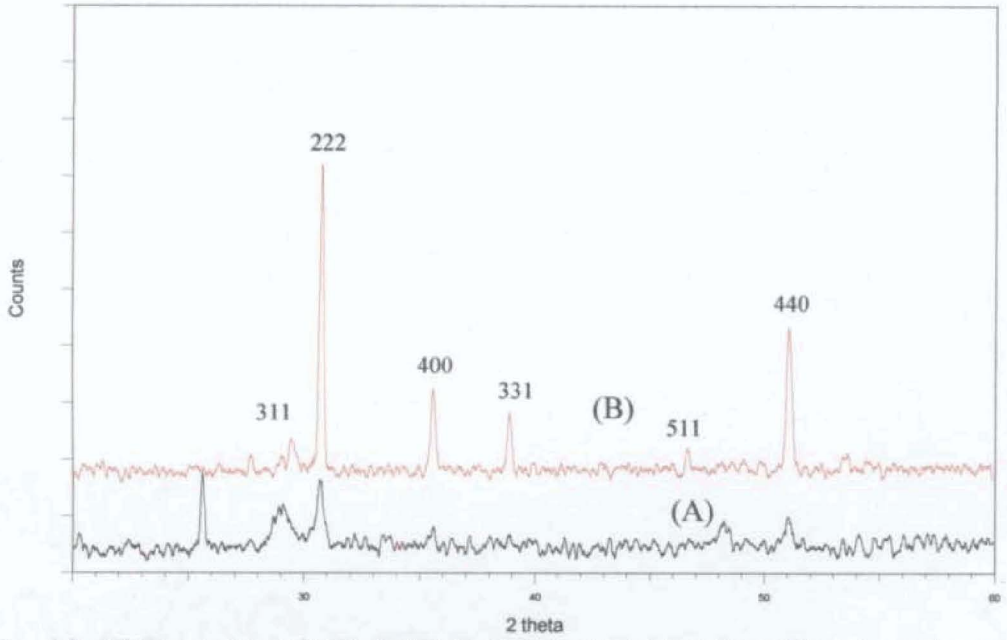


**Fig. 6.8. XRD spectra of [(SmY)$Ti_2O_7$] synthesized by (A) SHS-AA method & (B) calcined at 1200$^0$C [Match JCPDS: 42-413 $Y_2Ti_2O_7$ (cubic)]**

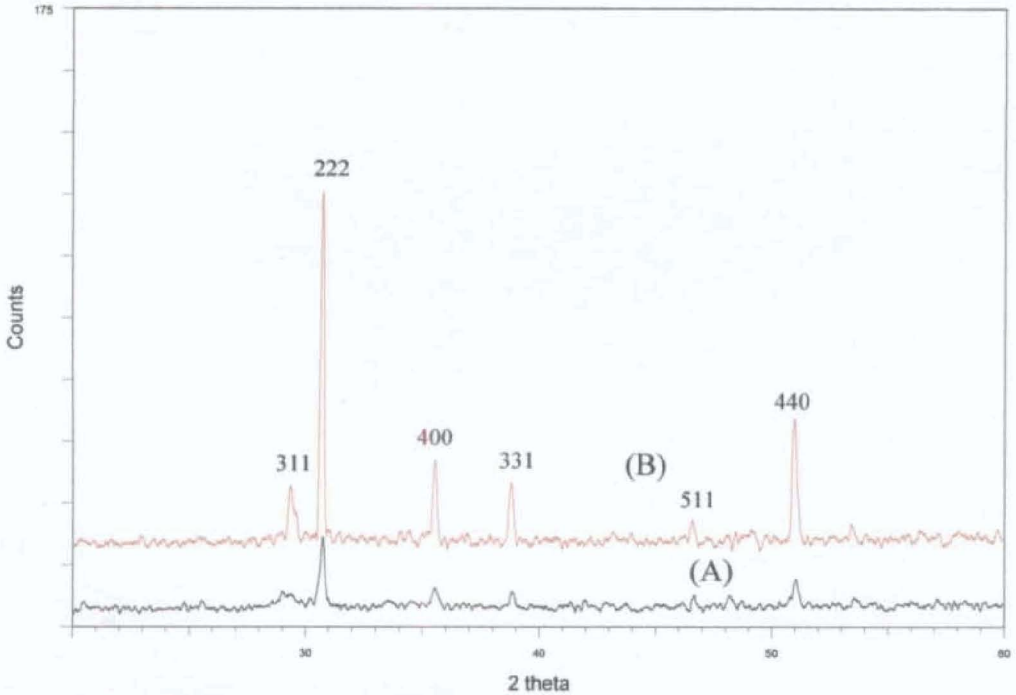


**Fig. 6.9. XRD spectra of [(GdDy)$Ti_2O_7$] synthesized by (A)SHS-AA method & (B)calcined at 1200$^0$C [Match JCPDS: 17-453 $Dy_2Ti_2O_7$ (cubic)]**

The XRD pattern of the (Gd,Y) also transformed to phase pure product on calcination at $1200^0$C ( Fig: 6.10).

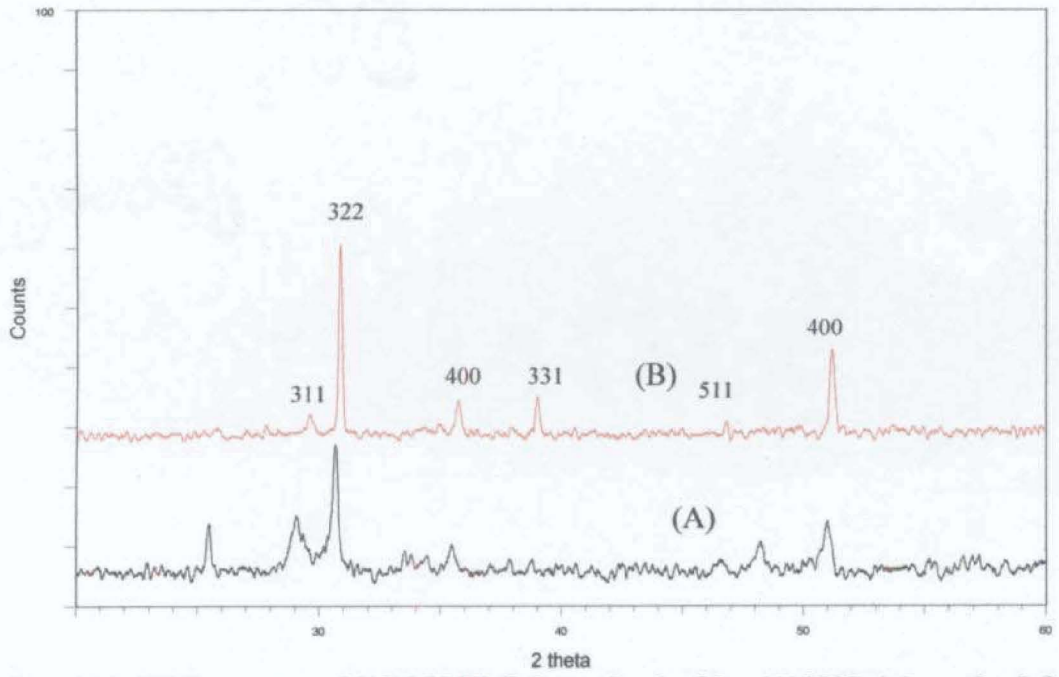


**Fig. 6.10. XRD spectra of [(Gd.Y)$Ti_2O_7$] synthesized by (A)SHS-AA method & (B) calcined at $1200^0$C [Match JCPDS: 23-259 $Gd_2Ti_2O_7$ (cubic), 42-413 $Y_2Ti_2O_7$ (cubic)]]**

Thus it appears that rare earth element which formed cubic $RE_2Ti_2O_7$ retained the crystal structure in the mixed rare earth titanates of the compositions (RE,RE')$Ti_2O_7$. Similarly, monoclinic mixed rare earth titanates are formed by the elements La, Pr and Nd which yielded monoclinic single rare earth titanates, $RE_2Ti_2O_7$.

**BET surface area analysis of cubic (RE,RE')$Ti_2O_7$**

The BET surface area of the four cubic mixed rare earth titanates, (Sm,Gd)$Ti_2O_7$ (Sm,Dy)$Ti_2O_7$, (Gd,Y)$Ti_2O_7$ and (Dy,Y)$Ti_2O_7$ and their average particle size (APS) calculated from the density data of the SHS

powders as per the empirical formula described in the section on monoclinic titanates are given in table 6.3.

**Table 6.3. BET surface area & APS of cubic mixed rare earth titanates $(RE,RE')Ti_2O_7$ synthesized by SHS method**

| $(RE,RE')Ti_2O_7$ | Density(g/cc) | Surface area($m^2$/g) | APS(nm) |
|---|---|---|---|
| Sm-Gd | 6.437 | 8.02 | 116 |
| Sm-Dy | 6.592 | 22.00 | 41 |
| Gd-Y | 5.889 | 22.56 | 45 |
| Dy-Y | 6.071 | 11.82 | 84 |

The BET plots of $1/[W(P_O/P)-1]$ against relative pressure, $P/P_O$ for the four cubic mixed rare earth titanates are given in figures 6.11 to 6.14. The data clearly suggest that all the mixed rare earth titanates are nanosized particles even before any mechanical processing like milling, grinding, etc.

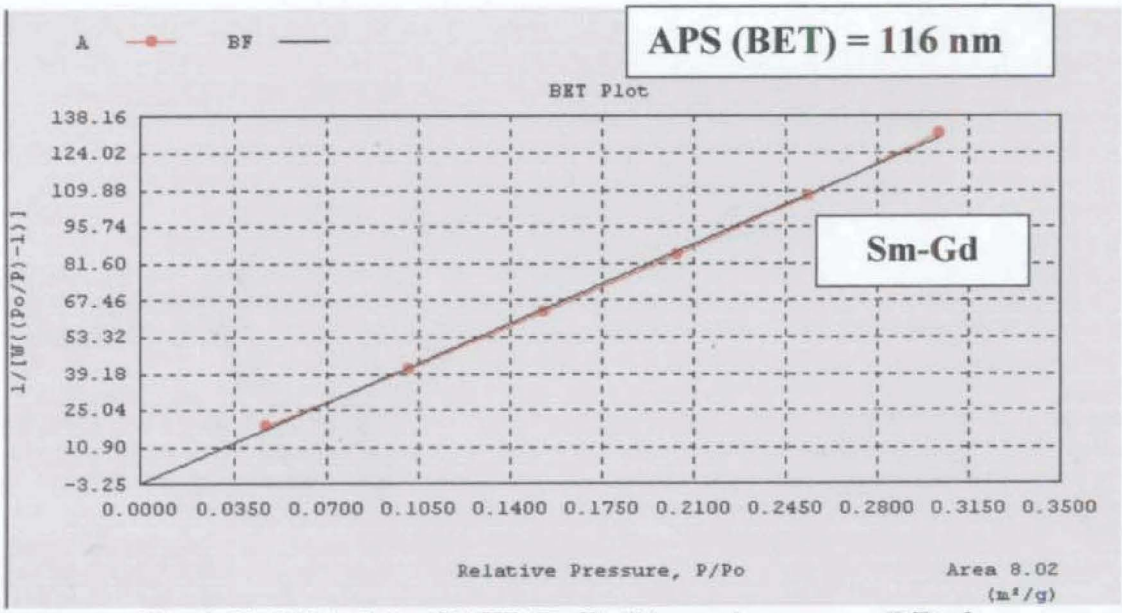


**Fig. 6.11. BET plots of $1/[W((P_O/P)-1)]$ vs rel. pressure, $P/P_O$ for cubic mixed rare earth titanates,$(Sm.Gd)Ti_2O_7$**

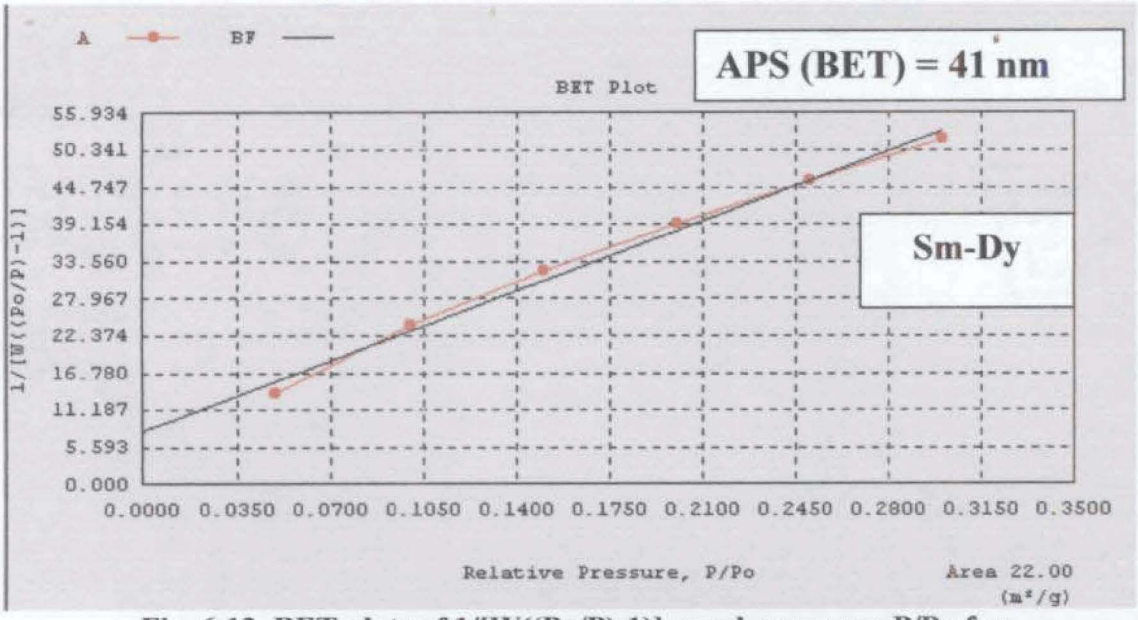


**Fig. 6.12. BET plots of $1/[W((P_O/P)-1)]$ vs rel. pressure, $P/P_O$ for cubic mixed rare earth titanates,$(Sm.Dy)Ti_2O_7$**

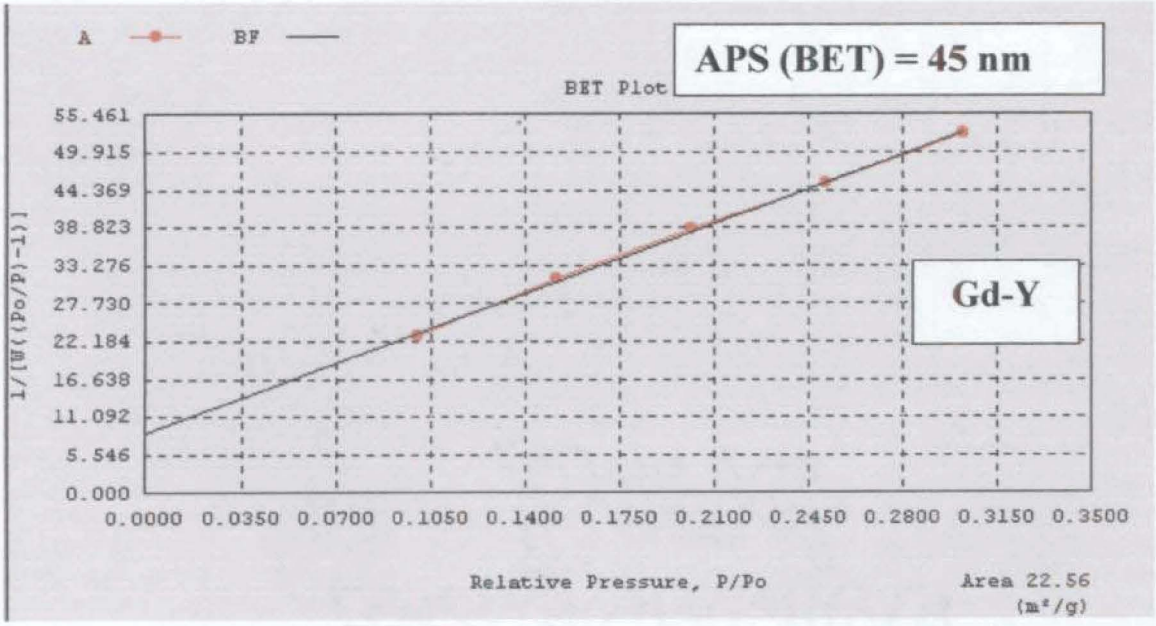


**Fig. 6.13. BET plots of $1/[W((P_O/P)-1)]$ vs rel. pressure, $P/P_O$ for cubic mixed rare earth titanates,$(Gd.Y)Ti_2O_7$**

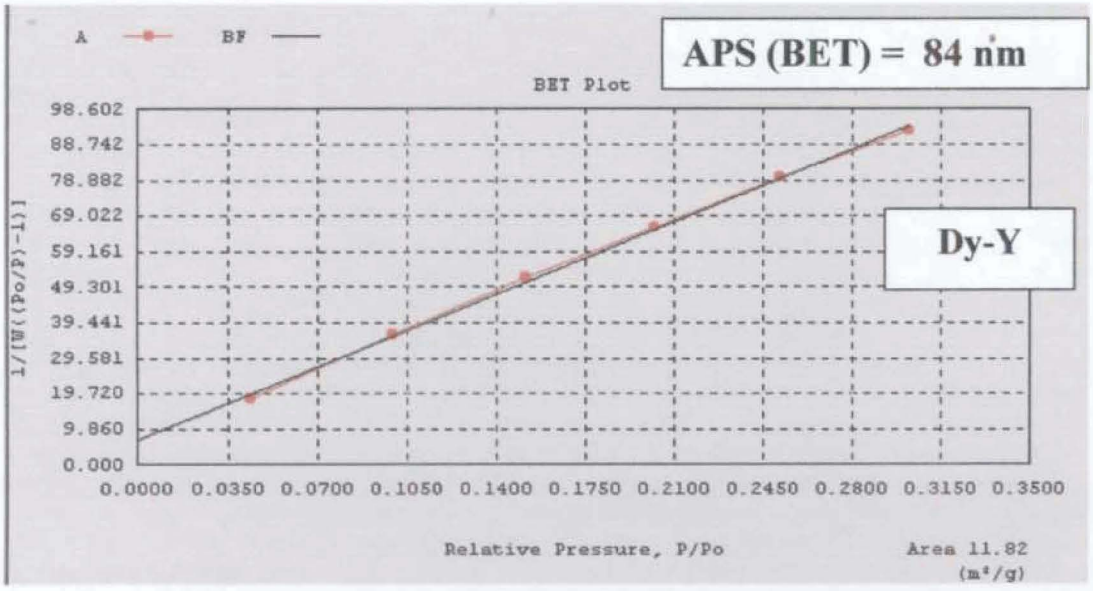


**Fig. 6.14. BET plots of $1/[W((P_O/P)-1)]$ vs rel. pressure, $P/P_O$ for cubic mixed rare earth titanates,$(Dy.Y)Ti_2O_7$**

## Dielectric properties

The dielectric properties of the mixed rare earth titanates prepared by solid state (SS) method and by SHS method were measured in the frequency range 100 Hz to 10 MHz after sintering at various temperatures. However consistent data were obtained only for samples sintered at 1525 $^0$C and 1575$^0$C. Therefore, only these results are considered. The permittivity and dissipation factor observed for the compounds are brought out in figs. 6.15 and 6.16. The data indicated that permittivity of the materials prepared by SHS method are well above that obtained by solid state route. The most important observation is that the permittivity remain a constant over the entire frequency range applied.

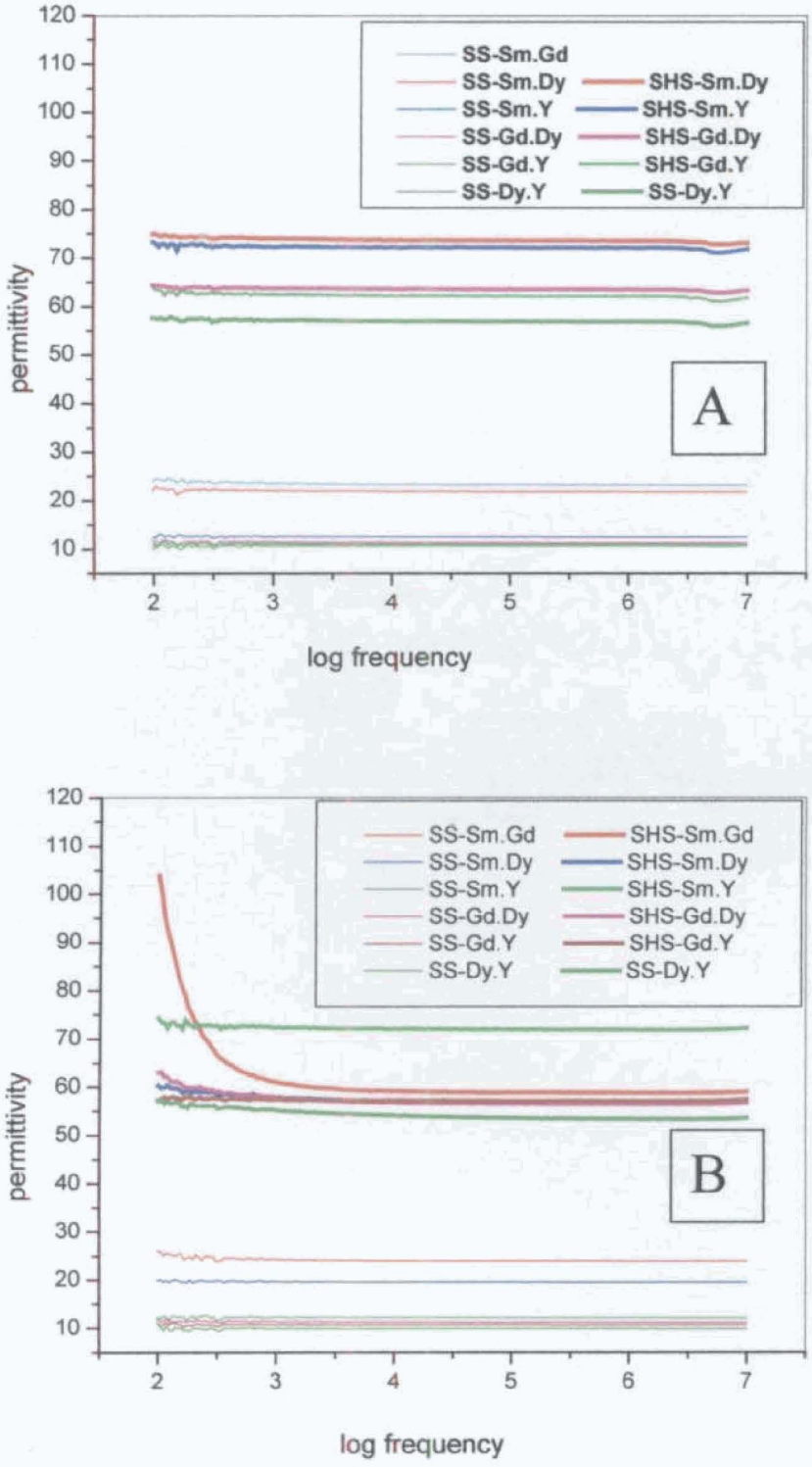


**Fig. 6.15. Changes in permittivity with frequency of RE.RE'$Ti_2O_7$ samples sintered at (A) 1575 $^0$C and (B)1525 $^0$C**

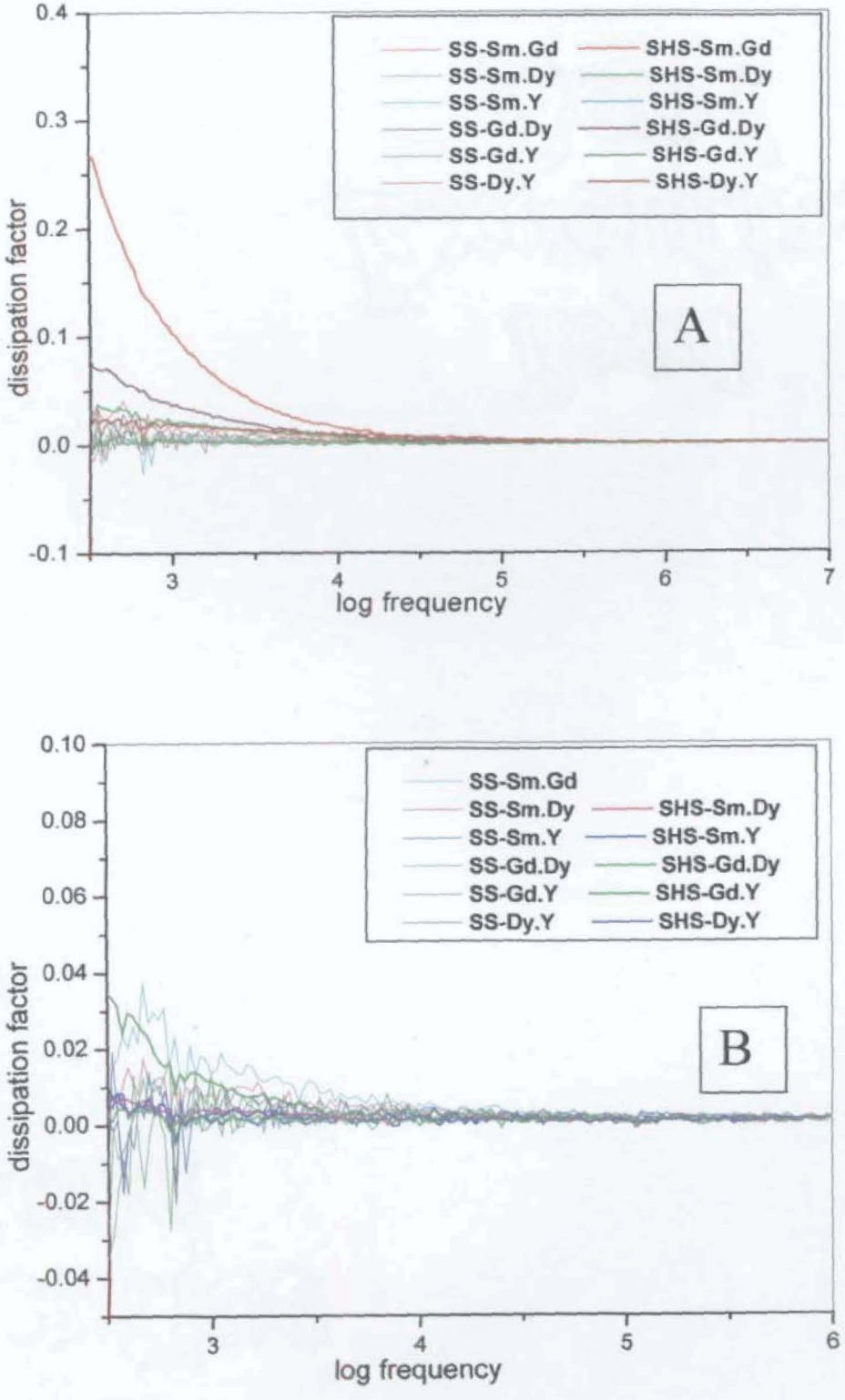


**Fig. 6.16. Changes in dissipation factor with frequency of RE.RE'$Ti_2O_7$ samples sintered at (A) 1575 $^0$C and (B)1525 $^0$C**

The dissipation factors remain more or less same for powders obtained from both methods and remain a constant after a definite frequency.

The permittivity values of the SHS sample sintered at 1575 $^0$C were also measured at different temperatures (20 $^0$C to 120 $^0$C) and the results are presented in fig: 6.17. It can be seen that changes in permittivity with temperature are negligible. These types of ceramic materials have number of applications particularly in microwave dielectrics.

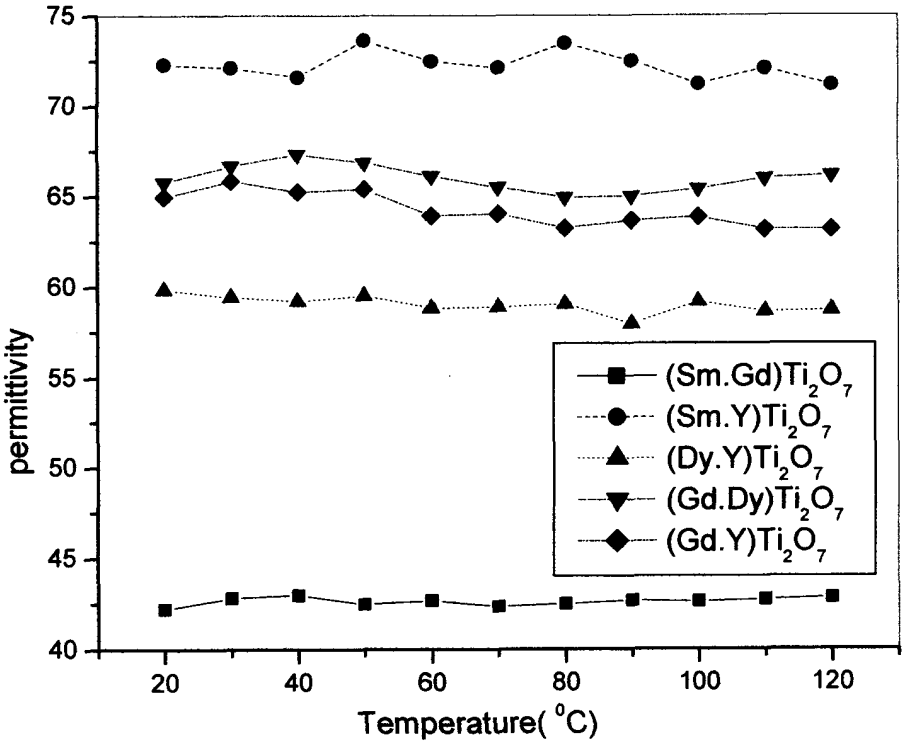


**Fig. 6.17. Changes in permittivity with temperature for the mixed titanates, (RE, RE')$Ti_2O_7$**

## Optical properties

**Reflectance spectra**: In the reflectance spectra of mixed rare earth titanates obtained by the SHS method, the monoclinic $(La,Pr)Ti_2O_7$ and $(Pr,Nd)Ti_2O_7$ exhibits no reflections in the wave length range 200 to 900 nm. In the case of cubic crystalline mixed rare earth titanates $(Dy,Y)Ti_2O_7$, $(Gd,Y)Ti_2O_7$, $(Sm,Gd)Ti_2O_7$, $(Gd,Dy)Ti_2O_7$, $(Sm,Dy)Ti_2O_7$, and $(Sm,Y)Ti_2O_7$, strong characteristic peaks are observed at around 280 nm. Among the cubic compounds most prominent reflection is shown by $(Gd,Y)Ti_2O_7$ at 280 nm; but other cubic titanates have more or less similar intensities for that peak. In addition, the cubic compounds $(Dy,Y)Ti_2O_7$, $(Sm,Dy)Ti_2O_7$ and $(Sm,Y)Ti_2O_7$ exhibit strong absorption peaks at 735 nm and at 794 nm, whereas other cubic titanates were not having any characteristic absorptions at that regions. The spectra are reproduced in fig. 6.18.

**Fluorescence spectra**: The fluorescence spectra of the compounds were recorded at the excitation wavelength 280 nm. In the spectra (fig: 6.19) of all the mixed rare earth titanates, strong emissions were observed at around 480 nm and 550 nm. All the mixed rare earth titanates have sufficient intensities for emission peak at 480 nm which made it suitable for photoacoustic studies.

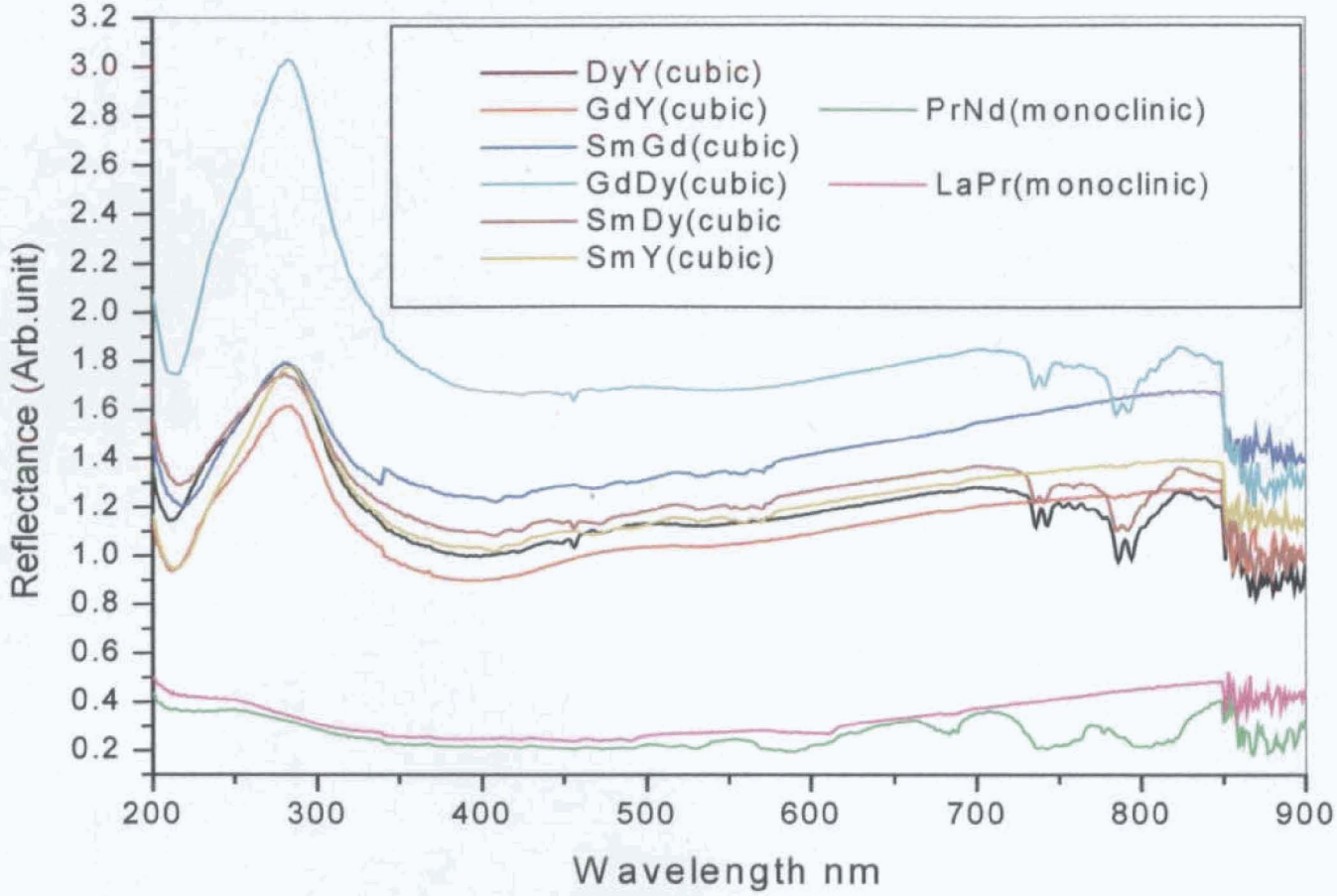


**Fig. 6.18. Reflectance spectra of mixed rare earth titanates, (RE.RE')$Ti_2O_7$ synthesized by the SHS method**

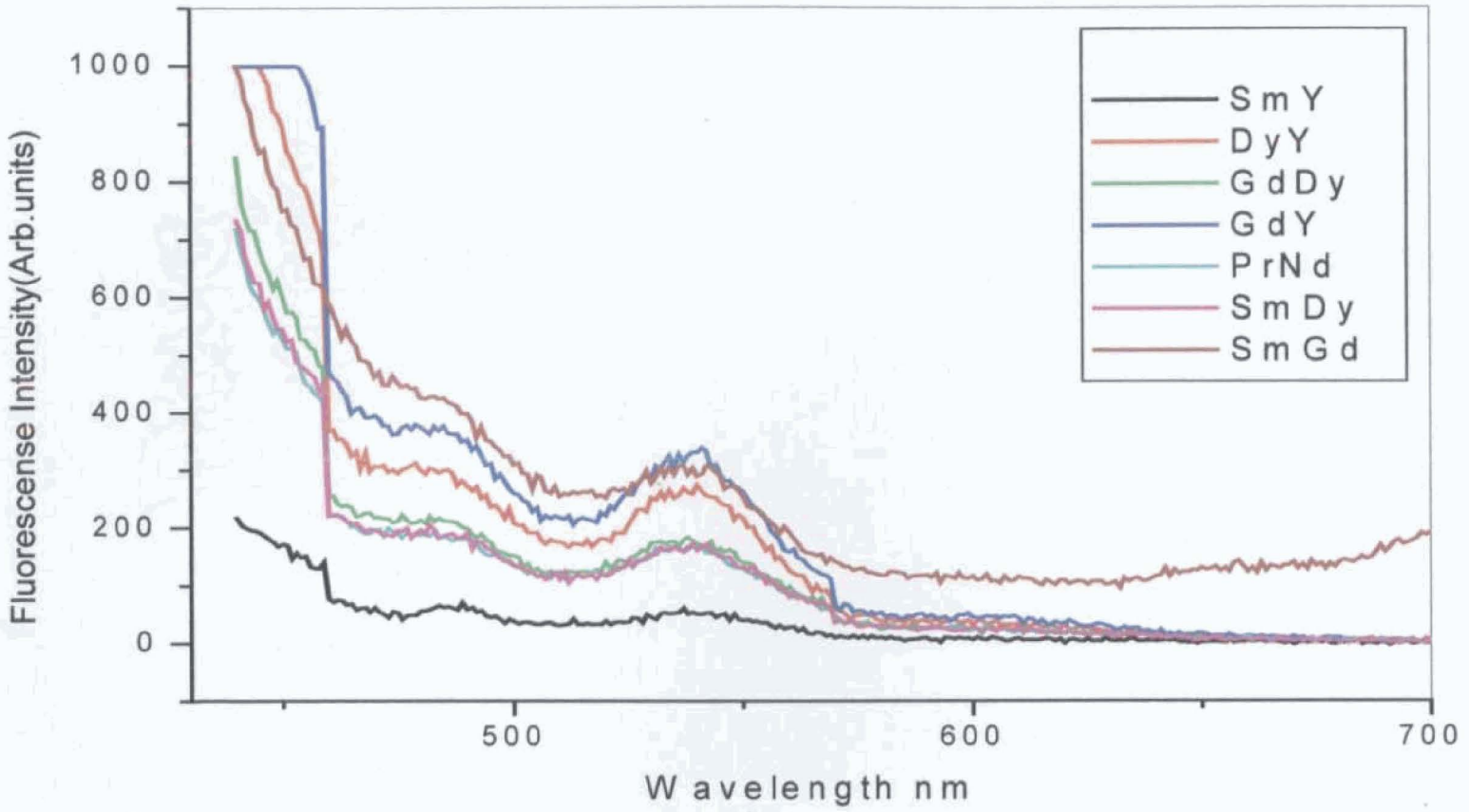


**Fig. 6.19. Fluorescence spectra of mixed rare earth titanates, (RE.RE')$Ti_2O_7$ synthesized by the SHS method**

**Photoacoustic properties:** Recently rare earth zirconates with pyrochlore structure similar to the rare earth titanates have been reported to show low thermal diffusivity, a characteristic property of materials for protective thermal barrier coatings. The cubic mixed rare earth titanates, $(Dy,Y)Ti_2O_7$, $(Sm,Y)Ti_2O_7$ and $(Gd,Y)Ti_2O_7$ synthesized by SHS method also showed interesting optical properties. Their thermal behavior was studied by using a laser beam of 488 nm and by photoacoustic (PA) technique and were found to exhibit good thermal diffusivity. Since, these mixed titanates exhibited sufficient absorption at 488 nm wavelength, their changes in phase and amplitude of PA signal against square root of frequency are given in figure 6.20 and 6.21. From the slope of the plot, thermal diffusivity was calculated as discussed earlier.

Though the phase and amplitude of the PA signal contains clear signature of the thermal properties of the specimen, phase data is more reliable for open cell configuration since the amplitude data depends on many external parameters such as sample surface quality and detector response at different wavelengths. Thermal diffusivity of the samples are calculated from the slopes of the straight line graphs of PA Phase Vs square root of frequency and are tabulated in table 6.4.

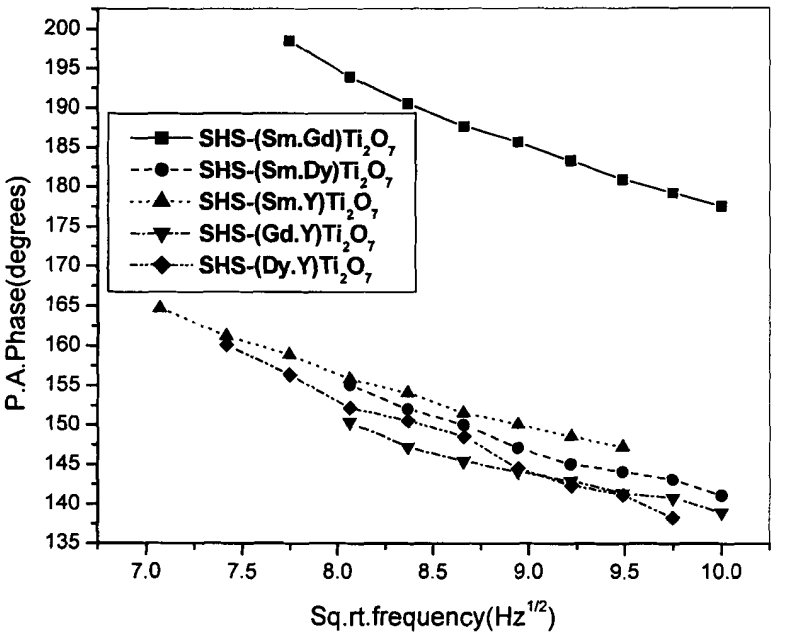


**Fig. 6.20. Variation of PA Phase difference with modulation frequency for mixed rare earth titanates,RE.RE'$Ti_2O_7$**

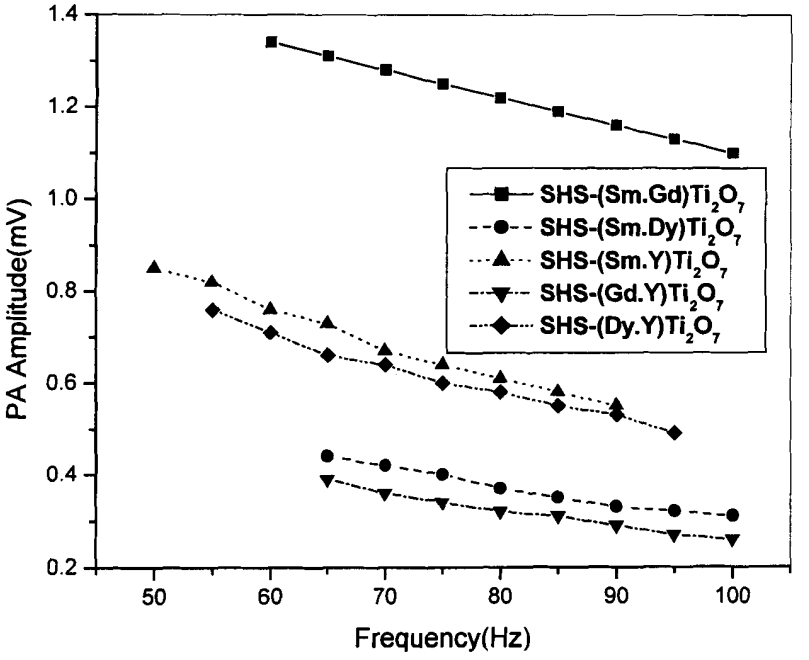


**Fig. 6.21. Variation of PA amplitude with modulation frequency for mixed rare earth titanates,RE.RE'$Ti_2O_7$**

**Table 6.4. Thermal diffusivity of mixed rare earth titanates,(RE,RE')$Ti_2O_7$**

| (RE,RE' )$Ti_2O_7$ where RE,RE' = | b | Thickness ls (cm) | α ($cm^2/s$) |
|---|---|---|---|
| Dy-Y | 8.52 | 0.155 | 0.0009 |
| Sm-Y | 7.22 | 0.113 | 0.0008 |
| Gd-Y | 5.41 | 0.086 | 0.0008 |

Thermal diffusivities of some of the known materials are given in table 6.5.

**Table 6.5. Thermal diffusivities of typical materials**

| Material | Thermal diffusivity, (α $cm^2$/ s) |
|---|---|
| Zirconia | 0.002- 0.005 |
| Silica carbide | 0.008 |
| Silicon | 0.08 |
| Barium Titanate | 0.0015 |
| Rare earth zirconate | 0.002 |

A comparison of the observed thermal diffusivity (α = $cm^2/s$) of the compound with that of some known materials (table 6.5) showed that the α values of the mixed rare earth titanates are several fold lower. Therefore these materials can function as superior thermal barrier coatings

## SUMMARY AND CONCLUSIONS

Mixed rare earth titanates of the type (RE, RE')$_2Ti_2O_7$ obtained by the SHS reaction between the earth nitrates and $TiO_2$ in presence of ammonium acetate were found to be phase pure monochronic or cubic structures having nanosized particles. The permitivity and dissipation factor obtained suggested that these compounds are superior to the rare earth titanates $RE_2Ti_2O_7$

(Chapter 4) as microwave dielectrics. From photoaccoustic studies, the thermal diffusivity ($\alpha$) of the mixed rare earth titanates were determined. The observed very low $\alpha$ values indicates that, these materials are highly suitable for thermal barrier coatings.

# REFERENCES


1. J. G. Bednortz and K. A. Muller, *Z. Phys. B.* **64**, 189 (1986).
2. M. K. Wu, J. R. Ashburn, C. J. Torrey, P. H. Hor, R .L. Meng, L. Gao, Z. J. Huang, Y. Q. Wang and C. W. Chu, *Phy. Rev. Lett.,* **58**, 908 (1987).
3. A. Schilling, M. Cantoni, K. J. D. Guo and H. R. Oh, *Nature,* **363**, 56 (1993).
4. Y. Z. Lu, P. Haldar, R. Markiwricz, S. Sridhar and B. C. Giesson, *Mater. Lett.*, **5**, 380 (1987).
5. 'Advanced Ceramic Materials', Noyes Publications (1985).
6. Relva C. Buchanan, 'Ceramic Materials for Electronics', Marcel Dekker Inc., New York (1993).
7. A. J. Moulson, J. M. Herbert, 'Electroceramics', Chapman and Hall (1990).
8. W. D. Kingery, H. K. Bowen and D. R. Uhlmann, 'Introduction to Ceramics', John Wiley, New York, 1976.
9. Shinroku Saito, 'Fine Ceramics', Elsevier Publishers, 1985.
10. 'Engineered Materials Handbook, Vol. Ceramics and Glasses', ASM International (1991).
11. L. L. Hench, D. R. Ulrich (eds.), 'Ultrastructure Processing of Ceramics: glasses and composites', Wiley, New York (1984).

12. I. Matsuyama, K. Suja, S. Satoh and T. Suganuma, *Bull. Am. Ceram. Soc.,* **63**, 1408 (1984).

13. R. Classen, *J. Mat. Sci. Lett.*, **7**, 477 (1988).

14. K. Kamiya, R. Uemura, J. Matsuoka and H. Nasu. *J. Ceram. Soc. Jpn*, **103**, 245 (1995).

15. G. De, M. Tapfer, M. Catalano, G. Battaglin, F. Caccavala, F. Goneka, P. Mazzoldi and R. Haglund, *Appl. Phys. Lett.* **68**, 3820 (1996).

16. T. R. Rama Mohan, D. D. Sood, V. N. Vaidya and Ram Prasad 'Fine Ceramics – Synthesis, Properties and Applications', Indian Ceramic Society, (1998)

17. J. B. Jaffe, W. R. Cook and H. Jaffe, 'Piezoelectric Ceramics', Academic Press Inc., New York (1971).

18. F.H. Norton, "Fine Ceramics Technology and Applications", McGraw Hill (1970).

19. D. L. Segal, 'Chemical Synthesis of advanced ceramic materials', Cambridge Univ. Press, Cambridge (1989).

20. V. N. Vaidya, S. K. Mukherjee, J. K. Joshi, R. V. Kamat and D. D. Sood, *J. Nucl. Mat.*, **148**, 324 (1987).

21. S. K. Mukherjee, J. V. Dehadraya, V. N. Vaidya and D. D. Sood,. *J. Nucl. Mater.,* **185**, 39 (1991).

22. D. D. Upadhyaya, S. K. Roy, G. K. Dey and S. Banerjee, *Bull. Mater. Sci.,* **17**, 875 (1994).

23. K. E. Spear, *J. Am. Ceram. Soc.*, **72**, 171 (1989).

24. D. M. Teter, *MRS Bull.* **23**, 22 (1998).

25. R. W. Rice, C. Cm. Wu and F. Borchelt, *J. Am. Ceram. Soc.*, **77**, 2539 (1994).

26. J. E. Butler and H. Windisehmann, *MKS Bull.*, **23**, 22 (1998).

27. S. Matsumoto, *J. Mater. Sci. Lett.*, **4**, 600 (1985).

28. A. M. Stoneham, I. J. Ford and P. Chalker, *MRS Bull.*, **23**, 28 (1998).

29. Ralf Riedel, 'Handbook of Ceramic Hard Materials', Vol.**1**, Wiley VCH, Germany, (2000).

30. J. M. Leger, J. Haines, M. Schmidt, J. P. Petietet, A. S. Pereira and J. A. H. da Jornada. *Nature*, **383**, 401 (1996).

31. A. Zerr, G. Meihe, G. Serghion, M. Schwarz, E. Kroke, R. Riedel, H. Fuez, P. Kroll and R. Boehler, *Nature*, **400**, 340 (1999).

32. D. M. Teter and R. J. Hemley, *Nature*, **271**, 53 (1996).

33. D. M. Gruen, *MRS Bull.*, **23**, 32 (1998).

34. C. S. Yoo, J. Akella and H. Cynn, *Phy. Rev. B*, **56**, 140 (1997).

35. I. W. Chen and A. Rosenflanz, *Nature*, **389**, 701 (1997).

36. H. R. Karfunkel and T. Dressler, *J. Am. Chem. Soc.*, **114**, 2285 (1992).

37. J. H. Nguyen and R. Jeanloz, *Mater. Sci. Eng.* A, **209**, 23 (1996).

38. Michael J. Reece, Clive A. Worrell, Graham J. Hill and Roger Morrell, *J. Am. Ceram. Soc.*, **79**[1], 17 (1996).

39. N. S. Van Damme, A. E. Sutherland, L. Jones, K. Bridger and S. R. Winzer, *J. Am. Ceram. Soc.*, **74** [8], 1785 (1991).

40. H. Sakata, M. Amano, Y. Kawashima, T. Okamoto, 16th *Int. Congr. Glass,* [4], 357(1992)

41. Sakata, Hironobu, Amano, Masatake, Kawashima, Yasuyuki, Okamoto, Tetsuya,. *J. Ceram. Soc. Jpn.*, **102** [4], 317(1994)

42. T. V. Vittal Rao, R. V. Kamat and V. N. Vaidya, *Ferro electries*, **189**, 1 (1996).

43. A. Ezis, 'Ceramics for high performance applications', Brook Hill, Massachusetts, 207 (1974).

44. D. W. Johnson Jr. and P. K. Gallagher, 'Ceramic Processing before Firing', John Wiley and Sons, New York, 125 (1978).

45. U. Nadkarni, 'Fine Ceramic Powders', edited by R. Freer, J. L. Woodhead, British Ceramic Proceedings, **47**, 81 (1991).

46. F. K. Van dijen, R. Metselaar, *J. Am. Ceram. Soc.*, **68**, 16 (1985).

47. D. C. Bradley, R. C. Mehrotra and D. P. Gaur, 'Metal Alkoxides', Academic Press, London (1978).

48. Richard. E. Riman, "Ceramic powder synthesis-Current status and future challenges" - 'Ceramic Processing Science and Technology', ed. Hans Hausner et al, Publ. Am. Cer. Soc., USA, Ceramic Transactions Vol.**51,** (1994).

49. F. Chaput, J. P. Boilot and A. Beauger, *J. Am. Ceram. Soc.*, **73**, 942 (1990).

50. T. Kasai, Y. Ozaki and S. Yamamoto, 'Preparation of $BaTiO_3$ and $SrTiO_3$ from metal alkoxides'. *Yogyo Kyokaishi*, **95**, 1000 (1987).

51. K. W. Kirby, *Mater. Res. Bull.*, **23**, 881 (1988).

52. A. S. Shaikh, and G. M. Vest,. *J. Am. Ceram. Soc.*, **69**, 682 (1986).

53. S. Katayama, I. Yoshinaga, N. Yamada, T. Nagai, *J. Am. Ceram. Soc.*, **79**, [8], 2059(1996)

54. James S. Reed, 'Introduction to the Principles of Ceramic Processing', John Wiley, New York (1989).

55. V. Hlavacek, *Acers. Bull.*, **70** [2], 240(1991)

56. V. Hlavacek, J. A. Puszynski, *Indust. and Eng. Chem. Res.*, **35**, [2], 349 (1996)

57. A. G. Merzhanov, I. P. Borovinskaya, *Zh. Vses. Khim. Ob-va im. D.I. Mendeleeva*, **24** [3], 223(1979)

58. A. G. Merzhanov, *J. Mater. Process. Technol.*, **56**, 222(1996)

59. A. G. Merzhanov, 'Combustion: new manifestations of an ancient process in: Chemistry of Advanced Materials' ed. C.N.R. Rao, Blackwell Sci. Publ., 19(1992)

60. A. G. Merzhanov,. *Combust. Sci. and Technol.*, **105** [4-6], 295(1995)

61. A. G. Merzhanov, 'Self-propagating high-temperature synthesis of ceramic (oxide) superconductors in: Ceramic Transactions.

Superconductivity and Ceramic Superconductors' ed. K. N. Nair, E. I. Dupont deNemours, E. A. Giess. Westerville, Ohio: Amer. Ceram. Soc. Publ., **13,** 519 (1990)

62. A. G. Merzhanov, *Int. J. of SHS*, **4** [4], 323 (1995)

63. A. G. Merzhanov, *Int. J. of SHS*, **2** [2], 113 (1993)

64. A. G. Merzhanov, *Int. J. of SHS*, **6** [2], 119 (1997)

65. Y. Miyamoto, *J. Mineralogical Soc. of Jpn.*, **18** [6], 383(1988)

66. O. A. Kaibyshev, N. G. Zaripov, *Int. J. of SHS*, **6** [2], 203 (1997)

67. J. W. McCauley, *Ceram. Eng. Proc.*, **11**, [9-10], 1137(1990)

68. K. C. Patil, S. T. Aruna, and T. Mimani, Curr. Op. *Solid State Mater. Sci.*, **6**, 507 (2002).

69. Y. M. Grigorev., A. G. Merzhanov, *Int. J. of SHS,* **1** [4], 600 (1992)

70. E. H. Grigoryan, *Intern. J. of SHS*, **6** [3], 307(1997)

71. J. B. Holt, 'Combustion Synthesis, a New Area of Research in Materials Science'. Energy & Technology Review LLNL, 11, (1984)

72. B. J. Matkowsky, A. P. Aldushin, K. G. Shkadinsky G. V. Shkadinskaya, *Int. J. of SHS*, **6** [3], 345(1997)

73. A.O. Odawara, A.Y. Kaieda, 'A New Synthesis Method for Ceramics: Self-Propagating High Temperature Synthesis Method' Sosei to Kako. **28** [312], 3(1987)

74. R. Pampuch, *Journal of the European Ceramic Society*, 2395 (1999)

75. R. Pampuch, J. Lis, L. Stobierski, *Sci. Ceram.* **14**,15(1988)

76. R. Pamlpuch, *Int. J. of SHS*, **6**, [2]187 (1997)

77. R. Pampuch, 'SHS powders: the present and future. In Ceramic Processing Science and Technology', ed.Shin-Ichi irano, H. Hausner and G. Messing. Ceramic Transactions, Vol. 51, Am. Ceram. Soc. Columbus, OH, (1995)

78. K. C. Patil, S.T. Aruna, S. Ekambaram, *Solid State & Mater. Sci.,***2**[2], 158 (1997)

79. J. Subrahmanyam, M. Vijayakumar, *J. Mater. Sci.,.***27**, 6249 (1992)

80. H. C. Yi, J. J. Moore, *J. Mater. Sci.*, **25** [14], 3693(1990),

81. D. Bahadur, S. Rajakumar and Ankit Kumar, *J. Chem. Sci.*, **118** [1], 15 **(2006)**

82. A. Varma, J. P. Lebrat, *Chem. Eng. Sci.*, **47** [9-11], 2179 (1992)

83. V. V. Barzykin, *Pure and Appl. Chem.*, **64** [7] ,909 (1992)

84. I. P. Borovinskaya, *Pure & Appl. Chem.*, **64** [7], 919 (1992)

85. H. J. Feng, K. R. Hunter, J. J. Moore, *J. Mater. Synth. Process*, **2**, 71 (1994)

86. J. S. Haggerty, Y. M. Chaing, *Ceram. Eng. Sci. Proc.*, **11**, [7-8], 758 (1990)

87. J. J. Moore, A. O. Kunrath, R. Torres, I. Reimanis, G. Mustoe, K. Upadhya, E. A. Levashov, *Int. J. of SHS,* **6**, [3],277 (1997)

88. J. Lis, R. Pampuch and L. Stobierski, "Specific aspects of sintering of powders prepared by Combustion method (SHS)"- 'Ceramic

Processing Science and Technology', Edited by Hans Hausner et al, Publ. Am. Cer. Soc., USA, Ceramic Transactions Vol.**51**(1994).

89. J. J. Moore, H. J. Feng, *Progr. Mater. Sci.*, **35**, [4-5] 243 (1995)

90. J. J. Moore, H. J. Feng, *Progr. Mater. Sci.*, **39**, [4-5] 275(1995)

91. Z. A. Munir, *Int. J. of SHS*, **6** [2], 165 (1997)

92. A. Shiryaev, *Int. J. of SHS*, **4**[4],351 (1995)

93. Chyi-Ching Hwang, Tsung-Yung Wu, Jun Wan & Jih-Sheng Tsai, *Mat. Sci. and Engg.B*, **111** [1], 49 (2004).

94. S. Polizzi, G. Fagherazzi, M. Battagliarin, M. Bettinelli & A. Speghini; *J. Mat. Res.*, **16** [1], 146 (2001).

95. M. R. Morelli and Brook, "Combustion Synthesis of $LaCrO_3$ powders"- 'Ceramic Processing Science and Technology', Edited by Hans Hausner et al, Am. Ceram. Soc., USA, Ceramic Transactions Vol.**51** (1994).

96. Gunter K. Muecke and Peter Muller "The not-so-rare-earths".

97. B. R. Lipin and G. A. McKay, 'Geochemistry and Mineralogy of Rare Earth Elements'

98. K. N. R. Taylor, "The Rare Earth Metals", Contemp. Phys. **11** [5], 423 (1970).

99. Encyclopedia Britanica, 2003

100. R. K. Garg, "Rare Earths-Conventional applications and Emerging Technologies" –Proceedings of 'Recent Dev. in the S&T of Rare Earths', Cochin, Kerala (1995)

101. W. Muller et al, "Heavy Element Properties", North Holland Publ. Co., Amsterdam, 68, (1975).

102. K. R. Dayas et al "Functional Advantages of RE elements in the Material Composition of Electronic Components and Devices" Proceedings of 'Recent Developments in the S&T of Rare Earths', Cochin, Kerala (1995)

103. Neeraj, C. N. R. Rao, *J. Mater. Chem.*, **8**[7], 1631 (1998)

104. S. Wang, Y. Jiang, Y. Zhang, J. Yan, W. Li, *J. Electrochem. Soc.*, **145** [6], 1932(1998)

105. I. R. Gibson, G. P. Dransfield, J. T. S. Irvine, *J. Mat. Sci.*, **33**[17], 4297 (1998)

106. S. P. S. Badwal, K. Foger, *J. Australas. Ceram. Soc.*, **34** [1],1 (1998)

107. T. Horita, N. Sakai, H. Yokokawa, M. Dokiya, T. Kawada, J. Van Herle, K. Sasaki *J. Electroceramics*, **1**[2], 155 (1997)

108. A. Q. Pham, R. S. Glass, *J. Electrochem. Soc.*, **144** [11], 3929 (1997)

109. T. Kato, A. Momma, S. Nagata, Y. Kasuga, *J. Ceram. Soc. Jap.*, **105** [12], 1057 (1997)

110. J. S. Lee, T. Matsubara, T. Sei, T. Tsuchiya, *J. Mat. Sci.*, **32** [19], 5249 (1997)

111. Alcock, Charles, *Rev. Int. Hautes Temp. Refract.*, **28** [1], 1 (1993)

112. F. Capel, P. Duran, J. R. Jurado, *Bull. Soc. Esp. Ceram. Vidrio*, **34** [5-6], 401(1995)

113. S. T. Aruna, M. Muthuraman, K. C. Patil, *J. Mater. Chem.*, **7** [12], 2499 (1997)

114. G. A. Tompsett, N. M. Sammes, *J. Am. Ceram. Soc.*, **80** [12], 3181 (1997)

115. K. Asano, H. Iwahara, *J. Electrochem. Soc.*, **144** [9], 3125 (1997)

116. Robert C. Weast, 'CRC Handbook of Chemistry and Physics', CRC Press Inc., USA (1988)

117. J. B. Mac Chesney and H. A. Sauer, *J. Am. Cer. Soc.*, **45** [9], 416 (1962).

118. Guillen and Bertaut, *Bull. Soc.. Fr. Ceram.*, **72**,57(1996).

119. *Natl. Bur. Stand. (US) Monogr. No. 25*, **15**, 35 (1978)

120. J. Guha and J. Kolav, *J. Mater. Sci. Lett.*, **1**, 312 (1982).

121. A. Sych, and T. Novik, Russ. J. *Inorg. Chem.* (Engl.Transl.), **22**, 35 (1977).

122. J. Haffel et al. *Ind. Eng. Chem.*, **14**, 154 (1975).

123. F. Litchenberg, D. Widmer, J. G. Bednorz, T. Williams and A. Reller, *Z, Phy.B: Condes. Matter*, **82** [2], 211 (1991).

124. B. Melekh et al , *Russ. J. Inorg. Chem.* (Engl.Transl.), **25**, 1761 (1980).

125. A. Sych et al, *Russ. J. Inorg. Chem.* (Engl.Transl.), **25**, 1139 (1980).

126. J. Guha and J. Kolav, *J. Mater. Sci. Lett.*, **1,** 312 (1982).

127. Pfoertsch, Mc Carthy, Penn State Univ., University Park, Pennsylvaniya, 'XRD data of $PrTiO_3$,' ICDD Grant (1997).

128. Z. K. Huang, Z. X. Lin and T. S. Yen, *Guisuanyan Xuebao*, **7** [1], 1 (1979).

129. A. V. Zagorodnyuk, L. V. Sadkovskaya, G. V. Shamrai, I. P. Kovalevskaya, R. L. Magunov and G. A. Teterin, *Zh. Neorg. Khim.*, **31** [9] 2389 (1986); *Russ. J. Inorg. Chem.* (Engl. Transl.) **31** [9], 1377 (1986).

130. G. A. Teterin, V. F. Zinchenko, A. V. Zagorodnyuk *Ukr. Khim. Zh.* (Russ.Ed.),**54** [3], 252 (1998); *Sov.Progr.Chem.* (Engl.Transl.) **54** [3], 31(1988).

131. *Natl. Bur. Stand. (US) Monogr.* 25, **18**, 48 (1981).

132. *Natl. Bur. Stand. (US) Monogr.* 25, **18**, 50 (1981).

133. D. Kolar et al *J. Less-Common Met.*, **60**, 137(1978).

134. *Natl. Bur. Stand. (US) Monogr. 25*, **18**, 52 (1981)

135. Pfoertsch, Mc Carthy, Penn State Univ., University Park, Pennsylvaniya, 'XRD data of $NdTiO_3$', ICDD Grant (1997)

136. A. V. Kolesnikov, G. E. Sukhanova, A. P. Zaitseva and L. G. Shcherbakova, Izv. Akad. Nauk SSSR, *Neorg. Mater.*, **22** [11] 1932 (1986); *Inorg. Mater.(Engl.Transl.),* **22** [11], 1695 (1986).

137. Mc Carthy et al *Inorg. Chem.*, **8**, 1236 (1969).

138. G. Sukhanova et al *Inorg. Mater.* (Engl. Transl.) **17**, 759 (1981).

139. Roth et al, *J. Res. Natl. Bur. Stand. Sect. A*, **56**, 17 (1956).

140. V. Zubkov, Ural Branch of Russian Academy of Sciences, Inst. of Solid State Chemistry, Ekaterinburg, Russia, 'XRD data of $Sm_2Ti_2O_7$', ICDD Grant (1995).

141. A. Kolesnikov, G. Sukhanova, A. Zaitseva and L. Shcherbakova, *Inorg. Mater.* (Engl. Transl.) **23**, 222 (1987).

142. Mc Carthy et al *Inorg. Chem.*, **8**, 1236 (1969).

143. G. V. Shamrai, R. L. Magunov and I. P. Kovalevskaya., Izv. Akad. Nauk SSSR, *Neorg. Mater.*, **23** [2] 255 (1987); *Inorg. Mater.*(Engl. Transl.), **23** [2], 222 (1987).

144. *Natl. Bur. Stand. (US) Monogr. 25*, **8**, 32 (1970).

145. L. Shcherbakova et al *Inorg. Mater.* (Engl. Transl.) **15**, 1724 (1979).

146. Moore, Mc Carthy, Brixner, Penn State Univ., University Park, Pennsylvaniya; *Inorg. Chem.* **3**, 1065 (1964).

147. Pfoertsch, Mc Carthy, Penn State Univ., University Park, Pennsylvaniya, 'XRD data of $GdTiO_3$', ICDD Grant (1997).

148. G. V. Shamrai, R. L. Magunov, I. V. Stasenko and A. P. Zhirnova, Izv. Akad. Nauk SSSR, *Neorg.Mater.*, **25**[2], 273 (1989); *Inorg. Mater.* (Engl. Transl.), **25**[2], 233 (1989).

149. Garton and Wanklyn, *J. Mater. Sci..*, **3**, 394 (1968).

150. Shcherbakova et al *Inorg. Mater.* (Engl. Trasl.) **15**, 1724 (1979).

151. M. Petrova, D. Romanov, R. Rakhmankulov, A. Novikova, and A. Grebenshchikov, *Russ. J. Inorg. Chem.*(Engl.Transl.)**31**, 761(1986).

152. Roth et al, *J. Res. Natl. Bur. Stand.* (US), **56**, 17 (1956).

153. N. Mizutani, A. Kitazava and M. Kato, *Nippon Kagaku Kaishi*, **9**, 1623 (1974); N. Mizutani, Y. Tajima and M. Kato, *J. Am. Cer. Soc.* **59** [3-4], 168 (1979).

154. M. Kato and N. Mizutani, *Kenkyu Hokoku-Asahi Garasu Kogyo Gijutsu Shoreikai,* **29**, 35 (1976); .D. Kushkov, A. M. Zaslavskii, I. S. Kozlov, A. V. Mel'nikov and A. E. Silvinskaya, *Probl. Spets. Elektrometall.*, No.**1**,50 (1991).

155. W. Syvinski and G. Mc Carthy, North Dakota State Univ., Fargo, North Dakota, USA, 'XRD data of $Y_2TiO_5$', ICDD Grant (1989).

156. N. Mizutani, Nippon Kagaku Kaishi, *J. Chem. Soc. Japan*, 1623 (1974).

157. F. Molter, W. Eysel, Minera–Petrograph. Istitut der Universitat Heidelberg, Germany, 'XRD data of $Y_2Ti_2O_7$', ICDD Grant (1991).

158. Shveikin, Baznev, *Russ. J. Inorg. Chem.* (Engl.Transl.), **18**, 155 (1973).

159. G.V. Shamrai, A.V. Zagorodnyuk R.L.Magunov, and A.P. Zhirnova, Zh. Neorg. Khim., **29**[12]3168 (1984); *Russ. J. Inorg. Chem.*(Engl. Transl.), **29**[12],1811(1984).

160. Francois Brisse & Osvald Knop,; *Canadian J. Chem.*, **45,** 609 (1967).

161. Osvald Knop, Francois Brisse & Lotte Castelliz, *Canadian J. Chem.* , **47,** 971 (1969).

162. Michael Kestigian, Roland Ward, *J. Am. Cer. Soc*, **77** [12], 6199 (1955).

163. B. J. Mulder, *Am. Cer. Soc. Bull.*, **49**, 990 (1970).

164. W. S. Clabaugh, E. M. Swiggard and R. Gilchrist, *J. Res. Natl. Bur. Stand* (U.S.), **56**, 289 (1956).

165. A. N. Christenson, and S. E. Rasmussen, *Acta Chem. Scand.*, **17**, 845 (1963).

166. S. Kaneko and F. Imoto, *J. Chem. Soc. Jpn.*, **6**, 985 (1975).

167. K. Kajiyoshi, N. Ishizawa and M. Yoshimura, *J. Am. Ceram. Soc.*, **74**, 369 (1991).

168. Zhili Ding, Mingfu Zhang and Jiecai Han, *Mater. Phys. Mech.* **4**, 107 (2001).

169. A. Kaiser, A. Berger, D. Sporn, H. Bertagnolli, "Lyothermal Synthesis of Nanocrystalline $BaTiO_3$ and $TiO_2$ Powders"-'Ceramic Processing Science and Technology', Edited by Hans Hausner et al, Am. Ceram. Soc.,USA, Ceramic Transactions Vol.**51**(1994).

170. N. N. Melnik, and L.M. Tsapenko, *Inorg. Mater*, **22**(4), 575 (1986).

171. S. D. Skapin, D. Kolar and D. Suvorov, *J. European. Ceram. Soc.*, **20** [8], 1179 (2000).

172. A. Navrotsky, S. V. Ushakov, K. B. Helean "Enthalpies of formation of Rare Earth Pyrochlores"- Thermochemistry Facility, Dept. of Chem. Engg. and Mater. Sci., University of California at Davis <anarotsky@ucdavis.edu>.

173. S. T. Bramwell and M. J. Harris, *J. Phys.: Condes. Matter* **10,** L215 (1998).

174. L. Minervini, R. W. Grimes & K. E. Sickafus *J. Am. Cer. Soc*, **83** [8] 1873 (2000).

175. N. P. Raju, M. Dion, M. J. Gingras, T. E. Mason & J. E. Greedan, *Phys. Rev. B* **59**[22], 14489 (1999-II).

176. Isabelle Mirebeau & Igor Goncharenko, *J.Phys.: Condes .Matter* **16,** S653 (2004).

177. J. S. Gardener, G. Ehlers, S. T. Bramwell and B. D. Gaulin, *J.Phys.: Condes. Matter* **16,** S643 (2004).

178. R. Moessner and J. T. Chalker, *Phys. Rev. Let.* **80** [13], 2929 (1998).

179. Ofer Porat & Harry. L. Tuller ; *J. Am. Cer. Soc*, **79** [12] 3078 (1996).

180. S. W. Han, J. S. Gardner & C. H. Booth, , *Phys. Rev.B*, **69** 024416 (2004).

181. J. S. Gardener et al, *Phys. Rev. Let.* **82** [5] 1012 (1999).

182. R. Moessner, *Phy. Rev. B*: **57**[10] R 5587 (1998-II).

183. M. J. Harris, S. T. Bramewell, D. F. McMorrow, T. Zeiske and K. W. Godfrey, *Phys.Rev.Let.* **79**[13] 2554 (1997).

184. G. Ehlers, A.L. Cornelius, T. Fennell, M. Koza, S. T. Bramwell and J. S. Gardener, *J. Phys.: Condes. Matter* **16,** S635 (2004).

185. O. Porat, M. A. Spears et al , *Solid State Ionics* , **86-88**, 285 (1996).

186. P. K. Moon and H. L. Tuller, *Solid State Ionics* **28-30**, 470 (1988).

187. O. Porat, C. Heremans and H. L. Tuller, *Solid State Ionics,* **94**,75 (1997).

188. Ofer Porat, Catherine Heremans and Harry. L. Tuller, *J. Am. Cer. Soc*, **80** [9], 2278 (1997).

189. J. K. Park, C. H. Kim, K. J. Choi, H. D. Park & S. Y. Choi; *J. Mat. Res.*, **16** [9], 2568 (2001).

190. Dan Goldschmidt and Harry. L. Tuller, *Phys. Rev.* B, **34** [8], 5558 (1986).

191. S. Kramer, M. Spears and H.L. Tuller, *Solid State Ionics* **72**, 59 (1994).

192. Holly, S. Shulman, Martin Testorf, Dragon Damjanovic and Nava Setter, *J. Am. Ceram. Soc.*, **79** [12], 3124 (1996).

193. R. L. Withers, J. G. Thompson and A. D. Rae,. *J. Solid State Chem.*, **94**, 404 (1991).

194. J. J. Xu, A. S. Shaikh and R. W. Vest, *IEEE Trans. Ultrason, Ferroelectr., Freq. Control*, **36**, 307 (1989).

195. Octavio Alvarez-Fregoso,. *J. Appl. Phys.*, **81**[3], 1387 (1997).

196. R. J. Cava, J. J. Krajewski, W. F. Peck, 'Compensation of the temperature coefficient of the dielectric constant of barium strontium titanate (BST)' US Patent 5552355 (1996).

197. Y. Park, Y. H. Kim, 'Dielectric Ceramic composition for high frequency and method for preparation of the same' US Patent 5538928 (1996)

198. Hiroaki Yanagida et al., 'The Chemistry of Ceramics', John Wiley & Sons, USA (1996).

199. Sanghun Jeon and Hyunsang Hwang, *Appl. Phy. Lett.*, **81**(25), 4856 (2002).

200. H. J. Jung, H. J. Kim, K. Y. Kim, S. J. Yoon, S. O. Yoon, T. Nakamura, et al. 'Compositions of High Frequency Dielectrics' US Patent 5569632 (1996)

201. C. W. A. Paschoal, R. L. Moreira, C. Fantini, M. T. Sebastian, *J. of Europ. Cer. Soc.*, **23**, 2661(2003)

202. P. Laffez, G. Desgardin and B. Raveau, *J.Mater.Sc.*,**27**, 5229 (1992).

203. M. T. Sebastian, S. Soloman and R. Ratheesh, *J.Am.Cer.Soc.*,**84** [7], 1487 (2001).

204. X. Qi, Han, T. P. J. Gallanger, H. G. Henderson et al., *J. Phy. Condes. Matter*, **8**, 4837(1996).

205. G. L. Roberts, R. J. Cava, W. F. Peck and J. J. Krajewski, *J. Mater. Res.*, **12**, 526 (1995)

206. R. W. Colins, P. Haasen and E. J. Kramer, 17A, "Tape Casting", 'Processing of Ceramics, Part I', Weinheim, New York (1996).

207. K. Scheunmann, and H. K. Muller, *J. Inorg. Nucl. Chem.*, **37**[9], 1879 (1975).

208. M. Kimura, et al., *Jpn. J. Appl. Phys.* **11**[6], 904 (1972).

209. S. B. Xiong et al, *Appl. Phys. Let.* **69** [2], 191 (1996).

210. A. V. Shlyaktina, O. K. Karyagina and L. G. Shcherbakova, *Inorg. Mater.* **40** [1], 59 (2004).

211. N. N. Mel'nick, L. M. Tsapenko, V. I. Larchev and G. G. Skrotskaya, *Inorg. Mater.* **26**[4], 676 (1990).

212. M. A. Petrova, A. S. Novikova and R. G. Grebenshchikov, *Inorg. Mater.* **18** [2], 236 (1982).

213. T. H. Sako, H. Shimizu, K. Kodama et al., *J. Appl. Phys.*, **42**, 6081 (2003).

214. A. Srinivas, Dong-Wan Kim, Kug Sun Hong and S. V. Suryanarayana, *Appl. Phys. Lett.*, **83** [11], 2217 (2003).

215. S. D. Kapin, and D. Kolar, *J. Euro. Ceram. Soc.*, **20**, 1179 (2000).

216. J. Moon, and J. A. Kerchner, *J. Mater. Res.*, **14**, 425 (1999).

217. J. Moon, and T. Li, *J. Mater. Res.*, **12**, 189 (1997).

218. P. A. M. Berdowski & G. Blasse, , *J. Solid State Chem.* **62**, 317(1986).

219. Jon. C. Goldsby, Serene .C. Farmer and Ali Sayir, 'Processing techniques developed to fabricate lanthanum titanate piezoelectric

material for high temperature smart structures' Jon.C.Goldsby@nasa.gov

220. S. Nanamatsu, M. Kimura, K. Doi, S. Matsushita and N. Yamada, *Ferroelectrics* **8**, 511(1974); H. Takeda et al Jap. J.Appl. Phys., **42**, 6081(2003)

221. C. Z. Bi et al , *Condens. Matter.* **17**, 5225 (2005)

222. Xiao Qiang Liu and Xiang Ming Chen, *J. Am. Cer. Soc.* **88** [2], 456(2005).

223. Amit Sinha and Beant Prakash Sharma, *J. Am. Cer. Soc.* **88** [4], 1064 (2005).

224. D. M. Todorovic, P. M. Nikolic, D. G. Vaseljevic and M. D. Dramicanin, *J. Appl.Phys.*, **76**,1, (1994)

225. S. Sankararaman, V. P. N. Nampoori , C. P. G. Vallabhan, G. Ambadas and S. Sugunan, *Appl.Phys. Lett.*, **67**, 20, (1995)

226. A. M. Mansanares, H. Vargas, F. Galembeck, J. Buijs and D. Bicanic, *Appl. Phys.*, **70** [11],7046,( 1991).

227. A. Rosencwaig, 'Photoacoustics and photoacoustic spectroscopy', John Wiley & Sons, New York, (1980)

228. K. Annieta Philip 'Characterization of Selected Photonic Materials and Systems using Photoacoustic Technique'. PhD thesis, International School of Photonics, Cochin University of Science and Technology, (2005)

229. A. Rosencwaig and A. Gersho, *J. Appl. Phys.*, **47**, 64 (1976)

230. H. S. Carlaw and J. C. Jaegar, 'Conduction of heat in solids' (Oxford press)

231. H. S. Carlaw, 'Introduction to the mathematical theory of the conduction of heat in solids' (McMillan).

232. Charpentier, F. Lepoutre and L. Bertrand, *J. Appl. Phys.*, **53**, [1] , 608, (1982).

233. Measurement Sci.& Technol. **12**, 2058 (2001)

234. National Physical Lab. TPAC News **7.**

235. Henry Lehmann et al, *J.Am.Ceram.Soc.*, **86**[8],1338 (2003).

236. Robert Vassen et al, *J. Am. Ceram. Soc.*, **83**[8], 2023 (2000).

237. N. P. Bansal, D. Zhu, *NASA /TM* 212896, (2003).

238. Regis, J. Betsch, H. L. Park, William B. White, *Mat. Res. Bull.* **26**, 613 (1991).

239. Manual Ocana, Jose V. Garcia-Ramos and Carlos J. Serna, *J. Am. Ceram. Soc.*, **75** [7], 2010 (1992).

240. S. X. Wang, L. M. Wang, R. C. Ewing, *Nucl. Inst. and Methods*, **B148**, 704 (1999).

241. Hobant H. Willard, Lynne L. Merrit Jr., John A. Dean and Frank A. Settle Jr., *Instrumental Methods of Analysis*, CBS Publishers, New Delhi (1986).

242. M. Signoretto, L. Oliva, F. Pinna, G. Strukul, *J. of Non Crystalline Solids*, **290**, 145 (2001).

243. Kazuo Nakamoto, 'IR and Raman spectra of Inorganic and Coordination Compounds', John Wiley & Sons, New York (1997).

244. S. D. Ross, 'Inorganic Infrared Raman spectra', McGraw Hill, U.K., 107 (1972).

245. S. Brunauer, P. Emmett and E. Teller, *J. Amer. Chem. Soc.*, **60**, 309 (1938).

246. S. Lowell and J. E. Shields, 'Powder surface area and porosity', 3rd edn., Chapman & Hall, London (1991).

247. Harold P. Klug, Lerroy E. Alexander, 'X-ray diffraction procedures', 2nd edn., John Wiley and Sons, New York, (1974).